

VIBRATION ANALYSIS AND INTELLIGENT CONTROL OF FLEXIBLE ROTOR SYSTEMS USING SMART MATERIALS

by

Lawrence Atepor



University
of Glasgow

THESIS SUBMITTED IN FULFILLMENT OF THE REQUIREMENTS
FOR THE DEGREE OF DOCTOR IN PHILOSOPHY
TO THE FACULTY OF ENGINEERING
DEPARTMENT OF MECHANICAL ENGINEERING
UNIVERSITY OF GLASGOW

© L. Atepor
October 2008

All Rights Reserved

This work may not be reproduced in whole or in part, by photocopy or other means without permission of the author.

To my Family

COPYRIGHT

Attention is drawn to the fact that copyright of this thesis rests with its author. This copy of the thesis has been supplied on the condition that anyone who consults it is understood to recognise that its copyright rests with the author and that no quotation from the thesis and no information derived from it may be published, without prior written consent of the author.

This thesis may not be consulted, photocopied or lent by any library without the permission of the author for a period of two years from the date of acceptance of the thesis.

ABSTRACT

Flexible rotor-bearing system stability is a very important subject impacting the design, control, maintenance and operating safety. As the rotor bearing-system dynamic nonlinearities are significantly more prominent at higher rotating speeds, the demand for better performance through higher speeds has rendered the use of linear approaches for analysis both inadequate and ineffective. To address this need, it becomes important that nonlinear rotor-dynamic responses indicative of the causes of nonlinearity, along with the bifurcated dynamic states of instabilities, be fully studied. The objectives of this research are to study rotor-dynamic instabilities induced by mass unbalance and to use smart materials to stabilise the performance of the flexible rotor-system. A comprehensive mathematical model incorporating translational and rotational inertia, bending stiffness and gyroscopic moment is developed. The dynamic end conditions of the rotor comprising of the active bearing-induced axial force is modelled, the equations of motion are derived using Lagrange equations and the Rayleigh-Ritz method is used to study the basic phenomena on simple systems. In this thesis the axial force terms included in the equations of motion provide a means for axially directed harmonic force to be introduced into the system. The Method of Multiple Scales is applied to study the nonlinear equations obtained and their stabilities. The *Dynamics 2* software is used to numerically explore the inception and progression of bifurcations suggestive of the changing rotor-dynamic state and impending instability.

In the context of active control of flexible rotors, smart materials particularly SMAs and piezoelectric stack actuators are introduced. The application of shape memory alloy (SMA) elements integrated within glass epoxy composite plates and shells has resulted in the design of a novel smart bearing based on the principle of antagonistic action in this thesis. Previous work has shown that a single SMA/composite active bearing can be very effective in both altering the natural frequency of the fundamental whirl mode as well as the modal amplitude. The drawback with that design has been the disparity in the time constant between the relatively fast heating phase and the much slower cooling phase which is reliant on forced air, or some other form of cooling. This thesis presents a modified design which removes the aforementioned existing shortcomings. This form of design means that the cooling phase of one half, still using forced air, is

significantly assisted by switching the other half into its heating phase, and vice versa, thereby equalising the time constants, and giving a faster push-pull load on the centrally located bearing; a loading which is termed ‘antagonistic’ in this present dissertation. The piezoelectric stack actuator provides an account of an investigation into possible dynamic interactions between two nonlinear systems, each possessing nonlinear characteristics in the frequency domain. Parametric excitations are deliberately introduced into a second flexible rotor system by means of a piezoelectric exciter to moderate the response of the pre-existing mass-unbalance vibration inherent to the rotor. The intended application area for this SMA/composite and piezoelectric technologies are in industrial rotor systems, in particular very high-speed plant, such as small light pumps, motor generators, and engines for aerospace and automotive application.

ACKNOWLEDGEMENTS

I am so grateful to God who has made this research possible and to those who have made my experience in the University of Glasgow one that I will always remember fondly.

Firstly, I would like to express my sincere gratitude to my supervisor, **Professor Matthew Philip Cartmell**, who has been like a father and a mentor to me. His advice and guidance throughout the course of my postgraduate studies were invaluable, as was his patience and politeness that never failed during his supervision. I have learnt a lot of positive things from him. Thank you for being an advisor, a mentor and a good friend.

Thanks also extend out to Mr. Brian Robb and Mr. Bernie Hoey who have been of great help to me in the fixing of my experimental rigs, and to Dr. Asif Israr, my office mate for three years, for his encouragement and for being a good office mate.

Also to the Ghana Education Trust Fund (GetFund) and the Ghana Scholarship Secretariat who provided me with the scholarships for this course of study, and the Dynamics Group of the Mechanical Engineering Department, University of Glasgow for their support and for the provision of the necessary facilities and equipment; these are greatly appreciated.

Lastly to my friends, the Tuwor family in Glasgow, and to my family for their never ending support, sacrifices, understanding and encouragement throughout my course of studying at the University of Glasgow. Without them, I would not have been able to achieve what I have today.

“Thank you so very much and may God bless you richly”

LIST OF FIGURES

Figure 2-1: Typical temperature-transformation curves of a NiTi alloy (Marc van der Wijst 1998).	30
Figure 2-2: Schematic cross-section of piezoelectric stack actuator	32
Figure 3-1: Reference frames for a disk on a rotating flexible shaft.	37
Figure 3-2: Coordinates of the geometric centre c and an arbitrary point B on the shaft (Lalanne & Ferraris, 1990)	40
Figure 3- 3: Mass Unbalance	44
Figure 3- 4: Coordinates.....	46
Figure 3- 5: Bearing stiffness and damping	50
Figure 4-1: Amplitudes of the response as functions of the frequency at mass unbalance $m_u=0.004\text{kg}$ and damping coefficient of 13.6Ns/m	81
Figure 4- 2: Amplitudes of the response as functions of the frequency at mass unbalance $3m_u$ and damping coefficient of 13.6Ns/m	82
Figure 4- 3: Amplitudes of the response as functions of the frequency at mass unbalance m_u and damping coefficient of 15Ns/m	82
Figure 4- 4: Amplitudes of the response as functions of the frequency at mass unbalance m_u and damping coefficient of 13.6Ns/m with parametric force term.	82
Figure 4- 5: Amplitudes of the response as functions of the frequency.....	85
Figure 4- 6: Amplitudes of the response as functions of the frequency at the inclusion of parametric force term.	85
Figure 4- 7: Plots of response for MMS and Numerical Integration together- without parametric force terms.....	86
Figure 4- 8: Plots of response for MMS and Numerical Integration together- with parametric force terms.....	86
Figure 5- 1: Stability plots for k values.....	100
Figure 5- 2: Stability plots for λ values	101
Figure 6- 1: Sketch of the change in distance between two nearby orbits used to define Lyapunov exponent	110
Figure 6- 2: Bifurcation diagrams showing amplitude as a function of Ω (X-axis: Ω ,Y-axis: x_1, x_2), where $x_1 = x_2 = x$	113

Figure 6- 3: Lyapunov exponent and Bifurcation diagrams of amplitude as a function of the normalised excitation acceleration in the horizontal direction.	114
Figure 6- 4: Lyapunov exponent and Bifurcation diagrams of amplitude as a function of the normalised excitation acceleration for the Model with Parametric force term in the horizontal direction.	115
Figure 6- 5: Dynamical analysis of response to normalised excitation acceleration at 250 in the horizontal direction.....	121
Figure 6- 6: Dynamical analysis of response to normalised excitation acceleration at 400 in the horizontal direction.....	122
Figure 6- 7: Dynamical analysis of response to normalised excitation acceleration at 460 in the horizontal direction.....	123
Figure 6- 8: Dynamical analysis of response to normalised excitation acceleration at 505 in the horizontal direction.....	124
Figure 6- 9: Dynamical analysis of response to normalised excitation acceleration at 618 in the horizontal direction.....	125
Figure 6- 10: Dynamical analysis of response to normalised excitation acceleration at 840 in the horizontal direction.....	125
Figure 6- 11: Dynamical analysis of response to normalised excitation acceleration of models with the parametric force term in the horizontal direction	126
Figure 6- 12: Poincaré maps for the Models from solutions obtained from bespoke integration code in <i>Mathematica</i> TM	128
Figure 6- 13: Phase planes and Time plots for m_u from solutions obtained from bespoke integration code in <i>Mathematica</i> TM	129
Figure 6- 14: Phase planes and Time plots for $3m_u$ from solutions obtained from bespoke integration code in <i>Mathematica</i> TM	130
Figure 6- 15: Phase planes and Time plots for $4m_u$ from solutions obtained from bespoke integration code in <i>Mathematica</i> TM	131
Figure 6- 16: Phase planes and Time plots for $5m_u$ from solutions obtained from bespoke integration code in <i>Mathematica</i> TM	132
Figure 6- 17: Dynamical analysis of response to normalised excitation acceleration at the various discrete points from solutions obtained from integration code in <i>Mathematica</i> TM	133

Figure 7- 1: SMA Experimental set-up for response measurements.....	137
Figure 7- 2: Schematic view of Instruments used for the Antagonistic SMA/Composite Smart Bearing experiment.....	138
Figure 7- 3: The Antagonistic SMA/Composite Smart Bearing Test Rig.....	138
Figure 7- 4: Schematic of the antagonistic SMA/Composite bearing housing....	140
Figure 7- 5: The amplitudes of disc vibration versus excitation frequency for the right hand side of the Antagonistic Bearing.	143
Figure 7- 6: The amplitudes of disc vibration versus excitation frequency for the left hand side of the Antagonistic Bearing.....	143
Figure 7- 7 : Close-up of the Piezoelectric Exciter.....	147
Figure 7- 8: Assembly of the Piezoexciter Test Rig.....	147
Figure 7- 9: (a) Shaft-end assembly when rotor is not whirling, (b) Shaft-end assembly when rotor is whirling at maximum amplitude and (c) Free length of spring.....	150
Figure 7- 10: Schematic of the piezoelectric exciter.	151
Figure 7- 11: The amplitudes of disc vibration versus frequency with a spring compression length of 20.2mm.....	155
Figure 7- 12: The amplitudes of disc vibration versus frequency with a spring compression length of 25.2mm.....	156
Figure A.1- 1: Model of the rotor	A-2
Figure A.1- 2: Schematic of the shafts movements.	A-5
Figure C- 1: Dynamics 2 Program Code for coupled Duffing equations.....	C-1

LIST OF TABLES

Table 4- 1: Data of graphs plotted.....	81
Table 5- 1: Summary of conditions for stability according to Routh's criterion .	96
Table 5- 2: Discrete mass unbalance values with their stability indicators.....	99
Table 6- 1: Data used for numerical simulations	107
Table 6- 2: Program command values for <i>Dynamic 2</i> Plotting	109
Table 7- 1: Material properties of a typical SMA material (Ni-Ti alloy), (http://www.sma-inc.com).....	142

TABLE OF CONTENTS

COPYRIGHT.....	ii
ABSTRACT	iii
ACKNOWLEDGEMENTS.....	v
LIST OF FIGURES	vi
LIST OF TABLES.....	ix
TABLE OF CONTENTS	x
NOMENCLATURE	xv
CHAPTER 1.....	1
INTRODUCTION	1
1.1 Background.....	1
1.2 Objectives	3
1.3 Outline and Methodology.....	5
CHAPTER 2.....	7
LITERATURE REVIEW	7
2.1 Historical Perspective	7
2.1.1 Jeffcott’s Rotor	7
2.1.2 Origins of Vibration Theory.....	8
2.1.3 Gyroscopic Effects	8
2.1.4 Shape Memory Alloys	9
2.1.5 Piezoelectric Materials	9
2.2 Vibration Control of Rotor Systems.....	10
2.3 Nonlinearities in Structures.....	14
2.3.1 Types of Nonlinearity.....	15
2.3.2 Nonlinearities of Beams/ Shafts	17
2.3.3 Nonlinearities in Bearings.....	18
2.4 Nonlinear Control	20

2.5	Perturbation Methods.....	22
2.6	Method of Multiple Scales (MMS).....	23
2.7	Smart Materials.....	26
2.8	Shape Memory Alloy (SMA).....	28
2.9	Piezoelectric Materials	31
CHAPTER 3.....		34
ANALYTICAL MODELLING OF FLEXIBLE ROTOR SYSTEMS		34
3.1	Introduction.....	34
3.2	Derivation of the Equations of Motion	35
3.2.1	Rotor Model	36
3.2.2	Kinetic Energy of the Rotating Disk	38
3.2.3	Kinetic Energy of the Shaft.....	39
3.2.4	Strain Energy of the Shaft	40
3.2.5	Kinetic Energy of the Mass Unbalance.....	43
3.2.6	Simplified Model.....	45
3.2.7	Nonlinear Bearing	48
3.2.8	Equations of Motion	52
3.2.8.1	Alternative Analytical Model A	53
3.2.8.2	Alternative Analytical Model B	53
3.2.8.3	Alternative Analytical Model C.....	54
3.2.9	Linear Viscous Damping	54
3.2.9.1	Model A.....	54
3.2.9.2	Model B.....	55
3.2.9.3	Model C	55
3.2.10	Parameter Estimation Procedure	55
3.2.10.1	Nonlinearity Estimation.....	56
3.2.11	Discussions.....	57
CHAPTER 4.....		58
APPROXIMATE ANALYTICAL AND NUMERICAL SOLUTIONS TO THE		
EQUATIONS OF MOTION		58
4.1	Introduction.....	58

4.2	Ordering of Terms	59
4.3	The Method of Multiple Scales	62
4.3.1	Introducing the Time Scales	62
4.3.2	Treatment of Coefficients to like Orders of \mathcal{E}	63
4.3.3	Secular Terms to First Order Perturbation.....	65
4.3.4	Modulation of First Order Perturbation Equations.....	68
4.3.5	Second Order Perturbation Equations.....	70
4.3.6	Secular Terms from the Second Order Perturbation Equations	71
4.3.7	Analysis of the Second Order Solvability Equations	72
4.3.8	General Solutions of the Equations of Motion (4.2-1) and (4.2-2)	77
4.3.9	Multiple Scales Results	80
4.3.9.1	Amplitude Response Plot – without Parametric Force Term.....	81
4.3.9.2	Amplitude Response Plot – with Parametric Force Term.....	82
4.4	Direct Numerical Integration.....	83
4.4.1	Results from <i>Mathematica</i> TM	85
4.4.1.1	Numerical Integration Plot- without Parametric Force Term	85
4.4.1.2	Numerical Integration Plot- with Parametric Force Term	85
4.5	Discussion of Results	87
CHAPTER 5.....	88
STABILITY OF STEADY-STATE SOLUTIONS	88
5.1	Introduction.....	88
5.2	Stability Matrix.....	88
5.3	The Routh-Hurwitz Stability Criterion	93
5.3.1	Stability Results.....	97
CHAPTER 6.....	102
INVESTIGATION OF SYSTEMS DYNAMICS	102
6.1	Introduction.....	102
6.2	Program Code.....	103
6.2.1	Dynamics 2 Code.....	103
6.2.1.1	Nondimensionalisation	104

6.2.2	<i>Mathematica</i> TM Code.....	106
6.2.3	Definition of Parameters.....	106
6.3	Bifurcation Analysis.....	107
6.4	Lyapunov Exponents.....	109
6.5	Bifurcations as Functions of Excitation Acceleration.....	110
6.6	Phase Planes, Poincaré Maps and Time Plots.....	116
6.6.1	Analysis of Phase Planes, Poincaré Maps and Time Plots.....	117
6.6.1.1	At Normalised Excitation Acceleration of 250 (Figure 6-5):.....	117
6.6.1.2	At Normalised Excitation Acceleration of 400 (Figure 6-6):.....	118
6.6.1.3	At Normalised Excitation Acceleration of 460 (Figure 6-7):.....	118
6.6.1.4	At Normalised Excitation Acceleration of 505 (Figure 6-8):.....	119
6.6.1.5	At Normalised Excitation Acceleration of 618 (Figure 6-9) and 840 (Figure 6-10):	120
6.6.1.6	Including Parametric Force Term (Figure 6-11):.....	120
6.7	Numerical investigations in <i>Mathematica</i>TM code.....	126
CHAPTER 7.....		134
EXPERIMENTAL INVESTIGATIONS.....		134
7.1	Controlling Flexible Rotor Vibration by means of an Antagonistic SMA/Composite Smart Bearing.....	134
7.1.1	Introduction.....	134
7.1.2	Overview of the Experimental Rig.....	136
7.1.3	Active Bearing Concept.....	139
7.1.4	Active Bearing Experiment.....	140
7.1.5	Experimental Results.....	141
7.2	Controlling Flexible Rotor Vibration by means of a Piezoelectric Stack Exciter.....	144
7.2.1	Introduction.....	144
7.2.2	Instrumentation.....	146
7.2.3	Design and Selection of Piezoexciter Component.....	147
7.2.4	Test Setup.....	149
7.2.5	Experimental Results.....	151
7.2.6	Piezoelectric Exciter Applications.....	153

CHAPTER 8.....	157
DISCUSSIONS OF RESULTS.....	157
8.1 Introduction.....	157
8.2 Analytical Results.....	157
8.3 Stability Analysis Results	159
8.4 Numerical Results	159
8.5 Experimental Results	162
8.6 Conclusions.....	162
CHAPTER 9.....	164
CONCLUSIONS AND RECOMMENDATIONS FOR FURTHER WORK	164
9.1 Summary	164
9.2 Recommendations for Further Work	167
REFERENCES	169
PUBLICATIONS	202
.....	202
CONTENTS OF APPENDICES	A-1
.....	A-1
.....	C-1

NOMENCLATURE

Symbols	Description
q_1, q_2	Displacement
c, C_1	Damping coefficients
ω	Natural frequency
k, C_3	Linear stiffness coefficient
b, C_4	Nonlinear cubic stiffness coefficient
m	Modal mass
θ, ϕ, ψ	Angles of rotation
$\omega_x, \omega_y, \omega_z$	Angular velocities
T	Kinetic energy
U	Strain energy
T_d	Kinetic energy of disk
T_s	Kinetic energy of shaft
T_u	Kinetic energy of mass unbalance
M_d	Mass of disk
m_u	Mass unbalance

d	Distance of mass unbalance from geometric centre of shaft
F_{q_i}	Generalised forces
δW_{q_i}	Virtual work associated with a generalised force
E	Modulus of elasticity
I	Area moment of inertia
I_{dx}, I_{dz}, I_{dy}	Diametral moment of inertia
S	Cross-sectional area of shaft
u, v, w	Displacement in the x, y, z directions
u^*, w^*	Displacement of the geometric centre with respect to the x and z directions
F_x, F_z	Bearing forces in the x and z directions
k_{ij}	Linear spring coefficients; $i, j = x, z$
\bar{k}_{ij}	Nonlinear spring coefficients; $i, j = x, z$
c_{ij}	Linear damping coefficients; $i, j = x, z$
ω_{nl}	Nonlinear frequency
k_b	Bearing stiffness coefficient
c_b	Bearing damping coefficient
c_s	Damping coefficient of shaft

a, b	Amplitude response
τ	Nondimensionalised time
T	Time
T_n	$n = 0$:Fast time scales; $n = 1, 2$:Slow time scales i.e, $T_0 = t$; $T_1 = \varepsilon t$; $T_2 = \varepsilon^2 t$
ε	Ordering parameter for method of multiple scales
A, C	Complex amplitudes
Γ, ρ	Excitation amplitude
Ω	Excitation frequency
$\frac{\Omega}{\omega}$	Nondimensionalised excitation frequency
α_1, α_2	Phase angles
$\bar{\sigma}$	Detuning parameter
Ω_2	Parametric excitation frequency; $\Omega_2 = 2\Omega$ for the case of exact principal parametric resonance
a_i	Characteristic equation coefficients; $a_i = k_i$; $i = 1$ to n
λ_i	Eigenvalues
λ	Lyapunov exponent
$F_{S\max}$	Maximum spring force

$F_{S\min}$	Minimum spring force
k_{SS}	Spring constant
$F_{act(max)}$	Maximum actuator force; $F_{act(max)} = F_{act} = F_{v0}$
δ_1	Spring ‘preload’ pre-compression
δ_2	Maximum spring compression
Δ	Maximum shaft end displacement
BIFD	No. of iterates (dots plotted) for each bifurcation parameter
BIFPI	Pre-iterates for each bifurcation parameter
BIFV	No. of parameter values in bifurcation diagram
CON	Connect consecutive dots of trajectories
I-H-B	Incremental harmonic balance
IPP	No. of iterates per plot
K-B	Krylov-Bogolioubov Method
K-B-M	Krylov-Bogolioubov-Mitropolski Method
L-P	Lindstedt-Poincaré Method
MMS	Method of multiple scales
NI	Direct numerical integration

ODE	Ordinary differential equation
PI	No. of pre-iterates before plotting
SMA	Shape memory alloy
SPC	Steps per cycle

CHAPTER 1

INTRODUCTION

1.1 Background

Rotating machinery play an important role in many different industries in our society. Some examples are in electrical power production, gas-turbines, aircraft engines, process machines in heavy industry, fans, pumps and ship engines, which are only a few of the applications in which rotating machinery has a central role. The designs of many rotating machines are now fifty to a hundred years old; however, the demands of these units are continuously changing. Hence, it becomes important to work on product development and research in the area of rotating machinery. The behaviour of these rotor-dynamic components can influence the performance of the whole system. Namely, for certain ranges of rotational speed, such systems can exhibit various types of vibration which can be so violent that it can cause significant damage. Consequently, the understanding of the dynamic behaviour of these systems is very important.

Vibration in dynamical systems can be caused by nonlinearities which induce forces locally in the system under consideration. However, their presence in general has important consequences for the overall dynamic behaviour. Some examples of nonlinearities in mechanical systems are friction forces, mass unbalance, and nonlinear spring and damper supports. Therefore, in order to gain understanding and to predict different types of vibration it is important to understand the causes of such vibrations, and also to understand the interactions between them where there exists more than one type of vibration. Lateral vibrations in rotor systems have been analysed extensively by Tondl, 1965; Fritz, 1970 (a, b) and Lee, 1993. They considered different types of rotor systems, and in all those systems, lateral vibrations are induced by the mass unbalance in a rotor. In all the systems considered it is noticed that increase of mass unbalance can have destabilising effects. For example, Tondl, 1965 and Lee, 1993

considered a simple disk with a mass unbalance connected to a shaft which is elastic in the lateral direction and found out that in such systems, under certain conditions, instabilities can appear if the mass unbalance increases. Since the rotating parts of these machines are mostly the main sources of vibration, adequate understanding and knowledge of the vibration phenomena of rotor-dynamics are necessary for finding ways to reduce or eliminate when possible vibrations. It has been observed that when the running speed exceeds certain critical speeds, various kinds of undesirable problems of rotor-dynamic instability would occur. Therefore, studying the static and dynamic response, both theoretically and experimentally, of the flexible rotor system under various loading conditions would help in understanding and explaining the behaviour of more complex, real structures under similar conditions.

The analysis of the nonlinear effects in rotor-bearing systems is extremely difficult and there are a few analytical procedures that will generate valid results over a wide range of parameters. Vibration problems involving nonlinearities do not generally lend themselves to closed form solutions obtained by using conventional analytical techniques. The Perturbation methods are a collection of techniques that can be used to simplify, and to solve, a wide variety of mathematical problems, involving small or large parameters. The solutions may often be constructed in explicit analytical form or, when it is impossible, the original equation may be reduced to a more simple one that is much easier to solve numerically. The techniques including Incremental Harmonic Balance, Averaging, Krylov-Bogolioubov, Lindstedt-Poincaré and the Method of Multiple Scales, usually assume the system has a simple periodic response, which is then successively iterated upon to converge to an acceptable approximation to the actual response. A common solution procedure for nonlinear vibration problems, such as rotor-bearing systems, is to perform a long time-transient numerical integration of the equations of motion. This procedure can yield the transient behaviour plus a stable steady state response for given system parameters and initial conditions.

Generally, vibration control in rotating machines is linked to a critical speed, to an excitation at rotation harmonics, or to rotordynamic instability. Active vibration control is usually divided into active and semi-active control. In active

control, a dynamic force is applied against the vibration to be controlled. In the semi-active case, the characteristics of a structure are adjusted in such a way that the vibration response is reduced. Applications of smart materials technology to various physical systems are evolving to actively control vibration. Smart materials involve distributed actuators and sensors and in the application of one or more of these, one may either integrate them in the structure making up an embedded system or develop control systems that can even cope with unexpected operating conditions.

This dissertation first establishes rotor-dynamic responses as function of control parameters and system configuration, which are obtained by an analytical model that describes the physical nature of the nonlinear mechanism within a flexible rotor-bearing system. The excitation is provided by the rotor unbalance and the nonlinearity is given by the inherent instability mechanism and nonlinear elements within the system. Thus, the set-in and progress of dynamic instability induced by nonlinearities in the rotary model is both analytically and numerically investigated. Experimental investigations are conducted to study the controllability of the flexible rotor system using Smart materials.

1.2 Objectives

It is established that nonlinear analysis is of great importance for understanding the behaviour of a rotor-dynamic system. Presently, research in rotor-dynamics is such that nonlinear analytical methods for rotating machines are either unavailable or insufficient. Effective methods of controlling vibrations in rotor-dynamic systems are still being sought. Therefore, the major objectives of this research are to:

Develop a dynamic mathematical model of a flexible rotor system described by differential equations including axial force terms, taking into consideration translational, rotational inertia, bending stiffness, gyroscopic moment and nonlinearities. The axial force term enables one to include or apply an external force axially into the rotor system. To control the vibrations of a dynamic rotor system using active control methods, it is first appropriate to apply a controller to a system in a theoretical setting. It therefore becomes necessary to build a

valid model on which to base the control. The model needs to reproduce accurately the dynamic response of the real system over the frequency range of interest and also needs to be versatile enough to model variations of the rotor dynamic properties.

Analyse vibrations of flexible rotor systems using appropriate analytical and numerical tools with and without the introduction of axial parametric force terms, with the focus of the analysis based on the steady-state behaviour of the system.

Construct test environments for active vibration control of rotors by employing the use of Smart actuators directed to the control of stability.

The main contributions of the thesis can be described as follows:

- Modifications have been made to the existing governing equations of motion of the flexible rotor system by accommodating large deflections and including axial force terms which allow the introduction of external axial forces in order to manipulate the behaviour of the flexible rotor system. The physical bases employed to model the axial force term is that the force term is modelled as a physical effect equivalent to the localised changing of the elastic part of the rotor shaft stiffness, which can then be manipulated to cause reduction in vibration amplitude and changes in critical speeds.
- Provision of knowledge by solving the nonlinear equations of motion analytically using the Perturbation Method of Multiple Scales to show how the introduction of parametric force terms can help in stabilising the otherwise unstable system due to mass unbalance, by reducing the amplitude values.
- Provision of knowledge that has not previously been available using dynamical systems analysis to show how a hard-driven nonlinear rotor system can be stabilised by the introduction of a parametrically excited force into the system. The availability of the knowledge would thus positively impact the operating safety of rotary machinery.

- New information on the alternatives to the traditional stability chart for better or instability-free rotary machine concept development and configuration design by
 - (a) Designing and experimentally testing an antagonistic SMA/Composite active bearing for controlling vibration by shifting the resonance frequency range of a flexible rotor system.
 - (b) Designing and experimentally testing a piezoelectric actuator exciter for controlling vibration by reducing the amplitude of vibration when parametric excitation is introduced into the system at a principal parametric resonance where the frequency of excitation is twice the first whirl mode frequency of the system.

This work presents and demonstrates an effective approach that integrates weakly nonlinear rotor-dynamics, and analytical and numerical modelling that applied to the detection and identification of instabilities. Under the influence of mass unbalance, the rotor-bearing system displays transitional behaviour typical of a nonlinear dynamic system, going from periodic to period-doubling to quasiperiodic and eventually to chaotic motions. When actuator forces are also considered, the model system demonstrates very different behaviour. As a result, dynamic methods of vibration controlling using specially designed devices made out of smart materials are proposed as alternatives to operating purely by the traditional stability chart. Observations and results such as these have important practical implications on the design and safe operation of high performance rotary machinery.

1.3 Outline and Methodology

This thesis is divided into nine chapters. It begins with an introduction in Chapter 1 followed by literature review in Chapter 2. The flexible rotor-bearing system is modelled mathematically in Chapter 3. Chapter 4 applies the Perturbation Method of Multiple Scales, and also applies a direct numerical integration method. In chapter 5 a stability analysis of steady-state solutions is investigated using the Routh-Hurwitz criterion.

Chapter 6 strengthens the above results with the numerical investigation of the system dynamics in the form of calculations leading to bifurcation diagrams and the Lyapunov exponent. Phase planes, Poincaré maps and time plots are also plotted for a more in-depth understanding into the system dynamics. This provides one with a better comprehension of the overall dynamics of the flexible rotor-bearing system.

Experiments have been carried out based on the theoretical work to control vibrations as a result of instabilities in the rotor system using smart materials in the form of Shape Memory Alloys and Piezoelectric actuators. These are discussed in Chapter 7.

Chapter 8 presents a discussion and comparison of results from the different methods employed in this thesis, and the conclusions and recommendations for further work are also presented in Chapter 9.

Publications produced during the course of this postgraduate research by the author, and others, are given after the Reference section.

CHAPTER 2

LITERATURE REVIEW

2.1 Historical Perspective

2.1.1 Jeffcott's Rotor

Rotordynamics as a subject first appeared in the last quarter of the 19th Century due to the problems associated with the high speed turbine of Gustaf de Laval who invented the elastically supported rotor, called de Laval Rotor, and observed its supercritical operation. Foepl (1895) explained analytically the dynamic behaviour of the de Laval rotor. Serious research on rotor dynamics started in 1869 when Rankine (1869) published his paper on whirling motions of a rotor. However, he did not realize the importance of the rotor unbalances and therefore concluded that a rotating machine never would be able to operate above the first critical speed. De Laval showed around 1900 that it is possible to operate above critical speed, with his one-stage steam turbine. In 1919 Jeffcott prescribed the first paper where the theory of unbalanced rotors is described. Jeffcott derived a theory which shows that it is possible for rotating machines to exceed the critical speeds. However, in the Jeffcott model the mass is basically represented as a particle or a point-mass, and the model can not correctly explain the characteristics of a rigid-body on a flexible rotating shaft (Gustavsson R., (2005)). DeLaval and Jeffcott's names are still in use as the name of the simplified rotor model with the disc in the mid-span of the shaft. Jeffcott's rotor is described by Vance (1988), for example as one that consists of a flexible shaft, with zero mass, supported at its ends. The supports are rigid and allow rotation around the centre axis of the shaft. The mass is concentrated in a disk, fixed at the midpoint of the shaft. The system is geometrically symmetrical with respect to its rotational axis, except for a mass imbalance attached to the disk. When rotating the mass imbalance provides excitation to the system.

2.1.2 Origins of Vibration Theory

The development of vibration theory, as a subdivision of mechanics, came as a natural result of the development of the basic sciences it draws from, mathematics and mechanics. The term “vibration” was used from Aeschylus times (Dimarogonas, 1992). Pythagoras of Samos (ca. 570-497 BC) conducted several vibration experiments with hammers, strings, pipes and shells. He established the first vibration research laboratory. That for a (linear) system there are frequencies at which the system can perform harmonic motion was known to musicians but it was stated as a law of nature for vibration systems by Pythagoras. Moreover, he proved with his hammer experiments that natural frequencies are system properties and do not depend on the magnitude of the excitation (Dimarogonas 1990, Dimarogonas and Haddad 1992).

Euler in 1744 obtained the differential equation for the lateral vibration of bars and determined the functions that are now known as normal functions and the equation now called frequency equation for beams with free, clamped or simply supported ends and Navier in 1821 investigated the general equations of equilibrium and vibration of elastic solids (Dimarogonas, 1992). He formed an expression for the work done in a small relative displacement by all forces and obtained the differential equations by way of the calculus of variations. Solutions of the differential equations of motion for an elastic solid were treated by Poisson (1829) who founded the general theory of vibrations. Poisson in 1829 brought under the general equations of vibration of elastic solids the theory of vibration of thin rods. Lord Rayleigh in 1889 formalised the idea of normal functions introduced by Daniel Bernoulli and Clebsch and introduced the ideas of generalised forces and generalised coordinates. He further introduced systematically the energy and approximate methods in vibration analysis. This idea was further developed by W. Ritz (1909), and Rayleigh introduced a correction to the lateral vibration of beams due to rotating inertia.

2.1.3 Gyroscopic Effects

The influence of gyroscopic effects on a rotating system was presented in 1924 by Stodola. The model that was presented consists of a rigid disk with a polar moment of inertia, transverse moment of inertia and mass. The disk is

connected to a flexible mass-less overhung rotor. The gyroscopic coupling terms in Stodola's rotor model resulted in the natural frequencies being dependent upon the rotational speed. The concept of forward and backward precession of the rotor was introduced as a consequence of the results from the natural frequencies analysis of the rotor model. When the natural frequencies of the rotor system changes with the rotational speed the result is often represented in a frequency diagram or Campbell diagram with natural frequencies as a function of the rotational speed (Lalanne and Ferraris, 1990).

2.1.4 Shape Memory Alloys

The first recorded observation of Shape Memory Alloy (SMA) transformation was made in 1932 on gold-cadmium. In addition, in 1938 the phase transformation was observed in brass (copper-zinc). It was not until 1962, however, that Beehler and co-workers found the transformation and attendant shape memory effect in Nickel-Titanium at the Naval Ordnance Laboratory. They named this family of alloy NiTiInol after their Laboratory. A few years after the discovery of NiTiInol, a number of other alloy systems with the shape memory effect were found, (Hodgson and Brown, 2000). Though product development using SMA began to accelerate after the discovery of NiTiInol, many of the SMAs contain expensive and exotic elements. Only the copper based alloys came close to challenging the NiTiInol family as a commercially attractive system. During the 1980s and early 1990s, a number of products, especially medical products, were developed to market (Hodgson and Brown, 2000 and DesRoches, 2002).

2.1.5 Piezoelectric Materials

Although as early as the 18th century, crystals of certain minerals were known to generate charge when heated (which became known as pyroelectricity) it was two brothers who actually came to develop the actual "piezoelectricity" used yet today. In 1880, the Curie brothers; Jacques and Pierre discovered the piezoelectric effect. They found out that when a mechanical stress was applied on crystals such as tourmaline, topaz, quartz, Rochelle salt and sugar cane, electrical charges appeared, and this voltage was proportional to the stress. Conversely piezoelectricity was mathematically deduced from fundamental thermodynamic properties by Lippmann in 1881. The first practical application

for piezoelectric devices was sonar, first developed during World War I. In France in 1917, Paul Langevin and his co-workers developed an ultrasonic submarine detector. An everyday life application example is the automotive airbag sensor. The material detects the intensity of the shock and sends an electrical signal which triggers the airbag (www. Piezomaterials.com, 2008).

2.2 Vibration Control of Rotor Systems

Reduction of vibration in structures has always been an important issue in mechanics. Lighter, more flexible constructions are more susceptible to oscillations, mechanical vibrations are associated with fatigue which can lead to a catastrophic failure, which often have to be eliminated as much as possible, since they can deteriorate performance and contribute to premature collapse. An effective means of controlling and reducing vibrations in rotating machinery is the use of external damping and elastic elements often provided via flexible bearings and /or bearing supports.

Rotor systems have been traditionally supported on oil-film bearings due to their robustness. The oil-film bearings introduce some damping to the rotor system, but can also lead to oil whip instability. In order to control the resonance and to delay the onset of instability, passive devices such as squeeze-film bearings have been used to augment the system damping (Cunningham, 1978). However, in supercritical systems several lateral bending modes of vibration are liable to be excited, and given a single passive device it is not possible to select the stiffness and damping parameters so as to exert a significant influence over all these modes (Stanway *et.al.*, 1981), and on the other hand, their success depends on accurate knowledge of the dynamic behaviour of the machine. Additionally, passive control techniques have low versatility, i.e., any change in the machine configuration or in the loading condition may require a new damping device. Therefore, passive vibration control devices are of limited use. This limitation together with the desire to exercise greater control over rotor vibration, with greatly enhanced performance, has led to a growing interest in the development of active control of rotor vibrations (Abduljabbar *et.al.* (1996)).

The development of microelectronics in the last three decades has allowed the implementation of active vibration control techniques. Active vibration control is based on a feedback control law that is applied to the mechanical system in order to obtain a suitable response. An important advantage of active vibration control is that it can be adjusted to suit different load conditions and machine configurations. In the field of rotating machinery active vibration control can be applied either to modify the structure characteristics such as damping and stiffness (Yao *et.al.*1999), or to introduce a control force. Application of control forces can be achieved either directly, using actuators which correspond to fixed position forces (Barret *et.al.* 1995), or by using active balancing devices, (Der Haopian *et.al.* 1999). The use of active balancing is restricted to attenuation of synchronous perturbations (Simões *et.al.* 2007)).

Allaire *et.al.* (1986) developed and tested magnetic bearings in a multimass flexible rotor both as support bearings and as vibration controller and demonstrated the beneficial effect of reducing vibration amplitudes by using an electromagnet applied to a transmission shaft respectively. They used two approaches to actively control flexible rotors. In the first approach magnetic bearings or electromagnetic actuators are used to apply control forces directly to the rotating rotor without contacting it. In the second approach, the control forces of the electro-magnetic actuators are applied to the bearing housings.

Subbiah *et.al.* (1988) and Viderman *et.al.* (1987) showed that a rotor has certain speed ranges in which large and unacceptable amplitude of vibration could be developed. These speed ranges are known as critical speeds (or critical frequencies) which could cause a bearing failure or result in excessive rotor deflection. Under these circumstances, the problem of ensuring that a rotor-bearing system performs with stable and low-level amplitude of vibration becomes increasingly important. The use of electromagnetic bearings in lowering the amplitude level has increased and Keith *et.al.* (1990) showed that they generate no mechanical loss and need no lubricants such as oil or air as they support the rotor without physical contact. However, the electromagnets are open loop unstable and all designs require external electronic control to regulate the forces acting on the bearing (Cheung *et.al.* (1994)). Abduljabbar *et.al.* (1996) derived an optimal controller based on characteristics peculiar to

rotor bearing systems which take into account the requirements for the free vibration and the persistent unbalance excitations. The controller uses as feedback signals, the states and the unbalance forces. A methodology of selecting the gains on the feedback signals has been presented based on separation of the signal effects: the plant states are the primary stimuli for stabilizing the rotor motion and augmenting system damping, while the augmented states representing the unbalance forces are the primary stimuli for counteracting the periodically excited vibration. The results demonstrate that the proposed controller can significantly improve the dynamical behaviour of the rotor-bearing systems with regard to resonance and instabilities.

Sun *et.al.* (1998) used a multivariable adaptive self-tuning controller to control forced vibrations in a rotor system. They used an active hydrodynamic bearing as a third bearing to add damping to the system. The self-tuning regulator was implemented to control oil-film thickness in the third bearing located between the load-carrying ball bearings. The system was designed to cope with nonlinear fluid-film bearing characteristics and parameter variations (Tammi (2003)). They showed that the self-tuning regulator was suitable for forced vibration compensation. Sun *et.al.* (1998) also used a multivariable self-tuning adaptive control strategy to control forced vibration of rotor systems incorporating a new type of active journal bearing, which has particular advantages compared with control strategies, such as requiring no pre-knowledge of the system parameters and imbalance distribution and being easy to implement. Such a proposed control strategy is especially significant in applications with complex rotor-bearing systems supported on fluid-film bearings (He *et.al.* (2007)).

The use of disk type Electrorheological (ER) damper in controlling vibration of rotor systems was carried out by Yao *et.al.* (1999). ER fluid is a kind of smart material which has the merits of fast response, easy control, low energy consumption and a broad application of vibration control. These authors designed a new disk type ER damper and attached its moving part to the outer ring of a bearing which was mounted on a squirrel cage. The suppression of the resonant vibration around the first critical speed and the suppression of the large response caused by the sudden unbalance were considered and achieved.

Yan *et.al.* (2000) presented an intelligent bearing system for passing through the critical speed of an aero engine rotor by changing the stiffness using SMA wires based on Nagata *et.al.* (1987) method. The authors considered vibration control with the rotating speed rising, and paid attention to avoiding the first critical speed of the rotating machine system. Their system has only two changeable stiffness values in the pedestal bearing, because the SMA character has two phases and therefore the SMA stiffness can be changed only twice. And when the rotational speed arrives at the critical speed, the stiffness of the rotor system is changed by the switch on/off of the SMA. Their result shows the effect of the avoidance of the first resonance (He *et.al.* (2007)). Ehmann *et.al.* (2003) used a third point in a rotor for controlling vibrations. A piezo-actuator was integrated with one of two bearings of a rotor. The shaft of the rotor had two disks attached. Two different controllers were considered: an integral-force-feedback controller and a robust controller designed with μ -synthesis. The use of active control reduced the response of the rotor.

Vibration control of nonlinear rotor systems using a dynamic absorber utilizing the Electromagnetic force was studied by Inoue *et.al.* (2001). Rotor systems supported by single-row deep groove ball bearings exhibit nonlinear spring characteristics. The vibration characteristics are changed due to the effect of nonlinearities. They clarified that the isotropic symmetrical nonlinearity has influence on the vibration control characteristics, and also that vibration control can be achieved by considering such effects of nonlinearity in designing the parameters of the dynamic absorber.

Nagata *et.al.* (1987) proposed a method of active vibration control for passing through critical speeds for rotating shafts by changing stiffness of the supports. In this method, the vibration of the shaft at the critical speed is controlled by means of heating and cooling the SMA for bearing supports. But the control of the vibration response worked only at every constant rotating speed rising from 0 rpm (He *et.al.* (2007)). Vibration control of a rotor-bearing system using a self-optimizing support system based on shape memory alloy was proposed by He *et.al.* (2007). The authors used SMA spring to construct a pedestal bearing for the rotor-bearing system. The principle of the dynamic absorber is utilized to calculate and change the stiffness of the SMA pedestal bearing in order for the

rotor shaft to be usually situated near anti-resonance with changes of the rotating speed, and its vibration can be controlled.

Simões *et.al.* (2007) worked on active vibration control of a rotor in both steady state and transient motion using piezoelectric stack actuators. They investigated the efficiency of the control strategy in the following conditions: Rotor at rest, steady state motion and transient motion. The piezoelectric actuators were orthogonally mounted in a single plane localized at one of the rotor bearings. They used the modal control technique to the dynamic behaviour of the structure. An optimal Linear Quadratic Regulator (LQR) controller associated with a state estimator Linear Quadratic Estimator (LQE) was used. These authors have shown that a simple optimal controller can be successfully used for vibration attenuation in flexible rotors and that a single active plane is enough to provide control effort. The results are very encouraging in the sense that piezoelectric actuators provide significant control forces over an important frequency band and that they can be used for balancing purposes.

A control method to eliminate the jump phenomena of the rotating speed and to restrain the whirling motion in a flexible rotor system by controlling torque is proposed by Inoue *et.al.* (2000). They derived a sufficient condition for stabilization of the system modelled by a second-order differential equation whose coefficients are continuous, bounded, time-varying and sign-definite. They showed that the jump of the rotating speed is eliminated and the maximum amplitude of the whirling motion is reduced.

2.3 Nonlinearities in Structures

Interesting physical phenomena occur in structures in the presence of nonlinearities, which cannot be explained by linear models. These phenomena include jumps, saturation, subharmonic, superharmonic and combination resonances, self-excited oscillation, modal interactions and chaos. Naturally no physical system is strictly linear and hence linear models of physical systems have limitations of their own. In general, linear models are applicable only in a very restrictive domain, for instance when the vibration amplitude is very small. Thus to accurately identify and understand the dynamic behaviour of a

structural system under general loading conditions, it is essential that nonlinearities present in the system also be modelled and studied (Malatkar (2003)).

2.3.1 Types of Nonlinearity

Nonlinearity exists in a system whenever there are products of dependent variables and their derivatives in the equations of motion and boundary conditions and whenever there are any sort of discontinuities or jumps in the system. Nayfeh *et.al.* (1979) and Moon (1987) have explained in detail the various types of nonlinearities with examples. However, the majority of physical systems belong to the class of weakly nonlinear (or quasi-linear) system. Most of these systems exhibit behaviours only slightly different from that of their linear counterparts. They also exhibit phenomena which do not exist in the linear domain. Therefore, for weakly nonlinear structures, the usual starting point is still the identification of the linear natural frequencies and mode shapes. Then, in the analysis, the dynamic response is usually described in terms of its linear natural frequencies and mode shapes. The effect of the small nonlinearities is seen in the equations governing the amplitude and phase of the structure response.

In structural mechanics and rotating machinery applications, relevant nonlinearities can in a broad sense be classified as follows:

1. Inertial nonlinearity which comes from nonlinear terms containing velocities and/or accelerations in equations of motion. The source of the inertial nonlinearity is the Kinetic energy of the system. Examples are the centripetal and Coriolis acceleration terms in motions of bodies moving relative to rotating frames.
2. Geometric nonlinearities are mostly found in systems undergoing large deformations or deflections. This nonlinearity arises from the potential energy of the system. In structural mechanics, large deformations mostly results in nonlinear strain-and curvature-displacement relations. Examples of this type can be found in the equations derived from nonlinear strain-displacement relations due to mid-plane stretching in strings, due to nonlinear curvature in beams and

due to shaft elongation of a rotor system (Ishida *et.al.* (1996) and Shaw, (1988)). Another example is the simple pendulum, the equation of motion of which is $\ddot{\theta} + \omega_0^2 \sin \theta = 0$; the nonlinear term $\omega_0^2 \sin \theta$ represents geometric nonlinearity, since it models large angular motions (Amabili *et.al.* (2003) and Nayfeh *et.al.* (2004)).

3. Damping is a nonlinear phenomenon and linear viscous damping in structures is an idealization. Some examples of nonlinear damping are hysteretic damping, Coulomb friction and aerodynamic drag. Caughey *et.al.* (1970), Tomlinson *et. al.* (1979), Sherif *et.al.* (2004) and Al-Bender *et. al.* (2004).

4. In boundary conditions nonlinearities can also be found. For example, free surfaces in fluid, vibro-impacts due to loose joints or contacts with rigid constraints. Also, in the situation when a pinned-free rod is attached to a nonlinear torsional spring at the pinned end and that resulting from clearance in bearings.

5. Material or Physical nonlinearity. This is when the constitutive law relating the stresses and strains is nonlinear. In other words nonlinear stress-strain relationship gives rise to this type of nonlinearity. Nonlinear beam problems with material nonlinearity have been studied by Papirno, (1982), Ditcher *et.al.* (1982) and Bert (1982). Examples are rubber Isolators, Richard *et.al.* (2001) and for metals, the nonlinear Ramberg-Osgood material model is used at elevated temperatures. Here Papirno (1982) conducted an experimental investigation to check the validity of the Ramberg-Osgood type nonlinear stress-strain relationship to various materials. Another example is the case in foams, White *et. al.* (2000), Schultze *et.al.* (2001) and Singh *et.al.* (2003).

6. Structural systems could also be affected physically by nonlinearities that stem from trigonometric functions of fixed angular co-ordinates. Examples can be found in flexible rotor systems, Adiletta *et.al.* (1997a, b). Tondl (1965) first applied nonlinear vibration theory to the rotor-bearing problem in 1965. Rotor systems with nonlinearities show interesting behaviours such as jump phenomena, subharmonic phenomena and bifurcation phenomena. Ishida, (1994)

and Yamamoto *et.al.* (2001) have investigated the effects of these nonlinearities on the dynamic characteristics of the vibrations of the rotor system.

2.3.2 Nonlinearities of Beams/ Shafts

Basic beam theories developed decades ago by Bernoulli, Coulomb, Euler, Kirchhoff, Rayleigh and Timoshenko and many others are still in use today. When dealing with small deformations linear beam theory would have been enough, but with moderately large deformations and accurate modelling several nonlinearities need to be included. Most of the nonlinear theories of transverse beam vibrations deal with the effect of midplane stretching for the case of a simply supported uniform beam with an infinite axial restraint. Burgreen in 1951 looked at free oscillations of a beam having hinged ends at a fixed distance apart. He also studied, both experimentally and theoretically, the effects of a compressive load. He derived the equation of motion containing a nonlinear term due to midplane stretching which results in nonlinear strain-displacement relations. He gave the solution in terms of elliptic functions and also found that the frequency of vibration varies with the amplitude. In agreement with the above theories Ray *et.al.* (1969), through experiment analyzed the effect of midplane stretching on the vibrations of a uniform beam with immovable ends for simply supported, clamped, and simply supported-clamped cases.

Nonlinear vibrations of a hinged beam with one end free to move in the axial direction were studied by Atluri (1973). Including rotatory inertia and nonlinearities due to inertia and geometry and ignoring the effects of midplane stretching and transverse shear deformation he found out that the effective nonlinearity depends on the contributions of the geometric and inertia nonlinearity terms and that the inertia nonlinearity is of the softening type.

Moyer Jr. *et.al.* (1984) considered the transient response of nonlinear beam vibration problems subjected to pulse loading using a numerical approach and Liebowitz (1983) also investigated vibrational response of geometrically nonlinear beams subjected to impulse and impact loading. Nonlinear vibrations of rotating shafts have been reported by Yamamoto *et.al.* (1981) and Vassilopoulos *et.al.* (1983). Pai *et.al.* (1990b) and Anderson *et.al.* (1996b) using equations derived by Crespo da Silva *et.al.* (1978a, b) who investigated the

nonlinear motions of cantilever beams and observed that, for the first mode, the geometric nonlinearity, which is of the hardening type, is dominant; whereas for the second and higher modes, the inertia nonlinearity, which is of the softening type, becomes dominant.

Hodges *et.al.* (1974) developed nonlinear equations of motion with quadratic nonlinearities to describe the dynamics of slender, rotating, extensional helicopter rotor blades undergoing moderately large deformations and Rosen *et.al.* (1979) derived a more accurate set of equations than those of Hodges *et.al.* (1974) by including some nonlinear terms of order three in which their numerical results are in agreement with the experimental data obtained by Dowell *et.al.* (1977). Retaining cubic nonlinearities effects in derived nonlinear differential equations of motion, Crespo da Silva *et.al.* (1986a, b) investigated their influence on the motion of a helicopter rotor blade. They concluded that the most significant cubic nonlinear terms are those associated with the structural geometric nonlinearity in the equation. Pai and Nayfeh (1990a) developed nonlinear equations containing structural coupling terms, quadratic and cubic nonlinearities due to curvature and inertia for vibration of slewing or rotating metallic beams.

2.3.3 Nonlinearities in Bearings

In rotor-bearing systems there are many sources of nonlinearities, such as play in bearings and fluid dynamics in journal bearings. The dynamic stiffness of the bearing which supports the rotating shaft has a significant effect on the vibration. In particular it affects the machine critical speeds and the vibration in between critical speeds and Yamamoto *et.al.* (1976) suggested that rolling bearings, which are frequently used in industry, sometimes have nonlinear spring characteristics due to coulomb friction and the angular clearance between roller and ring. Yamamoto *et.al.* (1981) and Ishida *et.al.* (1990) revealed that in practice all components of nonlinear forces appear markedly up to the third power of deflections in single-row deep groove ball bearings, and to the fourth power in double-row angular contact ball bearings.

Studies carried out by Gonsalves *et.al.* (1995), Nelson *et.al.* (1988), Kim *et.al.* (1990), Goldman *et.al.* (1994a,1994b and 1995) on nonlinear rotor systems

with bearing clearance subjected to out-of-balance phenomena showed that the presence of clearances invariably causes severe nonlinearities in the system, primarily in the form of discontinuous stiffness effects which can lead to very complex responses. Investigations carried out by Lee *et.al.* (1993) on rotor systems concluded that various spring constants of bearings giving rise to the jump phenomenon, and causing the frequency response curves to bend at various inclinations are due to nonlinearities in bearings. It has been shown by Azeez *et. al.* (1999) that very small free-plays in the bearings of a rotordynamic system lead to strong and potentially catastrophic nonlinear instabilities, evidenced by large-amplitude chaotic motions with frequencies close to linearised critical speeds. In the nonlinear analysis of a dynamic system, Zheng *et.al.* (2000), showed that a quasi-periodic bifurcation was found for a group of bearing parameters and after the bifurcation point a jump phenomenon was detected and in the system appeared a large number of closed branches of subharmonic motions occurring in very tiny frequency (rotating speed) intervals. As the rotating speed increases, the system undergoes bifurcation, and finally goes to chaos.

Shabaneh *et.al.* (2003) showed in their analysis of a rotor shaft with viscoelastically supported bearings that the primary resonance peak shifts to higher frequencies when the bearing elastic characteristic is increased. The nonlinearity occurs at the boundaries due to nonlinear characteristics of the bearings.

In a rotor-bearing system, the hydrodynamic pressure in journal bearings is generated entirely by the motion of the journal and depends on the viscosity of the lubricating fluid. However, the hydrodynamic pressure around the bearing is nonlinear and hence the fluid film rotor-bearing system has a strong nonlinearity which can cause substantial vibrations of the rotor and its bearings, Chang-Jian *et.al.* (2007). In 1978, Holmes *et.al.* (1978) published a paper dealing with aperiodic behaviour in journal bearings. In their work, the symmetrical, steady-state motion of a rigid shaft supported by two short journal bearings was studied. The behaviour of this test rig was found to be of two distinct types. For small eccentricity, the motion was asymptotically periodic and consisted of a small number of components, principally at synchronous and half-synchronous

frequencies. For high eccentricity, the motion observed was complex and did not settle to a limit cycle, remaining in a state of aperiodic motion.

In 1994, Brown *et.al.*(1994), developed a simple model of a rigid, hydrodynamically supported journal bearing using short bearing theory. It was shown that the journal behaved chaotically when the rotating unbalance force exceeded the gravitational load. High speed journal bearings lubricated with unconventional lubricants of low viscosity give rise to large Reynolds numbers, and therefore the flow of the bearing becomes turbulent. In 2000, Lahmar *et.al.*(2000), proved that the turbulent effects on the dynamic behaviour of rotor-bearing systems become more significant as the journal rotational speed increases.

2.4 Nonlinear Control

Interesting cases of nonlinear dynamics under principal parametric resonance have been investigated for some years now. While the disturbing force is a time-dependent excitation that is orthogonal to the coordinate of the structure and its frequency is close to twice that of one of the natural frequencies of the structure, the principal parametric resonance may occur and high-amplitude oscillation will take place in the structure. Nayfeh and Mook (1979) have studied this phenomenon and revealed that the high-amplitude vibration occurs because the system undergoes nonlinear vibrations such as bifurcations or limit cycles. Parametric resonance differs from the commonly encountered external resonances, i.e., when the frequency of the disturbing force is near to one of the natural frequencies of the structure. For parametric resonances, the excitation parameters such as frequency and amplitude are represented by time-dependent coefficients within the governing partial-differential equations of motion. In terms of their behaviour, parametrically excited systems may exhibit large responses even when the excitation is small and not close to the system's natural frequencies.

In recent years, chaos control has been a hot topic in scientific research in many important applications in physics, mechanics and engineering. The general principle of active nonlinear control is to introduce an action which affects a

change in behaviour of a dynamical system in a desirable manner. Several control methods leading to suppression of chaos have been presented. Asfar *et.al.* (1994) conducted numerical studies of vibration suppression of a single-degree-of-freedom system subjected to a principal parametric resonance. Passive vibration control techniques like the Lanchester-type dampers were used in their studies in order to increase the structural damping. Chow *et.al.* (2001) on vibrational control of a nonlinear elastic panel used a high frequency parametric vibration and amplitude modulation of the forcing function. The high frequency parametric vibration used introduced a change in some system parameter causing static stability, whilst the modulation of the forcing amplitude stabilizes unstable periodic motions.

Yabuno (1997) proposed a combined linear-plus-nonlinear displacement feedback and linear-velocity feedback control for a parametrically excited Duffing system. His numerical simulation shows that linear-velocity feedback stabilizes the trivial solution in the quasi-stationary frequency-response, while linear-plus-nonlinear displacement feedback reduces the quasi-stationary frequency-response. It has been shown by Queini *et.al.* (1999) that vibration amplitudes resulting from nonlinear resonance that cannot be fully controlled by conventional techniques such as the addition of linear damping or by the implementation of conventional mass absorber can be suppressed by cubic-velocity feedback. For their active control technique they used piezoelectric actuators to suppress the nonlinear vibrations of a cantilever steel beam.

Based on the work of Queini *et.al.* (1999), Chen *et.al.* (2003) proposed an alternative control method that combines linear and nonlinear velocity (cubic-velocity) feedback control to suppress the principal parametric resonance in a flexible cantilever beam structure. They further noted that combined bifurcation control and nonlinear feedback control can avoid actuator saturation and performs better than either linear feedback or nonlinear feedback control. The proposed nonlinear response modification in the context of this thesis is largely relevant to flexible rotor systems subjected to parametric excitations.

2.5 Perturbation Methods

Perturbation methods date back to the 18th Century, when Pierre Simon Laplace [1749-1827] a French astronomer, mathematician and physicist was the first to use perturbation methods to solve a problem of equilibrium of a large weightless drop on a plane. The perturbation methods, which have many similar qualities to asymptotic methods, are a collection of techniques that may be used to simplify, and to solve, a wide variety of mathematical problems involving small or large parameters. The solutions may often be constructed in explicit analytical form or, when it is impossible, the original equation may be reduced to a more simple one that is much easier to solve numerically (Lim (2003)).

The first comprehensive book on perturbation methods was written by Van Dyke (1964), with a focus on fluid mechanical applications. Cole (1968) introduced a text from the point of view of applied mathematics. Aziz (1984) gave a review of the various applications of perturbation methods in heat transfer area. Comprehensive material on perturbation methods can be found in the latest books by Nayfeh (1973), Bender and Orszag (1978), Lin and Segel (1988), and Hinch (1991).

In Nonlinear oscillations, Nayfeh and Mook (1979) provided examples of parametrically excited systems, and presented some analytical techniques for studying parametrically excited systems. They introduced perturbation techniques into the analysis of nonlinear and/or parametric vibrations. Some of the perturbation methods used in the resolution of nonlinear problems include Incremental Harmonic Balance (I-H-B), Averaging, Krylov-Bogolioubov (K-B), Krylov-Bogolioubov-Mitropolski (K-B-M), Lindstedt-Poincaré (L-P) and the Method of Multiple Scales (MMS). In the Incremental Harmonic Balance (I-H-B) and Lindstedt-Poincaré (L-P) methods one seeks directly a periodic steady state solution, which is assumed a priori to occur, whilst the Averaging, Krylov-Bogolioubov (K-B), Krylov-Bogolioubov-Mitropolski (K-B-M) and the Method of Multiple Scales (MMS) methods yield a set of first order differential equations which describe the slow time evolution of the amplitude and phase of the response.

Using computer analysis, Lau *et.al.* (1982) presented an incremental harmonic balance method (I-H-B) for determining the parametric instability of a nonlinear vibrating beam system with viscous damping. Pierre *et.al.* (1985) extended the I-H-B method to investigate the dynamic instability of viscous damped plates. Investigating the dynamic stability problems of a sandwich beam with a constrained layer and an electrorheological fluid core subjected to an axial dynamic force Yeh *et.al.* (2004) used the Harmonic Balance Method to calculate the instability regions of the sandwich band. Further to this Yeh *et.al.* (2005) used the I-H-B method to study the regions of dynamic instability of Magnetorheological material-based adaptive beams. These investigations demonstrated that the I-H-B method has been successfully applied to determine the dynamic instability of structural systems with viscous damping.

Averaging methods have been in use since the time of Lagrange and Laplace. Examples of applications of the method of averaging are provided by Mitropolsky (1967) and Nayfeh (1973). Sethna (1965) and Haxton *et.al.* (1972) used the method of averaging to analyze primary resonances of systems governed by equations with quadratic nonlinearities when one natural frequency is twice another. Palacios *et.al.* (2002) employed the Bogoliubov averaging method in their study of the vibrations of an elastic foundation consisting of a portal frame with quadratic nonlinearities, forced by a non-ideal energy source. Krylov-Bogoliubov-Mitropolsky (K-B-M) asymptotic method was used by Wickert (1992) to study the nonlinear vibrations and bifurcations of moving beams. Mockensturm *et.al.* (1996) applied the perturbation method of K-B-M to examine the stability and limit cycles of parametrically excited and axially moving strings in the presence of tension fluctuations.

2.6 Method of Multiple Scales (MMS)

The perturbation method of multiple scales has been associated primarily with the names of Sturrock (1957, 1963), Frieman (1963), Cole and Kevorkian (1963), Nayfeh (1965a, 1965b, 1968, 1973), and Sandri (1965, 1967) and applied by Kevorkian (1966a) and Cole (1968) to several examples. According to Nayfeh, ‘the method of multiple scales is so popular that it is being rediscovered just about every 6 months’. The underlying idea of the method of multiple scales is

to consider the expansion representing the response to be a function of multiple independent variables, or scales, instead of a single variable. This method has advantages over the Lindstedt-Poincaré method as it can treat damped systems conveniently and that it yields transient solutions as well as steady state solutions in contrast to some other techniques which yield only the steady state solution (Cartmell, 1984). The MMS is one of several tools used to study the nonlinear equations of motion; it appears particularly suitable for solving stability problems. The method of multiple scales was used by Ji *et.al.* (1998) for the analysis of a simple rotor with a disk located on the middle of the shaft.

Lee *et.al.* (1999) investigated a weakly nonlinear, harmonically excited, spring pendulum in which analysis was carried out using a second order multiple scales expansion, neglecting the zeroth order term. This led to the identification of stable and unstable regions, as well as routes to chaos. Poincaré maps for bifurcation analysis and Lyapunov exponent were generated, with differences showing quantitatively and qualitatively for the first order and second order approximations, with the suggestion that the second order approximation agrees better with the original system.

However, when employing higher order expansions, slightly different versions of the method are used in literature. The oldest version, called reconstitution method (called MMS version I), is due to Nayfeh (1981, 1985). In version I, for primary resonances, the damping and forcing terms are re-ordered such that they balance the effect of nonlinearities. The nearness of the external excitation frequency to one of the natural frequencies is represented by using only one correction term. The time derivatives for each time scale do not vanish separately, but their sum vanishes for finding the steady state solutions. In contrast, Rahman and Burton (1989) proposed a newer version of MMS (called MMS version II). They showed that the version I cannot capture well the steady-state solutions and that it yields extra solutions which are not physical for the case of a simple Duffing oscillator for example.

The version II method can be used to determine the periodic, steady-state, primary response of a single degree of freedom, lightly damped, and weakly nonlinear, forced oscillator. Rahman and Burton then suggested that the excitation and the damping should be expanded in a series and require that each

time-scale derivative vanish independently. However, unsteady-state solutions cannot be retrieved using the version II method. This led to Lee and Lee's (1997) modification of MMS version II by showing how to calculate the unsteady and steady state solutions. The details of the extended method were illustrated using a Duffing-type equation of the form

$$\ddot{u} + \hat{\delta}\dot{u} + u + \beta u^3 = \hat{p} \cos \Omega t, \quad (2.7-1)$$

Where, $\hat{\delta}$, β and \hat{p} are of the order ε which is a small parameter.

The above equation is similar to the example presented by Rahman and Burton (1989). Similar to version I, modified version II makes series expansions unnecessary for the frequency, damping and excitation amplitude. The damping and excitation are scaled to appear in the first nonlinear order. Transient solutions can also be obtained. In establishing this, time derivatives are taken to be non-zero only on their corresponding level of approximation, i.e., D_1 terms are non-zero on the first level of approximation but vanish on the second level of approximation. Where D_1 is an operator notation for the partial derivative with respect to a multiple scales slow time T_1

El-Bassiouny *et.al.* (2001) used the method of multiple scales to investigate a second-order approximate analytic solution. They determined the instability regions of the response of the considered oscillator via an algorithm that used Floquet theory to evaluate the stability of the investigated second-order approximate analytic solutions in the neighbourhood of the nonlinear resonance of the system. They constructed Bifurcation diagrams showing the locus of instabilities of periodic solutions, thereby predicting the qualitative changes that can be observed when either the frequency or the amplitude of excitation is varied across a bifurcation curve. By constructing the bifurcation diagram they investigated the solutions lose stability through three types of bifurcations; saddle-node, period-doubling, to other attractors (sequence of period-doubling to chaos).

A detailed review of the method of multiple scales has been done by Cartmell *et.al.* (2003). They studied the role of term ordering, the integration of the so-called small (perturbation) parameter within systems constant, nondimensionalisation and time scaling, series truncation, inclusion and exclusion of higher order nonlinearities and typical problems in the handling of secular terms. In the paper Cartmell *et.al.* (2003) showed that a consistent feature of all multiple scale analysis is the choice of the ordering scheme and the form of the power series expansion and that it is possible to obtain the same results for different structural combinations of each. According to the paper, the continual emergence of new and ingenious variations of the basic method as well as continual new problem applications makes it abundantly clear that multiple scales is set to continue as a cornerstone of analysis in nonlinear engineering dynamics.

Investigating the principal parametric resonance of a single-degree-of-freedom system with nonlinear two-frequency parametric and self-excitations, El-Bassiouny (2005) used the method of multiple scales to determine the equations that describe to first-order the modulation of the amplitude and phase and predicted the existence of the steady state responses and stabilities. Duchemin *et.al.*(2006) applied the method of multiple scales to study the dynamic behaviour and stability of a rotor under base excitation, when the system mounting is subjected to a sinusoidal rotation. They applied the method of multiple scales to identify the instability zone which are then obtained numerically using a step-by-step computation.

2.7 Smart Materials

Generally speaking the term “smart” or “intelligent” material systems refers to man-made structural systems inspired by natural models. Natural systems display numerous admirable qualities smart material systems emulate: precision, efficacy, functionality, durability and adaptability (adaptive materials and structures). To achieve these standards, smart material systems employ three basic tools. Sensors, analogous to the human nervous system, register important internal and external information. Actuators (motors) perform work like muscles. Finally, computerized control centres acts as the brains of a system,

making decisions and issuing orders. These materials exhibit non-negligible deformation or material property change with the application of thermal fields, electrical fields, or magnetic fields. These materials include Electrorheological (ER) fluids, Magnetorheological (MR) fluids, Electrostrictive materials, Shape Memory Alloys (SMA), Magnetic Shape Memory Alloys (MSMA), Magnetostrictive materials, and Piezoelectric materials.

Smart fluid is defined as fluid in which the flow can be controlled through the application of an electric or magnetic field. Electrorheological (ER) and Magnetorheological (MR) materials belong to the family of controllable fluids. The ER effect was first discovered by Winslow and the MR effect was discovered by Rabinow in the late 1940s. However, more active research studies on the ER and MR fluids and their applications began in the mid-1980s (Yalcintas and Dai 1999). Their rheological properties, such as viscosity, elasticity and plasticity, change in the order of milliseconds in response to applied electric and magnetic field levels. (Yalcintas and Dai 1999). The ability of controllable fluids to be directly used as fast-acting, fluid valves with no moving parts in semi-active vibration control has been one of the principle motivating factors for the development of such fluids (Carlson *et.al.* 1995, Carlson and Sproston, 2000 and Hietanen, 2002)

Magnetic shape memory alloy (MSMA) effect is a new invention in the actuator materials field, allowing 50 times greater strains than in Magnetostrictive materials. In MSMA materials the magnetic field moves the twins formed in the structure creating a net shape change in the material. The mechanism also enables more complicated shape changes than conventional linear strain, such as bending and shear. Typically, present MSMA's, such as Ni₂MnGa produce 2% strain at 0 to 2 MPa stress in actuator use. Other potential MSMA materials are Fe-Pd and Fe-Ni-Co-Ti alloys (AdaptaMat, Finland MSM actuators). The maximum strain of MSM material is about 5% and the application temperature range is from -130 °C to 70°C (Marke *et.al.* 2002).

Magnetostriction is observed in a substance when it strains upon application of a magnetic field. Conversely, a field is generated when the material is stressed; this is, however, proportional to the material's rate of strain. James Joule discovered the magnetostrictive effect first in nickel in 1840, however, the

modern era of Magnetostriction began in 1963 when strains approaching 1% were discovered in the rare earth materials of terbium and dysprosium at cryogenic temperatures. The most frequently used material is giant magnetostrictive Fe-Tb-Dy-alloy called Terfenol-D (Active Materials Laboratory, MIT, USA). Magnetostrictive material is usually sold as a complete actuator system because the Magnetostriction is optimised when the material is both mechanically and magnetically biased. The commercially-available actuators have total displacement capabilities of 0.2%, are capable of producing output forces of 1750N, and operate at frequencies up to 60 kHz. Terfenol-D transducers are used as positioners, sonar projectors, isolators, shock absorbing mounts, linear stepper motors, and to mimic the vibrations of an artificial heart (Shakeri *et.al.*(2002) and Marke *et.al.*2002).

Electrostrictive materials are similar to Piezoelectric materials, with about the same strain capabilities. However, they are very sensitive to temperature, have a monopolar, nonlinear relation between the applied field and induced strain, and exhibit negligible hysteresis. In the Electrostrictive material there is an interaction between the electric field and electric dipoles that is inherently nonlinear. Materials such as relaxor ferroelectrics undergo strain when an electric field is applied. Under this category of materials, lead magnesium niobate (PMN) alloys have sufficiently large dielectric permittivity that helps to generate significant polarization and hence strains. Electrostrictives are used as actuators in a wide range of applications. The maximum strain is of order 0.1% (Uchino1986, Blackwood *et.al.* 1993 and Chopra 2002).

2.8 Shape Memory Alloy (SMA)

Shape Memory Alloys (SMA) refers to a group of materials that have the ability to return to a predetermined shape when heated. This property is utilised in an SMA actuator, which, in its simplest form comprises an arrangement of SMA wires or strips. A shape memory alloy, when deformed (in the martensitic phase) with the external stresses removed and heated above its characteristic transition temperatures, will regain its original “memory” shape (in the austenitic phase). This unique effect of retuning to its original geometry after inelastic deformation (more than 1%) is known as the shape memory effect (SME). The

first observation of the shape memory effect (SME) was made in 1932 with gold-cadmium. The phase transformation associated with the shape memory effect was later discovered in 1938 with brass (Perkins *et.al.*, 1975). Several years after in 1962 Buehler and Wiley (1965) at the Naval Ordnance Laboratory (NOL) discovered a series of nickel-titanium alloys that demonstrated this shape memory effect. This SMA discovered by Buehler *et al.* was later named NiTiInol, and has been made commercially available ever since.

SMA's can thus transform thermal energy directly to mechanical work (Liang *et.al.* 1993). The characteristic transformation temperatures are defined as follows (Ju *et.al.* 1999, Otsuka *et.al.* 1999).

M_s : martensite start temperature upon cooling

M_f : martensite finish temperature upon cooling

A_s : reverse transformation start temperature upon heating

A_f : reverse transformation finish temperature upon heating

The thermoelastic martensite transformations are characterised by a small hysteresis between the starting temperature transformation (M_s) and its reverse (A_s), and the continuous growth of the martensite, and this is shown graphically in the Figure 2-1 below. The transformation also exhibits hysteresis, and it varies with the alloy system (Otsuka *et.al.* 1999, Zhao 2001, Marke *et.al.*2002).

The superelasticity (SE) effect is common for SMA intermetallics. SE, which is pseudoelasticity occurring at a temperature above A_f (slightly above their transformation temperatures). This provides a very springy, "rubberlike" elasticity in these alloys. Apart from NiTiInol (nickel-titanium alloys), there are other metallic materials that are known to exhibit shape memory effect. These include the copper alloy systems Cu-Zn, Cu-Zn-Al, Cu-Zn-Ga, Cu-Zn-Sn, Cu-Zn-Si, Cu-Al-Ni, Cu-Au-Zn, and the alloys of Au-Cd, Ni-Al, etc.

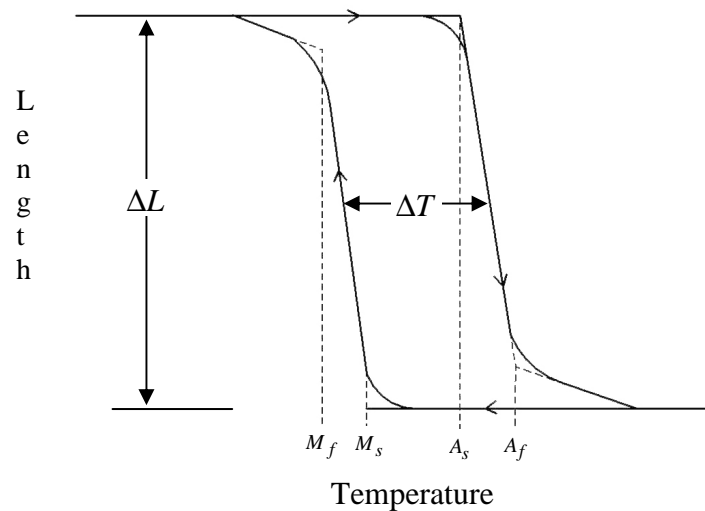


Figure 2-1: Typical temperature-transformation curves of a NiTi alloy (Marc van der Wijst 1998).

SMA are highly adaptive, compact, and lightweight and have a high force-to-weight ratio. They are the only materials that can impart both large strains and large forces but their poor energy conversion remains a problem (Barsoum, 1997). In dynamic applications, as in the case of this research, which require heating and cooling of the strips to start and stop, the recovery process, the heating and cooling rates become a limiting factor. Electric heating can drive the transformation; while cooling depends on heat conduction, which is a slower process for many applications.

Investigations on using SMA to damping vibrations have been carried out by many research groups. Rogers (1988) suggested that SMA fibres could be embedded into conventional composites such as graphite/epoxy to control the structural response including static deformation, vibration, buckling, and structural acoustic radiation/transmission. Nagaya *et.al.*(1987) suggested that shape memory alloys could be used to control the critical speed of rotating shafts. SMA wires and tendons have been applied for active damping of flexural vibrations of cantilever beams by Baz *et.al.* (1990), Ikegami *et.al.* (1990), Rhee (1992), Choi and Cheong (1996) and Shahin (1997), and the results indicate that active vibration control is possible using SMA wires and tendons. It has also been shown by Rogers *et.al.* 1990, 1991, Baz *et.al.* (1994, 1995) and Bideaux *et.al.* (1995) that vibration of structures can be reduced by shifting the resonance frequencies away from the disturbing frequencies by heating SMA wires

embedded in a cantilever beam or plate. In this thesis SMA (in the form of strips) applications to rotordynamics are introduced, specifically the use of single-ended and antagonistic active bearing housings, and some prototypical experiments have given encouraging results for the reduction in the resonant amplitude for forward whirl in a flexible rotor.

2.9 Piezoelectric Materials

Piezoelectric materials produce electric charge (voltage) if their crystalline structure is deformed by an external force. This effect is called the *direct effect* of piezoelectricity. On the other hand, piezoelectric materials change their crystalline structure with the application of an external electric field. This phenomenon is known as the *converse effect* of piezoelectricity. Pierre and Jacques Curie discovered the direct effect of piezoelectricity in 1880. The converse piezoelectric effect was first predicted by Lippmann via methods of analytical thermodynamics in 1881 which was confirmed by the Curies in 1881. Thus they can be used both as actuators and sensors (Chopra 2002). Over time the use of the converse effect of piezoelectricity has become critical in applications that require oscillators with relatively large amplitude and very slow rate of decay.

The most commonly used piezoelectric ceramics are barium titanate (BaTiO_3), lead lanthanum zirconate (PLZT), lead magnesium niobate (PMN) and lead zirconate titanate PZT (PbZrTiO_3). These materials exhibit nonlinear coupling between a mechanical and an electric response. Piezoelectric ceramics can either be monolithic or made of thin, stacked ceramic layers. They are high-force, but low stroke devices, have a very broad operating frequency bandwidth, and exhibit precise positioning response and repeatability. They can achieve precision that is measured in nanometres (Piezoelectric ceramics- Noliac A/S, Denmark). One common actuator design, that addresses the limitation in achievable stroke, is the stack actuator depicted schematically in Figure 2-2. The stack is created by bonding thin layers of piezoelectric together such that their polarization directions alternate along the major axis. Electrodes separate the layers nearly entirely. When a voltage difference is applied across the

electrodes, a complicated electric field and mechanical response result if one considers the fine scales of the devices.

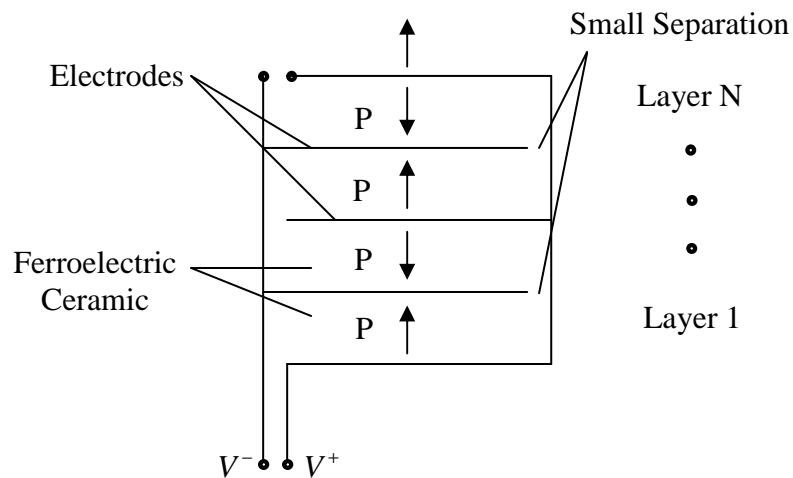


Figure 2-2: Schematic cross-section of piezoelectric stack actuator

Piezoelectric stack actuators are often used in motion control applications where precise positioning and fast response are critical. They are typically available with displacements ranges of up to $200\ \mu\text{m}$, with force capacities of up to 10,000 N, and maximum voltage ratings from 150 V to 1000V. Electrically, the piezoelectric actuators behave as a nonlinear capacitive load. The actuator can be expanded or contracted by applying a positive or negative voltage. The elongation or contraction of the piezoelectric material is the result of the in-place realignment of electrical dipoles in the crystalline domains (Yi *et.al.* 2005).

Piezoelectric materials are currently being considered for a number of actuator applications including precision positioning, vibration suppression, noise control and inkjet printing. Piezoelectric actuators have been used for the active shape, vibration and acoustic control of structures. Their ability to be easily integrated into structures makes them very attractive in structural control. Multilayer actuators have advantages such as fast switching time, high block force and low driving voltage (Steinkopff *et.al.* 2000).

Bailey and Hubbard (1985) introduced piezoelectric actuators to active vibration control. They used the actuators bonded to the surface of a cantilever beam in their feedback vibration damping design. Crawley and de Luis (1987) presented an analytical and experimental development of piezoelectric actuators as vibration exciters. Using the models they developed from the stress/strain relationships, they were able to predict the displacement of three real cantilevered beam and piezoelectric actuator arrangements under steady-state resonance vibration conditions. Dimitriadis *et.al.* (1991) had performed a two dimensional extension of Crawley and de Luis's work, applying pairs of laminated piezoelectric actuators to a plate. They demonstrated that the location and shape of the actuator dramatically affected the vibration response of the plate.

Other researchers such as Fansen and Chen (1986) and Baz and Poh (1988, 1990) have used piezoelectric actuators in active vibration control experiments, showing again the potential of piezoelectric actuators as control actuators in vibration control. The application of piezoelectric stack actuators to control of vibrations in rotating machinery was considered by Palazzolo *et.al.* (1989). The authors showed that significant reductions in the vibration of rotating machinery could be achieved using two of these actuators in the support structure of the rotating shaft. In this thesis the author is deliberately introducing parametric excitations into a flexible rotor by means of a piezoelectric exciter and with the intention of using this to moderate the responses of the pre-existing mass-unbalance vibration inherent to the rotor.

CHAPTER 3

ANALYTICAL MODELLING OF FLEXIBLE ROTOR SYSTEMS

3.1 Introduction

For several years, a wide variety of phenomena concerning industrial rotor dynamic systems have been studied and much attention has been given to one of them, namely the behaviour of rotors under mass unbalance excitation. One important phenomenon is the self-excited oscillation which has been shown to be stemming from deviations from assumptions employed such as linearity. Resonances induced without periodic excitations are called self-excited oscillations. In the system having a single degree of freedom, the self-excited oscillation occurs due to the effect of negative damping and the amplitude grows with time (Kunitoh *et.al.*, (2004)). The dynamic behaviour of rotors has been extensively studied by Lalanne and Ferraris (1990), Rao (1991), Ehrich (1992), and Childs (1992). The books by Lalanne and Ferraris (1990) and Rao (1991) describe the discretisation of the system into components for the shaft, mass unbalance, bearings and disks. The mathematical model derived and used in this research is based on the work of Lalanne and Ferraris (1990). Two models for the equations of motion have been derived using Lagrangian dynamics and the Rayleigh-Ritz method, and are used to study some phenomena in rotor systems. The equations of motion include rotary inertia, gyroscopic coupling, axial load effects and the influence of nonlinear bearings. Nonlinearities in the system due to inertia and geometric properties are also considered in the modelling of the equations of motion. The equations are obtained in the following systematic way. First the expressions of the kinetic and strain energies of the rotor elements are constructed and the Rayleigh-Ritz method is applied for the simplification of the energy expressions. Then, the virtual work of external forces is modelled and finally Lagrange's equations are employed to derive the coupled equations.

3.2 Derivation of the Equations of Motion

In deriving the equations of motion, the scalar method of Lagrangian dynamics or the vectorial approach of Newtonian mechanics can both be applied to problems of this sort depending on preference. Lagrangian dynamics permits the derivation of the equation of motion from three scalar quantities; the kinetic energy, potential energy, and virtual work of the nonconservative forces.

The rotor equations are derived by means of the following steps:

Derivation of the kinetic energy of the disk, the shaft and the mass unbalance. Derivation of strain energy of the shaft. Use of Lagrange's equation of the form

$$\frac{d}{dt} \left(\frac{\partial T}{\partial \dot{q}_i} \right) - \frac{\partial T}{\partial q_i} + \frac{\partial U}{\partial q_i} = \frac{\partial W}{\partial q_i} = F_{q_i} \quad (3.2-1)$$

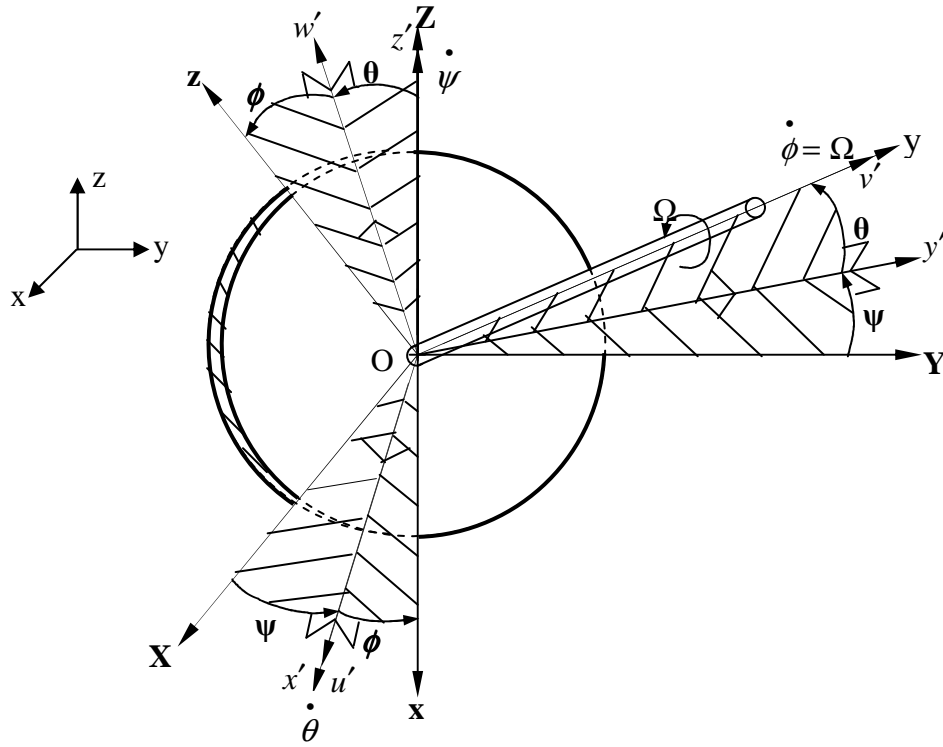
where, $i=1,2$, T represents the kinetic energy, U is the strain energy, q_i are generalised independent coordinates, and F_{q_i} are generalised forces. ∂W represents the virtual work of the nonconservative forces under a virtual displacement ∂q_i .

The Rayleigh-Ritz method has been used to obtain a simple model. It is a method in which a single function can be replaced by a series of shape functions multiplied by constant coefficients. It is used for finding the approximate real resonant frequencies and mode shapes of multi degree of freedom systems, such as spring mass systems or flywheels on a shaft. In this work it is used to obtain the displacement functions in terms of the generalised coordinates for the first mode shape of the shaft with a constant cross-section in bending that is simply supported at both ends.

3.2.1 Rotor Model

In many dynamical problems involving spinning bodies it is convenient to express the motion in terms of components along and about rotating frames of reference, which, by definition, are noninertial frames. In relating this motion to the inertial space authors such as Dimarogonas (1983), Meirovitch (1990), and Lalanne and Ferraris (1990) developed expressions relating the components of the rotating and the fixed systems of axes. In considering the movement of the rotor, two reference frames are used. $R_0(x, y, z)$ is an inertial frame, and $R(X, Y, Z)$ is a frame fixed to the disk (see Figure 3-1). The movement of the rotor is defined using six parameters (3 translational, 3 rotational). Therefore, the three coordinates of a point on the disk with respect to R_0 are expressed by X, Y, Z . Similarly, the three components of the angular velocity vector from R_0 to R expressed in frame R are ω_x , ω_y and ω_z . The movement of the frame R fixed to the disk with respect to R_0 is described by angles ψ , θ , and ϕ . To orientate the disk, a rotation into a vibration mode through angle ψ around the Z axis brings the triad into coincidence with axes x', y', z' . A further rotation of the axes x', y', z' through angle θ about axes x puts the disk into the orientation of u', v', w' where axis x is sometimes referred to as the nodal axis, and it remains in the horizontal plane at all times. Finally a rotation of axes u', v', w' through angle ϕ about v' makes the triad coincide with the body axes, x, y, z (see Figure 3-1). The instantaneous angular velocity vector of the xyz frame, as stated in Lalanne and Ferraris (1990) is

$$\omega_{R/R_0} = \dot{\psi}Z + \dot{\theta}x' + \dot{\phi}y \quad (3.2- 2)$$



(a) 3-D view of the rotor

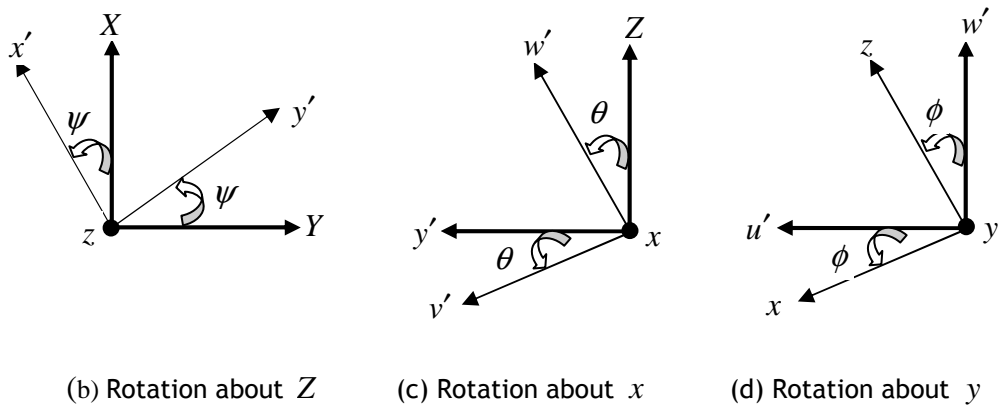


Figure 3-1: Reference frames for a disk on a rotating flexible shaft.

3.2.2 Kinetic Energy of the Rotating Disk

The disk is assumed to be rigid and is thus characterized solely by its kinetic energy. The kinetic energy of the disk about its centre of mass O is calculated within the frame R_0 . In this system the angular velocity vector becomes

$$\omega_{R/R_0}^R = \begin{bmatrix} \omega_x \\ \omega_y \\ \omega_z \end{bmatrix} = \begin{bmatrix} -\dot{\psi} \cos \theta \sin \phi + \dot{\theta} \cos \phi \\ \dot{\phi} + \dot{\psi} \sin \theta \\ \dot{\psi} \cos \theta \cos \phi + \dot{\theta} \sin \phi \end{bmatrix} \quad (3.2-3)$$

Let u and w designate the coordinates of O in R_0 , the coordinate along y being constant. In addition, the mass of the disk is M_d and its tensor of inertia in O is given by $I_{/O}$, where xyz are the principal axes of the inertia, as follows

$$I_{/O} = \begin{bmatrix} I_{dx} & 0 & 0 \\ 0 & I_{dy} & 0 \\ 0 & 0 & I_{dz} \end{bmatrix} \quad (3.2-4)$$

The angular velocity of the frame R with respect to frame R_0 is

$$\Omega_R^0 = \begin{bmatrix} \omega_x \\ \omega_y \\ \omega_z \end{bmatrix} \quad (3.2-5)$$

The kinetic energy due to the rotation of the disk is more difficult to calculate, therefore we assume that the disk is symmetric so that the inertia properties may be calculated using the polar moment of inertia I_{dy} , about the shaft, and the diametral moment of inertia, I_{dx} about any axis perpendicular to the shaft line. The kinetic energy due to the rotational motion of the disk is then,

$$T_d = \frac{1}{2} M_d (\dot{u}^2 + \dot{w}^2) + \frac{1}{2} (I_{dx} \omega_x^2 + I_{dy} \omega_y^2 + I_{dz} \omega_z^2) \quad (3.2-6)$$

For a symmetric disk $I_{dx} = I_{dz}$

Substituting the angular velocity vector, equation (3.2-3) into the kinetic energy of the disk equation (3.2-6) we have

$$T_d = \frac{1}{2}M_d(\dot{u}^2 + \dot{w}^2) + \frac{1}{2}I_{dx}(\dot{\theta}^2 + \dot{\psi}^2 \cos^2 \theta) + \frac{1}{2}I_{dy}(\dot{\phi}^2 + \dot{\psi}^2 \sin^2 \theta + 2\dot{\phi}\dot{\psi} \sin \theta) \quad (3.2-7)$$

which can be simplified here as the disk is symmetric ($I_{dx} = I_{dz}$), the angles ψ and θ are small angles, and the angular velocity of the rotor is constant; that is,

$$\phi = \Omega t \quad \text{and} \quad \dot{\phi} = \Omega \quad (3.2-8)$$

Therefore the kinetic energy of the disk becomes,

$$T_d = \frac{1}{2}M_d(\dot{u}^2 + \dot{w}^2) + \frac{1}{2}I_{dx}(\dot{\theta}^2 + \dot{\psi}^2 \cos^2 \theta) + \frac{1}{2}I_{dy}(\Omega^2 + \dot{\psi}^2 \sin^2 \theta + 2\Omega\dot{\psi} \sin \theta) \quad (3.2-9)$$

where, M_d is the mass of the disk and $I_{dy}\Omega\dot{\psi} \sin \theta$ represents the gyroscopic effect.

3.2.3 Kinetic Energy of the Shaft

The general formulation of the kinetic energy of the shaft is from an extension of the disk equation (3.2-9). For an element of length l , the expression for the kinetic energy is,

$$T_s = \frac{\rho S}{2} \int_0^l (\dot{u}^2 + \dot{w}^2) dy + \frac{\rho I}{2} \int_0^l (\dot{\theta}^2 + \dot{\psi}^2 \cos^2 \theta) dy + \rho I L \Omega^2 + \frac{\rho I}{2} \int_0^l (\dot{\psi}^2 \sin^2 \theta) dy + 2\rho I \Omega \int_0^l (\dot{\psi} \sin \theta) dy \quad (3.2-10)$$

where, ρ is mass per unit volume, S is the cross-sectional area of the shaft, I is area moment of Inertia of the shaft cross-section about the neutral axis,

dy is the thickness of the shaft, $\frac{\rho S}{2} \int_0^l (\dot{u} + \dot{w}) dy$ is the classical expression for

the kinetic energy of the shaft in bending, $\frac{\rho I}{2} \int_0^l (\dot{\theta}^2 + \dot{\psi}^2 \cos^2 \theta) dy$ is the

secondary effect of rotatory inertia, and $2\rho I\Omega\int_0^l(\dot{\psi}\sin\theta)dy$ represents the gyroscopic term.

3.2.4 Strain Energy of the Shaft

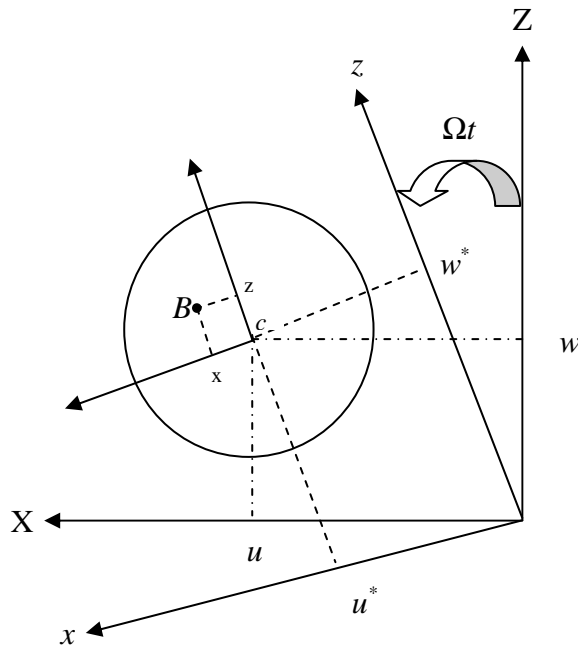


Figure 3-2: Coordinates of the geometric centre c and an arbitrary point B on the shaft (Lalanne & Ferraris, 1990)

Considering the cross-section of the shaft, where, c is the geometric centre of the shaft, $B(x, z)$ is a typical point on the cross-section, E is the Young's modulus of the material, ε is the longitudinal strain, σ is stress, u^* and w^* are displacements of the geometric centre with respect to the x and z axis and including second-order terms in the expression, the longitudinal strain of point B of the rotating shaft can be shown to be

$$\varepsilon = -x \frac{\partial^2 u^*}{\partial y^2} - z \frac{\partial^2 w^*}{\partial y^2} + \frac{1}{2} \left(\frac{\partial u^*}{\partial y} \right)^2 + \frac{1}{2} \left(\frac{\partial w^*}{\partial y} \right)^2 \quad (3.2- 11)$$

Let

$$\varepsilon_l = -x \frac{\partial^2 u^*}{\partial y^2} - z \frac{\partial^2 w^*}{\partial y^2} \quad (3.2- 12)$$

and

$$\varepsilon_{nl} = \frac{1}{2} \left(\frac{\partial u^*}{\partial y} \right)^2 + \frac{1}{2} \left(\frac{\partial w^*}{\partial y} \right)^2 \quad (3.2- 13)$$

where, ε_l contains the linear strain terms and ε_{nl} contains the nonlinear strain terms. Thus equation (3.2-11) can be written as

$$\varepsilon = \varepsilon_l + \varepsilon_{nl} \quad (3.2- 14)$$

The strain energy of the shaft is

$$U_1 = \frac{1}{2} \int_{\tau} \varepsilon \sigma d\tau \quad (3.2- 15)$$

where τ is the volume of the shaft and the relationship between stress and strain is

$$\sigma = E\varepsilon \quad (3.2- 16)$$

Substituting equations (3.2-14) and (3.2-16) into the strain energy equation (3.2-15) we get,

$$U_1 = \frac{E}{2} \int_{\tau} \left(\varepsilon_l^2 + 2\varepsilon_l \varepsilon_{nl} + \varepsilon_{nl}^2 \right) d\tau \quad (3.2- 17)$$

The second integral in equation (3.2-17) gives rise to a stiffness term, which couples the linear and nonlinear strains. It is assumed that the cross-section of the shaft is circular, and the arbitrary point B will be symmetrical about the axes x and z , thus making the shaft cross-section with respect to x and z symmetrical. The symmetry of the shaft cross-section with respect to x and z results in the second term being

$$\int_{\tau} \varepsilon_{nl} \varepsilon_l d\tau = 0 \quad (3.2- 18)$$

The strain energy therefore becomes,

$$U_1 = \frac{E}{2} \int_0^l \int_s \left\{ \left(-x \frac{\partial^2 u^*}{\partial y^2} - z \frac{\partial^2 w^*}{\partial y^2} \right)^2 + \left(\frac{1}{2} \left(\frac{\partial u^*}{\partial y} \right)^2 + \frac{1}{2} \left(\frac{\partial w^*}{\partial y} \right)^2 \right)^2 \right\} dS dy \quad (3.2-19)$$

Expanding equation (3.2-19) gives,

$$U_1 = \frac{E}{2} \int_0^l \int_s \left\{ x^2 \left(\frac{\partial^2 u^*}{\partial y^2} \right)^2 + z^2 \left(\frac{\partial^2 w^*}{\partial y^2} \right)^2 + \left(2xz \frac{\partial^2 u^*}{\partial y^2} \frac{\partial^2 w^*}{\partial y^2} \right) + \frac{1}{4} \left(\frac{\partial u^*}{\partial y} \right)^4 + \frac{1}{2} \left(\frac{\partial u^*}{\partial y} \right)^2 \left(\frac{\partial w^*}{\partial y} \right)^2 + \frac{1}{4} \left(\frac{\partial w^*}{\partial y} \right)^4 \right\} dS dy \quad (3.2-20)$$

Because of symmetry, the integral of the third term in equation (3.2-20) is equal to zero. Introducing area moments of Inertia with respect to x and z

$$I_x = \int_s z^2 ds \quad (3.2-21)$$

$$I_z = \int_s x^2 ds \quad (3.2-22)$$

where s is the cross-sectional area. The strain energy expression is thus

$$U_1 = \frac{E}{2} \int_0^l \left\{ I_z \left(\frac{\partial^2 u^*}{\partial y^2} \right)^2 + I_x \left(\frac{\partial^2 w^*}{\partial y^2} \right)^2 \right\} dy \quad (3.2-23)$$

If the shaft is subjected to a constant axial force F_0 there is a further contribution to the strain energy of the shaft given by

$$U_2 = \int_0^l \frac{F_0}{s} (\varepsilon_l + \varepsilon_{nl}) d\tau \quad (3.2-24)$$

Owing to symmetry, the first term under the integral will vanish over the cross-sectional area; substituting equations (3.2-12) and (3.2-13) into equation (3.2-24) gives

$$U_2 = \frac{F_0}{2} \int_0^l \left\{ \left(\frac{\partial u^*}{\partial y} \right)^2 + \left(\frac{\partial w^*}{\partial y} \right)^2 \right\} dy \quad (3.2-25)$$

The combined strain energy, $U_1 + U_2$ is then

$$U = \frac{E}{2} \int_0^l \left\{ I_z \left(\frac{\partial^2 u^*}{\partial y^2} \right)^2 + I_x \left(\frac{\partial^2 w^*}{\partial y^2} \right)^2 \right\} dy + \frac{F_0}{2} \int_0^l \left\{ \left(\frac{\partial u^*}{\partial y} \right)^2 + \left(\frac{\partial w^*}{\partial y} \right)^2 \right\} dy \quad (3.2-26)$$

To avoid periodic terms explicitly as a function of time, it is necessary, because of the bearing properties, to express the strain energy as a function of u and w , components of the displacement in R_0 using equations (3.2-27) and (3.2-28) deduced from Figure 3-2,

$$u^* = u \cos \Omega t - w \sin \Omega t \quad (3.2-27)$$

$$w^* = u \sin \Omega t + w \cos \Omega t \quad (3.2-28)$$

Therefore equation (3.2-26) can be written as

$$\begin{aligned} U &= \frac{E}{2} \int_0^l \left\{ I_z \left(\cos \Omega t \frac{\partial^2 u}{\partial y^2} - \sin \Omega t \frac{\partial^2 w}{\partial y^2} \right)^2 \right\} dy \\ &+ \frac{E}{2} \int_0^l \left\{ I_x \left(\sin \Omega t \frac{\partial^2 u}{\partial y^2} + \cos \Omega t \frac{\partial^2 w}{\partial y^2} \right)^2 \right\} dy \\ &+ \frac{F_0}{2} \int_0^l \left\{ \left(\frac{\partial u}{\partial y} \right)^2 + \left(\frac{\partial w}{\partial y} \right)^2 \right\} dy \end{aligned} \quad (3.2-29)$$

Finally, for the most common case of a symmetric shaft (i.e. $I_x = I_z = I$), the strain energy becomes

$$U = \frac{EI}{2} \int_0^l \left\{ \left(\frac{\partial^2 u}{\partial y^2} \right)^2 + \left(\frac{\partial^2 w}{\partial y^2} \right)^2 \right\} dy + \frac{F_0}{2} \int_0^l \left\{ \left(\frac{\partial u}{\partial y} \right)^2 + \left(\frac{\partial w}{\partial y} \right)^2 \right\} dy \quad (3.2-30)$$

3.2.5 Kinetic Energy of the Mass Unbalance

Unbalance is one load that is impossible to avoid and can be conveniently defined by a small mass m_u situated at a distance d from the geometric centre of the shaft, and so its kinetic energy T_u has to be calculated.

The mass remains in a plane perpendicular to the y axis and its coordinate along the y axis is a constant or zero depending on the origin of the reference frame (Lalanne and Ferraris, 1990).

Considering a positive (counter clockwise) rotation through the angle Ωt , or θ

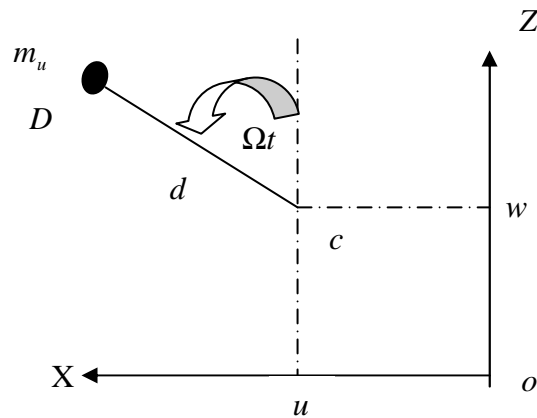


Figure 3- 3: Mass Unbalance

The displacement in the X direction is

$$OD_x = u + d \sin \Omega t \quad (3.2- 31)$$

The displacement in the Z direction is

$$OD_y = w + d \cos \Omega t \quad (3.2- 32)$$

and is a constant in the Y direction

Therefore the displacement of the mass in the X , Z and Y directions can be written as

$$OD = \begin{vmatrix} u + d \sin \Omega t \\ const \\ w + d \cos \Omega t \end{vmatrix} \quad (3.2- 33)$$

where const here represents the word constant.

Then velocity can be stated as

$$V = \frac{d(OD)}{dt} = \begin{vmatrix} \dot{u} + d\Omega \cos \Omega t \\ 0 \\ \dot{w} - d\Omega \sin \Omega t \end{vmatrix} \quad (3.2- 34)$$

and the kinetic energy of the mass unbalance is

$$T_u = \frac{m_u}{2} (\dot{u}^2 + \dot{w}^2 + \Omega^2 d^2 + 2\Omega d \dot{u} \cos \Omega t - 2\Omega d \dot{w} \sin \Omega t) \quad (3.2- 35)$$

The term $m_u \Omega^2 d^2 / 2$ is a constant in this context and has no subsequent influence on the equations. The mass unbalance m_u is smaller than the mass of the rotor, so the expression for the kinetic energy can be written as

$$T_u \cong m_u \Omega d (\dot{u} \cos \Omega t - \dot{w} \sin \Omega t) \quad (3.2- 36)$$

3.2.6 Simplified Model

The Rayleigh-Ritz method is used to study a model composed of a shaft of length l , supporting a disk located at l_1 along the shaft (see Figure 3-4). It is used to devise new expressions for the displacement in the x and z directions in terms of the generalised coordinates. The rotor is assumed to be simply supported at both ends and neglecting the argument t for simplicity, the expression for the displacement in the x and z directions are

$$u(y, t) = f(y)q_1(t) = f(y)q_1 \quad (3.2- 37)$$

$$w(y, t) = f(y)q_2(t) = f(y)q_2 \quad (3.2- 38)$$

where, q_1 and q_2 are generalised independent coordinates and $f(y)$ is the displacement function, and it is chosen as the normalised first mode shape of a beam with a constant cross section in bending and simply supported at both ends, and is given as

$$f(y) = \sin\left(\frac{\pi y}{l}\right) \quad (3.2-39)$$

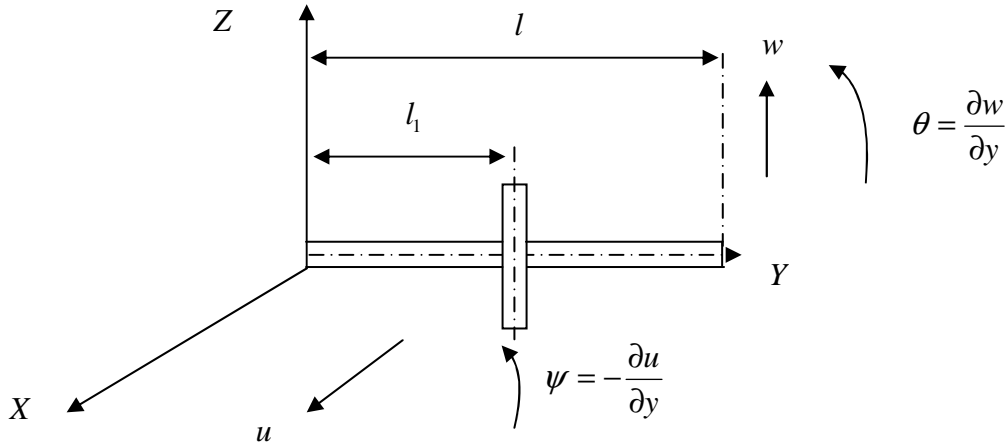


Figure 3-4: Coordinates

θ in Figure 3-4 is the angular displacement in the Z direction and ψ is the angular displacement in the X direction. As angular displacements θ and ψ are small, they are approximated by

$$\theta = \frac{\partial w}{\partial y} = \frac{df(y)}{dy} q_2 = g(y) q_2 \quad (3.2-40)$$

$$\psi = -\frac{\partial u}{\partial y} = -\frac{df(y)}{dy} q_1 = -g(y) q_1 \quad (3.2-41)$$

where, $g(y) = \frac{\pi}{l} \cos \frac{\pi y}{l}$ and it is coming from differentiating the displacement function. Introducing the displacement function (equation (3.2-39)) into the kinetic energy of the system, we have, for the disk,

$$T_d = \frac{1}{2} M_d f^2(l_1) (\dot{q}_1^2 + \dot{q}_2^2) + \frac{1}{2} I_{dx} g^2(l_1) \{ \dot{q}_2^2 + \dot{q}_1^2 \cos^2(g(l_1) q_2) \} \quad (3.2-42)$$

$$+ \frac{1}{2} I_{dy} \Omega^2 + \frac{1}{2} I_{dy} g^2(l_1) \dot{q}_1^2 \sin^2(g(l_1) q_2) - I_{dy} \Omega g(l_1) \dot{q}_1 \sin(g(l_1) q_2)$$

For the shaft

$$T_s = \frac{\rho s}{2} \int_0^l f^2(y) dy (\dot{q}_1^2 + \dot{q}_2^2) + \frac{\rho I}{2} \int_0^l g^2(y) dy \{ \dot{q}_2^2 + q_1^2 \cos^2(g(l_1)q_2) \} \quad (3.2-43)$$

$$+ \rho I L \Omega^2 + \frac{\rho I}{2} \int_0^l g^2(y) dy \{ \dot{q}_1^2 \sin^2(g(l_1)q_2) \} - 2\rho I \Omega \int_0^l g(y) dy \dot{q}_1 \sin(g(l_1)q_2)$$

For the disk and shaft combined

$$T = \frac{1}{2} \left[M_d f^2(l_1) + \rho s \int_0^l f^2(y) dy \right] (\dot{q}_1^2 + \dot{q}_2^2) \quad (3.2-44)$$

$$+ \frac{1}{2} \left[I_{dx} g^2(l_1) + \rho I \int_0^l g^2(y) dy \right] \{ \dot{q}_2^2 + \dot{q}_1^2 \cos^2(g(l_1)q_2) \}$$

$$+ \Omega^2 \left(\frac{1}{2} I_{dy} + \rho I L \right) + \frac{1}{2} \left[I_{dy} g^2(l_1) + \rho I \int_0^l g^2(y) dy \right] \{ \dot{q}_1^2 \sin^2(g(l_1)q_2) \}$$

$$- \Omega \left[I_{dy} g(l_1) + 2\rho I \int_0^l g(y) dy \right] \{ \dot{q}_1 \sin(g(l_1)q_2) \}$$

Simplifying equation (3.2-44) gives

$$T = \frac{1}{2} m (\dot{q}_1^2 + \dot{q}_2^2) + \Omega^2 \left(\frac{1}{2} I_{dy} + \rho I L \right) - \Omega a_2 (\dot{q}_1 \sin(\Upsilon q_2)) \quad (3.2-45)$$

where,

$$\Upsilon = g(l_1), m = m_1 + P, m_1 = M_d f^2(l_1) + \rho s \int_0^l f^2(y) dy, P = I_{dx} g^2(l_1) + \rho I \int_0^l g^2(y) dy,$$

$$I_{dx} \approx I_{dy}, a_2 = I_{dy} g(l_1) + 2\rho I \int_0^l g(y) dy, f(l_1) = \sin\left(\frac{\pi l_1}{l}\right), \text{ and } g(l_1) = \frac{\pi}{l} \cos\frac{\pi l_1}{l}. \quad l_1$$

and l values are obtained from the experimental rig.

Also introducing the displacement function (equation (3.2-39)) into the kinetic energy of the mass unbalance expression of equation (3.2-36) gives

$$T_u = m_u \Omega d f(l_1) (\dot{q}_1 \cos \Omega t - \dot{q}_2 \sin \Omega t) \quad (3.2-46)$$

Likewise, introducing this displacement function into the strain energy of the shaft results in,

$$U = \frac{EI}{2} \int_0^l h^2(y) dy (q_1^2 + q_2^2) + \frac{F_0}{2} \int_0^l g^2(y) dy (q_1^2 + q_2^2) \quad (3.2- 47)$$

where, $h(y) = \frac{d^2 f(y)}{dy^2}$. Simplifying equation (3.2-47) gives

$$U = \frac{1}{2} k_s (q_1^2 + q_2^2) \quad (3.2- 48)$$

where, $k_s = EI \int_0^l h^2(y) dy + F_0 \int_0^l g^2(y) dy$ and is the stiffness of the shaft .

Equations (3.2-45), (3.2-46) and (3.2-48) are the kinetic energy expression for the disk and shaft combined, the kinetic energy expression for the mass unbalance and the strain energy expression for the shaft respectively, in terms of the generalised coordinates.

3.2.7 Nonlinear Bearing

In rotating machinery, the dynamic stiffness of the bearing which supports the rotating shaft can have a significant quantitative and qualitative effect on the vibration within the machine. In particular it affects the machine critical speeds and the vibration in between critical speeds. Rolling bearings sometimes have nonlinear spring characteristics due to Coulomb friction and the angular clearance between roller and ring (An-Chen *et.al.*1993). Brown *et.al.*(1994) assuming linear damping force and using short bearing theory verified that a simple model of a rigidly supported hydrodynamic journal bearing can be shown to behave chaotically when the rotating unbalance force exceeds the gravitational load. Chen *et.al.* (1998) in the study of chaos in the unbalanced response of a flexible rotor supported by oil film bearings with nonlinear suspension assumed a linear damping force and their findings showed that the dimension of the bearing centre trajectory is fractal and greater than two in some operating conditions, indicating that the system is in a state of chaotic motion. For simplification, the damping forces of the bearing are assumed to be linear. Thus, the equations of the bearing forces as shown in Figure 3-5 are expressed in the following.

$$F_x = k_{xx}x + k_{xz}z + \bar{k}_{xx}x^n + \bar{k}_{xz}z^n + C_{xx}\dot{x} + C_{xz}\dot{z} \quad (3.2- 49)$$

$$F_z = k_{zx}x + k_{zz}z + \bar{k}_{zx}x^n + \bar{k}_{zz}z^n + C_{zx}\dot{x} + C_{zz}\dot{z} \quad (3.2- 50)$$

where, $n = 1, 2, \dots$,

k_{ij} are linear spring coefficients; $i, j = x, z$

\bar{k}_{ij} are nonlinear spring coefficients; $i, j = x, z$

C_{ij} are linear damping coefficients; $i, j = x, z$

In practice, all components of these nonlinear forces appear markedly up to the third power of deflections in single-row ball bearings (Yamamoto *et.al.* 1981). Therefore, the bearing is assumed to have cubic nonlinear spring, and linear damping characteristics is also assumed. The generalised force from the bearing can be written as

$$F = F_x + F_z \quad (3.2- 51)$$

The virtual work associated with a generalised force is

$$\delta W_{q_i} = [F_{q_i}] \delta q_i \quad (3.2- 52)$$

where the generalised force F_{q_i} is associated with the generalised coordinate q_i . Taking u and w as lateral displacements of the centre of mass of the disk with respect to the fixed frame X, Y, Z , then the virtual work, which is the sum of the virtual work terms for the damping and stiffness effects of the bearing, can be expressed if $u \rightarrow u + \delta u$ and $\delta w = 0$, to give

$$\begin{aligned} \delta W_{(u)} = & [-k_{xx}u] \delta u + [-k_{xz}w] \delta u + [-\bar{k}_{xx}u^3] \delta u \\ & + [-\bar{k}_{xz}w^3] \delta u + [-c_{xx}\dot{u}] \delta u + [-c_{xz}\dot{w}] \delta u \end{aligned} \quad (3.2- 53)$$

For the case where $w \rightarrow w + \delta w$ and $\delta u = 0$, then,

$$\begin{aligned} \delta W_{(w)} = & [-k_{zz}w] \delta w + [-k_{zx}u] \delta w + [-\bar{k}_{zz}w^3] \delta w \\ & + [-\bar{k}_{zx}u^3] \delta w + [-c_{zz}\dot{w}] \delta w + [-c_{zx}\dot{u}] \delta w \end{aligned} \quad (3.2-54)$$

The generalised forces are negative because of work done by the bearing on the shaft.

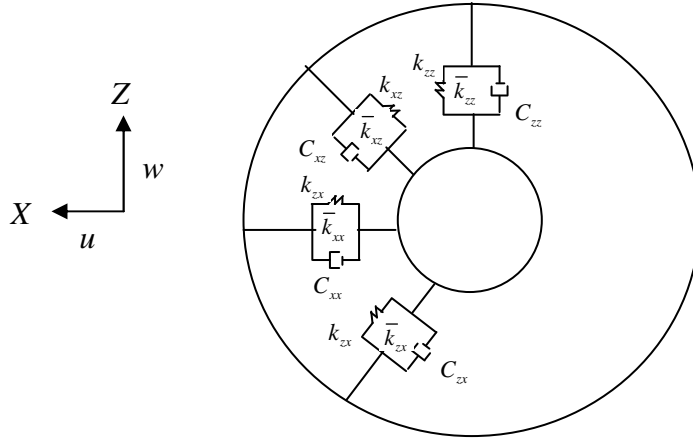


Figure 3- 5: Bearing stiffness and damping

For $k_{xz} = k_{zx} = 0$ (3.2-55)

and applying equation (3.2-55) to equations (3.2-53) and (3.2-54) we have

$$\delta W_{(u)} = [-k_{xx}u] \delta u + [-\bar{k}_{xx}u^3] \delta u + [-c_{xx}\dot{u}] \delta u \quad (3.2-56)$$

$$\delta W_{(w)} = [-k_{zz}w] \delta w + [-\bar{k}_{zz}w^3] \delta w + [-c_{zz}\dot{w}] \delta w \quad (3.2-57)$$

so, $\delta W = \delta W_u + \delta W_w$ (3.2-58)

giving

$$\delta W = [F_u] \delta u + [F_w] \delta w \quad (3.2-59)$$

For $u \rightarrow u + \delta u$ the δu is coaxial with the F_u components and for $w \rightarrow w + \delta w$ the δw is also coaxial with the F_w components, thus equations (3.2-56) and (3.2-57) become

$$F_u = -k_{xx}x - \bar{k}_{xx}x^3 - C\dot{x} \quad (3.2- 60)$$

$$F_w = -k_{zz}z - \bar{k}_{zz}z^3 - C\dot{z} \quad (3.2- 61)$$

Applying equations (3.2-37) and (3.2-38) to (3.2-60) and (3.2-61) we have,

$$F_{q_1} = -k_{xx}f(l_2)q_1 - \bar{k}_{xx}[f(l_2)q_1]^3 - C_{xx}f(l_2)\dot{q}_1 \quad (3.2- 62)$$

$$F_{q_2} = -k_{zz}f(l_2)q_2 - \bar{k}_{zz}[f(l_2)q_2]^3 - C_{zz}f(l_2)\dot{q}_2 \quad (3.2- 63)$$

For a symmetrical bearing

$$k_{xx}f(l_2) = k_{zz}f(l_2) = kf(l_2) \quad (3.2- 64)$$

$$\bar{k}_{xx}f^3(l_2) = \bar{k}_{zz}f^3(l_2) = \bar{k}f^3(l_2) \quad (3.2- 65)$$

$$C_{xx}f(l_2) = C_{zz}f(l_2) = C_b f(l_2) \quad (3.2- 66)$$

Then, letting,

$$kf(l_2) = k_b \quad (3.2- 67)$$

$$\bar{k}f^3(l_2) = b \quad (3.2- 68)$$

$$C_b f(l_2) = c_b \quad (3.2- 69)$$

where, k_b is the bearing stiffness coefficient and c_b is the bearing damping coefficient. Substituting equations (3.2-64) to (3.2-69) into equations (3.2-62) and (3.2-63) we obtain

$$F_{q_1} = -k_b q_1 - b q_1^3 - c_b \dot{q}_1 \quad (3.2-70)$$

$$F_{q_2} = -k_b q_2 - b q_2^3 - c_b \dot{q}_2 \quad (3.2-71)$$

where; F_{q_1} and F_{q_2} are the two components of the force.

The Smart Actuator introduces a Y directed axial force component into the bearing force. This is a force F_v directed along Y when switched on, and therefore the virtual work expression of equation (3.2-59) extends to

$$\delta W = [F_u] \delta u + [F_w] \delta w + [F_v] \delta v \quad (3.2-72)$$

F_v is assumed to be positive because it is external. Therefore expressing F_v in terms of q_1 and q_2 we have $F_{v_{q_1}} = F_{act} q_1$ and $F_{v_{q_2}} = F_{act} q_2$ respectively. Where, F_{act} is the actuator force. (See Appendix A-1 for the derivation of the actuator force term). For $v \rightarrow v + \delta v$, the δv is coaxial with the F_v components, so the two components of the forces extend to

$$F_{q_1} = -k_b q_1 - b q_1^3 - c_b \dot{q}_1 + F_{act} q_1 \quad (3.2-73)$$

$$F_{q_2} = -k_b q_2 - b q_2^3 - c_b \dot{q}_2 + F_{act} q_2 \quad (3.2-74)$$

3.2.8 Equations of Motion

Now applying Lagrange's equations (3.2.1) to the kinetic energy given by the addition of (3.2-45) and (3.2-46) and the strain energy given by (3.2-48) and using q_1 and q_2 as generalised coordinates and the generalised forces as F_{q_1} and F_{q_2} results in the equations in the following subsections.

3.2.8.1 Alternative Analytical Model A

In this model large deflections are accommodated within the equations.

$$m\ddot{q}_1 - \Omega a_5 \dot{q}_2 \cos(\Upsilon q_2) + kq_1 + bq_1^3 + c_b \dot{q}_1 - F_{act} q_1 = m_u d \Omega^2 \sin \Omega t \quad (3.2-75)$$

$$m\ddot{q}_2 + \Omega a_5 \dot{q}_1 \cos(\Upsilon q_2) + kq_2 + bq_2^3 + c_b \dot{q}_2 - F_{act} q_2 = m_u d \Omega^2 \cos \Omega t \quad (3.2-76)$$

where; $k = k_s + k_b$; $a_5 = a_2 \Upsilon$, $\Upsilon = g(l_1) = 1.325$, this is calculated using data from the experimental rig, and k is the rotor-bearing radial stiffness representing the combined circumferentially-symmetric stiffness of the rotor shaft and bearings.

Reference to Appendix A-2 provides a discussion of the equations (3.2-75) and (3.2-76).

3.2.8.2 Alternative Analytical Model B

Going back to the kinetic energy expression equation (3.2-45) and applying small angle approximation of the form $\sin \theta \approx \theta$ and $\cos \theta \approx 1$, leads to

$$T = \frac{1}{2} m (\dot{q}_1^2 + \dot{q}_2^2) + \Omega^2 \left(\frac{1}{2} I_{dy} + \rho IL \right) - \Omega a_2 \dot{q}_1 q_2 (\Upsilon) \quad (3.2-77)$$

Thus equation (3.2-77) becomes

$$T = \frac{1}{2} m (\dot{q}_1^2 + \dot{q}_2^2) + \Omega^2 \left(\frac{1}{2} I_{dy} + \rho IL \right) - \Omega a_5 \dot{q}_1 q_2 \quad (3.2-78)$$

Applying Lagrange's equations (3.2-1) to the kinetic energy given by the addition of (3.2-78) and (3.2-46) and the strain energy given by (3.2-48) gives the equations

$$m\ddot{q}_1 - \Omega a_5 \dot{q}_2 + kq_1 + bq_1^3 + c_b \dot{q}_1 - F_{act} q_1 = m_u d \Omega^2 \sin \Omega t \quad (3.2-79)$$

$$m\ddot{q}_2 + \Omega a_5 \dot{q}_1 + kq_2 + bq_2^3 + c_b \dot{q}_2 - F_{act} q_2 = m_u d \Omega^2 \cos \Omega t \quad (3.2-80)$$

3.2.8.3 Alternative Analytical Model C

Taking a small angle approximation to the Model A equations, using the Maclaurin Series in the form $\sin q_2 = q_2 - \frac{q_2^3}{3!} + \frac{q_2^5}{5!} - + \dots$ and $\cos q_2 = 1 - \frac{q_2^2}{2!} + \frac{q_2^4}{4!} - + \dots$ to expand the trigonometrical functions in equations (3.2-75) and (3.2-76) by assuming the flexible rotor lateral oscillations to be finite, but not very large, and for small angles of q_2 , the expansions of $\sin q_2$ and $\cos q_2$ will be dominated by the leading term. Thus for small vibrations we can make the approximation of replacing $\sin(\Upsilon q_2)$ by (Υq_2) and $\cos(\Upsilon q_2)$ by 1, equations (3.2-75) and (3.2-76) therefore become,

$$m\ddot{q}_1 - \Omega a_5 \dot{q}_2 + kq_1 + bq_1^3 + c_b \dot{q}_1 - F_{act} q_1 = m_u d \Omega^2 \sin \Omega t \quad (3.2- 81)$$

$$m\ddot{q}_2 + \Omega a_5 \dot{q}_1 + kq_2 + bq_2^3 + c_b \dot{q}_2 - F_{act} q_2 = m_u d \Omega^2 \cos \Omega t \quad (3.2- 82)$$

3.2.9 Linear Viscous Damping

Damping is a nonlinear phenomenon and some examples are hysteretic damping, Coulomb dry friction and aerodynamic drag. Linear viscous damping is an idealisation, which provides a term proportional to velocity. Including linear viscous term ($c_s \dot{q}$) into equations (3.2-75), (3.2-76), (3.2-79), (3.2-80), (3.2-81) and (3.2-82) we get the three equation models as,

3.2.9.1 Model A

$$m\ddot{q}_1 + c\dot{q}_1 - \Omega a_5 \dot{q}_2 \cos(\Upsilon q_2) + kq_1 + bq_1^3 - F_{act} q_1 = m_u d \Omega^2 \sin \Omega t \quad (3.2- 83)$$

$$m\ddot{q}_2 + c\dot{q}_2 + \Omega a_5 \dot{q}_1 \cos(\Upsilon q_2) + kq_2 + bq_2^3 - F_{act} q_2 = m_u d \Omega^2 \cos \Omega t \quad (3.2- 84)$$

3.2.9.2 Model B

$$m\ddot{q}_1 + c\dot{q}_1 - \Omega a_5 \dot{q}_2 + kq_1 + bq_1^3 - F_{act} q_1 = m_u d \Omega^2 \sin \Omega t \quad (3.2- 85)$$

$$m\ddot{q}_2 + c\dot{q}_2 + \Omega a_5 \dot{q}_1 + kq_2 + bq_2^3 - F_{act} q_2 = m_u d \Omega^2 \cos \Omega t \quad (3.2- 86)$$

3.2.9.3 Model C

$$m\ddot{q}_1 + c\dot{q}_1 - \Omega a_5 \dot{q}_2 + kq_1 + bq_1^3 - F_{act} q_1 = m_u d \Omega^2 \sin \Omega t \quad (3.2- 87)$$

$$m\ddot{q}_2 + c\dot{q}_2 + \Omega a_5 \dot{q}_1 + kq_2 + bq_2^3 - F_{act} q_2 = m_u d \Omega^2 \cos \Omega t \quad (3.2- 88)$$

where; c is the damping coefficient and $c = c_s + c_b$, and c_s is the damping coefficient of the shaft . A close look at Models B and C show that they are identical in structure and they all assume small angle approximations.

3.2.10 Parameter Estimation Procedure

We estimate the parameters (c, b) describing the weakly damping and weakly nonlinear cubic stiffness coefficients experimentally by measuring the rate of decay of free amplitude oscillations for the linear viscous damping coefficient c (see Appendix A.4 for the estimation of the linear viscous damping coefficient) and from frequency-response results for b respectively. It is known that, for a given excitation level, the amplitude at the peak of the corresponding frequency-response curve depends on the damping value, and the effect of the nonlinearity is essentially to shift the peak away from the natural frequency ω . For a system with hardening nonlinearity, the peak is shifted to the right; and in the case of a softening nonlinearity it is shifted to the left. The magnitude of the shift depends on the strength of the nonlinearity (Nayfeh and Mook, 1979). Thus, knowing the amplitude at the peak and the frequency shift, it is possible to estimate approximately the effective nonlinearity coefficient of a system. The detailed estimation procedure is described in the following subsection.

3.2.10.1 Nonlinearity Estimation

Using Duffing's equation as given by (Thomson, 1993)

$$\ddot{y} + \omega^2 y + by^3 = F \cos \Omega t \quad (3.2- 89)$$

where, by^3 is the nonlinear cubic stiffness term and F is excitation amplitude. The solution of the nonlinear natural frequency of vibration is given by

$$\omega_{nl}^2 = \omega^2 + \frac{3}{4}bA^2 - \frac{F}{A} \quad (3.2- 90)$$

Equation (3.2-90) is adopted for this work, where ω is the linear natural frequency and ω_{nl} is the nonlinear natural frequency. The term ω_{nl} is a function of A , which is the response amplitude.

As A increases, ω_{nl} also increases correspondingly as is expected for a hardening spring (Thomson, 1993). If large amplitude A is chosen and denoted as A_1 , we have the following

$$\omega_{nl(1)}^2 = \omega^2 + \frac{3}{4}bA_1^2 - \frac{F}{A_1} \quad (3.2- 91)$$

Where $\omega_{nl(1)}$ is the first nonlinear natural frequency. The value of A can be increased or decreased slightly by either increasing or decreasing the excitation level. Let this altered response amplitude be called A_2 (Wong, 1988). Thus the equation (3.2-90) becomes

$$\omega_{nl(2)}^2 = \omega^2 + \frac{3}{4}bA_2^2 - \frac{F}{A_2} \quad (3.2- 92)$$

Where $\omega_{nl(2)}$ is taken as the second nonlinear frequency. By manipulating equations (3.2-91) and (3.2-92), b is evaluated to be

$$b = \frac{4(\omega_{nl(1)}^2 - \omega_{nl(2)}^2)}{3(A_1^2 - A_2^2)} - \frac{4F}{3A_1A_2(A_1 + A_2)} \quad (3.2- 93)$$

This is obtained by an experiment as conducted and described in Appendix A.5. It should be noted that $\omega_{nl(1)}$ and $\omega_{nl(2)}$ will be very close, and that accurate work on a spectrum analyser is the only practical way of identifying

this shift as the response amplitude itself shifts from A_1 to A_2 during the small change introduced by shifting the excitation amplitude level.

3.2.11 Discussions

A rotor system can be considered a vibrating system in the classical sense. It is represented by a system of equations which relates excitations and responses, where responses of interest are motions of the geometric centre of the shaft. Excitations can be due to rotating mass unbalance. A resonance condition exists when the frequency of excitation due to mass unbalance coincides with the natural frequency. The rotating system has several unique features compared to other vibrating systems due to its rotation. Mass unbalance provides excitation which is present whenever the rotor spins; for this reason mass unbalance is considered an integral part of the analysis as opposed to an excitation term. The tendency of a rotor disk's angular momentum or the momentum of the rotor itself, to couple with rotations about the bearing is called the "gyroscopic effect" and causes the natural frequencies to vary with rotor speed. Equations of the rotor system are obtained systematically in the following way. First the expressions of the disk kinetic, shaft kinetic, mass unbalance kinetic and strain energies of the rotor elements are constructed. Then the virtual work of external forces, including, bearing and axial force terms are formed. The axial force term enables one to include or apply an external force axially into the rotor system. A numerical method, Rayleigh-Ritz method which gives simple models that are useful to understanding of the basic phenomena, has been used to simplify the model. Lagrange's equations are applied to the expressions, firstly by accommodating large deflections to obtain the model A equations, and secondly, by making small angle approximations to obtain the model B and C equations.

CHAPTER 4

APPROXIMATE ANALYTICAL AND NUMERICAL SOLUTIONS TO THE EQUATIONS OF MOTION

4.1 Introduction

In this chapter nonlinear vibrations of the flexible rotor while passing through primary resonance and the associated stability behaviour are analysed, with and without an axial parametric excitation. Solutions are developed based on an appropriate Jeffcott rotor model, which consists of a single unbalanced disk attached to an elastic shaft at mid-span. The classical perturbation Method of Multiple Scales (MMS) has been chosen for the analysis of the equations of motion because the solution is a function of multiple independent time-scales, so the fast scale can be used for capturing motions at frequencies comparable to the linear frequency of the system, whilst the slow scale accounts for slow modulations of amplitudes and phases. This method is well discussed in the books of Nayfeh and Mook (1979), Cartmell (1990), and Murdock (1999). Cartmell *et.al.* (2003) reviewed the Multiple Scales Method as applied to the weakly nonlinear dynamics of mechanical systems. The MMS is one of several tools used to study the nonlinear equations of motion and is sometimes suitable for solving stability problems. The principal difference between this and other perturbation methods is that the time (independent variable) is represented by independent time scales. Its chief advantage over other perturbation techniques, such as the Lindstedt-Poincaré method, is that it is easily applicable to damped systems. It also generates all possible resonance conditions and allows the user great control over the overall accuracy of the solution (Cartmell,1984). The underlying idea of this method is to consider an expansion of the dependent variables as a function of multiple independent variables, or scales, instead of a single independent variable. Extended expansions based on “slow” and “fast” time scales are applied to obtain uniform expansions for the amplitudes of the motion. Expressions for the amplitude and phase modulation functions are explicitly obtained, and manipulated to yield steady-state solutions. Frequency-

amplitude relationships which describe approximate general solutions resulting from mass unbalance and combined parametric and mass unbalance, are derived.

Stability regions in the parameter space are obtained numerically for a suitable solution in terms of the perturbed steady-state solutions of the governing nonlinear equations of motion. The sensitivity of vibration amplitudes to various rotor-dynamic system parameters is illustrated through a numerical study. In addition direct numerical integration within *Mathematica*TM is also performed for the comparison of numerical solutions for the model of the rotor system.

4.2 Ordering of Terms

Referring to chapter 3, the equations of Models B and C are identical. The Model A equations contain trigonometrical terms in coordinate q_2 whereas Models B and C use small angle approximations to these. Since it is not possible to apply the method of multiple scales to systems such as the Model A equations without first removing the trigonometrical terms, removing them takes us to the equations of Models B and C. So, the multiple scales method can only be applied to the equations of Models B and C. The necessity now is to order the two sets of equations in terms of the small perturbation parameter ε .

The equations are for Model B;

$$\ddot{q}_1 + \hat{c}\dot{q}_1 - \Omega\hat{a}_5\dot{q}_2 + \omega^2q_1 + \hat{b}q_1^3 = \mu d\Omega^2 \sin \Omega t \quad (4.2- 1)$$

$$\ddot{q}_2 + \hat{c}\dot{q}_2 + \Omega\hat{a}_5\dot{q}_1 + \omega^2q_2 + \hat{b}q_2^3 = \mu d\Omega^2 \cos \Omega t \quad (4.2- 2)$$

where, $\hat{a}_5 = \frac{a_5}{m}, \omega^2 = \frac{k}{m}, \hat{b} = \frac{b}{m}, \hat{c} = \frac{c}{m}, \mu = \frac{m_u}{m}$

We nondimensionalise the time scale t and order the equations by introducing the small parameter ε . Let nondimensional time τ be $\tau = \omega t$, where $\omega = \sqrt{\frac{k}{m}}$,

and it is the natural frequency. ω is normalised to unity, therefore $\tau \equiv 1$. Also we let

$$q_1 = \varepsilon \bar{q}_1; \quad q_2 = \varepsilon \bar{q}_2 \quad (4.2- 3)$$

on the assumption that q_1 and q_2 are fairly small.

Substituting for q_1 and q_2 across the two equations of motion we have, for the second time derivative terms,

$$\ddot{q}_1 = \frac{d^2 q_1}{dt^2} = \frac{d^2 q_1}{d\tau^2} \omega^2 \equiv q_1'' \omega^2 \Rightarrow \varepsilon \omega^2 \bar{q}_1'' \quad (4.2- 4)$$

where the dots denote differentiation with respect to t and the primes denote differentiation with respect to timescale τ , and

$$\ddot{q}_2 = \frac{d^2 q_2}{dt^2} = \frac{d^2 q_2}{d\tau^2} \omega^2 \equiv q_2'' \omega^2 \Rightarrow \varepsilon \omega^2 \bar{q}_2'' \quad (4.2- 5)$$

The other terms transform as follows, in the sequence that they appear in the equations of motion,

$$\dot{q}_1 = \frac{dq_1}{dt} = \frac{dq_1}{d\tau} \omega \equiv q_1' \omega \Rightarrow \varepsilon \omega \bar{q}_1' \quad (4.2- 6)$$

$$\dot{q}_2 = \frac{dq_2}{dt} = \frac{dq_2}{d\tau} \omega \equiv q_2' \omega \Rightarrow \varepsilon \omega \bar{q}_2' \quad (4.2- 7)$$

$$q_1 \Rightarrow \varepsilon \bar{q}_1 \quad \text{and} \quad q_2 \Rightarrow \varepsilon \bar{q}_2 \quad (4.2- 8)$$

$$q_1^3 \Rightarrow \varepsilon^3 \bar{q}_1^3 \quad \text{and} \quad q_2^3 \Rightarrow \varepsilon^3 \bar{q}_2^3 \quad (4.2- 9)$$

For the right hand side, since $\mu = \frac{m_u}{m}$ and this is necessarily small, then it is agreed that it is possible to set $\mu = \bar{\mu} \varepsilon$; similarly for uniformity we set $d = \varepsilon \bar{d}$.

Assembling the terms now, from equations (4.2-1) and (4.2-2) we have

$$\varepsilon\omega^2\bar{q}_1'' + \varepsilon\omega\hat{c}\bar{q}_1' - \varepsilon\omega\Omega\hat{a}_5\bar{q}_2' + \varepsilon\omega^2\bar{q}_1 + \varepsilon^3\hat{b}\bar{q}_1^3 = \varepsilon^2\bar{\mu}\bar{d}\Omega^2 \sin \Omega t \quad (4.2- 10)$$

$$\varepsilon\omega^2\bar{q}_2'' + \varepsilon\omega\hat{c}\bar{q}_2' + \varepsilon\omega\Omega\hat{a}_5\bar{q}_1' + \varepsilon\omega^2\bar{q}_2 + \varepsilon^3\hat{b}\bar{q}_2^3 = \varepsilon^2\bar{\mu}\bar{d}\Omega^2 \cos \Omega t \quad (4.2- 11)$$

The following equations result from dividing through by $\varepsilon\omega^2$,

$$\bar{q}_1'' + \frac{\hat{c}}{\omega}\bar{q}_1' - \frac{\Omega}{\omega}\hat{a}_5\bar{q}_2' + \bar{q}_1 + \varepsilon^2\frac{\hat{b}}{\omega^2}\bar{q}_1^3 = \varepsilon\bar{\mu}\bar{d}\left(\frac{\Omega}{\omega}\right)^2 \sin\left(\frac{\Omega}{\omega}\tau\right) \quad (4.2- 12)$$

$$\bar{q}_2'' + \frac{\hat{c}}{\omega}\bar{q}_2' + \frac{\Omega}{\omega}\hat{a}_5\bar{q}_1' + \bar{q}_2 + \varepsilon^2\frac{\hat{b}}{\omega^2}\bar{q}_2^3 = \varepsilon\bar{\mu}\bar{d}\left(\frac{\Omega}{\omega}\right)^2 \cos\left(\frac{\Omega}{\omega}\tau\right) \quad (4.2- 13)$$

The equations are now scaled as well, with a normalised natural frequency of unity. The gyroscopic terms $\frac{\Omega}{\omega}\hat{a}_5\bar{q}_i'$, $i=1,2$, and the linear viscous damping terms $\frac{\hat{c}}{\omega}\bar{q}_i'$, $i=1,2$, are to $O(\varepsilon^0)$ i.e. the zeroth order, which is mathematically inconvenient since their effects will appear within the zeroth order perturbation equations and they are not fundamental to the motion and do not strongly contribute to the resonance of interest. To make them less inconvenient, they are re-formulated in terms of the small parameter, ε , so that they appear in the same perturbation equation as the excitation term. This also ensures that their effects only appear within the higher order perturbation equations. We therefore propose \hat{a}_5 and \hat{c} as small hence $\hat{a}_5 = \varepsilon\bar{a}_5$ and $\hat{c} = \varepsilon\bar{c}$ leading to

$$\bar{q}_1'' + \varepsilon\frac{\bar{c}}{\omega}\bar{q}_1' - \varepsilon\frac{\Omega}{\omega}\bar{a}_5\bar{q}_2' + \bar{q}_1 + \varepsilon^2\frac{\hat{b}}{\omega^2}\bar{q}_1^3 = \varepsilon\bar{\mu}\bar{d}\left(\frac{\Omega}{\omega}\right)^2 \sin\left(\frac{\Omega}{\omega}\tau\right) \quad (4.2- 14)$$

$$\bar{q}_2'' + \varepsilon\frac{\bar{c}}{\omega}\bar{q}_2' + \varepsilon\frac{\Omega}{\omega}\bar{a}_5\bar{q}_1' + \bar{q}_2 + \varepsilon^2\frac{\hat{b}}{\omega^2}\bar{q}_2^3 = \varepsilon\bar{\mu}\bar{d}\left(\frac{\Omega}{\omega}\right)^2 \cos\left(\frac{\Omega}{\omega}\tau\right) \quad (4.2- 15)$$

This retains the linear Inertia and stiffness terms at the zeroth order perturbation level from which generating solutions are obtained, the damping, gyroscopic coupling and excitation terms appear to first order perturbation, and the cubic nonlinearity term to second order perturbation. This philosophy is pragmatic and realistic in that it permits the pre-ordained generation of linear, homogeneous, generating solutions for each coordinate.

4.3 The Method of Multiple Scales

4.3.1 Introducing the Time Scales

As required by the method of multiple scales, the coordinates $\bar{q}_{1,2}(t)$ are stated in power series form, as are their derivatives with respect to time. The solution of the equations (4.2-14) and (4.2-15) are approximated by uniformly valid expressions of the form as indicated in equations (4.2-16) and (4.2-17),

$$\bar{q}_1(t, \varepsilon) = \bar{q}_{10}(T_0, T_1, T_2) + \varepsilon \bar{q}_{11}(T_0, T_1, T_2) + \varepsilon^2 \bar{q}_{12}(T_0, T_1, T_2) + O(\varepsilon^3) \quad (4.2-16)$$

$$\bar{q}_2(t, \varepsilon) = \bar{q}_{20}(T_0, T_1, T_2) + \varepsilon \bar{q}_{21}(T_0, T_1, T_2) + \varepsilon^2 \bar{q}_{22}(T_0, T_1, T_2) + O(\varepsilon^3) \quad (4.2-17)$$

where, $\bar{q}_{10}(T_0, T_1, T_2) \dots \bar{q}_{22}(T_0, T_1, T_2)$ are functions of time scales T_n for $n=0,1,2,\dots$ yet to be determined and ε is an arbitrarily small parameter. The derivative perturbations rely on the notion that the real time t , can be expressed in the form of a set of successively independent time scales, T_n , given by

$$T_n = \varepsilon^n t \text{ for } n=0,1,2,\dots, \quad (4.2-18)$$

In equations (4.2-16) and (4.2-17), T_0 is nominally considered as a fast time-scale and T_1, T_2 as slower time-scales, such that $T_0 = t$, $T_1 = \varepsilon t$ and $T_2 = \varepsilon^2 t$ as from equation (4.2-18). Each time-scale is treated as an independent variable and the required order of approximation to the solution dictates the number of time scales used. It follows that the derivatives with respect to t become expansions in terms of the partial derivatives with respect to the T_n according to

$$\frac{d}{dt} = \frac{dT_0}{dt} \frac{\partial}{\partial T_0} + \frac{dT_1}{dt} \frac{\partial}{\partial T_1} + \frac{dT_2}{dt} \frac{\partial}{\partial T_2} = D_0 + \varepsilon D_1 + \varepsilon^2 D_2 \quad (4.2-19)$$

$$\frac{d^2}{dt^2} = D_0^2 + 2\varepsilon D_0 D_1 + 2\varepsilon^2 D_0 D_2 + \varepsilon^2 D_1^2 \quad (4.2-20)$$

The partial derivatives of equations (4.2-19) and (4.2-20) are stated in the D operator notation where $D_i^j = \frac{\partial^j}{\partial T_i^j}$. Series (4.2-16) to (4.2-20) inclusive are truncated after the second order ε terms, because this perturbation analysis has been deliberately limited to the second order perturbation level. Higher order terms, ε^3 and so on, may be neglected, because the associated higher order perturbation equations will yield negligible corrections for the problem, as set up here.

4.3.2 Treatment of Coefficients to like Orders of ε

Applying the method of multiple scales in the conventional manner by substituting equations (4.2-16), (4.2-17), (4.2-19) and (4.2-20) into the differential equations of motion (4.2-14) and (4.2-15), these become,

$$\begin{aligned}
& (\bar{q}_{10} + \varepsilon \bar{q}_{11} + \varepsilon^2 \bar{q}_{12}) [D_0^2 + 2\varepsilon D_0 D_1 + 2\varepsilon^2 D_0 D_2 + \varepsilon^2 D_1^2] \\
& + \varepsilon \frac{\bar{c}}{\omega} (\bar{q}_{10} + \varepsilon \bar{q}_{11} + \varepsilon^2 \bar{q}_{12}) [D_0 + \varepsilon D_1 + \varepsilon^2 D_2] \\
& - \varepsilon \frac{\Omega}{\omega} \bar{a}_5 [(\bar{q}_{20} + \varepsilon \bar{q}_{21} + \varepsilon^2 \bar{q}_{22})(D_0 + \varepsilon D_1 + \varepsilon^2 D_2)] + (\bar{q}_{10} + \varepsilon \bar{q}_{11} + \varepsilon^2 \bar{q}_{12}) \\
& + \varepsilon^2 \frac{\hat{b}}{\omega^2} (\bar{q}_{10} + \varepsilon \bar{q}_{11} + \varepsilon^2 \bar{q}_{12})^3 + o(\varepsilon)^4 = \varepsilon \bar{\mu} \bar{d} \left(\frac{\Omega}{\omega} \right)^2 \text{Sin} \left(\frac{\Omega}{\omega} \tau \right)
\end{aligned} \tag{4.2- 21}$$

$$\begin{aligned}
& (\bar{q}_{20} + \varepsilon \bar{q}_{21} + \varepsilon^2 \bar{q}_{22}) [D_0^2 + 2\varepsilon D_0 D_1 + 2\varepsilon^2 D_0 D_2 + \varepsilon^2 D_1^2] \\
& + \varepsilon \frac{\bar{c}}{\omega} (\bar{q}_{20} + \varepsilon \bar{q}_{21} + \varepsilon^2 \bar{q}_{22}) [D_0 + \varepsilon D_1 + \varepsilon^2 D_2] \\
& + \varepsilon \frac{\Omega}{\omega} \bar{a}_5 [(\bar{q}_{10} + \varepsilon \bar{q}_{11} + \varepsilon^2 \bar{q}_{12})(D_0 + \varepsilon D_1 + \varepsilon^2 D_2)] + (\bar{q}_{20} + \varepsilon \bar{q}_{21} + \varepsilon^2 \bar{q}_{22}) \\
& + \varepsilon^2 \frac{\hat{b}}{\omega^2} (\bar{q}_{20} + \varepsilon \bar{q}_{21} + \varepsilon^2 \bar{q}_{22})^3 + o(\varepsilon)^4 = \varepsilon \bar{\mu} \bar{d} \left(\frac{\Omega}{\omega} \right)^2 \text{Cos} \left(\frac{\Omega}{\omega} \tau \right)
\end{aligned} \tag{4.2- 22}$$

Then, collecting the coefficients of like order of ε^n , and equating them to zero in order to construct the perturbation equations, leads to,

Order ε^0

$$D_0^2 \bar{q}_{10} + \bar{q}_{10} = 0 \quad (4.2- 23)$$

$$D_0^2 \bar{q}_{20} + \bar{q}_{20} = 0 \quad (4.2- 24)$$

where the natural frequency of free undamped vibration is normalised to unity, thus $\omega^2 = 1$. These are linear, homogeneous, second order perturbation equations and can be thought of as ordinary differential equations with respect to timescale T_0 . They are the zeroth order perturbation equations.

Order ε^1

$$D_0^2 \bar{q}_{11} + \bar{q}_{11} = -2D_0 D_1 \bar{q}_{10} - \frac{\bar{c}}{\omega} D_0 \bar{q}_{10} + \frac{\Omega}{\omega} \bar{a}_5 D_0 \bar{q}_{20} + \bar{\mu} \bar{d} \left(\frac{\Omega}{\omega} \right)^2 \text{Sin} \left(\frac{\Omega}{\omega} \tau \right) \quad (4.2- 25)$$

$$D_0^2 \bar{q}_{21} + \bar{q}_{21} = -2D_0 D_1 \bar{q}_{20} - \frac{\bar{c}}{\omega} D_0 \bar{q}_{20} - \frac{\Omega}{\omega} \bar{a}_5 D_0 \bar{q}_{10} + \bar{\mu} \bar{d} \left(\frac{\Omega}{\omega} \right)^2 \text{Cos} \left(\frac{\Omega}{\omega} \tau \right) \quad (4.2- 26)$$

The equations (4.2-25) and (4.2-26) are the first order perturbation equations.

Order ε^2

$$D_0^2 \bar{q}_{12} + \bar{q}_{12} = -2D_0 D_2 \bar{q}_{10} - D_1^2 \bar{q}_{10} - 2D_0 D_1 \bar{q}_{11} - \frac{\bar{c}}{\omega} D_1 \bar{q}_{10} - \frac{\bar{c}}{\omega} D_0 \bar{q}_{11} + \frac{\Omega}{\omega} \bar{a}_5 D_0 \bar{q}_{21} + \frac{\Omega}{\omega} \bar{a}_5 D_1 \bar{q}_{20} - \frac{\hat{b}}{\omega^2} \bar{q}_{10}^3 \quad (4.2- 27)$$

$$D_0^2 \bar{q}_{22} + \bar{q}_{22} = -2D_0 D_2 \bar{q}_{20} - D_1^2 \bar{q}_{20} - 2D_0 D_1 \bar{q}_{21} - \frac{\bar{c}}{\omega} D_1 \bar{q}_{20} - \frac{\bar{c}}{\omega} D_0 \bar{q}_{21} - \frac{\Omega}{\omega} \bar{a}_5 D_1 \bar{q}_{10} - \frac{\Omega}{\omega} \bar{a}_5 D_0 \bar{q}_{11} - \frac{\hat{b}}{\omega^2} \bar{q}_{20}^3 \quad (4.2- 28)$$

Equations (4.2-27) and (4.2-28) are the second order perturbation equations. It is clear that each perturbation order requires explicit solutions to \bar{q}_{10} and \bar{q}_{20} , and then \bar{q}_{11} and \bar{q}_{21} by means of appropriate treatment of the emergent structures on the right hand sides of the perturbation equations starting with the zeroth order generating equations.

4.3.3 Secular Terms to First Order Perturbation

Harmonic solutions of (4.2-23) and (4.2-24), the zeroth order perturbation equations are stated in convenient polar form. Respectively, these are,

$$\bar{q}_{10} = A(T_1, T_2)e^{iT_0} + \bar{A}(T_1, T_2)e^{-iT_0} \quad (4.2-29)$$

$$\bar{q}_{20} = C(T_1, T_2)e^{iT_0} + \bar{C}(T_1, T_2)e^{-iT_0} \quad (4.2-30)$$

where, $\omega=1$, and A and C are as yet unknown complex amplitudes, with their complex conjugates denoted by \bar{A} and \bar{C} .

Substituting the zeroth order perturbation solutions from equations (4.2-29) and (4.2-30) into the first order perturbation equations (4.2-25) and (4.2-26), and henceforth neglecting the arguments T_1 and T_2 for simplicity, gives

$$D_0^2 \bar{q}_{11} + \bar{q}_{11} = -2iD_1 A e^{iT_0} + 2iD_1 \bar{A} e^{-iT_0} - i \frac{\bar{C}}{\omega} A e^{iT_0} + i \frac{\bar{C}}{\omega} \bar{A} e^{-iT_0} \quad (4.2-31)$$

$$+ i \frac{\Omega \bar{a}_5}{\omega} C e^{iT_0} - i \frac{\Omega \bar{a}_5}{\omega} \bar{C} e^{-iT_0} + \Gamma \text{Sin} \left(\frac{\Omega}{\omega} \tau \right)$$

$$D_0^2 \bar{q}_{21} + \bar{q}_{21} = -2iD_1 C e^{iT_0} + 2iD_1 \bar{C} e^{-iT_0} - i \frac{\bar{C}}{\omega} C e^{iT_0} + i \frac{\bar{C}}{\omega} \bar{C} e^{-iT_0} \quad (4.2-32)$$

$$- i \frac{\Omega \bar{a}_5}{\omega} A e^{iT_0} + i \frac{\Omega \bar{a}_5}{\omega} \bar{A} e^{-iT_0} + \Gamma \text{Cos} \left(\frac{\Omega}{\omega} \tau \right)$$

where $\Gamma = \bar{\mu} \bar{d} \left(\frac{\Omega}{\omega} \right)^2$. Also, substituting the zeroth order perturbation solutions, equations (4.2-29) and (4.2-30) into the second order perturbation equations (4.2-27) and (4.2-28), and also neglecting the arguments T_1 and T_2 for simplicity from hereon gives

$$D_0^2 \bar{q}_{12} + \bar{q}_{12} = -2iD_2 A e^{iT_0} + 2iD_2 \bar{A} e^{-iT_0} - D_1^2 A e^{iT_0} - D_1^2 \bar{A} e^{-iT_0} \quad (4.2-33)$$

$$- 2D_1 D_0 \bar{q}_{11} - \frac{\bar{C}}{\omega} D_1 A e^{iT_0} - \frac{\bar{C}}{\omega} D_1 \bar{A} e^{-iT_0} - \frac{\bar{C}}{\omega} D_0 \bar{q}_{11}$$

$$+ \frac{\Omega \bar{a}_5}{\omega} D_0 \bar{q}_{21} + \frac{\Omega \bar{a}_5}{\omega} D_1 C e^{iT_0} + \frac{\Omega \bar{a}_5}{\omega} D_1 \bar{C} e^{-iT_0}$$

$$- \frac{\hat{b}}{\omega^2} \left[A^3 e^{3iT_0} + 3A^2 \bar{A} e^{iT_0} + 3A \bar{A}^2 e^{-iT_0} + \bar{A}^3 e^{-3iT_0} \right]$$

$$\begin{aligned}
 D_0^2 \bar{q}_{22} + \bar{q}_{22} = & -2iD_2 C e^{iT_0} + 2iD_2 \bar{C} e^{-iT_0} - D_1^2 C e^{iT_0} - D_1^2 \bar{C} e^{-iT_0} \\
 & - 2D_1 D_0 \bar{q}_{21} - \frac{\bar{c}}{\omega} D_1 C e^{iT_0} - \frac{\bar{c}}{\omega} D_1 \bar{C} e^{-iT_0} - \frac{\bar{c}}{\omega} D_0 \bar{q}_{21} \\
 & - \frac{\Omega \bar{a}_5}{\omega} D_1 A e^{iT_0} - \frac{\Omega \bar{a}_5}{\omega} D_1 \bar{A} e^{-iT_0} - \frac{\Omega \bar{a}_5}{\omega} D_0 \bar{q}_{11} \\
 & - \frac{\hat{b}}{\omega^2} \left[C^3 e^{3iT_0} + 3C^2 \bar{C} e^{iT_0} + 3C \bar{C}^2 e^{-iT_0} + \bar{C}^3 e^{-3iT_0} \right]
 \end{aligned} \tag{4.2-34}$$

Terms proportional to e^{iT_0} and e^{-2iT_0} are resonant, and they will cause secular terms to appear in the particular solutions if they are not removed. Retaining the secular terms would create a disproportionate increase in the relative magnitude of the additional correction generated by solving at this order of perturbation. Expressing $\Gamma \text{Sin}\left(\frac{\Omega}{\omega} \tau\right)$ and $\Gamma \text{Cos}\left(\frac{\Omega}{\omega} \tau\right)$ in exponential forms and substituting into the first order perturbation equations (4.2-31) and (4.2-32), and taking the common factor of e^{iT_0} out from the right hand sides, the secular terms are immediately identified. Thus we have,

$$D_0^2 \bar{q}_{11} + \bar{q}_{11} = e^{iT_0} \left(\begin{array}{l} -2iD_1 A + 2iD_1 \bar{A} e^{-2iT_0} - i \frac{\bar{c}}{\omega} A + i \frac{\bar{c}}{\omega} \bar{A} e^{-2iT_0} \\ + i \frac{\Omega \bar{a}_5}{\omega} C - i \frac{\Omega \bar{a}_5}{\omega} \bar{C} e^{-2iT_0} + i \frac{\Gamma}{2} e^{i\left(\frac{\Omega}{\omega}-1\right)T_0} - i \frac{\Gamma}{2} e^{-i\left(\frac{\Omega}{\omega}+1\right)T_0} \end{array} \right) \tag{4.2-35}$$

$$D_0^2 \bar{q}_{21} + \bar{q}_{21} = e^{iT_0} \left(\begin{array}{l} -2iD_1 C + 2iD_1 \bar{C} e^{-2iT_0} - i \frac{\bar{c}}{\omega} C + i \frac{\bar{c}}{\omega} \bar{C} e^{-2iT_0} \\ - i \frac{\Omega \bar{a}_5}{\omega} A + i \frac{\Omega \bar{a}_5}{\omega} \bar{A} e^{-2iT_0} + \frac{\Gamma}{2} e^{i\left(\frac{\Omega}{\omega}-1\right)T_0} + \frac{\Gamma}{2} e^{-i\left(\frac{\Omega}{\omega}+1\right)T_0} \end{array} \right) \tag{4.2-36}$$

It can be seen that all terms in the right hand side of the first order perturbation equations (4.2-35) and (4.2-36) are secular. The general approach in multiple scales is to equate the secular terms of equations such as (4.2-35) and (4.2-36) to zero, so as to preserve the uniformity of the expansions of the dependent variables. Therefore, terms proportional to e^{iT_0} constitute a set of secular terms and are removed from the equations (4.2-35) and (4.2-36), and to eliminate them we must put,

$$-2iD_1A - i\frac{\bar{c}}{\omega}A + i\frac{\Omega}{\omega}\bar{a}_5C + i\frac{\Gamma}{2}e^{i\left(\frac{\Omega}{\omega}-1\right)T_0} = 0 \quad (4.2- 37)$$

$$-2iD_1C - i\frac{\bar{c}}{\omega}C - i\frac{\Omega}{\omega}\bar{a}_5A + \frac{\Gamma}{2}e^{i\left(\frac{\Omega}{\omega}-1\right)T_0} = 0 \quad (4.2- 38)$$

Considering terms proportional to e^{-2iT_0} , we get another set of secular terms becoming,

$$2iD_1\bar{A} + i\frac{\bar{c}}{\omega}\bar{A} - i\frac{\Omega}{\omega}\bar{a}_5\bar{C} - i\frac{\Gamma}{2}e^{-i\left(\frac{\Omega}{\omega}+1\right)T_0} = 0 \quad (4.2- 39)$$

$$2iD_1\bar{C} + i\frac{\bar{c}}{\omega}\bar{C} + i\frac{\Omega}{\omega}\bar{a}_5\bar{A} + \frac{\Gamma}{2}e^{-i\left(\frac{\Omega}{\omega}+1\right)T_0} = 0 \quad (4.2- 40)$$

Further, since by the assumption that $\Omega \approx \omega$, the term $\frac{\Gamma}{2}e^{i\frac{\Omega}{\omega}T_0}$ will then be near-resonant, causing small divisor terms to appear in the particular solutions. To include near-resonant terms within the secular terms a detuning parameter σ is introduced, this being a measure of the nearness to resonance, for the nondimensionalised case, by means of

$$\frac{\Omega}{\omega} = \frac{\omega + \varepsilon\sigma}{\omega} = 1 + \frac{\varepsilon\sigma}{\omega} = 1 + \varepsilon\bar{\sigma} \quad (4.2- 41)$$

This means the solvability equations (4.2-37) and (4.2-38) can now be expressed as

$$-2iD_1A - i\frac{\bar{c}}{\omega}A + i\frac{\Omega}{\omega}\bar{a}_5C + i\frac{\Gamma}{2}e^{i\varepsilon\bar{\sigma}T_0} = 0 \quad (4.2- 42)$$

$$-2iD_1C - i\frac{\bar{c}}{\omega}C - i\frac{\Omega}{\omega}\bar{a}_5A + \frac{\Gamma}{2}e^{i\varepsilon\bar{\sigma}T_0} = 0 \quad (4.2- 43)$$

Applying the time-scale transformation $\frac{\Omega}{\omega}T_0 = \frac{\omega T_0 + \varepsilon\sigma T_0}{\omega} = T_0 + \bar{\sigma}T_1$ to (4.2-42)

and (4.2-43) gives,

$$-2iD_1A - i\frac{\bar{c}}{\omega}A + i\frac{\Omega}{\omega}\bar{a}_5C + i\frac{\Gamma}{2}e^{i\bar{\sigma}T_1} = 0 \quad (4.2- 44)$$

$$-2iD_1C - i\frac{\bar{c}}{\omega}C - i\frac{\Omega}{\omega}\bar{a}_5A + \frac{\Gamma}{2}e^{i\bar{\sigma}T_1} = 0 \quad (4.2- 45)$$

With the solvability conditions fulfilled, the first order perturbation equations (4.2-35) and (4.2-36) are reduced to homogeneous linear oscillators becoming,

$$D_0^2 \bar{q}_{11} + \bar{q}_{11} = 0 \quad (4.2- 46)$$

$$D_0^2 \bar{q}_{21} + \bar{q}_{21} = 0 \quad (4.2- 47)$$

Trial solutions of equations (4.2-46) and (4.2-47) are taken by stating them in the following assumed polar form,

$$\bar{q}_{11} = E(T_1, T_2) e^{iT_0} + \bar{E}(T_1, T_2) e^{-iT_0} \quad (4.2- 48)$$

$$\bar{q}_{21} = F(T_1, T_2) e^{iT_0} + \bar{F}(T_1, T_2) e^{-iT_0} \quad (4.2- 49)$$

which, upon substituting into equations (4.2-46) and (4.2-47) give the particular solutions as,

$$\bar{q}_{11} = 0 \quad (4.2- 50)$$

$$\bar{q}_{21} = 0 \quad (4.2- 51)$$

The solutions to the first order perturbation equations are null because all terms in the right hand sides of the equations (4.2-35) and (4.2-36) are secular and have been removed.

4.3.4 Modulation of First Order Perturbation Equations

In solving equations (4.2-44) and (4.2-45) the complex amplitudes A and C can conveniently be expressed in polar form,

$$A = \frac{1}{2} a e^{i\alpha_1}, C = \frac{1}{2} b e^{i\alpha_2} \quad (4.2- 52)$$

where, a and b are amplitudes and α_1 and α_2 are the associated phase angles and are real valued functions of (T_1, T_2) . The physical reasoning behind this is so that real amplitude and phase quantities can be obtained. Substituting these

forms into equations (4.2-44) and (4.2-45), and then separating out the real and imaginary parts of the resulting equations, leads to a set of modulation equations, sometimes known as the slow-time solvability equations which can be stated here as,

$$\left(\bar{\sigma} - \gamma_1'\right)a - \frac{\Omega \bar{a}_5}{2\omega} b \text{Sin} \psi_1 = \frac{\Gamma}{2} \text{Sin} \gamma_1 \quad (4.2- 53)$$

$$a' + \frac{\bar{c}}{2\omega} a - \frac{\Omega \bar{a}_5}{2\omega} b \text{Cos} \psi_1 = \frac{\Gamma}{2} \text{Cos} \gamma_1 \quad (4.2- 54)$$

$$\left(\bar{\sigma} - \gamma_2'\right)b + \frac{\Omega \bar{a}_5}{2\omega} a \text{Sin} \psi_2 = -\frac{\Gamma}{2} \text{Cos} \gamma_2 \quad (4.2- 55)$$

$$b' + \frac{\bar{c}}{2\omega} b + \frac{\Omega \bar{a}_5}{2\omega} a \text{Cos} \psi_2 = \frac{\Gamma}{2} \text{Sin} \gamma_2 \quad (4.2- 56)$$

where,

$$\gamma_1 = \bar{\sigma} T_1 - \alpha_1; \quad \gamma_2 = \bar{\sigma} T_1 - \alpha_2; \quad \psi_1 = \alpha_2 - \alpha_1; \quad \psi_2 = \alpha_1 - \alpha_2 \quad (4.2- 57)$$

and the prime is used to indicate differentiation with respect to the slow-time scale T_1 . The form of equations (4.2-53) to (4.2-56) renders the system autonomous i.e. one in which T_1 does not appear explicitly because of the use of equations (4.2-58). For steady-state conditions, the slowly varying amplitudes and phases are set to zero, thus,

$$a' = b' = \gamma_1' = \gamma_2' = 0 \quad (4.2- 58)$$

This is done on the basis that the dependence on the slow time-scale T_1 provides a reasonable justification for doing this. In order to obtain the steady-state solutions, it is necessary to differentiate equations (4.2-57) with respect to T_1 leading to,

$$\alpha_1' = \bar{\sigma} - \gamma_1'; \quad \alpha_2' = \bar{\sigma} - \gamma_2' \quad (4.2- 59), (4.2- 60)$$

Substituting equations (4.2-58) to (4.2-60) into equations (4.2-53) to (4.2-56) generates the steady-state solutions, which correspond to the singular points of equations (4.2-53) to (4.2-56); that is, they correspond to the solutions of

$$\bar{\sigma}a - \frac{\Omega\bar{a}_5}{2\omega} b \text{Sin}\psi_1 = \frac{\Gamma}{2} \text{Sin}\gamma_1 \quad (4.2- 61)$$

$$\frac{\bar{c}}{2\omega} a - \frac{\Omega\bar{a}_5}{2\omega} b \text{Cos}\psi_1 = \frac{\Gamma}{2} \text{Cos}\gamma_1 \quad (4.2- 62)$$

$$\bar{\sigma}b - \frac{\Omega\bar{a}_5}{2\omega} a \text{Sin}\psi_2 = -\frac{\Gamma}{2} \text{Cos}\gamma_2 \quad (4.2- 63)$$

$$\frac{\bar{c}}{2\omega} b + \frac{\Omega\bar{a}_5}{2\omega} a \text{Cos}\psi_2 = \frac{\Gamma}{2} \text{Sin}\gamma_2 \quad (4.2- 64)$$

Squaring and adding equations (4.2-61) and (4.2-62), and (4.2-63) and (4.2-64) and rearranging leads to equations (4.2-65) and (4.2-66) which give the amplitudes of response a and b as functions of the detuning parameter $\bar{\sigma}$. These are the frequency-response equations which is a measure of deviation from the perfect forced resonance condition. These are first order results and they miss the cubic nonlinearity term which is a second order perturbation phenomena.

$$\bar{\sigma} = \pm \sqrt{\left(\frac{\Gamma}{2a}\right)^2 + \left(\frac{\Omega\bar{a}_5 b}{2\omega a}\right)^2 - \left(\frac{\bar{c}}{2\omega}\right)^2 + \frac{\Gamma\Omega\bar{a}_5 b}{2\omega a^2}} \quad (4.2- 65)$$

$$\bar{\sigma} = \pm \sqrt{\left(\frac{\Gamma}{2b}\right)^2 + \left(\frac{\Omega\bar{a}_5 a}{2\omega b}\right)^2 - \left(\frac{\bar{c}}{2\omega}\right)^2 + \frac{\Gamma\Omega\bar{a}_5 a}{2\omega b^2}} \quad (4.2- 66)$$

4.3.5 Second Order Perturbation Equations

Going back to the second order perturbation equations (4.2-33) and (4.2-34) and appropriately substituting the particular solutions of the first order equations (4.2-50) and (4.2-51) leads to these final forms for the second order perturbation equations ,

$$D_0^2 \bar{q}_{12} + \bar{q}_{12} = e^{iT_0} \left(\begin{array}{l} -2iD_2 A + 2iD_2 \bar{A} e^{-2iT_0} - D_1^2 A - D_1^2 \bar{A} e^{-2iT_0} \\ -\frac{\bar{c}}{\omega} D_1 A - \frac{\bar{c}}{\omega} D_1 \bar{A} e^{-2iT_0} + \frac{\Omega\bar{a}_5}{\omega} D_1 C + \frac{\Omega\bar{a}_5}{\omega} D_1 \bar{C} e^{-2iT_0} \\ -\frac{\hat{b}}{\omega^2} A^3 e^{2iT_0} - \frac{3\hat{b}}{\omega^2} A^2 \bar{A} - \frac{3\hat{b}}{\omega^2} A \bar{A}^2 e^{-2iT_0} - \frac{\hat{b}}{\omega^2} \bar{A}^3 e^{-4iT_0} \end{array} \right) \quad (4.2- 67)$$

$$D_0^2 \bar{q}_{22} + \bar{q}_{22} = e^{iT_0} \begin{pmatrix} -2iD_2 C + 2iD_2 \bar{C} e^{-2iT_0} - D_1^2 C - D_1^2 \bar{C} e^{-2iT_0} \\ -\frac{\bar{c}}{\omega} D_1 C - \frac{\bar{c}}{\omega} D_1 \bar{C} e^{-2iT_0} - \frac{\Omega \bar{a}_5}{\omega} D_1 A - \frac{\Omega \bar{a}_5}{\omega} D_1 \bar{A} e^{-2iT_0} \\ -\frac{\hat{b}}{\omega^2} C^3 e^{2iT_0} - \frac{3\hat{b}}{\omega^2} C^2 \bar{C} - \frac{3\hat{b}}{\omega^2} C \bar{C}^2 e^{-2iT_0} - \frac{\hat{b}}{\omega^2} \bar{C}^3 e^{-4iT_0} \end{pmatrix} \quad (4.2-68)$$

4.3.6 Secular Terms from the Second Order Perturbation Equations

Once again considering terms proportional to e^{iT_0} in equations (4.2-67) and (4.2-68), we get a pair of secular terms equations representing the solvability conditions.

$$-2iD_2 A - D_1^2 A - \frac{\bar{c}}{\omega} D_1 A + \frac{\Omega \bar{a}_5}{\omega} D_1 C - \frac{3\hat{b}}{\omega^2} A^2 \bar{A} = 0 \quad (4.2-69)$$

$$-2iD_2 C - D_1^2 C - \frac{\bar{c}}{\omega} D_1 C - \frac{\Omega \bar{a}_5}{\omega} D_1 A - \frac{3\hat{b}}{\omega^2} C^2 \bar{C} = 0 \quad (4.2-70)$$

Also, considering terms proportional to e^{-2iT_0} in equations (4.2-67) and (4.2-68), we get another set of secular terms equations representing the solvability conditions.

$$2iD_2 \bar{A} - D_1^2 \bar{A} - \frac{\bar{c}}{\omega} D_1 \bar{A} + \frac{\Omega \bar{a}_5}{\omega} D_1 \bar{C} - \frac{3\hat{b}}{\omega^2} A \bar{A}^2 = 0 \quad (4.2-71)$$

$$2iD_2 \bar{C} - D_1^2 \bar{C} - \frac{\bar{c}}{\omega} D_1 \bar{C} - \frac{\Omega \bar{a}_5}{\omega} D_1 \bar{A} - \frac{3\hat{b}}{\omega^2} C \bar{C}^2 = 0 \quad (4.2-72)$$

With the solvability conditions fulfilled, the second order perturbation equations (4.2-67) and (4.2-68) become,

$$D_0^2 \bar{q}_{12} + \bar{q}_{12} = -\frac{\hat{b}}{\omega^2} A^3 e^{3iT_0} - \frac{\hat{b}}{\omega^2} \bar{A}^3 e^{-3iT_0} \quad (4.2-73)$$

$$D_0^2 \bar{q}_{22} + \bar{q}_{22} = -\frac{\hat{b}}{\omega^2} C^3 e^{3iT_0} - \frac{\hat{b}}{\omega^2} \bar{C}^3 e^{-3iT_0} \quad (4.2-74)$$

Hence, the particular solutions for the second order perturbation equations shown in terms of the complex amplitudes A and C after removing secular terms are as follows,

$$\bar{q}_{12} = \frac{\hat{b}}{8\omega^2} A^3 e^{3iT_0} + \frac{\hat{b}}{8\omega^2} \bar{A}^3 e^{-3iT_0} \quad (4.2-75)$$

$$\bar{q}_{22} = \frac{\hat{b}}{8\omega^2} C^3 e^{3iT_0} + \frac{\hat{b}}{8\omega^2} \bar{C}^3 e^{-3iT_0} \quad (4.2-76)$$

4.3.7 Analysis of the Second Order Solvability Equations

The second order solvability equations (4.2-69) and (4.2-70) contain the terms $D_1^2 A$ and $D_1^2 C$, and going back to the solvability conditions of the first order perturbation equations (4.2-44) and (4.2-45) and differentiating with respect to T_1 and rearranging leads to expressions for these terms,

$$D_1^2 A = -\frac{\bar{c}}{2\omega} D_1 A + \frac{\Omega}{2\omega} \bar{a}_5 D_1 C + i\bar{\sigma} \frac{\Gamma}{4} e^{i\bar{\sigma}T_1} \quad (4.2-77)$$

$$D_1^2 C = -\frac{\bar{c}}{2\omega} D_1 C - \frac{\Omega}{2\omega} \bar{a}_5 D_1 A + \bar{\sigma} \frac{\Gamma}{4} e^{i\bar{\sigma}T_1} \quad (4.2-78)$$

Now, substituting the differentiated first order solvability equations, (4.2-77) and (4.2-78), into the solvability conditions of the second order perturbation equations, (4.2-69) and (4.2-70), and rearranging gives,

$$\begin{aligned} D_2 A = & \frac{\bar{c}}{4i\omega} \left(-\frac{\bar{c}}{2\omega} A + \frac{\Omega}{2\omega} \bar{a}_5 C + \frac{\Gamma}{4} e^{i\bar{\sigma}T_1} \right) \\ & - \frac{\Omega \bar{a}_5}{4i\omega} \left(-\frac{\bar{c}}{2\omega} C + \frac{\Omega}{2\omega} \bar{a}_5 A + \frac{\Gamma}{4i} e^{i\bar{\sigma}T_1} \right) \\ & - \bar{\sigma} \frac{\Gamma}{8} e^{i\bar{\sigma}T_1} - \frac{\bar{c}}{2i\omega} \left(-\frac{\bar{c}}{2\omega} A + \frac{\Omega}{2\omega} \bar{a}_5 C + \frac{\Gamma}{4} e^{i\bar{\sigma}T_1} \right) \\ & + \frac{\Omega \bar{a}_5}{2i\omega} \left(-\frac{\bar{c}}{2\omega} C + \frac{\Omega}{2\omega} \bar{a}_5 A + \frac{\Gamma}{4i} e^{i\bar{\sigma}T_1} \right) - \frac{3\hat{b}}{2i\omega^2} A^2 \bar{A} \end{aligned} \quad (4.2-79)$$

$$\begin{aligned}
 D_2 C = & \frac{\bar{c}}{4i\omega} \left(-\frac{\bar{c}}{2\omega} C + \frac{\Omega}{2\omega} \bar{a}_5 A + \frac{\Gamma}{4i} e^{i\bar{\sigma}T_1} \right) \\
 & + \frac{\Omega \bar{a}_5}{4i\omega} \left(-\frac{\bar{c}}{2\omega} A + \frac{\Omega}{2\omega} \bar{a}_5 C + \frac{\Gamma}{4} e^{i\bar{\sigma}T_1} \right) \\
 & - \bar{\sigma} \frac{\Gamma}{8i} e^{i\bar{\sigma}T_1} - \frac{\bar{c}}{2i\omega} \left(-\frac{\bar{c}}{2\omega} C - \frac{\Omega}{2\omega} \bar{a}_5 A + \frac{\Gamma}{i4} e^{i\bar{\sigma}T_1} \right) \\
 & - \frac{\Omega \bar{a}_5}{2i\omega} \left(-\frac{\bar{c}}{2\omega} A + \frac{\Omega}{2\omega} \bar{a}_5 C + \frac{\Gamma}{4} e^{i\bar{\sigma}T_1} \right) - \frac{3\hat{b}}{2i\omega^2} C^2 \bar{C}
 \end{aligned} \tag{4.2- 80}$$

The time variance of the complex amplitudes to second perturbation order with respect to the original time scale t can be expressed using a form of reconstituted derivatives. Thus,

$$\frac{dA}{dt} = \varepsilon D_1 A + \varepsilon^2 D_2 A \tag{4.2- 81}$$

$$\frac{dC}{dt} = \varepsilon D_1 C + \varepsilon^2 D_2 C \tag{4.2- 82}$$

Substituting the first order perturbation equations (4.2-44) and (4.2-45) and the solvability conditions of the second order perturbation equations (4.2-79) and (4.2-80) into the equations (4.2-81) and (4.2-82) leads to,

$$\begin{aligned}
 \frac{dA}{dt} = & -\frac{\varepsilon \bar{c}}{2\omega} A + \frac{\varepsilon \Omega \bar{a}_5}{2\omega} C + \frac{\varepsilon \Gamma}{4} e^{i\varepsilon \bar{\sigma} T_0} - \frac{\varepsilon^2 \bar{c}^2}{8i\omega^2} A + \frac{\varepsilon^2 \Omega \bar{a}_5 \bar{c}}{8i\omega^2} C \\
 & + \frac{\varepsilon^2 \bar{c} \Gamma}{16i\omega} e^{i\varepsilon \bar{\sigma} T_0} + \frac{\varepsilon^2 \Omega \bar{c} \bar{a}_5}{8i\omega^2} C - \frac{\varepsilon^2 \Omega^2 \bar{a}_5^2}{8i\omega^2} A + \frac{\varepsilon^2 \Omega \bar{a}_5 \Gamma}{16\omega} e^{i\varepsilon \bar{\sigma} T_0} \\
 & - \varepsilon^2 \bar{\sigma} \frac{\Gamma}{8} e^{i\varepsilon \bar{\sigma} T_0} + \frac{\varepsilon^2 \bar{c}^2}{4i\omega^2} A - \frac{\varepsilon^2 \Omega \bar{a}_5 \bar{c}}{4i\omega^2} C - \frac{\varepsilon^2 \bar{c} \Gamma}{8i\omega} e^{i\varepsilon \bar{\sigma} T_0} \\
 & - \frac{\varepsilon^2 \Omega \bar{c} \bar{a}_5}{4i\omega^2} C - \frac{\varepsilon^2 \Omega^2 \bar{a}_5^2}{4i\omega^2} A - \frac{\varepsilon^2 \Omega \bar{a}_5 \Gamma}{8\omega} e^{i\varepsilon \bar{\sigma} T_0} - \frac{\varepsilon^2 3\hat{b}}{2i\omega^2} A^2 \bar{A}
 \end{aligned} \tag{4.2- 83}$$

$$\begin{aligned}
 \frac{dC}{dt} = & -\frac{\varepsilon \bar{c}}{2\omega} C - \frac{\varepsilon \Omega \bar{a}_5}{2\omega} A + \frac{\varepsilon \Gamma}{4i} e^{i\varepsilon \bar{\sigma} T_0} - \frac{\varepsilon^2 \bar{c}^2}{8i\omega^2} C - \frac{\varepsilon^2 \Omega \bar{a}_5 \bar{c}}{8i\omega^2} A \\
 & - \frac{\varepsilon^2 \bar{c} \Gamma}{16\omega} e^{i\varepsilon \bar{\sigma} T_0} - \frac{\varepsilon^2 \Omega \bar{c} \bar{a}_5}{8i\omega^2} A + \frac{\varepsilon^2 \Omega^2 \bar{a}_5^2}{8i\omega^2} C + \frac{\varepsilon^2 \Omega \bar{a}_5 \Gamma}{16i\omega} e^{i\varepsilon \bar{\sigma} T_0} \\
 & - \varepsilon^2 \bar{\sigma} \frac{\Gamma}{8i} e^{i\varepsilon \bar{\sigma} T_0} + \frac{\varepsilon^2 \bar{c}^2}{4i\omega^2} C + \frac{\varepsilon^2 \Omega \bar{a}_5 \bar{c}}{4i\omega^2} A + \frac{\varepsilon^2 \bar{c} \Gamma}{8\omega} e^{i\varepsilon \bar{\sigma} T_0} \\
 & + \frac{\varepsilon^2 \Omega \bar{c} \bar{a}_5}{4i\omega^2} A - \frac{\varepsilon^2 \Omega^2 \bar{a}_5^2}{4i\omega^2} C - \frac{\varepsilon^2 \Omega \bar{a}_5 \Gamma}{8i\omega} e^{i\varepsilon \bar{\sigma} T_0} - \frac{\varepsilon^2 3\hat{b}}{2i\omega^2} C^2 \bar{C}
 \end{aligned} \tag{4.2- 84}$$

In order to obtain amplitude and phase information within an autonomous representation we re-define the complex amplitudes A and C in this form

$$\begin{aligned} A &= ue^{i\varepsilon\bar{\sigma}t/2}; \quad \bar{A} = \bar{u}e^{-i\varepsilon\bar{\sigma}t/2} \\ C &= ve^{i\varepsilon\bar{\sigma}t/2}; \quad \bar{C} = \bar{v}e^{-i\varepsilon\bar{\sigma}t/2} \end{aligned} \quad (4.2-85)$$

where the substitutions for A and C admit the conditions $du/dt = dv/dt = 0$, as required for $A = A(T_1, T_2)$ and $C = C(T_1, T_2)$. Substituting the amplitude transformations of equation (4.2-85) into equations (4.2-83) and (4.2-84), and removing the common factor of $e^{i\varepsilon\bar{\sigma}t/2}$ leaves the equations in terms of \dot{u} and \dot{v} respectively and these produce autonomous equations in u, \bar{u}, v and \bar{v} giving

$$\begin{aligned} \dot{u} = & -\frac{\varepsilon\bar{c}}{2\omega}u + \frac{\varepsilon\Omega\bar{a}_5}{2\omega}v + \frac{\varepsilon\Gamma}{4}e^{i\varepsilon\bar{\sigma}t/2} - \varepsilon^2\bar{\sigma}\frac{\Gamma}{8}e^{i\varepsilon\bar{\sigma}t/2} + \frac{\varepsilon^2\bar{c}^2}{8i\omega^2}u \\ & - \frac{\varepsilon^2\bar{c}\Gamma}{16i\omega}e^{i\varepsilon\bar{\sigma}t/2} - \frac{\varepsilon^2\Omega\bar{c}\bar{a}_5}{4i\omega^2}v - \frac{\varepsilon^23\Omega^2\bar{a}_5^2}{8i\omega^2}u - \frac{\varepsilon^2\Omega\bar{a}_5\Gamma}{16\omega}e^{i\varepsilon\bar{\sigma}t/2} \\ & - \frac{\varepsilon^23\hat{b}}{2i\omega^2}u^2\bar{u} \end{aligned} \quad (4.2-86)$$

$$\begin{aligned} \dot{v} = & -\frac{\varepsilon\bar{c}}{2\omega}v - \frac{\varepsilon\Omega\bar{a}_5}{2\omega}u + \frac{\varepsilon\Gamma}{4i}e^{i\varepsilon\bar{\sigma}t/2} - \varepsilon^2\bar{\sigma}\frac{\Gamma}{8i}e^{i\varepsilon\bar{\sigma}t/2} + \frac{\varepsilon^2\bar{c}^2}{8i\omega^2}v \\ & + \frac{\varepsilon^2\bar{c}\Gamma}{16\omega}e^{i\varepsilon\bar{\sigma}t/2} + \frac{\varepsilon^2\Omega\bar{c}\bar{a}_5}{4i\omega^2}u - \frac{\varepsilon^2\Omega^2\bar{a}_5^2}{8i\omega^2}v - \frac{\varepsilon^2\Omega\bar{a}_5\Gamma}{16i\omega}e^{i\varepsilon\bar{\sigma}t/2} \\ & - \frac{\varepsilon^23\hat{b}}{2i\omega^2}v^2\bar{v} \end{aligned} \quad (4.2-87)$$

For a steady state solution \dot{u} and \dot{v} are taken to be zero resulting in the following equations, where the substitutions made in equations (4.2-10) and (4.2-11) have been reversed to recover the original parameters of equations (4.2-1) and (4.2-2).

$$\begin{aligned} & -\frac{\hat{c}}{2\omega}u + \frac{\Omega\hat{a}_5}{2\omega}v + \frac{\Gamma}{4}e^{i\varepsilon\bar{\sigma}t/2} - \bar{\sigma}\frac{\Gamma}{8}e^{i\varepsilon\bar{\sigma}t/2} + \frac{\hat{c}^2}{8i\omega^2}u \\ & - \frac{\hat{c}\Gamma}{16i\omega}e^{i\varepsilon\bar{\sigma}t/2} - \frac{\Omega\hat{c}\hat{a}_5}{4i\omega^2}v - \frac{3\Omega^2\hat{a}_5^2}{8i\omega^2}u - \frac{\Omega\hat{a}_5\Gamma}{16\omega}e^{i\varepsilon\bar{\sigma}t/2} - \frac{3\hat{b}}{2i\omega^2}u^2\bar{u} = 0 \end{aligned} \quad (4.2-88)$$

$$\begin{aligned}
 & -\frac{\hat{c}}{2\omega}v - \frac{\Omega\hat{a}_5}{2\omega}u + \frac{\Gamma}{4i}e^{i\varepsilon\bar{\sigma}t/2} - \bar{\sigma}\frac{\Gamma}{8i}e^{i\varepsilon\bar{\sigma}t/2} + \frac{\hat{c}^2}{8i\omega^2}v \\
 & + \frac{\hat{c}\Gamma}{16\omega}e^{i\varepsilon\bar{\sigma}t/2} + \frac{\Omega\hat{c}\hat{a}_5}{4i\omega^2}u - \frac{\Omega^2\hat{a}_5^2}{8i\omega^2}v - \frac{\Omega\hat{a}_5\Gamma}{16i\omega}e^{i\varepsilon\bar{\sigma}t/2} - \frac{3\hat{b}}{2i\omega^2}v^2\bar{v} = 0
 \end{aligned} \tag{4.2- 89}$$

In order to solve the equations (4.2-88) and (4.2-89) it is helpful to state the complex transformed amplitudes u , \bar{u} , v and \bar{v} in the following forms

$$\begin{aligned}
 u &= p + iq, & \bar{u} &= p - iq \\
 v &= r + is, & \bar{v} &= r - is
 \end{aligned} \tag{4.2- 90}$$

Therefore further substitution of equations (4.2-90) into (4.2-88) and (4.2-89) leads to further forms of these equations in which real and imaginary parts are explicit,

$$\begin{aligned}
 & -\frac{\hat{c}}{2\omega}p - i\frac{\hat{c}}{2\omega}q + \frac{\Omega\hat{a}_5}{2\omega}r + i\frac{\Omega\hat{a}_5}{2\omega}s + \frac{\Gamma}{4}e^{i\varepsilon\bar{\sigma}t/2} - \bar{\sigma}\frac{\Gamma}{8}e^{i\varepsilon\bar{\sigma}t/2} + \frac{\hat{c}^2}{8i\omega^2}p \\
 & + \frac{\hat{c}^2}{8\omega^2}q - \frac{\hat{c}\Gamma}{16i\omega}e^{i\varepsilon\bar{\sigma}t/2} - \frac{\Omega\hat{c}\hat{a}_5}{4i\omega^2}r - \frac{\Omega\hat{c}\hat{a}_5}{4\omega^2}s - \frac{3\Omega^2\hat{a}_5^2}{8i\omega^2}p - \frac{3\Omega^2\hat{a}_5^2}{8\omega^2}q \\
 & - \frac{\Omega\hat{a}_5\Gamma}{16\omega}e^{i\varepsilon\bar{\sigma}t/2} - \frac{3\hat{b}}{2i\omega^2}p^3 - \frac{3\hat{b}}{2\omega^2}p^2q - \frac{3\hat{b}}{2i\omega^2}pq^2 - \frac{3\hat{b}}{2\omega^2}q^3 = 0
 \end{aligned} \tag{4.2- 91}$$

$$\begin{aligned}
 & -\frac{\hat{c}}{2\omega}r - i\frac{\hat{c}}{2\omega}s - \frac{\Omega\hat{a}_5}{2\omega}p - i\frac{\Omega\hat{a}_5}{2\omega}q + \frac{\Gamma}{4i}e^{i\varepsilon\bar{\sigma}t/2} - \bar{\sigma}\frac{\Gamma}{8i}e^{i\varepsilon\bar{\sigma}t/2} \\
 & + \frac{\hat{c}^2}{8i\omega^2}r + \frac{\hat{c}^2}{8\omega^2}s + \frac{\hat{c}\Gamma}{16\omega}e^{i\varepsilon\bar{\sigma}t/2} + \frac{\Omega\hat{c}\hat{a}_5}{4i\omega^2}p + \frac{\Omega\hat{c}\hat{a}_5}{4\omega^2}q - \frac{\Omega^2\hat{a}_5^2}{8i\omega^2}r \\
 & - \frac{\Omega^2\hat{a}_5^2}{8\omega^2}s - \frac{\Omega\hat{a}_5\Gamma}{16i\omega}e^{i\varepsilon\bar{\sigma}t/2} - \frac{3\hat{b}}{2i\omega^2}r^3 - \frac{3\hat{b}}{2\omega^2}r^2s - \frac{3\hat{b}}{2i\omega^2}rs^2 - \frac{3\hat{b}}{2\omega^2}s^3 = 0
 \end{aligned} \tag{4.2- 92}$$

Separating out the real and imaginary terms leads to the steady-state amplitude and phase equations in p , q , r and s .

$$\begin{aligned}
 & -\frac{\hat{c}}{2\omega}p + \frac{\Omega\hat{a}_5}{2\omega}r + \frac{\Gamma}{4}\left(1 - \frac{\bar{\sigma}}{2} - \frac{\Omega\hat{a}_5}{4\omega}\right)\cos\phi + \frac{\hat{c}^2}{8\omega^2}q \\
 & - \frac{\hat{c}\Gamma}{16\omega}\sin\phi - \frac{\Omega\hat{c}\hat{a}_5}{4\omega^2}s - \frac{3\Omega^2\hat{a}_5^2}{8\omega^2}q - \frac{3\hat{b}}{2\omega^2}p^2q - \frac{3\hat{b}}{2\omega^2}q^3 = 0
 \end{aligned} \tag{4.2- 93}$$

$$-\frac{\hat{c}}{2\omega}q + \frac{\Omega\hat{a}_5}{2\omega}s + \frac{\Gamma}{4}\left(1 - \frac{\bar{\sigma}}{2} - \frac{\Omega\hat{a}_5}{4\omega}\right)\sin\phi + \frac{\hat{c}^2}{8\omega^2}p \quad (4.2-94)$$

$$-\frac{\hat{c}\Gamma}{16\omega}\cos\phi - \frac{\Omega\hat{c}\hat{a}_5}{4\omega^2}r - \frac{3\Omega^2\hat{a}_5^2}{8\omega^2}p - \frac{3\hat{b}}{2\omega^2}pq^2 - \frac{3\hat{b}}{2\omega^2}p^3 = 0$$

$$-\frac{\hat{c}}{2\omega}r - \frac{\Omega\hat{a}_5}{2\omega}p + \frac{\Gamma}{4}\left(1 - \frac{\bar{\sigma}}{2} - \frac{\Omega\hat{a}_5}{4\omega}\right)\sin\phi + \frac{\hat{c}^2}{8\omega^2}s \quad (4.2-95)$$

$$+\frac{\hat{c}\Gamma}{16\omega}\cos\phi + \frac{\Omega\hat{c}\hat{a}_5}{4\omega^2}q - \frac{\Omega^2\hat{a}_5^2}{8\omega^2}s - \frac{3\hat{b}}{2\omega^2}r^2s - \frac{3\hat{b}}{2\omega^2}s^3 = 0$$

$$-\frac{\hat{c}}{2\omega}s - \frac{\Omega\hat{a}_5}{2\omega}q + \frac{\Gamma}{4}\left(1 - \frac{\bar{\sigma}}{2} - \frac{\Omega\hat{a}_5}{4\omega}\right)\cos\phi + \frac{\hat{c}^2}{8\omega^2}r \quad (4.2-96)$$

$$+\frac{\hat{c}\Gamma}{16\omega}\sin\phi + \frac{\Omega\hat{c}\hat{a}_5}{4\omega^2}p - \frac{\Omega^2\hat{a}_5^2}{8\omega^2}r - \frac{3\hat{b}}{2\omega^2}rs^2 - \frac{3\hat{b}}{2\omega^2}r^3 = 0$$

Equations (4.2-93) to (4.2-96) can be expressed more compactly, thus,

$$m\cos\phi - n\sin\phi + \eta_1 = 0 \quad (4.2-97)$$

$$m\sin\phi - n\cos\phi + \eta_2 = 0 \quad (4.2-98)$$

$$m\sin\phi + n\cos\phi + \eta_3 = 0 \quad (4.2-99)$$

$$m\cos\phi + n\sin\phi + \eta_4 = 0 \quad (4.2-100)$$

where, m , n , η_1 , η_2 , η_3 and η_4 are defined as,

$$m = \frac{\Gamma}{4}\left(1 - \frac{\bar{\sigma}}{2} - \frac{\Omega\hat{a}_5}{4\omega}\right) \quad (4.2-101)$$

$$n = \frac{\hat{c}\Gamma}{16\omega} \quad (4.2-102)$$

$$\eta_1 = -\frac{\hat{c}}{2\omega}p + \frac{\Omega\hat{a}_5}{2\omega}r + \frac{\hat{c}^2}{8\omega^2}q - \frac{\Omega\hat{c}\hat{a}_5}{4\omega^2}s - \frac{3\Omega^2\hat{a}_5^2}{8\omega^2}q - \frac{3\hat{b}}{2\omega^2}p^2q - \frac{3\hat{b}}{2\omega^2}q^3 \quad (4.2-103)$$

$$\eta_2 = -\frac{\hat{c}}{2\omega}q + \frac{\Omega\hat{a}_5}{2\omega}s + \frac{\hat{c}^2}{8\omega^2}p - \frac{\Omega\hat{c}\hat{a}_5}{4\omega^2}r - \frac{3\Omega^2\hat{a}_5^2}{8\omega^2}p - \frac{3\hat{b}}{2\omega^2}pq^2 - \frac{3\hat{b}}{2\omega^2}p^3 \quad (4.2-104)$$

$$\eta_3 = -\frac{\hat{c}}{2\omega}r - \frac{\Omega\hat{a}_5}{2\omega}p + \frac{\hat{c}^2}{8\omega^2}s + \frac{\Omega\hat{c}\hat{a}_5}{4\omega^2}q - \frac{\Omega^2\hat{a}_5^2}{8\omega^2}s - \frac{3\hat{b}}{2\omega^2}r^2s - \frac{3\hat{b}}{2\omega^2}s^3 \quad (4.2-105)$$

$$\eta_4 = -\frac{\hat{c}}{2\omega} s - \frac{\Omega \hat{a}_5}{2\omega} q + \frac{\hat{c}^2}{8\omega^2} r + \frac{\Omega \hat{c} \hat{a}_5}{4\omega^2} p - \frac{\Omega^2 \hat{a}_5^2}{8\omega^2} r - \frac{3\hat{b}}{2\omega^2} r s^2 - \frac{3\hat{b}}{2\omega^2} r^3 \quad (4.2-106)$$

Adding equations (4.2-97) and (4.2-100) we get,

$$2m \cos \phi + \eta_1 + \eta_4 = 0 \quad (4.2-107)$$

Then, by adding equations (4.2-98) and (4.2-99) it can be shown that

$$2m \sin \phi + \eta_2 + \eta_3 = 0 \quad (4.2-108)$$

Squaring and adding equations (4.2-107) and (4.2-108) and rearranging leads to the equation (4.2-109) describing the relationship between excitation amplitude, Γ , detuning parameter, $\bar{\sigma}$, and the system's responses.

$$\bar{\sigma} = 2 - \frac{\Omega \hat{a}_5}{2\omega} \pm \frac{4}{\Gamma} \sqrt{(\eta_1 + \eta_4)^2 + (\eta_2 + \eta_3)^2} \quad (4.2-109)$$

4.3.8 General Solutions of the Equations of Motion (4.2-1) and (4.2-2)

After finding the solvability equations a return is made to the main analysis to substitute the zeroth order perturbation solutions, equations (4.2-29) and (4.2-30), the first order perturbation solutions, equations (4.2-50) and (4.2-51), and the second order perturbation solutions, equations (4.2-75) and (4.2-76) into the approximated solutions of the equations (4.2-16) and (4.2-17) to get the full time-domain solutions to the equations of motion (4.2-1) and (4.2-2). We then substitute the re-defined A and C of equation (4.2-85) and further substitute equation (4.2-90) to get the full time-domain solutions in the original parameters of equations of motion (4.2-1) and (4.2-2) as

$$\begin{aligned} \bar{q}_1 = & 2p \cos\left(\frac{\Omega t}{2\omega}\right) - 2q \sin\left(\frac{\Omega t}{2\omega}\right) + \frac{\hat{b}}{4\omega^2} p^3 \cos\left(\frac{3\Omega t}{2\omega}\right) \\ & - \frac{3\hat{b}}{4\omega^2} p^2 q \sin\left(\frac{3\Omega t}{2\omega}\right) - \frac{3\hat{b}}{4\omega^2} p q^2 \cos\left(\frac{3\Omega t}{2\omega}\right) + \frac{\hat{b}}{4\omega^2} q^3 \sin\left(\frac{3\Omega t}{2\omega}\right) \end{aligned} \quad (4.2-110)$$

$$\begin{aligned} \bar{q}_2 = & 2r \cos\left(\frac{\Omega t}{2\omega}\right) - 2s \sin\left(\frac{\Omega t}{2\omega}\right) + \frac{\hat{b}}{4\omega^2} r^3 \cos\left(\frac{3\Omega t}{2\omega}\right) \\ & - \frac{3\hat{b}}{4\omega^2} r^2 s \sin\left(\frac{3\Omega t}{2\omega}\right) - \frac{3\hat{b}}{4\omega^2} r s^2 \cos\left(\frac{3\Omega t}{2\omega}\right) + \frac{\hat{b}}{4\omega^2} s^3 \sin\left(\frac{3\Omega t}{2\omega}\right) \end{aligned} \quad (4.2-111)$$

We likewise applied the Method of Multiple Scales solutions to the equations of motion with axial force terms included. The axial forces are introduced into the system as time-dependent excitations. The excitations appear as coefficients in the equations of motion. Since the excitations when they are time-dependent appear as parameters in the equations, these excitations are called parametric excitations. A small parametric excitation can produce a large response when the frequency of the excitation is close to twice one of the natural frequencies of the system (principal parametric resonance), (Nayfeh *et.al.*, (1995)). The parametric excitations are introduced into the system to investigate the interactions between forced vibrations and the parametric excitations. Therefore, applying the method of multiple scales to the equations of motion with axial parametric excitation terms in the form $F_{act} \cos(\Omega_2 t) q_i$ included, where $i=1,2$, $F_{act} q_i$ are the force terms in equations (3.2-85) and (3.2-86) in chapter 3, and Ω_2 is the parametric excitation frequency for the system operating in principal parametric resonance, we get,

$$\begin{aligned}
 \bar{q}_1 = & 2p \cos\left(\frac{\Omega t}{2\omega}\right) - 2q \sin\left(\frac{\Omega t}{2\omega}\right) + \frac{\hat{b}}{4\omega^2} p^3 \cos\left(\frac{3\Omega t}{2\omega}\right) - \frac{3\hat{b}}{4\omega^2} p^2 q \sin\left(\frac{3\Omega t}{2\omega}\right) \\
 & - \frac{3\hat{b}}{4\omega^2} p q^2 \cos\left(\frac{3\Omega t}{2\omega}\right) + \frac{\hat{b}}{4\omega^2} q^3 \sin\left(\frac{3\Omega t}{2\omega}\right) - \frac{2\hat{F}_{act} p}{2\Omega_2^2 + 4\Omega_2 \omega} \cos\left(\frac{5\Omega_2 t}{4\omega}\right) \\
 & + \frac{2\hat{F}_{act} q}{2\Omega_2^2 + 4\Omega_2 \omega} \sin\left(\frac{5\Omega_2 t}{4\omega}\right) - \frac{2\hat{F}_{act} \Omega_2 \hat{c} k p}{2\Omega_2^2 \omega^2 + 4\Omega_2 \omega^3} \sin\left(\frac{5\Omega_2 t}{4\omega}\right) \\
 & - \frac{2\hat{F}_{act} \Omega_2 \hat{c} k q}{2\Omega_2^2 \omega^2 + 4\Omega_2 \omega^3} \cos\left(\frac{5\Omega_2 t}{4\omega}\right) + \frac{2\hat{F}_{act} \hat{c} k p}{2\Omega_2^2 \omega + 4\Omega_2 \omega^2} \sin\left(\frac{5\Omega_2 t}{4\omega}\right) \\
 & - \frac{2\hat{F}_{act} \hat{c} k q}{2\Omega_2^2 \omega + 4\Omega_2 \omega^2} \cos\left(\frac{5\Omega_2 t}{4\omega}\right) + \frac{2\hat{F}_{act} \Omega \Omega_2 \hat{a}_5 k r}{2\Omega_2^2 \omega^2 + 4\Omega_2 \omega^3} \sin\left(\frac{5\Omega_2 t}{4\omega}\right) \\
 & + \frac{2\hat{F}_{act} \Omega \Omega_2 \hat{a}_5 k s}{2\Omega_2^2 \omega^2 + 4\Omega_2 \omega^3} \cos\left(\frac{5\Omega_2 t}{4\omega}\right) + \frac{2\hat{F}_{act} \Omega \hat{a}_5 k r}{2\Omega_2^2 \omega + 4\Omega_2 \omega^2} \sin\left(\frac{5\Omega_2 t}{4\omega}\right) \\
 & + \frac{2\hat{F}_{act} \Omega \hat{a}_5 k s}{2\Omega_2^2 \omega + 4\Omega_2 \omega^2} \cos\left(\frac{5\Omega_2 t}{4\omega}\right) - \frac{2\hat{F}_{act} Q p}{4\Omega_2^2 \omega^2 + 8\Omega_2 \omega^3} \cos\left(\frac{9\Omega_2 t}{4\omega}\right) \\
 & + \frac{2\hat{F}_{act} Q q}{4\Omega_2^2 \omega^2 + 8\Omega_2 \omega^3} \sin\left(\frac{9\Omega_2 t}{4\omega}\right)
 \end{aligned} \tag{4.2- 112}$$

$$\begin{aligned}
 \bar{q}_2 = & 2r \cos\left(\frac{\Omega t}{2\omega}\right) - 2s \sin\left(\frac{\Omega t}{2\omega}\right) + \frac{\hat{b}}{4\omega^2} r^3 \cos\left(\frac{3\Omega t}{2\omega}\right) - \frac{3\hat{b}}{4\omega^2} r^2 s \sin\left(\frac{3\Omega t}{2\omega}\right) \\
 & - \frac{3\hat{b}}{4\omega^2} r s^2 \cos\left(\frac{3\Omega t}{2\omega}\right) + \frac{\hat{b}}{4\omega^2} s^3 \sin\left(\frac{3\Omega t}{2\omega}\right) - \frac{2\hat{F}_{act} r}{2\Omega_2^2 + 4\Omega_2 \omega} \cos\left(\frac{5\Omega_2 t}{4\omega}\right) \\
 & + \frac{2\hat{F}_{act} s}{2\Omega_2^2 + 4\Omega_2 \omega} \sin\left(\frac{5\Omega_2 t}{4\omega}\right) - \frac{2\hat{F}_{act} \Omega_2 \hat{c} k r}{2\Omega_2^2 \omega^2 + 4\Omega_2 \omega^3} \sin\left(\frac{5\Omega_2 t}{4\omega}\right) \\
 & - \frac{2\hat{F}_{act} \Omega_2 \hat{c} k s}{2\Omega_2^2 \omega^2 + 4\Omega_2 \omega^3} \cos\left(\frac{5\Omega_2 t}{4\omega}\right) - \frac{2\hat{F}_{act} \hat{c} k r}{2\Omega_2^2 \omega + 4\Omega_2 \omega^2} \sin\left(\frac{5\Omega_2 t}{4\omega}\right) \\
 & - \frac{2\hat{F}_{act} \hat{c} k s}{2\Omega_2^2 \omega + 4\Omega_2 \omega^2} \cos\left(\frac{5\Omega_2 t}{4\omega}\right) - \frac{2\hat{F}_{act} \Omega \Omega_2 \hat{a}_5 k p}{2\Omega_2^2 \omega^2 + 4\Omega_2 \omega^3} \sin\left(\frac{5\Omega_2 t}{4\omega}\right) \\
 & - \frac{2\hat{F}_{act} \Omega \Omega_2 \hat{a}_5 k q}{2\Omega_2^2 \omega^2 + 4\Omega_2 \omega^3} \cos\left(\frac{5\Omega_2 t}{4\omega}\right) - \frac{2\hat{F}_{act} \Omega \hat{a}_5 k p}{2\Omega_2^2 \omega + 4\Omega_2 \omega^2} \sin\left(\frac{5\Omega_2 t}{4\omega}\right) \\
 & - \frac{2\hat{F}_{act} \Omega \hat{a}_5 k q}{2\Omega_2^2 \omega + 4\Omega_2 \omega^2} \cos\left(\frac{5\Omega_2 t}{4\omega}\right) - \frac{2\hat{F}_{act} Q r}{4\Omega_2^2 \omega^2 + 8\Omega_2 \omega^3} \cos\left(\frac{9\Omega_2 t}{4\omega}\right) \\
 & + \frac{2\hat{F}_{act} Q s}{4\Omega_2^2 \omega^2 + 8\Omega_2 \omega^3} \sin\left(\frac{9\Omega_2 t}{4\omega}\right)
 \end{aligned} \tag{4.2- 113}$$

$$\text{where, } k = \left(\frac{1}{-\frac{\Omega_2^2}{\omega^2} - \frac{2\Omega_2}{\omega}} \right) \text{ and } Q = \left(\frac{1}{-\frac{4\Omega_2^2}{\omega^2} - \frac{4\Omega_2}{\omega}} \right)$$

From the standpoint of these solvability and general solutions, the next section shows the results of the frequency-response and amplitude plots for the Models of equations with and without parametric force terms under appropriately varying conditions and parameters.

4.3.9 Multiple Scales Results

Four algebraic solutions for the amplitudes and phases, equations (4.2-93) to (4.2-96) were derived from the real and imaginary parts of the secular terms equations for perturbations \bar{q}_{12} and \bar{q}_{22} . The function of the secular terms equations is to remove those terms from the right hand sides of the perturbation equations that would otherwise have invalidated the uniformity of the power series. The secular terms equations are then processed separately in order to find the steady-state amplitudes of the solutions. After this, a return is made to the main analysis to find the particular solutions for the system variables (i.e. co-ordinates), into which the analytical forms that have been found for the steady state amplitudes can be substituted to give the complete solutions. In order to get the required results, *Mathematica*TM code was then used to solve numerically for \bar{q}_1 and \bar{q}_2 within equations (4.2-110) and (4.2-111) and those within Models B equations with the parametric force terms, equations (4.2-112) and (4.2-113). To obtain the values for p, q, r and s *Mathematica*TM code was used to solve the equations (4.2-93) to (4.2-96) simultaneously. (See Appendices B.1 and B.2 for the solutions). The results obtained are in the time domain and are transformed into the frequency domain by running the *Mathematica*TM code several times for a range of frequency values from 243.2 rad/s to 252.8 rad/s to obtain a list of amplitude values. While going through all the data individually one selects that portion of the amplitude values where the values are in steady state condition, for the amplitude response plots.

Graphs of amplitude versus forcing frequency Ω , i.e., the frequency of the excitation are plotted for some varying parameter values and for the case where the parametric force term is included in the equations. Table 4-1 represents the values of the constants for the graphs in Figures 4-1 to 4-4. These values are obtained from the coefficients of the modelled equations in Chapter 3 using the experimental set up and from the Appendices A3 and A4.

Parameters			
Stiffness (Linear) k	Damping Coefficient c	Actuator Force F_{act}	Stiffness (Cubic) b
$[Nm^{-1}]$	$[Nsm^{-1}]$	$[N]$	$[m^{-2}s^{-2}]$
38379	13.6 15	532	5.05×10^9

Coefficient $a_5 = 0.001 \text{ kg}$; Resonance frequency: $\Omega = 248.8 \text{ rad / s}$;
 Parametric frequency: $\Omega_2 = 497.6 \text{ rad / s}$; Modal mass: $m = 0.62 \text{ kg}$;
 Mass unbalance: $m_u = 0.004 \text{ kg}$

Table 4- 1: Data of graphs plotted

4.3.9.1 Amplitude Response Plot – without Parametric Force Term

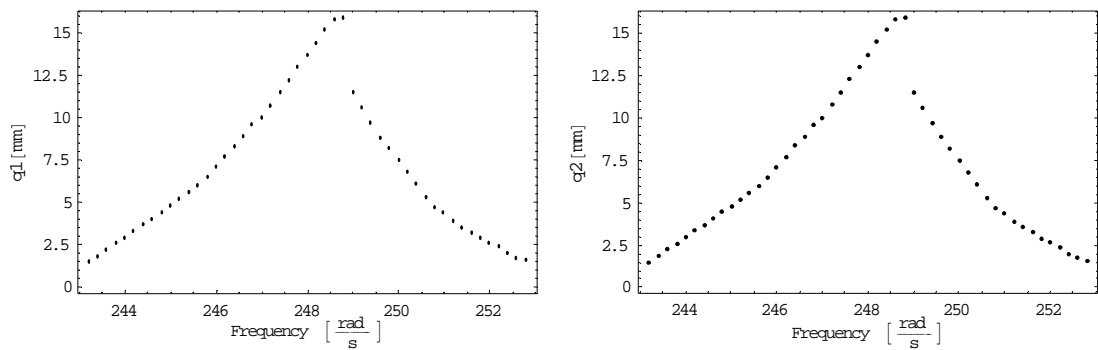


Figure 4-1: Amplitudes of the response as functions of the frequency at mass unbalance $m_u=0.004 \text{ kg}$ and damping coefficient of 13.6 Ns/m .

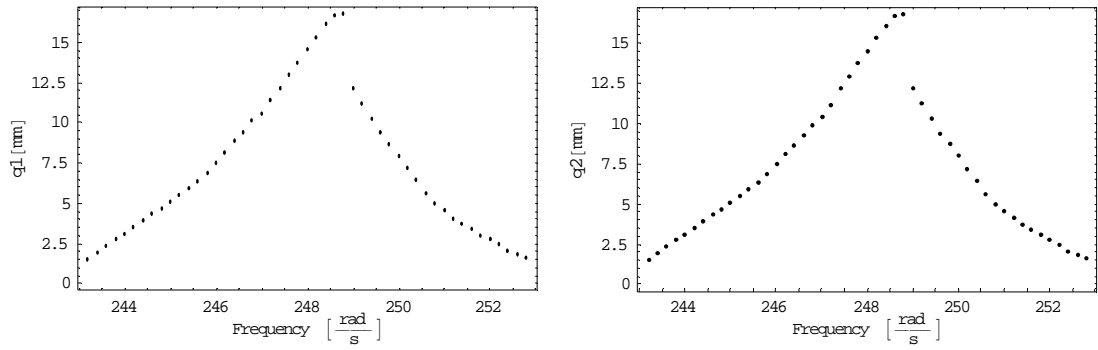


Figure 4- 2: Amplitudes of the response as functions of the frequency at mass unbalance $3m_u$ and damping coefficient of 13.6 Ns/m.

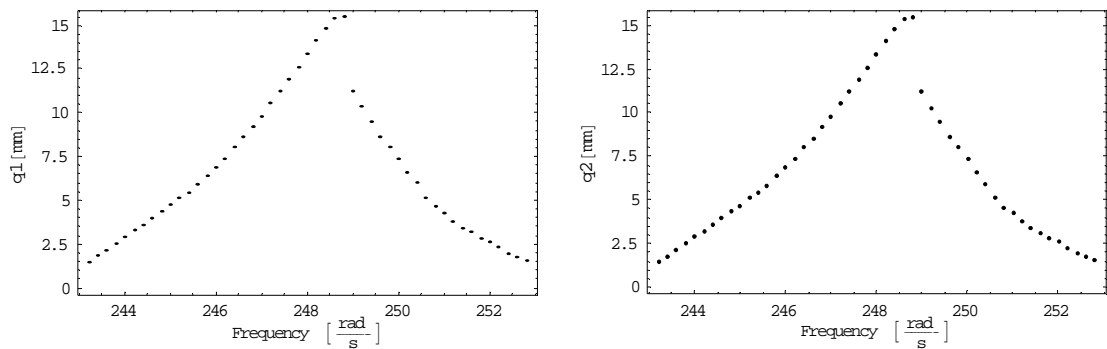


Figure 4- 3: Amplitudes of the response as functions of the frequency at mass unbalance m_u and damping coefficient of 15 Ns/m.

4.3.9.2 Amplitude Response Plot – with Parametric Force Term

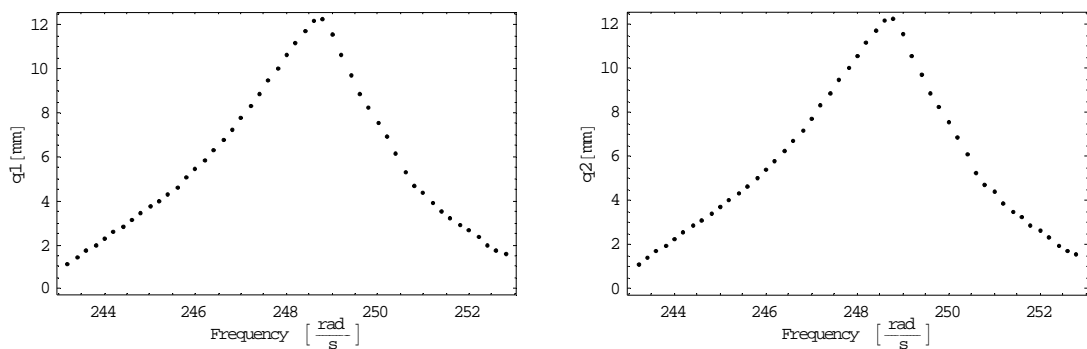


Figure 4- 4: Amplitudes of the response as functions of the frequency at mass unbalance m_u and damping coefficient of 13.6 Ns/m with parametric force term.

- Each dot on the curves corresponds to a singular point.
- Figure 4-1 shows plots of amplitudes \bar{q}_1 and \bar{q}_2 versus forcing frequency Ω when the mass unbalance is m_u and the damping coefficient is 13.6 Nsm^{-1} . Peak amplitudes of 16mm are observed for \bar{q}_1 and \bar{q}_2 . Jump phenomena of the rotating speed are also observed.
- In Figure 4-2, increasing the mass unbalance to $3m_u$ shows increases in the amplitudes to 16.8mm for \bar{q}_1 and \bar{q}_2 , resulting in a further increase in the jump.
- Maintaining the mass unbalance at m_u and increasing the damping coefficient to 15 Nsm^{-1} resulted in Figure 4-3, with amplitudes decreasing to 15.5mm for \bar{q}_1 and \bar{q}_2 . Although there are decreases in the amplitudes, they are relatively very small and the jump phenomena are not eliminated.
- In Figure 4-4 including parametric force terms in the equations and at mass unbalance of m_u and damping coefficient of 13.6 Nsm^{-1} , the amplitudes reduced to 12.3mm for \bar{q}_1 and \bar{q}_2 . It is also observed that the jump of the rotating speed is eliminated and the peak amplitudes of the whirling motion are reduced by about 23%.

4.4 Direct Numerical Integration

Direct numerical integration of the governing equations of motion in the time domain is the most general approach for the solution of the dynamic response of the system. The solution is initially defined at time zero and then convergence is sought thereafter at discrete points in time. Most of the methods use equal time steps at $\delta t, 2\delta t, 3\delta t \dots n\delta t$, however, highly nonlinear systems benefit from more sophisticated alternatives where variable step size is employed in an attempt to achieve convergence. The most common methods for integrating ordinary differential equations are Runge-Kutta, Bulirsch-Stoer, Adams-Moulton, Adams, Newmark and Gear methods. The Gear method (Gear, 1971) is mostly used for

stiff systems. Stiff systems are models where the ratio between the slowest and the fastest rate constants is greater than 500 (stiffness ratio >500).

In this section, the Runge-Kutta technique is used to integrate numerically the equations of motion, equations (4.2-1) and (4.2-2) so that these can be compared with the results that were generated by the method of multiple scales. The *Mathematica*TM program developed by Wolfram Research (Wolfram, 1996), has been used to carry out this analysis. *NDSolve integrator* is the function used within this *Mathematica*TM code to solve the set of differential equations since it can handle a wide range of ordinary differential equations as well as some partial differential equations. In solving differential equations there can be any number of unknown functions y_i , but all these functions must depend on a single “independent variable” x , which is the same for each function. *NDSolve integrator* represents solutions for the functions y_i which are represented as *Interpolating Function* objects. The *Interpolating Function* objects provide approximations to the y_i over the range of values x_{\min} to x_{\max} for the independent variable x . The integrator method selected within the function *NDSolve integrator* is the fourth order Runge-Kutta (i.e. *Method* \rightarrow *Runge-Kutta*). This is because the relevant equations of motion are non-stiff. The Runge-Kutta method numerically integrates differential equations by using a trial step at the midpoint of an interval to cancel out lower-order error terms. The fourth order Runge-Kutta method requires four gradient or ‘ k ’ terms to calculate for y_{n+1}

$$y_{n+1} = y_n + \frac{1}{6}(k_1 + 2k_2 + 2k_3 + k_4) \quad (4.2- 114)$$

where, h is the incremental independent variable and,

$$\begin{aligned} k_1 &= hf(t_n, y_n); & k_2 &= hf\left(t_n + \frac{h}{2}, y_n + \frac{k_1}{2}\right) \\ k_3 &= hf\left(t_n + \frac{h}{2}, y_n + \frac{k_2}{2}\right); & k_4 &= hf(t_n + h, y_n + k_3) \end{aligned} \quad (4.2- 115)$$

4.4.1 Results from *Mathematica*TM

Results from the bespoke *Mathematica*TM integrator are given for a range of frequency values varied from 243.2 rad/s to 252.8 rad/s. The results obtained are in the time domain and are transformed into the frequency domain by running the NDSolve code several times for the range of frequency values from 243.2 rad/s to 252.8 rad/s to obtain a list of amplitude values. Values from the steady state conditions are selected and their averages obtained for the amplitude versus frequency plots. The results obtained from this method provide a basis for comparison with the multiple scales solution.

4.4.1.1 Numerical Integration Plot- without Parametric Force Term

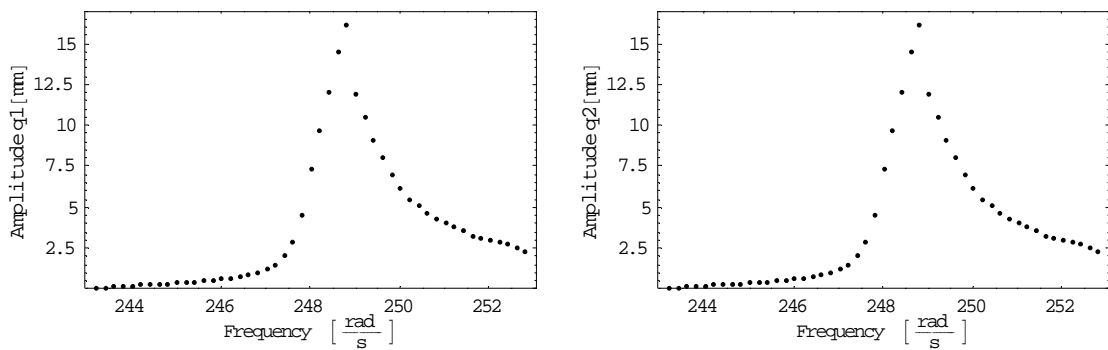


Figure 4- 5: Amplitudes of the response as functions of the frequency.

4.4.1.2 Numerical Integration Plot- with Parametric Force Term

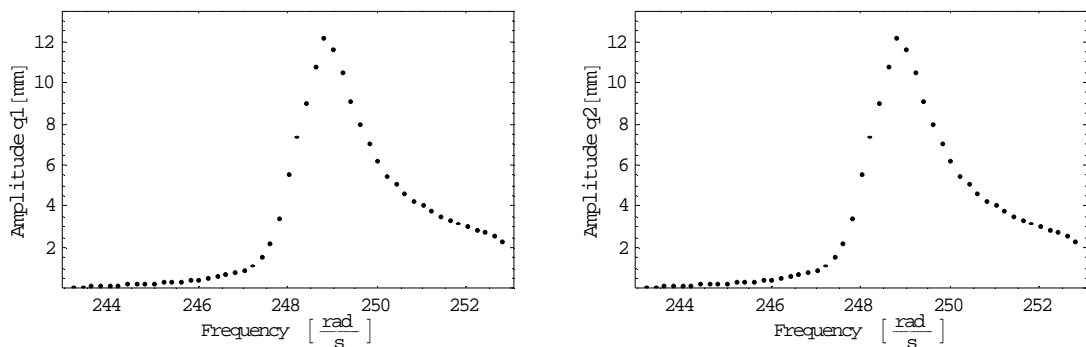


Figure 4- 6: Amplitudes of the response as functions of the frequency at the inclusion of parametric force term.

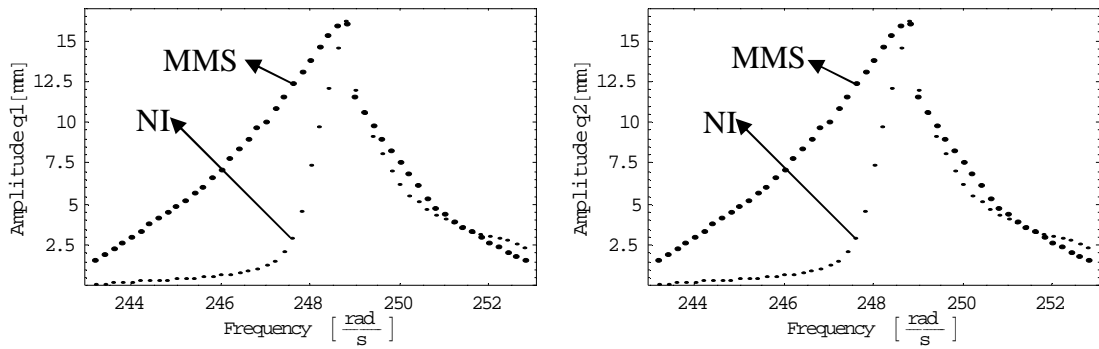


Figure 4- 7: Plots of response for MMS and Numerical Integration together- without parametric force terms.

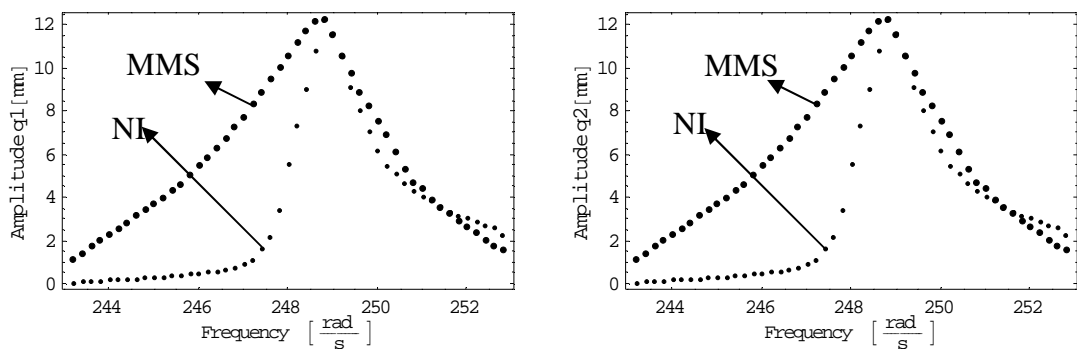


Figure 4- 8: Plots of response for MMS and Numerical Integration together- with parametric force terms.

- Where MMS is the method of multiple scales plot and NI is the direct integration plot.
- Figure 4-5 shows the response of the flexible rotor system obtained from direct integration by the use of NDSolve within *Mathematica*TM for the nonlinear Duffing ODE without the parametric force term. In Figure 4-7 reasonable agreement in terms of the amplitude levels and the jump phenomena can be observed comparing Figure 4-5 with the multiple scales results in Figure 4-1.
- Figure 4-6 shows the response obtained from the direct integration method with the parametric force term included. Also in Figure 4-8 reasonable agreement in terms of the amplitude levels and the elimination of the jump phenomena can be observed comparing Figure 4-6 with the multiple scales results in Figure 4-4.

4.5 Discussion of Results

Comparison between the results from the multiple scales analysis and the numerical integration benchmark summarised here shows evidence of a consistent phenomenon whereby both the responses in the first mode of \bar{q}_1 and \bar{q}_2 show hardening characteristics, jump phenomena and both stable and unstable solutions when the equations of motion contain no parametric force term. Including the parametric force terms, the two solutions show decreases in amplitude values, elimination of the jump phenomena and stable solutions.

CHAPTER 5

STABILITY OF STEADY-STATE SOLUTIONS

5.1 Introduction

The usual approach adopted in the literature for investigating the stability of rotor-bearing systems depends mainly upon solving the system governing equations of motion after simplification under certain assumptions and transformation into an eigenvalue problem. Then, from the evolution of exponential growth or decay, stability criteria are established based on the resulting eigenvalues and their systems parametric dependence. Many authors, including Kisk *et.al.*, (1964), Chivens (1973), Chang *et.al.*, (1993) and El-Marhomy (1994, 1998) have studied the nonlinear dynamics and stability of rotating shaft-disk systems by using perturbation methods in conjunction with well known stability techniques.

In this work the governing differential equations are solved analytically using the approximate method of multiple scales, in Chapter 4, and then the ensuing nonautonomous slow-time modulation equations are used to construct a stability matrix by applying small perturbations to the equilibrium. The stability of the flexible rotor-bearing system is then analysed by using the Routh-Hurwitz stability criterion.

5.2 Stability Matrix

From the multiple scales analysis in Chapter 4 the nonautonomous slow-time modulation equations emerge in the following form

$$a\alpha'_1 - \frac{\Omega\bar{a}_5}{2\omega} b \text{Sin}(\alpha_2 - \alpha_1) - \frac{\Gamma}{2} \text{Sin}(\bar{\sigma}T_1 - \alpha_1) = 0 \quad (5.2-1)$$

$$a' + \frac{\bar{c}}{2\omega} a - \frac{\Omega\bar{a}_5}{2\omega} b \text{Cos}(\alpha_2 - \alpha_1) - \frac{\Gamma}{2} \text{Cos}(\bar{\sigma}T_1 - \alpha_1) = 0 \quad (5.2-2)$$

$$b\alpha'_2 + \frac{\Omega\bar{a}_5}{2\omega} a \text{Sin}(\alpha_1 - \alpha_2) + \frac{\Gamma}{2} \text{Cos}(\bar{\sigma}T_1 - \alpha_2) = 0 \quad (5.2- 3)$$

$$b' + \frac{\bar{c}}{2\omega} b + \frac{\Omega\bar{a}_5}{2\omega} a \text{Cos}(\alpha_1 - \alpha_2) - \frac{\Gamma}{2} \text{Sin}(\bar{\sigma}T_1 - \alpha_2) = 0 \quad (5.2- 4)$$

where, a , b are the response amplitudes, α_1 , α_2 are the associated phase angles, Γ is the excitation amplitude, and \bar{c} is the damping coefficient , $\Omega\bar{a}_5$ is a mass coupling coefficient, and Ω is the excitation frequency, ω is the linear undamped natural frequency of the free vibration, $\varepsilon\sigma = \Omega - \omega$ is a detuning parameter , and T_1 is slow time scale.

Applying small perturbations to the amplitudes and phases we have,

$$a = a_0 + \delta a \quad (5.2- 5)$$

$$b = b_0 + \delta b \quad (5.2- 6)$$

$$\alpha_1 = \alpha_{10} + \delta\alpha_1 \quad (5.2- 7)$$

$$\alpha_2 = \alpha_{20} + \delta\alpha_2 \quad (5.2- 8)$$

These are notionally small perturbations around the equilibria, a_0 , b_0 , α_{10} , α_{20} .

Substituting equations (5.2-5) to (5.2-8) into equations (5.2-1) to (5.2-4) leads to,

$$(a_0 + \delta a)(\alpha'_{10} + \delta\alpha'_1) - \frac{\Omega\bar{a}_5}{2\omega} (b_0 + \delta b) \text{Sin}(\alpha_{20} + \delta\alpha_2 - \alpha_{10} - \delta\alpha_1) - \frac{\Gamma}{2} \text{Sin}(\bar{\sigma}T_1 - \alpha_{10} - \delta\alpha_1) = 0 \quad (5.2- 9)$$

$$(\alpha'_0 + \delta\alpha') + \frac{\bar{c}}{2\omega} (a_0 + \delta a) - \frac{\Omega\bar{a}_5}{2\omega} (b_0 + \delta b) \text{Cos}(\alpha_{20} + \delta\alpha_2 - \alpha_{10} - \delta\alpha_1) - \frac{\Gamma}{2} \text{Cos}(\bar{\sigma}T_1 - \alpha_{10} - \delta\alpha_1) = 0 \quad (5.2- 10)$$

$$(b_0 + \delta b)(\alpha'_{20} + \delta\alpha'_2) + \frac{\Omega\bar{a}_5}{2\omega}(a_0 + \delta a)\text{Sin}(\alpha_{10} + \delta\alpha_1 - \alpha_{20} - \delta\alpha_2) \quad (5.2- 11)$$

$$+ \frac{\Gamma}{2}\text{Cos}(\bar{\sigma}T_1 - \alpha_{20} - \delta\alpha_2) = 0$$

$$(b'_0 + \delta b') + \frac{\bar{c}}{2\omega}(b_0 + \delta b) + \frac{\Omega\bar{a}_5}{2\omega}(a_0 + \delta a)\text{Cos}(\alpha_{10} + \delta\alpha_1 - \alpha_{20} - \delta\alpha_2) \quad (5.2- 12)$$

$$- \frac{\Gamma}{2}\text{Sin}(\bar{\sigma}T_1 - \alpha_{20} - \delta\alpha_2) = 0$$

It is convenient to make the system autonomous, i.e. one in which T_1 does not appear explicitly, at the equilibrium points by introducing the following,

$$\bar{\sigma}T_1 - \alpha_{10} \Rightarrow \gamma_{10} ; \bar{\sigma}T_1 - \alpha_{20} \Rightarrow \gamma_{20} \quad (5.2- 13), (5.2- 14)$$

Also, for convenience let

$$\alpha_{20} - \alpha_{10} \Rightarrow \psi_{10} ; \alpha_{10} - \alpha_{20} \Rightarrow \psi_{20} ; \psi_{20} = -\psi_{10} \quad (5.2- 15), (5.2- 16), (5.2- 17)$$

Expanding the trigonometric terms as necessary, and then substituting equations (5.2-13) to (5.2-17) into equations (5.2-9) to (5.2-12) gives,

$$a_0\alpha'_{10} - Zb_0\text{Sin}\psi_{10} - m\text{Sin}\gamma_{10} = -a_0\delta\alpha'_1 - \alpha'_{10}\delta a - \delta a\delta\alpha'_{10} + Z\delta b\text{Sin}\psi_{10} \quad (5.2- 18)$$

$$+ Zb_0\delta\alpha_2\delta\alpha_1\text{Sin}\psi_{10} + Z\delta b\delta\alpha_2\delta\alpha_1\text{Sin}\psi_{10} + Zb_0\delta\alpha_2\text{Cos}\psi_{10}$$

$$+ Z\delta b\delta\alpha_2\text{Cos}\psi_{10} - Zb_0\delta\alpha_1\text{Cos}\psi_{10} - Z\delta b\delta\alpha_1\text{Cos}\psi_{10} - m\delta\alpha_1\text{Cos}\gamma_{10}$$

$$a'_0 + na_0 - Zb_0\text{Cos}\psi_{10} - m\text{Cos}\gamma_{10} = -\delta\alpha' - n\delta a + Z\delta b\text{Cos}\psi_{10} \quad (5.2- 19)$$

$$+ Zb_0\delta\alpha_2\delta\alpha_1\text{Cos}\psi_{10} + Z\delta b\delta\alpha_2\delta\alpha_1\text{Cos}\psi_{10} - Zb_0\delta\alpha_2\text{Sin}\psi_{10}$$

$$- Z\delta b\delta\alpha_2\text{Sin}\psi_{10} + Zb_0\delta\alpha_1\text{Sin}\psi_{10} + Z\delta b\delta\alpha_1\text{Sin}\psi_{10} + m\delta\alpha_1\text{Sin}\gamma_{10}$$

$$b_0\alpha'_{20} - Za_0\text{Sin}\psi_{10} + m\text{Cos}\gamma_{20} = +b_0\delta\alpha'_2 + \alpha'_{20}\delta b + \delta b\delta\alpha'_2 + Z\delta a\text{Sin}\psi_{10} \quad (5.2- 20)$$

$$+ Za_0\delta\alpha_1\delta\alpha_2\text{Sin}\psi_{10} + Z\delta a\delta\alpha_1\delta\alpha_2\text{Sin}\psi_{10} - Za_0\delta\alpha_1\text{Cos}\psi_{10}$$

$$- Z\delta a\delta\alpha_1\text{Cos}\psi_{10} + Za_0\delta\alpha_2\text{Cos}\psi_{10} + Z\delta a\delta\alpha_2\text{Cos}\psi_{10} - m\delta\alpha_2\text{Sin}\gamma_{20}$$

$$b'_0 + nb_0 + Zb_0\text{Cos}\psi_{10} - m\text{Sin}\gamma_{20} = -\delta b' - n\delta b - Z\delta a\text{Cos}\psi_{10} \quad (5.2- 21)$$

$$- Za_0\delta\alpha_1\delta\alpha_2\text{Cos}\psi_{10} - Z\delta a\delta\alpha_1\delta\alpha_2\text{Cos}\psi_{10} - Za_0\delta\alpha_1\text{Sin}\psi_{10}$$

$$- Z\delta a\delta\alpha_1\text{Sin}\psi_{10} + Za_0\delta\alpha_2\text{Sin}\psi_{10} + Z\delta a\delta\alpha_2\text{Sin}\psi_{10} - m\delta\alpha_2\text{Cos}\gamma_{20}$$

where, $Z = \frac{\Omega\bar{a}_5}{2\omega}$, $n = \frac{\bar{c}}{2\omega}$, $m = \frac{\Gamma}{2}$

Equations (5.2-18) to (5.2-21) are deliberately arranged so that the left hand sides are structural re-statements of the former equations (5.2-1) to (5.2-4), in terms of the equilibrium points, therefore they can be equated to zero, and hence, the right hand sides must also equate to zero,

$$\begin{aligned} & -a_0\delta\alpha'_1 - \alpha'_{10}\delta a - \delta a\delta\alpha'_1 + Z\delta b\text{Sin}\psi_{10} + Zb_0\delta\alpha_2\delta\alpha_1\text{Sin}\psi_{10} + Z\delta b\delta\alpha_2\delta\alpha_1\text{Sin}\psi_{10} \\ & + Zb_0\delta\alpha_2\text{Cos}\psi_{10} + Z\delta b\delta\alpha_2\text{Cos}\psi_{10} - Zb_0\delta\alpha_1\text{Cos}\psi_{10} - Z\delta b\delta\alpha_1\text{Cos}\psi_{10} \\ & - m\delta\alpha_1\text{Cos}\gamma_{10} = 0 \end{aligned} \quad (5.2- 22)$$

$$\begin{aligned} & -\delta\alpha' - n\delta a + Z\delta b\text{C os}\psi_{10} + Zb_0\delta\alpha_2\delta\alpha_1\text{C os}\psi_{10} + Z\delta b\delta\alpha_2\delta\alpha_1\text{C os}\psi_{10} \\ & - Zb_0\delta\alpha_2\text{Sin}\psi_{10} - Z\delta b\delta\alpha_2\text{Sin}\psi_{10} + Zb_0\delta\alpha_1\text{Sin}\psi_{10} + Z\delta b\delta\alpha_1\text{Sin}\psi_{10} \\ & + m\delta\alpha_1\text{Sin}\gamma_{10} = 0 \end{aligned} \quad (5.2- 23)$$

$$\begin{aligned} & b_0\delta\alpha'_2 + \alpha'_{20}\delta b + \delta b\delta\alpha'_2 + Z\delta a\text{Sin}\psi_{10} + Za_0\delta\alpha_1\delta\alpha_2\text{Sin}\psi_{10} + Z\delta a\delta\alpha_1\delta\alpha_2\text{Sin}\psi_{10} \\ & - Za_0\delta\alpha_1\text{Cos}\psi_{10} - Z\delta a\delta\alpha_1\text{Cos}\psi_{10} + Za_0\delta\alpha_2\text{Cos}\psi_{10} + Z\delta a\delta\alpha_2\text{Cos}\psi_{10} \\ & - m\delta\alpha_2\text{Sin}\gamma_{20} = 0 \end{aligned} \quad (5.2- 24)$$

$$\begin{aligned} & -\delta b' - n\delta b - Z\delta a\text{C os}\psi_{10} - Za_0\delta\alpha_1\delta\alpha_2\text{C os}\psi_{10} - Z\delta a\delta\alpha_1\delta\alpha_2\text{C os}\psi_{10} \\ & - Za_0\delta\alpha_1\text{Sin}\psi_{10} - Z\delta a\delta\alpha_1\text{Sin}\psi_{10} + Za_0\delta\alpha_2\text{Sin}\psi_{10} + Z\delta a\delta\alpha_2\text{Sin}\psi_{10} \\ & - m\delta\alpha_2\text{Cos}\gamma_{20} = 0 \end{aligned} \quad (5.2- 25)$$

In terms of “smallness” $a_0\delta\alpha'_1 \rightarrow 0$ and $b_0\delta\alpha'_2 \rightarrow 0$ because they are quadratic and include the derivative with respect to slow time T_1 , of already small terms $\delta\alpha_1$ and $\delta\alpha_2$. Also, the products of the perturbed amplitudes and phases are definitionally small and therefore tend to zero.

Thus, equations (5.2-22) to (5.2-25) reduce to,

$$\begin{aligned} & -a_0\delta\alpha'_1 - \alpha'_{10}\delta a + Z\delta b\text{Sin}\psi_{10} + Zb_0\delta\alpha_2\text{Cos}\psi_{10} - Zb_0\delta\alpha_1\text{Cos}\psi_{10} \\ & - m\delta\alpha_1\text{Cos}\gamma_{10} = 0 \end{aligned} \quad (5.2- 26)$$

$$\begin{aligned} & -\delta\alpha' - n\delta a + Z\delta b\text{C os}\psi_{10} - Zb_0\delta\alpha_2\text{Sin}\psi_{10} + Zb_0\delta\alpha_1\text{Sin}\psi_{10} \\ & + m\delta\alpha_1\text{Sin}\gamma_{10} = 0 \end{aligned} \quad (5.2- 27)$$

$$\begin{aligned} & b_0\delta\alpha'_2 + \alpha'_{20}\delta b + Z\delta a\text{Sin}\psi_{10} - Za_0\delta\alpha_1\text{Cos}\psi_{10} + Za_0\delta\alpha_2\text{Cos}\psi_{10} \\ & - m\delta\alpha_2\text{Sin}\gamma_{20} = 0 \end{aligned} \quad (5.2- 28)$$

$$\begin{aligned} -\delta b' - n\delta b - Z\delta a C \cos\psi_{10} - Za_0\delta\alpha_1 \sin\psi_{10} + Za_0\delta\alpha_2 \sin\psi_{10} \\ -m\delta\alpha_2 \cos\gamma_{20} = 0 \end{aligned} \quad (5.2-29)$$

Equations (5.2-26) to (5.2-29) are first order ordinary differential equations with respect to slow time T_1 , in δa , δb , $\delta\alpha_1$ and $\delta\alpha_2$, with solutions which can be stated in the exponential form,

$$\delta a = \delta a^* e^{\lambda T_1} \quad (5.2-30)$$

$$\delta b = \delta b^* e^{\lambda T_1} \quad (5.2-31)$$

$$\delta\alpha_1 = \delta\alpha_1^* e^{\lambda T_1} \quad (5.2-32)$$

$$\delta\alpha_2 = \delta\alpha_2^* e^{\lambda T_1} \quad (5.2-33)$$

where, δa^* and δb^* are the small real perturbation amplitudes and $\delta\alpha_1^*$ and $\delta\alpha_2^*$ are the small real perturbation phase angles.

Substituting equations (5.2-30) to (5.2-33) into equations (5.2-26) to (5.2-29) and after removing the common factor of $e^{\lambda T_1}$, and with some rearrangement, we have,

$$\begin{aligned} -\alpha'_{10}\delta a^* + (Z\sin\psi_{10})\delta b^* - (Zb_0\cos\psi_{10} + a_0\lambda + m\cos\gamma_{10})\delta\alpha_1^* \\ + (Zb_0\cos\psi_{10})\delta\alpha_2^* = 0 \end{aligned} \quad (5.2-34)$$

$$\begin{aligned} -(n + \lambda)\delta a^* + (Z\cos\psi_{10})\delta b^* + (Zb_0\sin\psi_{10} + m\sin\gamma_{10})\delta\alpha_1^* \\ - (Zb_0\sin\psi_{10})\delta\alpha_2^* = 0 \end{aligned} \quad (5.2-35)$$

$$\begin{aligned} (Z\sin\psi_{10})\delta a^* + \alpha'_{20}\delta b^* - (Za_0\cos\psi_{10})\delta\alpha_1^* \\ + (Za_0\cos\psi_{10} + b_0\lambda - m\sin\gamma_{20})\delta\alpha_2^* = 0 \end{aligned} \quad (5.2-36)$$

$$\begin{aligned} (-Z\cos\psi_{10})\delta a^* - (n + \lambda)\delta b^* - (Za_0\sin\psi_{10})\delta\alpha_1^* \\ + (Za_0\sin\psi_{10} - m\cos\gamma_{20})\delta\alpha_2^* = 0 \end{aligned} \quad (5.2-37)$$

Equations (5.2-34) to (5.2-37) can now be stated in matrix form, from which the associated determinant can be obtained, and equated to zero in order to generate the characteristic equation.

$$\begin{vmatrix} \alpha'_{10} & Z\text{Sin}\psi_{10} & (-Zb_0\text{Cos}\psi_{10} - a_0\lambda - m\text{Cos}\gamma_{10}) & Zb_0\text{Cos}\psi_{10} \\ -n - \lambda & Z\text{Cos}\psi_{10} & (Zb_0\text{Sin}\psi_{10} + m\text{Sin}\gamma_{10}) & -Zb_0\text{Sin}\psi_{10} \\ Z\text{Sin}\psi_{10} & \alpha'_{20} & -Za_0\text{Cos}\psi_{10} & (Za_0\text{Cos}\psi_{10} + b_0\lambda - m\text{Sin}\gamma_{20}) \\ -Z\text{Cos}\psi_{10} & -n - \lambda & -Za_0\text{Sin}\psi_{10} & (Za_0\text{Sin}\psi_{10} - m\text{Cos}\gamma_{20}) \end{vmatrix} = 0 \quad (5.2-38)$$

From equation (5.2-38) the characteristic equation is obtained

$$\lambda^4 k_1 + \lambda^3 k_2 + \lambda^2 k_3 + \lambda^1 k_4 + \lambda^0 k_5 = 0 \quad (5.2-39)$$

where the coefficients k_1 to k_5 are defined in Appendix B3.

5.3 The Routh-Hurwitz Stability Criterion

Instead of computing the roots of the characteristic equation, and then using these to determine stability, it is possible to utilize the characteristic polynomial to determine whether all the roots have negative real parts without actually having to solve for the roots. A large number of stability criteria have been developed for this purpose and the most commonly used is the Routh-Hurwitz stability criterion. In the late 1800s, Routh E. J., (1875) and Hurwitz A., (1895) published independently a method of investigating the stability of a linear system. The Routh-Hurwitz stability criterion provides necessary and sufficient conditions for the accurate delineation of the relevant parameter space into stable and unstable regions. The Routh-Hurwitz stability criterion states:

(a) For there to be roots with negative real parts there is a necessary, but not sufficient, condition that all coefficients in the characteristic equation, have the same sign and that none are zero.

If (a) above is satisfied, then the necessary and sufficient condition for stability is either,

(b) all the Hurwitz determinants of the polynomial are positive, or alternatively

(c) all the coefficients of the first column of Routh's array have the same sign. The number of sign changes indicates the number of unstable roots.

Bhattacharyya and Dutt, (1997) used the Routh-Hurwitz criterion to perform an approximate stability analysis when studying the unbalance response and stability of a rotor shaft system mounted on nonlinear rolling element bearings with viscoelastic support. A stability analysis of rotor-bearing system by El-Marhomy *et.al.*, (2004) also applied the Routh-Hurwitz criterion. These authors derived sufficient conditions for asymptotic stability of both the translational and rotational modes of motion of the system and presented the system's stability boundaries graphically in terms of the various systems parameters, to afford a comprehensive demonstration of the effects of these parameters on the system's stability of motion.

Using this technique, it is possible to determine immediately the stability of the system if the polynomial is the characteristic equation. This criterion is also useful for determining the ranges of coefficients of the characteristic equation for stability.

Considering the general n^{th} order characteristic polynomial written in the form

$$a_0s^n + a_1s^{n-1} + a_2s^{n-2} + \dots + a_{n-2}s^2 + a_{n-1}s^1 + a_n = 0 \quad (5.2- 40)$$

where the coefficients a_i ($i=0,1,\dots,n$) are real quantities. Then, we consider if any of the a_i components are zero, or negative, in the presence of at least one zero eigenvalue, or if there is at least one eigenvalue which has a positive real part, or if there are eigenvalues which are imaginary. Then the system is unstable, and it is not necessary to follow the procedure described below. It is also possible to divide the characteristic equation by a_0 , and then the coefficient of s^n will be unity. The condition that all the a_i coefficients are present, and they are all positive, is a necessary and sufficient condition for stability, taking into account that if all the coefficients are negative, they can be made positive by multiplying both sides of the characteristic equation by -1.

Therefore the only case that is considered here is where all the coefficients are positive. The Routh-Hurwitz criterion is based on ordering the coefficients of the characteristic equation into the well established Routh array:

$$\begin{aligned}
s^n &: a_0 & a_2 & a_4 & a_6 \\
s^{n-1} &: a_1 & a_3 & a_5 & a_7 \\
s^{n-2} &: b_1 & b_2 & b_3 & \\
s^{n-3} &: c_1 & c_2 & & \\
s^{n-4} &: d_1 & & &
\end{aligned}
\tag{5.2- 41}$$

The elements of the Routh array are obtained whereby each new row is derived from the two rows immediately above it, these being called the *working rows*. The first column of the 2x2 matrix in the expressions is always the first column of the two working rows of the Routh-Hurwitz array. The remaining column is the column of the working rows just to the right of the position of the unknown. The denominator of the expression is the first number of the lower of the two working rows.

Thus the elements are obtained as:

$$b_1 = \frac{-1}{a_1} \begin{vmatrix} a_0 & a_2 \\ a_1 & a_3 \end{vmatrix} = \frac{-1}{a_1} (a_0 a_3 - a_1 a_2) = a_2 - \frac{a_0 a_3}{a_1} \tag{5.2- 42}$$

$$b_2 = \frac{-1}{a_1} \begin{vmatrix} a_0 & a_4 \\ a_1 & a_5 \end{vmatrix} = a_4 - \frac{a_0 a_5}{a_1} \tag{5.2- 43}$$

$$b_3 = \frac{-1}{a_1} \begin{vmatrix} a_0 & a_6 \\ a_1 & a_7 \end{vmatrix} = a_6 - \frac{a_0 a_7}{a_1} \tag{5.2- 44}$$

The evaluation of the b_i coefficients is performed until the rest of them are equal to zero. The c_i coefficients are obtained as:

$$c_1 = \frac{-1}{b_1} \begin{vmatrix} a_1 & a_3 \\ b_1 & b_2 \end{vmatrix} = a_3 - \frac{a_1 b_2}{b_1} \tag{5.2- 45}$$

$$c_2 = \frac{-1}{b_1} \begin{vmatrix} a_1 & a_5 \\ b_1 & b_3 \end{vmatrix} = a_5 - \frac{a_1 b_3}{b_1} \tag{5.2- 46}$$

And the coefficients d_i are determined in a similar way where,

$$d_1 = \frac{-1}{c_1} \begin{vmatrix} b_1 & b_2 \\ c_1 & c_2 \end{vmatrix} = b_2 - \frac{b_1 c_2}{c_1} \tag{5.2- 47}$$

The Routh-Hurwitz criterion states that the number of roots of the characteristic equation with positive real parts is equal to the number of changes in sign of the first column of the array. According to Routh's stability criterion, the necessary and sufficient condition that all the eigenvalues of the characteristic equation have negative real parts is that all the coefficients of the characteristic equation are positive and all the terms in the first column of the Routh Array have positive signs, for a stable system, and this is summarised in table 5-1. Thus if the sign of the coefficients in the first column of the Routh Array changes p times, it follows that the characteristic equation has p roots with positive real parts, and thus the system is unstable.

For the flexible rotor-bearing system being considered here, it follows from equation (5.2-39) that $n=4$, therefore

$$a_0s^4 + a_1s^3 + a_2s^2 + a_3s^1 + a_4s^0 = 0 \quad (5.2- 48)$$

So from equation (5.2-39)

$$a_0 = k_1; a_1 = k_2; a_2 = k_3; a_3 = k_4; a_4 = k_5 \quad (5.2- 49)$$

$a_0 > 0$	$a_2 > 0$	$a_4 > 0$	$a_6 > 0$
$a_1 > 0$	$a_3 > 0$	$a_5 > 0$	$a_7 > 0$
$b_1 > 0$	b_2	b_3	
$c_1 > 0$	c_2		
$d_1 > 0$			

Table 5- 1: Summary of conditions for stability according to Routh's criterion

Hence, equations (5.2-42) to (5.2-47) can be re-stated as,

$$b_1 = k_3 - \frac{k_1 k_4}{k_2} \quad (5.2-50)$$

$$b_2 = k_5 - \frac{k_1(0)}{k_2} = k_5 \quad (5.2-51)$$

$$b_3 = 0 - 0 = 0 \quad (5.2-52)$$

$$c_1 = k_4 - \frac{k_2 k_5}{b_1} \quad (5.2-53)$$

$$c_2 = 0 - \frac{k_2(0)}{b_1} = 0 \quad (5.2-54)$$

$$d_1 = b_2 - \frac{b_1(0)}{c_1} = b_2 \quad (5.2-55)$$

Therefore the elements of the first column of the Routh Array are

$$a_0 = k_1, \quad a_1 = k_2, \quad b_1 = k_3 - \frac{k_1 k_4}{k_2}, \quad c_1 = k_4 - \frac{k_2 k_5}{\left(k_3 - \frac{k_1 k_4}{k_2}\right)}, \quad \text{and} \quad d_1 = k_5.$$

The Routh-Hurwitz criterion requires that all the first column elements are positive and all $a_i > 0$, i.e. $k_1 > 0$, $k_2 > 0$, $k_3 > 0$, $k_4 > 0$, $k_5 > 0$, $k_3 - \frac{k_1 k_4}{k_2} > 0$, and

$$k_4 - \frac{k_2 k_5}{\left(k_3 - \frac{k_1 k_4}{k_2}\right)} > 0 \quad \text{for stability.}$$

5.3.1 Stability Results

The results of the stability of the steady-state solutions at various mass unbalance values of the flexible rotor-bearing system are presented in Table 5-2 and Figures 5-1 and 5-2. The results show that there are values of mass unbalance for which the system can be stable or unstable. Table 5-2 shows discrete mass unbalance values with their coefficient values and eigenvalues.

For a mass unbalance of $m_u = 0.004\text{kg}$, all first column elements are greater than zero, and all $a_i > 0$, i.e. $k_1 = 0.000256$, $k_2 = 0.077$, $k_3 = 1.5$, $k_4 = 7.84$, $k_5 = 0.16$, $b_1 = 1.47$, $c_1 = 7.839$, $d_1 = 0.16$. Also the eigenvalues have negative real parts indicating stable motion.

At mass unbalances of $3m_u$, $4m_u$ and $5m_u$ all the first column elements and a_i are greater than zero, except k_5 and d_1 which are less than zero, and since $d_1 = k_5$, and with eigenvalues λ_4 being real but positive, the motion is unstable.

A further increase in mass unbalance to $6m_u$ and $7m_u$ shows their respective k_5 and d_1 values to be greater than zero, and all eigenvalues as real and negative indicating stability at these values.

Figures 5-1 and 5-2 show stability graphs of coefficients and mass unbalance, and eigenvalues and mass unbalance, with Figures 5-1(b) and 5-2(b) showing enlarged views of coefficients k_5 and mass unbalance, and eigenvalues λ_4 and mass unbalance plots respectively, and they show the transitions between stability and instability.

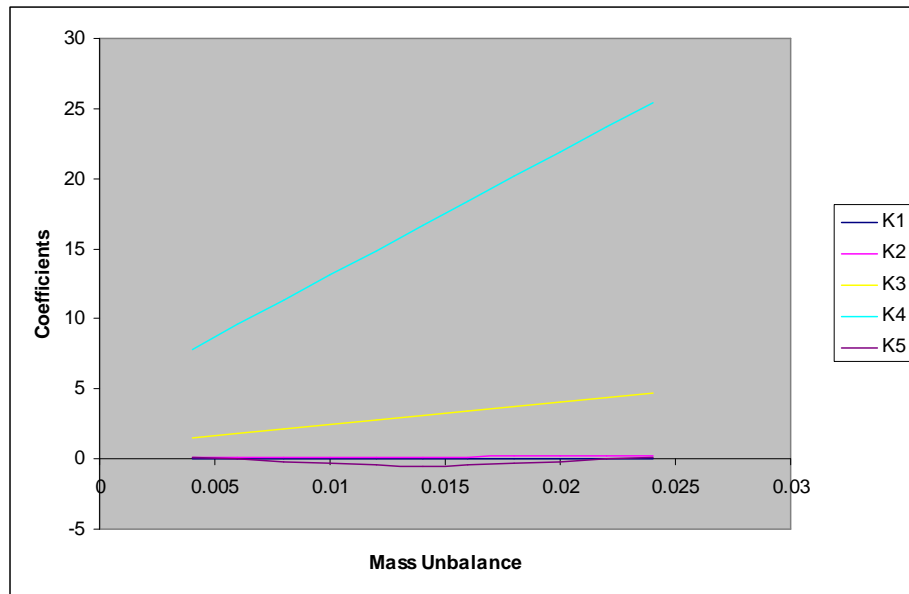
From Figures 5-1 and 5-2, at mass unbalance values between zero and 0.006kg, all the coefficients k_1 to k_5 values are greater than zero and there are no sign changes in the first columns of the Routh arrays. Also all the eigenvalues λ_1 to λ_4 are negative indicating stable motions.

At mass unbalance values from 0.006kg to 0.022kg, the system is unstable. The coefficients k_1 to k_4 values are greater than zero, but k_5 values are negative, also negative numbers are found in the first columns of the Routh arrays, meaning there are sign changes in the first column. The eigenvalues λ_4 are either zero or positive.

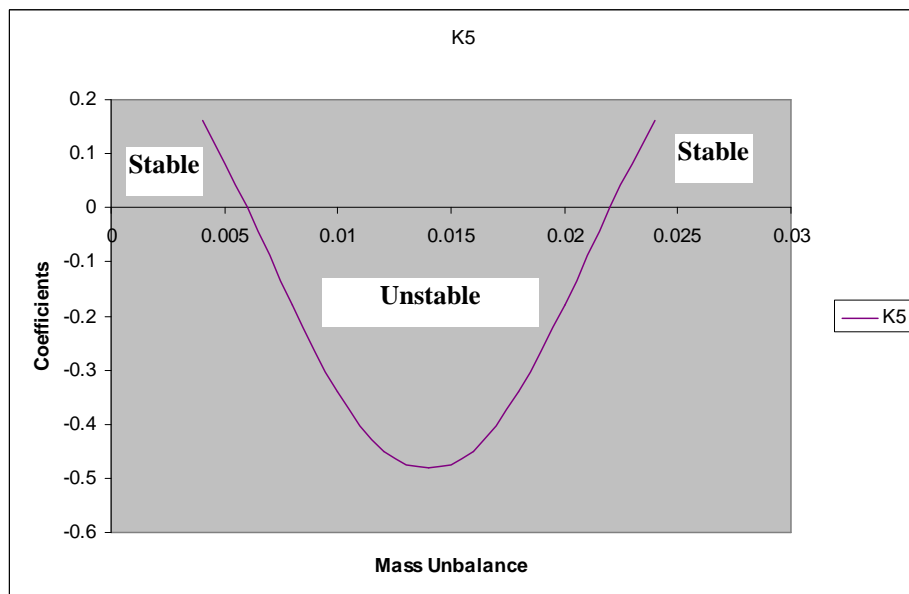
At mass unbalance values greater than 0.022kg, the system is stable because all the coefficients k_1 to k_5 values are greater than zero, and there are no sign changes in the first columns of the Routh arrays. Also all the eigenvalues λ_1 to λ_4 are negative.

Mass Unbalance (m_u)[kg]	a_i Values	Eigenvalues λ_i	Stable (S)/Unstable (U)
$m_u = 0.004$	$k_1 = 0.000256; k_2 = 0.077;$ $k_3 = 1.5; k_4 = 7.84; k_5 = 0.16$	$\lambda_1 = -292.3; \lambda_2 = -11.15;$ $\lambda_3 = -10.24; \lambda_4 = -0.044;$	S
$3m_u$	$k_1 = 0.000256; k_2 = 0.135;$ $k_3 = 2.79; k_4 = 14.87; k_5 = -0.45$	$\lambda_1 = -475.9; \lambda_2 = -11.44;$ $\lambda_3 = -10.07; \lambda_4 = 0.032;$	U
$4m_u$	$k_1 = 0.000256; k_2 = 0.163;$ $k_3 = 3.44; k_4 = 18.39; k_5 = -0.46$	$\lambda_1 = -567.7; \lambda_2 = -11.58;$ $\lambda_3 = -9.99; \lambda_4 = 0.033;$	U
$5m_u$	$k_1 = 0.000256; k_2 = 0.192;$ $k_3 = 4.08; k_4 = 21.9; k_5 = -0.18$	$\lambda_1 = -659.5; \lambda_2 = -11.73;$ $\lambda_3 = -9.9; \lambda_4 = 0.0158;$	U
$6m_u$	$k_1 = 0.000256; k_2 = 0.221;$ $k_3 = 4.73; k_4 = 25.42; k_5 = 0.16$	$\lambda_1 = -751.3; \lambda_2 = -11.87;$ $\lambda_3 = -9.82; \lambda_4 = -0.045;$	S
$7m_u$	$k_1 = 0.000256; k_2 = 0.250;$ $k_3 = 5.38; k_4 = 28.94; k_5 = 0.48$	$\lambda_1 = -843.1; \lambda_2 = -12.01;$ $\lambda_3 = -9.72; \lambda_4 = -0.0602;$	S

Table 5- 2: Discrete mass unbalance values with their stability indicators

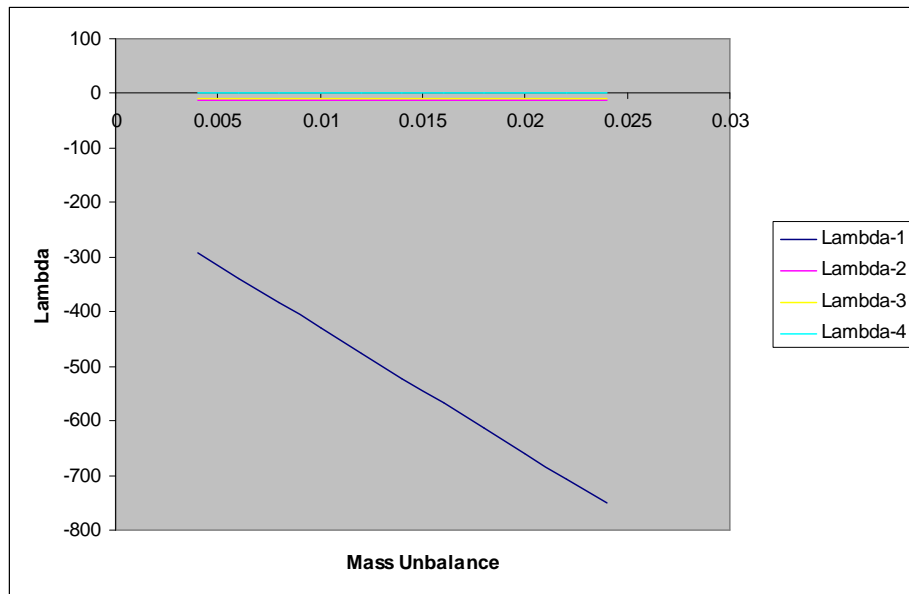


(a) Combined plots for k values

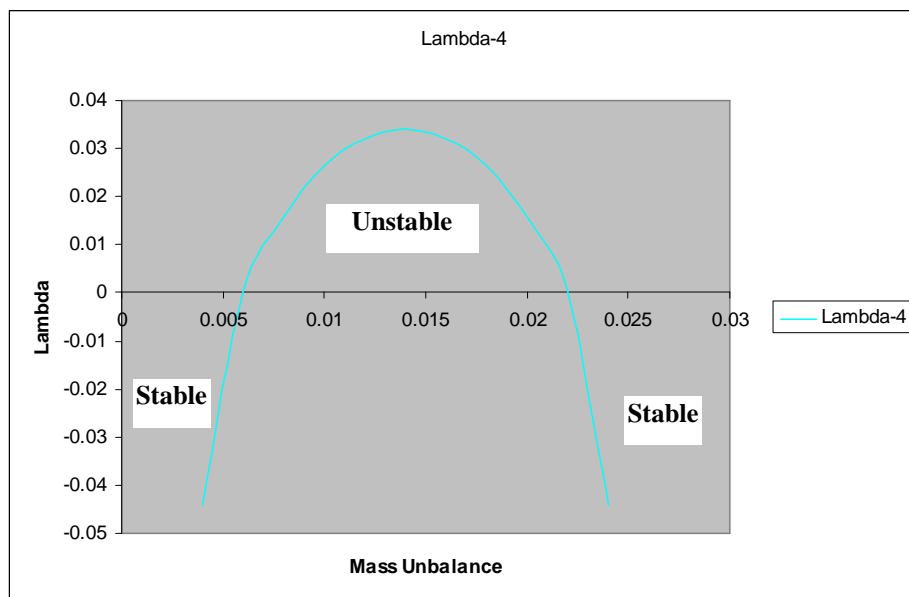


(b) Enlarged view of k5 values

Figure 5- 1: Stability plots for k values



(a) Combined plots for λ values



(b) Enlarged view of λ_4 values

Figure 5- 2: Stability plots for λ values

CHAPTER 6

INVESTIGATION OF SYSTEMS DYNAMICS

6.1 Introduction

In nonlinear dynamical systems analysis, exact solutions are hard, if not impossible to find. In addition to relying on analytical solutions for the flexible rotor, emphasis can also be placed on its qualitative behaviour. The analysis methods employed in this study are inclusive of the dynamic trajectories of the rotor, displacement-time plots, Poincaré maps, and bifurcation diagrams. Maximum Lyapunov exponent analysis is also used, together with the above mentioned feature properties to determine the onset conditions for chaotic motion. If a system falls into a chaotic regime, its behaviour is difficult to predict and control. Hence identifying chaotic motion and preferably taking steps to avoid generating the conditions which induce it are both highly important. Therefore, understanding the dynamics of an analytically modelled system can be extended further by recourse to techniques based on specialized numerical investigations. Over the years, numerous software namely, *Dynamics Solver*, *XPPAUT* and *AUTO* among others have been specifically designed for the analysis of dynamical systems. These softwares packages can be employed to generate plots of equilibria, limit cycles, bifurcation diagrams and Lyapunov exponents. The primary function of these system dynamics software packages is to perform numerical integrations and numerical continuation. The numerical integration technique is iterative and is applied for the majority of nonlinear systems that are not analytically solvable, and the trajectory is approximated by calculating a sequence of solutions at a given period of time. On the other hand, the numerical continuation technique is employed to trace the path of solutions to a given system as one or more parameter values varies, allowing one to find the bifurcations, and the tracing of stable and unstable solutions. Nusse and Yorke (1994) have developed numerical analysis software, *Dynamics*, for computational numerical investigations of system dynamics. Nusse *et. al.*, (1994, 1995) and Chin *et.al.*, (1994) have used this software for calculating bifurcation diagrams, basins of attraction, and Lyapunov exponents for a range of physically

interesting systems. A newer edition, *Dynamics 2*, also developed by Nusse and York in 1998 has since been in use. In this study, the *Dynamics 2* and *Mathematica*TM softwares are being employed here as computational basis for the qualitative assessments of bifurcation and to acquire the bifurcation set that expresses the boundary of the stable and unstable motions, with and without the introduction of parametric force terms into the governing equations developed in Chapter 3.

6.2 Program Code

6.2.1 Dynamics 2 Code

The *Dynamics 2* programming environment has numerous examples of maps and differential equations built in. Examples of built-in maps are the Henon map, Ikeda map, Kaplan/Yorke map, Logistic map, Quasiperiodicity map, Tinkerbell map, Tent map, and the Piecewise linear map amongst others. The differential equations include Chua's circuit, Goodwin's equation, examples of Hamiltonian systems, the Lorenz systems, the Lotka/Volterra equations, forced-damped pendulum equation, a parametrically excited Duffing equation, the Rossler equation, and the forced Van der Pol equation. Some of the defined equations from the program are as follows,

Henon map:

$$H(x, y) = (\rho - x^2 + C_1, x)$$

Logistic map:

$$L(x) = \rho x(1 - x)$$

Forced-damped pendulum:

$$x'' + C_1 x' + C_2 \sin x = \rho(C_3 + \cos[\Omega t])$$

Parametrically excited Duffing equation:

$$x'' + C_1 x' - x + C_3 (1 + \rho \sin[\Omega t]) x^2 + C_3 (1 + \rho \sin[\Omega t]) x^3 = 0$$

Forced van der Pol equation:

$$x'' - C_1 x' (1 - x^2) + C_2 x + C_3 x^3 = \rho \sin[\Omega t]$$

where ρ is the excitation amplitude, Ω is the excitation frequency, and C_1, C_2 and C_3 are all constants.

Although code is provided for a variety of maps and differential equations in the *Dynamics 2* program, coupled differential equations are not pre-defined. However, options within *Dynamics 2* allow the addition of bespoke mathematical models to the program. Figure C1 in Appendix C shows a screen dump of the code that was created for the analysis of the coupled differential equations. The reader is referred to Appendix C for the definition of the program code used in Figure C1, and also for a summary of detailed procedures for adding bespoke differential equations into *Dynamics 2*. The models of the flexible rotor system as discussed in Chapter 3 are used after some modifications for analyzing the behaviour of the dynamical system using the *Dynamics 2* software. We therefore write Model A equations in the following form:

$$\ddot{x} + \bar{C}_1 \dot{x} - \bar{C}_2 \dot{y} \cos(y) + \bar{C}_3 x + \bar{C}_4 x^3 = \rho \sin(\Omega t) \quad (6.2-1)$$

$$\ddot{y} + \bar{C}_1 \dot{y} + \bar{C}_2 \dot{x} \cos(y) + \bar{C}_3 y + \bar{C}_4 y^3 = \rho \cos(\Omega t) \quad (6.2-2)$$

Where, $\bar{C}_1 = \frac{c}{m}$; $\bar{C}_2 = \frac{a_5 \Omega}{m}$; $\bar{C}_3 = \frac{k}{m}$; $\bar{C}_4 = \frac{b}{m}$; $\rho = \frac{m_u \Omega^2 d}{m}$

6.2.1.1 Nondimensionalisation

The equations of motion contain dimensional parameters and one way of reducing the order of the design-space is to scale the equations of motion. The resulting parameters may after this operation become nondimensional.

Nondimensional numbers themselves can reveal much about a system. Nondimensionalisation does not change the dynamics of the system. This can be used to scale a good design to give the new design the same dynamical behaviour. For numerical simulation reasons scaling can be used to condition the equations better. By proper scaling, the difference in order of magnitude between numbers can be significantly reduced. Proper scaling will also reduce the computational time. The time t is nondimensionalised by using the rotor system natural frequency ω . Nondimensionalisation of the timescale in equations (6.2-1) and (6.2-2) is introduced by stating $\tau = \sqrt{\omega}t$, where, ω is the natural frequency of the first mode of the flexible rotor system. Therefore,

$$\ddot{x} = \frac{d^2x}{dt^2} = \frac{d^2x}{d\left(\frac{\tau}{\sqrt{\omega}}\right)^2} = \omega \frac{d^2x}{d\tau^2} \quad \therefore \ddot{x}(t) = \omega x''(\tau) \quad (6.2-3), (6.2-4)$$

$$\dot{x} = \frac{dx}{dt} = \frac{dx}{d\left(\frac{\tau}{\sqrt{\omega}}\right)} = \sqrt{\omega} \frac{dx}{d\tau} \quad \therefore \dot{x}(t) = \sqrt{\omega} x'(\tau)$$

$$\ddot{y} = \frac{d^2y}{dt^2} = \frac{d^2y}{d\left(\frac{\tau}{\sqrt{\omega}}\right)^2} = \omega \frac{d^2y}{d\tau^2} \quad \therefore \ddot{y}(t) = \omega y''(\tau) \quad (6.2-5), (6.2-6)$$

$$\dot{y} = \frac{dy}{dt} = \frac{dy}{d\left(\frac{\tau}{\sqrt{\omega}}\right)} = \sqrt{\omega} \frac{dy}{d\tau} \quad \therefore \dot{y}(t) = \sqrt{\omega} y'(\tau)$$

In terms of the dimensionless timescale, τ , equations (6.2-1) and (6.2-2) become

$$\omega x'' + \sqrt{\omega} \bar{C}_1 x' - \sqrt{\omega} \bar{C}_2 y' \cos(y) + \bar{C}_3 x + \bar{C}_4 x^3 = \rho \sin\left(\frac{\Omega}{\sqrt{\omega}}\right) \tau \quad (6.2-7)$$

$$\omega y'' + \sqrt{\omega} \bar{C}_1 y' + \sqrt{\omega} \bar{C}_2 x' \cos(y) + \bar{C}_3 y + \bar{C}_4 y^3 = \rho \cos\left(\frac{\Omega}{\sqrt{\omega}}\right) \tau \quad (6.2-8)$$

where the prime (') denotes differentiation with respect to dimensionless time τ . Dividing equations (6.2-7) and (6.2-8) by ω , gives

$$x'' + C_1 x' - C_2 y' \cos(y) + C_3 x + C_4 x^3 = \frac{\rho}{\omega} \sin(\phi t) \quad (6.2-9)$$

$$y'' + C_1 y' + C_2 x' \cos(y) + C_3 y + C_4 y^3 = \frac{\rho}{\omega} \cos(\phi t) \quad (6.2-10)$$

$$\text{where, } C_1 = \frac{\bar{C}_1}{\sqrt{\omega}}; C_2 = \frac{\bar{C}_2}{\sqrt{\omega}}; C_3 = \frac{\bar{C}_3}{\omega}; C_4 = \frac{\bar{C}_4}{\omega}; \phi = \omega$$

The second order ordinary differential equations are then split into first order ordinary differential equations making them more compact.

$$x' = u \quad (6.2-11)$$

$$u' = \frac{\rho}{\omega} \sin(\phi t) - C_1 u + C_2 v \cos(y) - C_3 x - C_4 x^3 \quad (6.2-12)$$

$$y' = v \quad (6.2-13)$$

$$v' = \frac{\rho}{\omega} \cos(\phi t) - C_1 v - C_2 u \cos(y) - C_3 y - C_4 y^3 \quad (6.2-14)$$

6.2.2 *Mathematica*TM Code

Nonlinear dynamic analysis of the rotor can also be carried out by using the NDSolve numerical integrator within *Mathematica*TM. The program code has been developed for phase plane construction, Poincaré map generation and time plot calculation, and is presented in Appendix C2. For effective and efficient analysis the second order ordinary differential equations are split into two first order ordinary differential equations as at equations (6.2-11) to (6.2-14). These first order equations can then be used to calculate time responses, phase plane trajectories, and predictions of bifurcations.

6.2.3 Definition of Parameters

The parameter values for the program codes are presented in Table 6-1 for the models of coupled equations with and without the parametric force term, corresponding to all the data described in Chapters 3 and 4.

Dynamics 2 Program Parameters

Dimensional Parameters

Stiffness (Linear)	Damping Coefficient	Actuator Force	Stiffness (Cubic)	Excitation Amplitude
$[s^{-2}]$	$[s^{-1}]$	$[ms^{-2}]$	$[m^{-2}s^{-2}]$	$[m s^{-2}]$
$C_3 = 61901.6$	$C_1 = 21.9$	$C_7 = 1533.7$	$C_4 = 8.15 \times 10^9$	$\rho = 12$

Gyroscopic term $C_2 = 0.4 s^{-1}$;

Reference frequency: $\omega = 248.8 \text{ rad/s}$; Parametric frequency: $\Omega_2 = 497.6 \text{ rad/s}$

Nondimensional Parameters

Stiffness (Linear)	Damping Coefficient	Actuator Force	Stiffness (Cubic)	Excitation Amplitude
$C_3 = 248.8$	$C_1 = 1.4$	$C_7 = 6.16$	$C_4 = 3.28 \times 10^7$	$\frac{\rho}{\omega} = 0.048$

Gyroscopic term $C_2 = 0.025$; $\phi = 248.8 \text{ rad/s}$; $\phi_2 = 497.6 \text{ rad/s}$

Table 6- 1: Data used for numerical simulations

6.3 Bifurcation Analysis

In the study of dynamical systems, a sudden qualitative or topological change can occur under the variation in a parameter of the system. These changes occurring in the dynamics of the system are called **bifurcation**. Poincaré (1854-1912) originally introduced the term bifurcation, into nonlinear dynamics. In bifurcation representations, it is useful to consider a space formed

by using the state variable(s) and chosen control parameter(s), called the state-control space. Locations at which bifurcations occur in this space are called bifurcation points. It is often desirable to know where in the parameter space nonperiodic motion exists. Bifurcation diagrams can be used to indicate such domains. A bifurcation diagram provides a summary of the essential dynamics of systems and is therefore a useful way of observing nonlinear dynamic behaviour (Chang-Jian *et.al.*, 2007).

A periodic motion may become unstable if the control parameters are allowed to vary, a scenario signifying dynamic deterioration of stability that could lead to eventual chaos. In literature, there are various types of bifurcations, however, in the present analysis a period doubling bifurcation can mostly be observed and is analysed in the following sections in detail. It is a bifurcation in which the system's behaviour changes at integer multiples of the periodicity of the original response. If the control parameter is further varied, the motion may become chaotic. Appearance of multi-periodic motion indicates the set-in of dynamic instability. Bifurcation helps in identifying instabilities in dynamical systems and provides theoretical and practical ideas for controlling these systems and optimizing their operation.

In understanding the dynamics within the models in Chapter 3, the *Dynamics 2* software was used to plot the bifurcatory behaviour of the amplitude responses as a function of normalised excitation acceleration and the Lyapunov exponent, and these are illustrated in Figures 6-2 to 6-4. All data used for these plots are system parameters taken from the experimental rig and graphs are plotted using nondimensionalised parameters tabulated in Table 6-1. All the figures are plotted using certain necessary *Dynamics 2* commands and are summarised in Table 6-2.

For a full understanding of these commands, the reader is referred to the definitions of these commands in Appendix C and the text entitled "Numerical Explorations" by Nusse and Yorke (1998).

	SPC	IPP	PI	BIFPI	BIFD	BIFV	CON
Time Plots	30	1	0	0	200	400	On
Phase Planes	30	1	0	0	200	400	On
Poincare Maps	30	30	0	0	200	400	Off
Bifurcation diagrams	30	30	0	500	1000	1000	Off
Lyapunov diagrams	30	30	0	500	1000	1000	On

Table 6- 2: Program command values for *Dynamic 2* Plotting

6.4 Lyapunov Exponents

Lyapunov Exponent is named after the Russian scientist Aleksandr Mikhailovich Lyapunov (1857-1918), who introduced a bespoke method for providing ways to determine the stability of sets of ordinary differential equations. The Lyapunov exponent has proved to be a powerful diagnostic tool for chaotic systems. The Lyapunov exponents of a system are a set of invariant geometric measures which describe, in an intuitive way, the dynamical content of the system and can serve as a measure of how easy it is to perform prediction on the system. Lyapunov exponents quantify the average rate of convergence or divergence of nearby trajectories generally, in a global sense. A positive exponent implies divergence and a negative one convergence. Any continuous time-dependent dynamical system without a fixed point will have at least one zero exponent and a zero exponent indicates the continuous nature of a flow in time. Systems with positive exponents have positive entropies and their trajectories that were initially close together move apart overtime. The more positive the exponent, the faster they move apart. Any system containing at least one positive Lyapunov exponent is defined to be chaotic or having a strange attractor, with the magnitude of the exponent reflecting the time scale on which systems dynamics become unpredictable. For systems with negative exponents, the

trajectories move together. Such systems exhibit asymptotic stability and the more negative the exponent the greater the stability. Systems with zero Lyapunov exponents are said to be in some sort of steady state mode and are conservative physically. The Lyapunov exponent, λ is defined by taking the natural logarithm of the Lyapunov number (defined by the divergence ratio).

$$\lambda = \lim_{\substack{t \rightarrow \infty \\ |\Delta x_0| \rightarrow 0}} \frac{1}{t} \ln \frac{|\Delta x(X_0, t)|}{|\Delta x_0|} \quad (6.2-15)$$

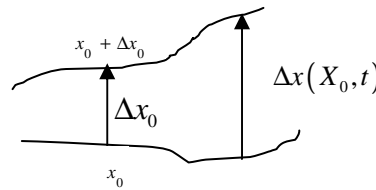


Figure 6- 1: Sketch of the change in distance between two nearby orbits used to define Lyapunov exponent

Figure 6-2 shows the normalised bifurcation diagrams of amplitudes x_1 and x_2 as a function of the excitation frequency Ω . Where, x_1 is the amplitude in the horizontal direction and x_2 is the amplitude in the vertical direction. The first mode is examined around the resonant region. It is evident that as the mass unbalance (m_u) is increased from the values of Figure 6-2(a) to those of 6-2(d), the response amplitudes increase, hence broadly correlating with the multiple scales results of Figure 4-2. Figure 6-2 also shows the Lyapunov exponents plotted for the respective bifurcations of the various mass unbalances. Periodic motions are evident from the negative values of the Lyapunov exponents. It is again evident that the increase in mass unbalance makes the hardening effect more noticeable.

6.5 Bifurcations as Functions of Excitation Acceleration

Figure 6-3 shows the Lyapunov exponent and Bifurcation diagrams of amplitude as controlled by the normalised excitation acceleration, when the excitation frequency is set equal to the first mode resonance frequency. In this thesis a weakly nonlinear system is being investigated, and for the physical system to

become more intrinsically nonlinear the excitation acceleration and the nonlinear cubic coefficient values have to be increased either by increasing the mass unbalance or by making the shaft more flexible, or both. Therefore in order to obtain and investigate the situation when the system is more strongly nonlinear the mass unbalance value is artificially increased to various multiples of the actual value. This manipulation increases the excitation value to a high level driving the weakly nonlinear system into more nonlinear reaches of the response range making the effect of the nonlinear terms proportionally greater than they would otherwise be. This effect causes the system to show possible bifurcations to chaos. The periodic response for the case based on the smallest mass unbalance in Figure 6-3(a) (i.e. the most weakly nonlinear response in Chapters 4 to 6), bifurcates to chaos as the mass unbalance increases. Positive Lyapunov exponents for figures 6-3(a)-(d) respectively show clear indication of chaos, while the negative Lyapunov exponents show stable motion. Also from these graphs, as the response become chaotic, less excitation acceleration is required in each of the four cases successively. One finds that five kinds of system motion exists over the range of excitation acceleration values. These are stable single period motion, stable period two motion, stable period four motion, stable quasi-periodic or multiperiod motion, and chaotic motion.

Figure 6-3(a) shows the bifurcation in the horizontal direction as controlled by the normalised excitation acceleration at a mass unbalance of $m_u = 0.004 \text{ kg}$, using the first mode resonance frequency value Ω from Table 6-1. It appears that for normalised excitation acceleration values from 200 to 730, the iterates settle down onto a fixed point. This is considered to be period one motion. At the value of 730 the fixed point becomes unstable and the period doubles, i.e. the iterates visit two different values in turn. At this value the period one motion becomes unstable in favour of a stable period two motion. Figure 6-3(b) and (c) show the bifurcation in the horizontal direction as controlled by excitation acceleration for the mass unbalance values $3m_u$ and $4m_u$ respectively. By increasing the mass unbalance values the periodic response bifurcates to period doubling and finally to chaos. Negative Lyapunov exponents show stable motion, while the positive Lyapunov exponents show clear indication of chaos.

Period doubling bifurcation is observed with a further increase of mass unbalance value in Figure 6-3(d). Period two, period four and multiperiod motions can be found for the regions of excitation acceleration leading to chaos. Also shown is a period doubling bifurcation process leading to a second chaotic motion after the first chaotic motion. It can also be observed from Figure 6-3 that any time the system bifurcates to higher multiples of periodic motion, a jump up to the zero level in the Lyapunov exponent plot occur, which is also an indication that the system moves to higher multiples of the period.

Figure 6-4 shows the bifurcation as controlled by normalised excitation acceleration in the horizontal direction, and using the first mode resonance frequency value, when a parametric force term is included at a parametric frequency of twice the first mode resonance frequency value. By increasing the mass unbalance values, the periodic responses remain periodic. The bifurcation diagrams do not change qualitatively, while the negative Lyapunov exponents show stable periodic motion. This means upon introducing the parametric force terms into the system all the period doubling and chaotic motions present in the system, and observed in Figure 6-3, become stable. This indicates that the period doubling and chaotic motions, which is bounded by the bifurcation set, is automatically shifted resulting in stable periodic motions.

Discrete excitation acceleration points in Figures 6-3 and 6-4 are selected for the plotting of phase planes, Poincaré maps and time plots for a more detailed understanding of the system's dynamics in the next section.

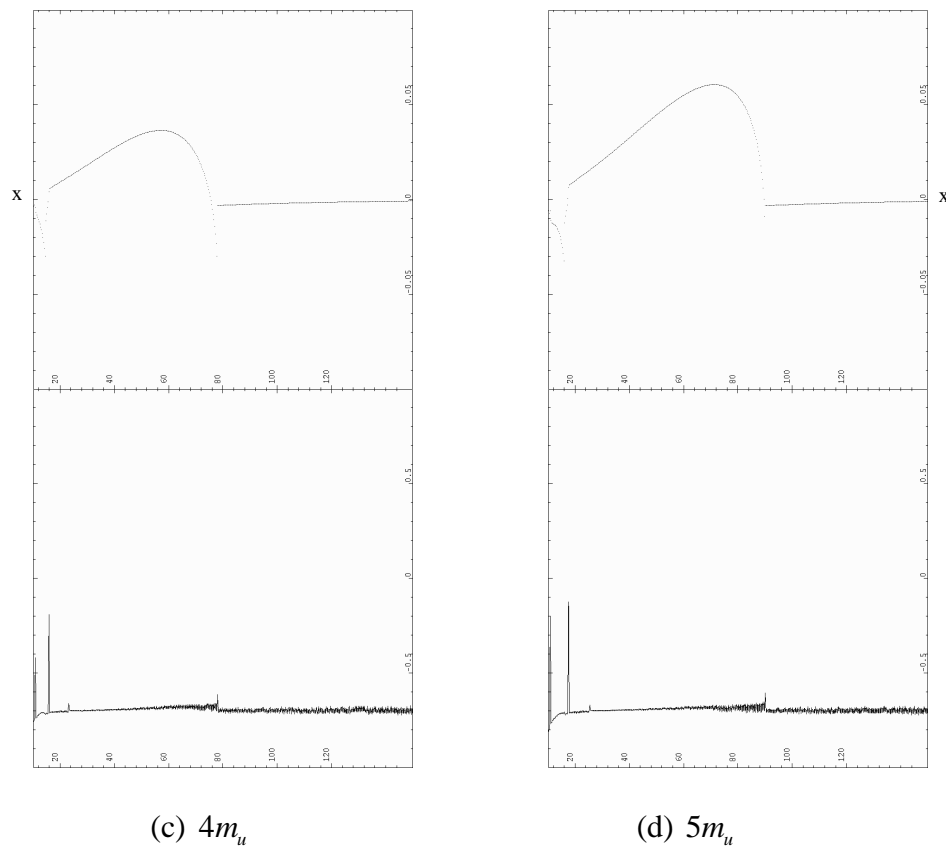
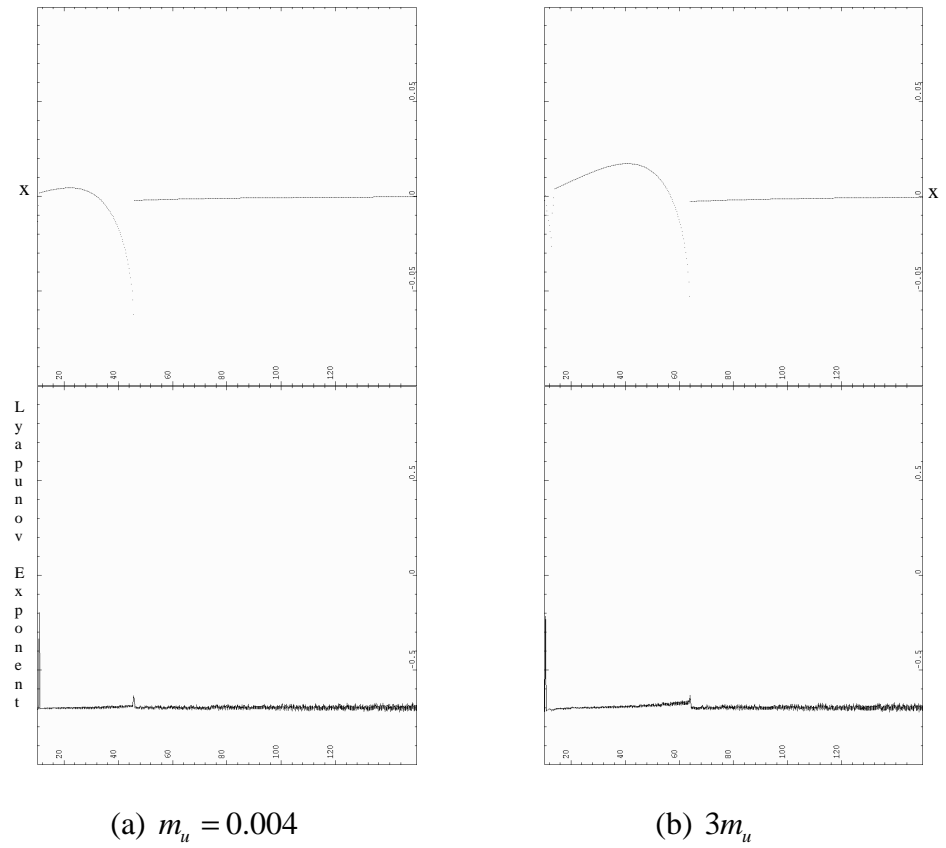
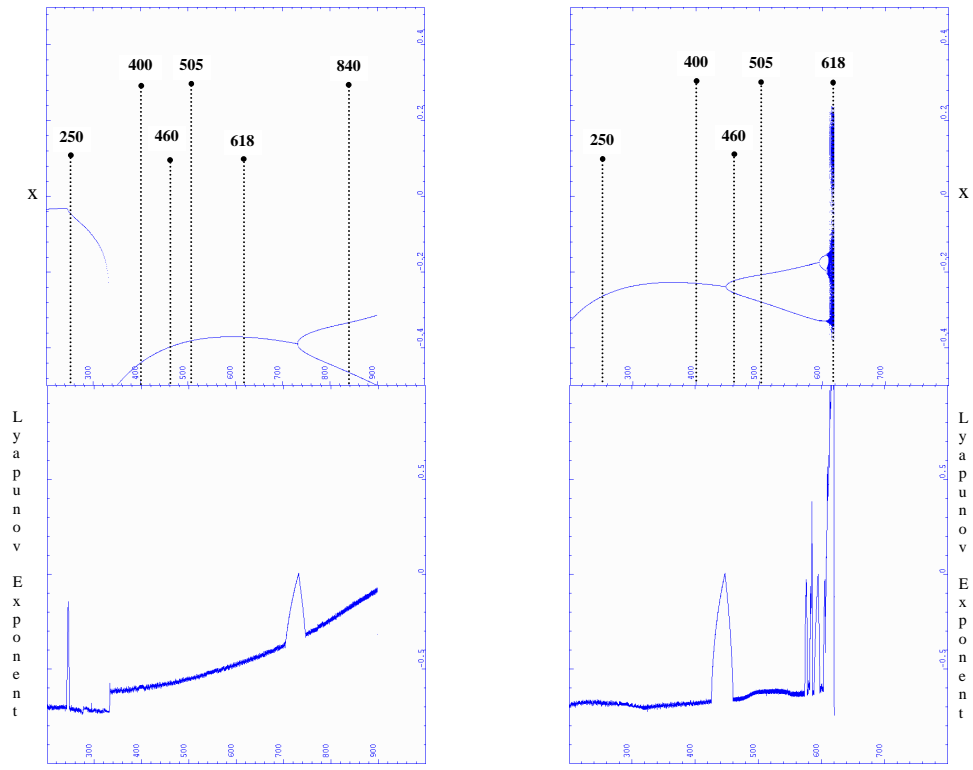
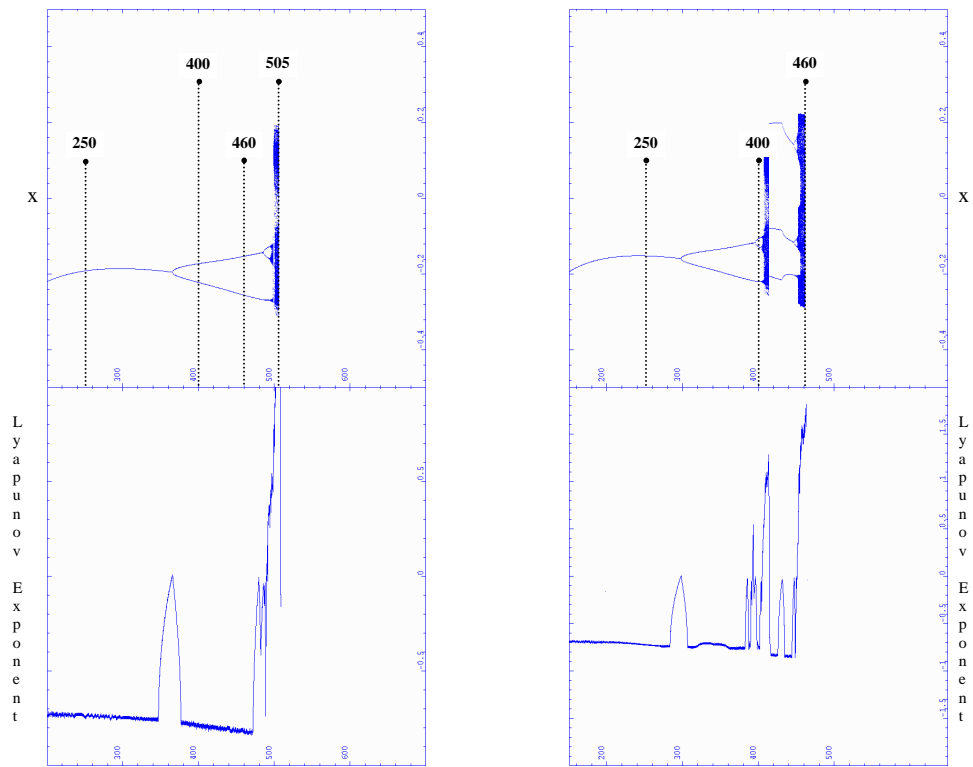


Figure 6- 2: Bifurcation diagrams showing amplitude as a function of Ω (X-axis: Ω , Y-axis: x_1, x_2), where $x_1 = x_2 = x$.



(a) m_u

(b) $3m_u$



(c) $4m_u$

(d) $5m_u$

Figure 6- 3: Lyapunov exponent and Bifurcation diagrams of amplitude as a function of the normalised excitation acceleration in the horizontal direction.

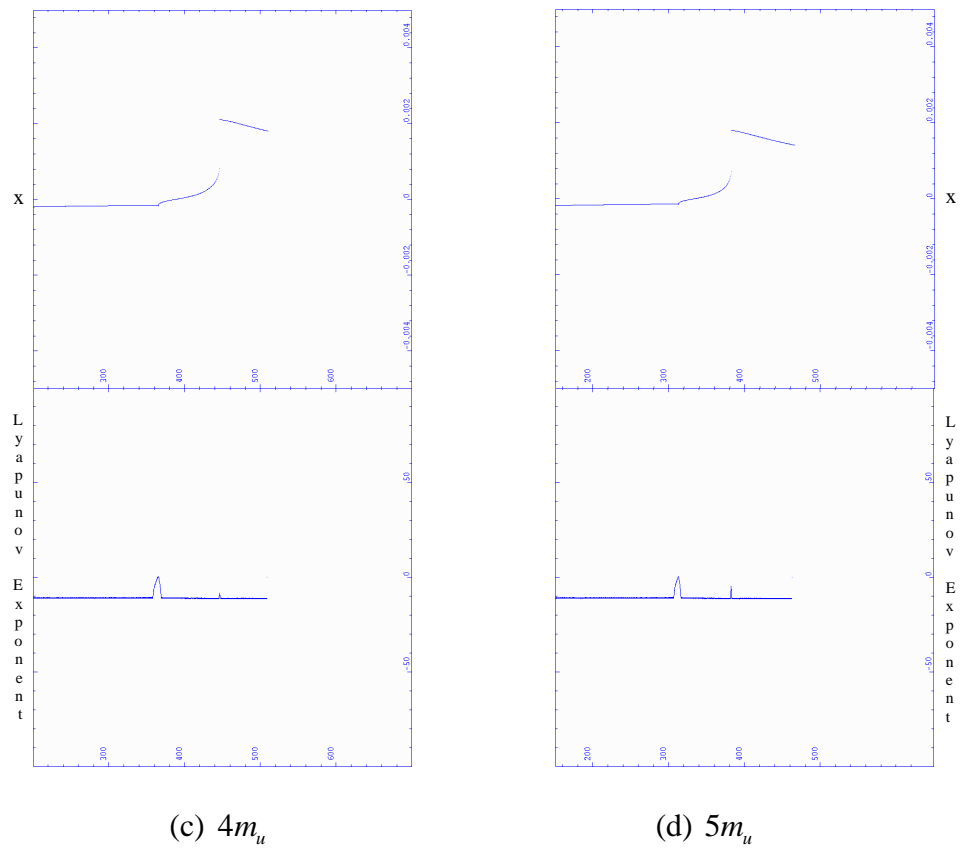
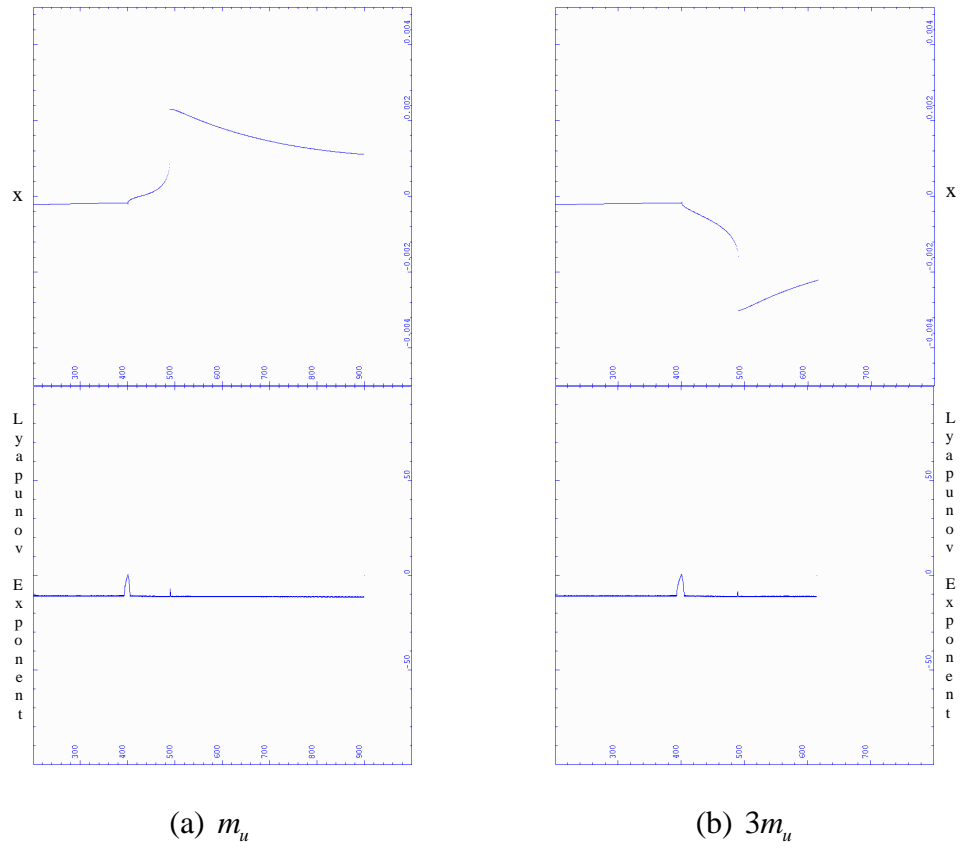


Figure 6- 4: Lyapunov exponent and Bifurcation diagrams of amplitude as a function of the normalised excitation acceleration for the Model with Parametric force term in the horizontal direction.

6.6 Phase Planes, Poincaré Maps and Time Plots

The response of a dynamic system in general could be a fixed point, a periodic solution, or a non-periodic solution. By studying the geometric characteristics and flow paths of the solution trajectory in the state space, the stability near the trajectory can be determined using phase portraits. For a trajectory that follows a close orbit in the phase portrait and returns precisely to where it first started after a period T , the motion is periodic and the closed orbit is called a limit cycle. Chaotic motions, on the other hand, have orbits that never close or repeat. Thus, the trajectory of the orbits in the phase plane will tend to fill up a section of the phase space. Although wandering of orbits is a clue to chaos, continuous phase plots provide very little information and one must use a modified phase plane technique called Poincaré mapping.

Poincaré map is a qualitative topological approach widely applied to the predictions of chaos and the study of stability in the phase space through exploring the geometric features of the sequence of points on a Poincaré section. A Poincaré section is a hypersurface in the state phase transverse to the flow of a system. In non-autonomous systems, points on the Poincaré sections represent the return points of the time series at a constant interval T , where T is the driving period of the existing force. The projection of all points in a Poincaré section to their image points by following trajectories until they first return to the Poincaré section is referred to as Poincaré map of the dynamic system. For a periodically forced, second-order nonlinear oscillator, a Poincaré map can be obtained by stroboscopically observing the position and velocity at a particular phase of the forcing functions. For quasi-periodic motion, the returns points in the Poincaré map form a closed curve. For a system undergoing chaotic motion, its associated Poincaré map shows specific shapes or many irregular points and features indicating the state and extent of bifurcation. For nT -periodic motion, the return points in the Poincaré map are n discrete points.

6.6.1 Analysis of Phase Planes, Poincaré Maps and Time Plots

More detailed analysis of Figures 6-3 and 6-4 are extended to phase planes, Poincaré maps and time plots (i.e. Figures 6-5 to 6-11) at discrete excitation acceleration points. The phase plane and time plots are plotted at assumed steady-state conditions, taken to be during the interval $t=995-1000$ seconds. However, the Poincaré maps are plotted from the transient time (i.e. $t=0$ to 1000 seconds) as most of them converge to a period one motion with just a point, therefore richer diagrams are preferred and so these maps converge to darker areas and finally to a point attractor. Those that are not in period one motion show irregular structures, or strange attractors, or a number of irregular points. A break-down of the observations for the sets of coupled equations with and without parametric terms is as follows.

6.6.1.1 At Normalised Excitation Acceleration of 250 (Figure 6-5):

- All the bifurcation diagrams for the different values of mass unbalance show periodic and stable motions with negative Lyapunov exponents as depicted in Figures 6-3 (a) to (d).
- The phase planes show a single closed orbit, showing only stationary, post-transient motion. The orbit is single and periodic, corresponding with the bifurcation diagrams. It indicates a period one motion. The solutions show regular patterns in the steady-state region of time $t=995-1000$ seconds and are indicative of stable periodic solutions.
- All the Poincaré maps converge into a single point (circled). As the maps consist of one point, which implies periodic motion, it indicates a period one motion with a stable attractor.
- All the time plots show evidence of a periodic response.

6.6.1.2 At Normalised Excitation Acceleration of 400 (Figure 6-6):

- The bifurcation diagrams in Figure 6-3(a) and (b) show period one motion whereas Figure 6-3 (c) and (d) show period two and period four motions, respectively. All the motions are stable, with negative Lyapunov exponents.
- Their corresponding phase planes indicate the period doubling phenomena. Figures 6-6(a) and (b) show single closed orbits indicating a period one motion and 6-6(c) show a closed orbit crossing itself, and depicts a period two motion as in their bifurcation diagrams. Figure 6-6(d) show a period four motion as in their bifurcation diagrams. The orbits show regular pattern indicating stable solutions.
- The Poincaré maps consist of a finite number of points, implying periodic motions. In Figures 6-6(a),(b),(c) and (d), the maps converge to one, two and four distinct points indicating stable period one, period two and period four motions, respectively.
- All the time plots show evidence of periodic motions.

6.6.1.3 At Normalised Excitation Acceleration of 460 (Figure 6-7):

- The bifurcation diagrams for $5m_u$, in Figure 6-3(d), show chaotic motion with positive Lyapunov exponents, whereas that for $4m_u$, in Figure 6-3(c) shows period two motion with a negative Lyapunov exponent. All the others are in period one motion.
- The phase planes underpin the above. For the chaotic motions densely filled phase planes are obtained. The plots have overlaid, complicated and repeated orbit cross-overs. Had the simulation been allowed to continue, the plane would be even more overlaid by repeated orbit cross-overs. A complicated phase plot is one indicator of chaotic motion; however, motion that rides on a complicated looking orbit may very well be fully-predictable, and thus non-chaotic, because a phase plot with very

large numbers of degrees-of-freedom may look similarly complicated, even if the system is in fact linear and thus certainly non-chaotic.

- In Figures 6-7(a) and (b) the Poincaré maps show one distinct point indicating stable period one motion, and in Figures 6-7(c), 2 distinct points are shown indicating stable period two motion, whereas in Figures 6-7(d) the Poincaré map shows irregular shape and is that of chaotic motion, where more and more points are added to the map as the simulation time marches on, filling out the details of the strange attractor on which the chaotic motion rides, and therefore indicative of chaotic motion.
- The time plots are in periodic motion, except for one in Figure 6-7(d) where the oscillations never repeat. This is another qualitative visual indicator of chaotic motions.

6.6.1.4 At Normalised Excitation Acceleration of 505 (Figure 6-8):

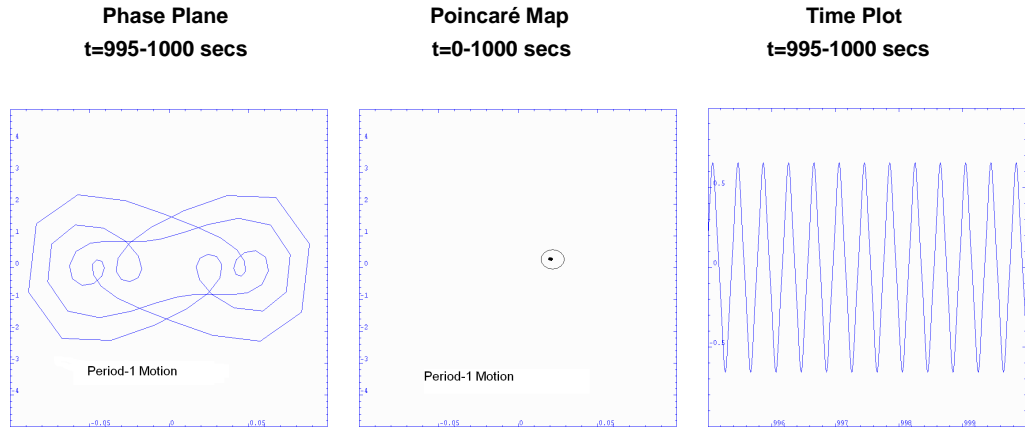
- Bifurcation diagrams in Figures 6-3(a) and (b) show period one and period two motions respectively with negative Lyapunov exponents, whereas Figure 6-3(c) show chaotic motions with positive Lyapunov exponents.
- The phase planes underpin the above. For the chaotic motions densely filled phase planes are obtained. The plots have overlaid, complicated and repeated orbit cross-overs. Figures 6-8(a) and (b) show closed orbits indicating period one and period two motions respectively.
- In Figures 6-8(a) and (b) the Poincaré maps show one and two distinct points respectively indicating stable period one and period two motions respectively, and in Figures 6-8(c) the Poincaré map shows an irregular shape and is that of chaotic motion.
- The time plots in Figures 6-8(a) and (b) show stable motions, but the plot in Figure 6-8(c) is non-periodic, the oscillations do not repeat, indicating chaotic motion.

6.6.1.5 At Normalised Excitation Acceleration of 618 (Figure 6-9) and 840 (Figure 6-10):

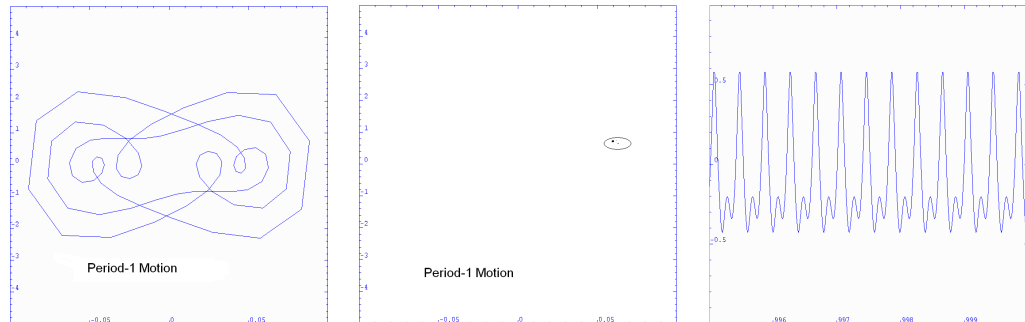
- The phase planes, Poincaré maps and time plots for these discrete normalised excitation acceleration display periodic or chaotic motions corresponding with their bifurcation diagrams in Figure 6-3.

6.6.1.6 Including Parametric Force Term (Figure 6-11):

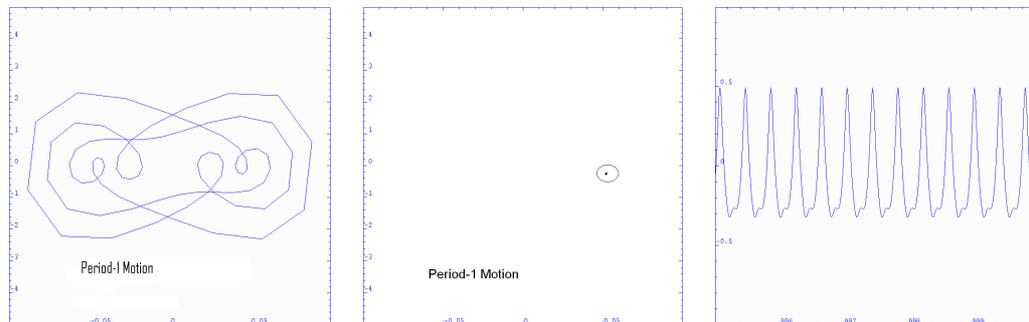
- All the bifurcation diagrams for models in Figure 6-4 show stable periodic motions with negative Lyapunov exponents.
- By analysing the system at the excitation levels, Figure 6-11 shows the phase plane, Poincaré map and time plot for the discrete normalised excitation acceleration displaying stable periodic motions corresponding with their bifurcation diagrams and Lyapunov exponents.



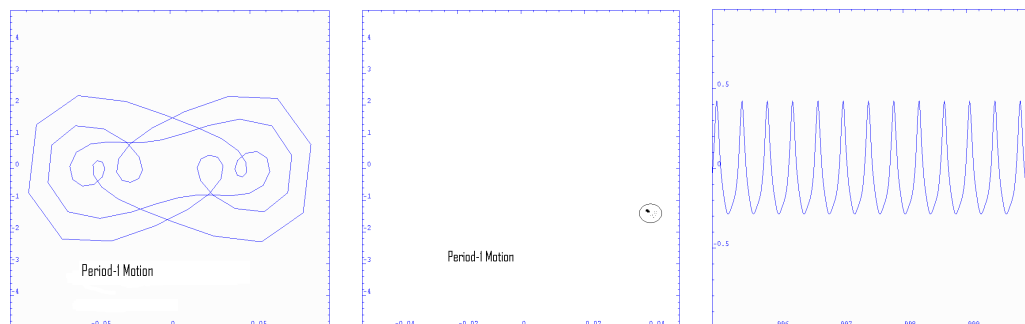
(a) m_u



(b) $3m_u$



(c) $4m_u$



(d) $5m_u$

Figure 6- 5: Dynamical analysis of response to normalised excitation acceleration at 250 in the horizontal direction

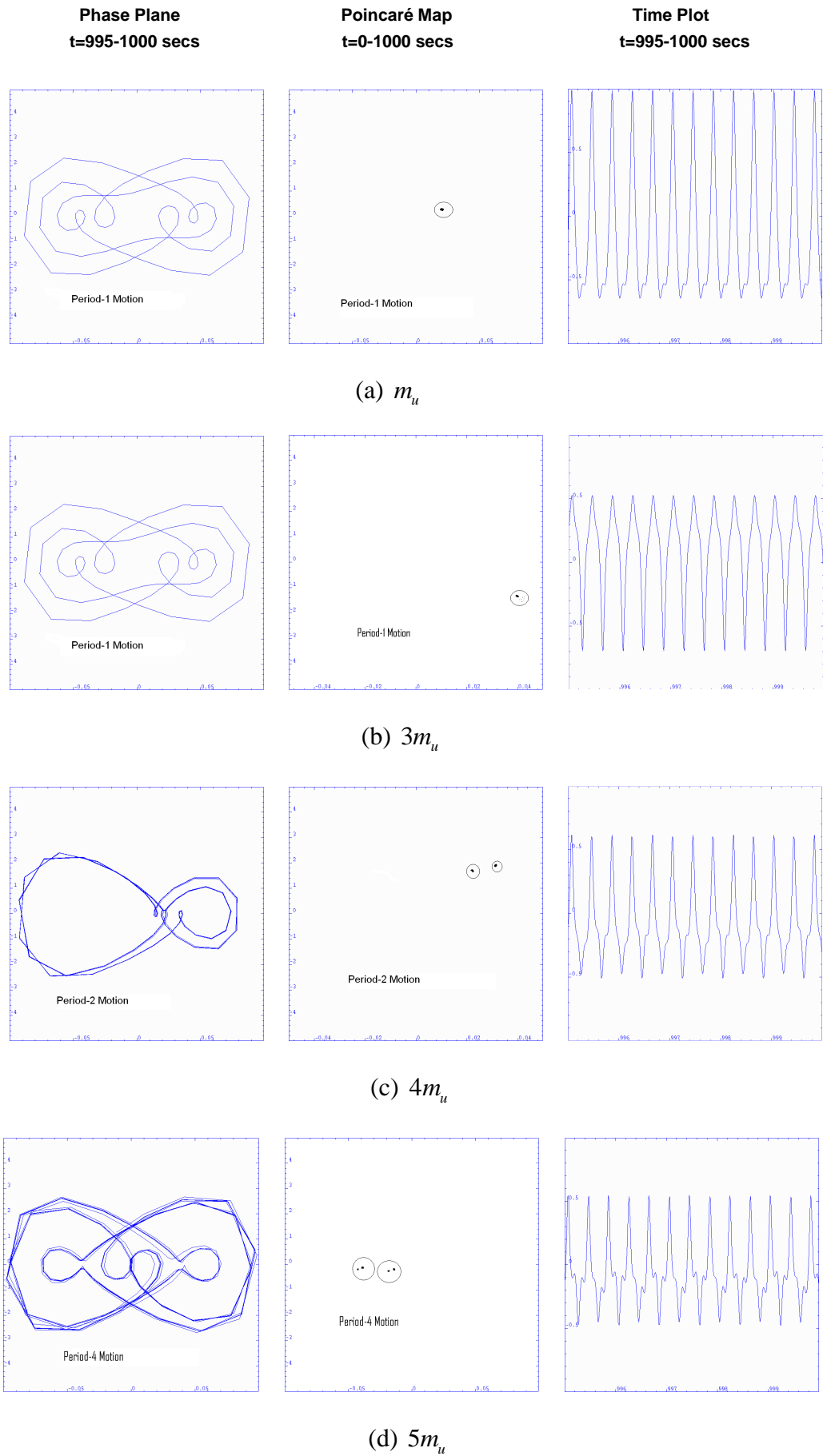


Figure 6- 6: Dynamical analysis of response to normalised excitation acceleration at 400 in the horizontal direction

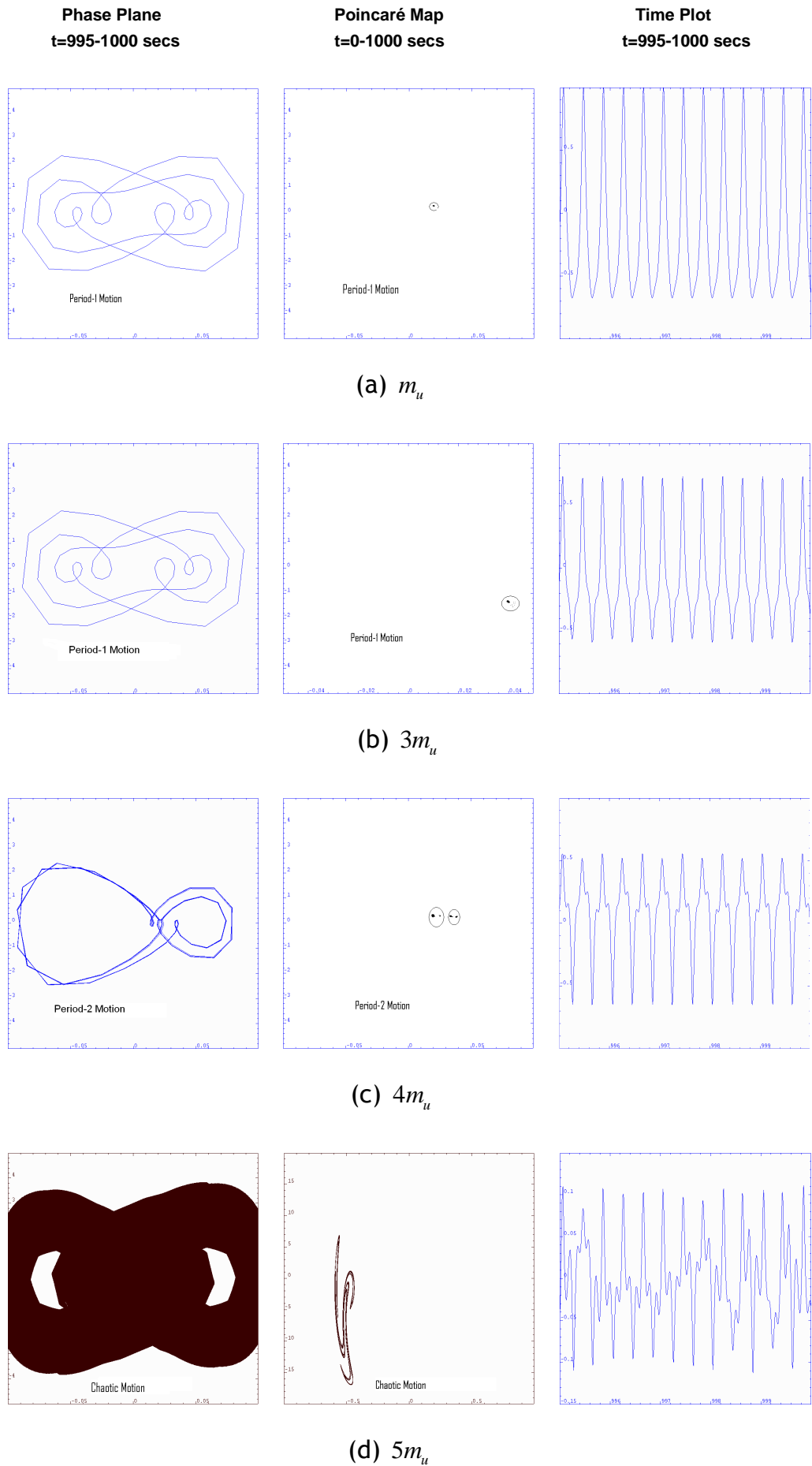


Figure 6- 7: Dynamical analysis of response to normalised excitation acceleration at 460 in the horizontal direction

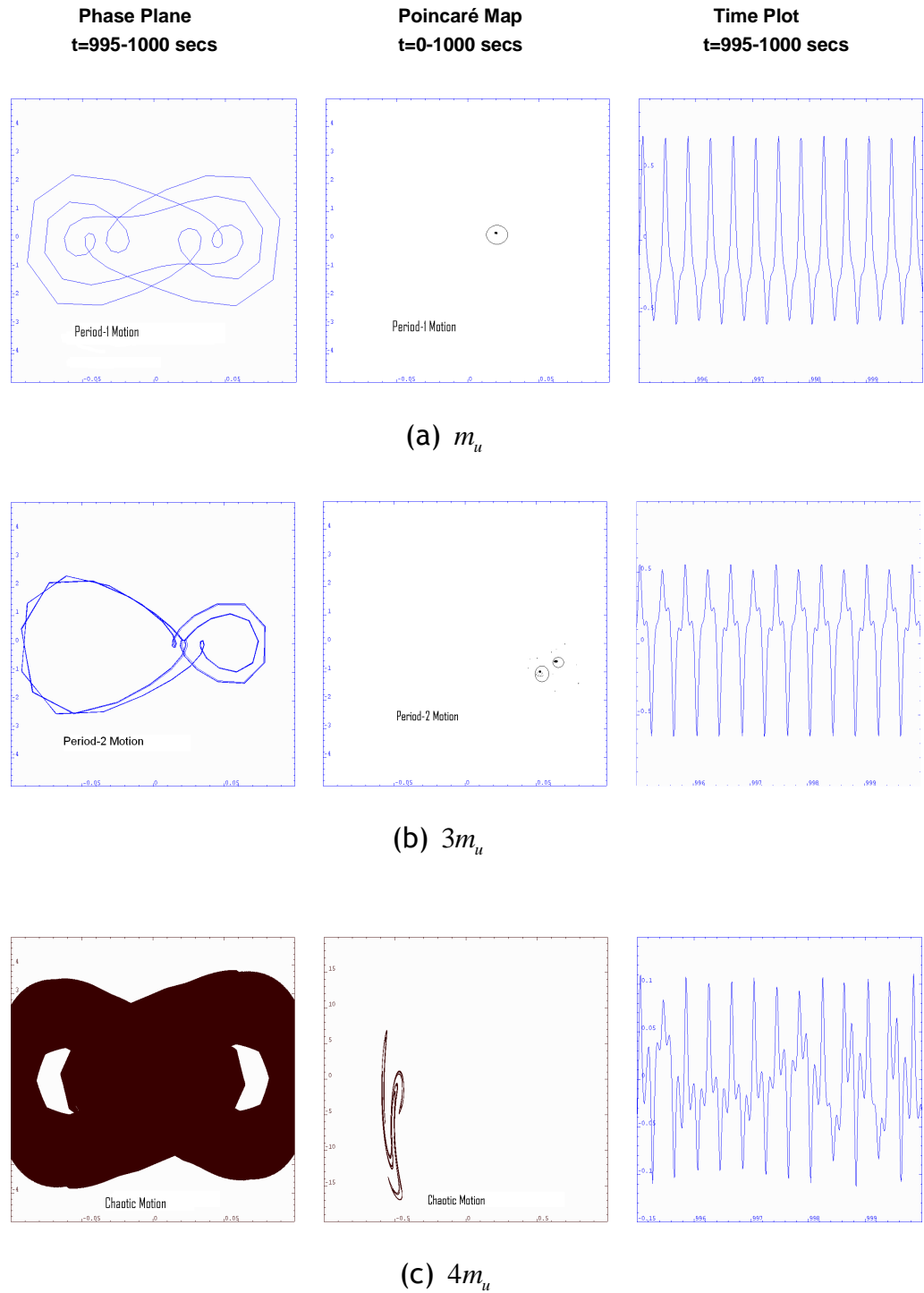
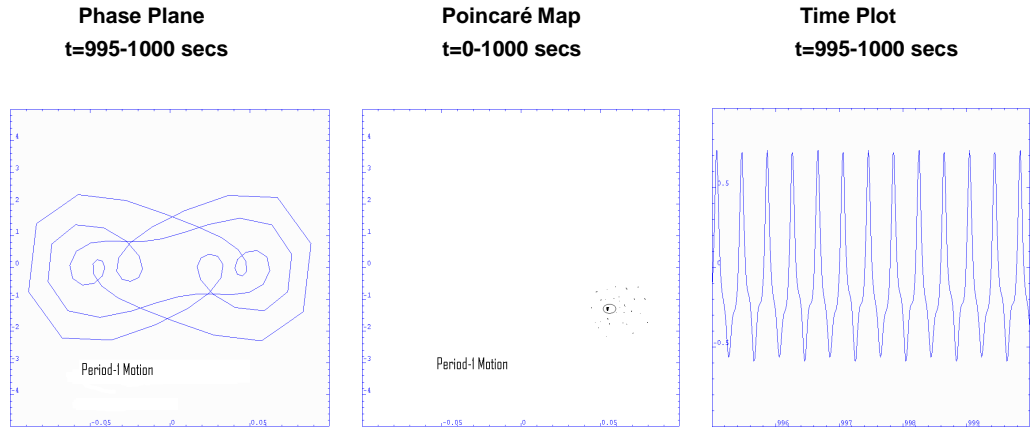
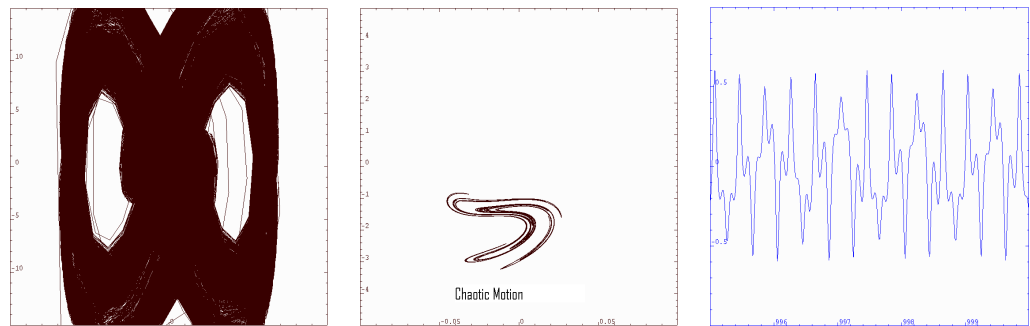


Figure 6- 8: Dynamical analysis of response to normalised excitation acceleration at 505 in the horizontal direction

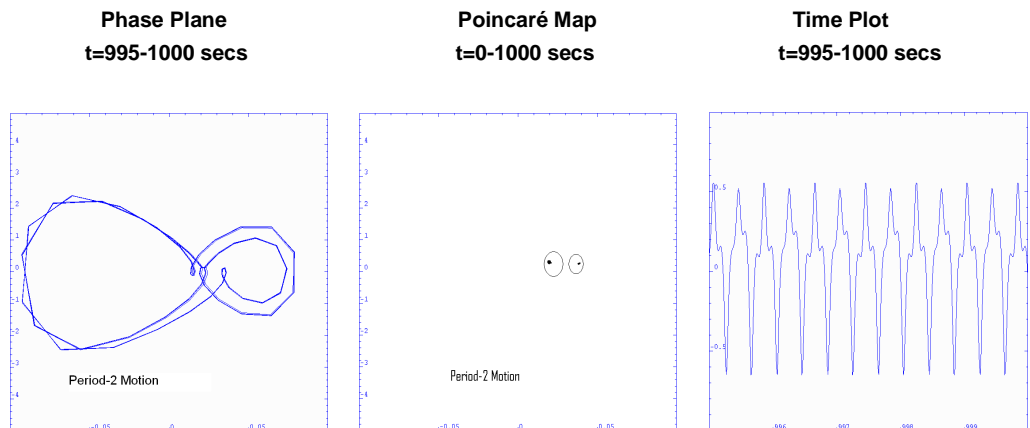


(a) m_u



(b) $3m_u$

Figure 6- 9: Dynamical analysis of response to normalised excitation acceleration at 618 in the horizontal direction



(a) m_u

Figure 6- 10: Dynamical analysis of response to normalised excitation acceleration at 840 in the horizontal direction

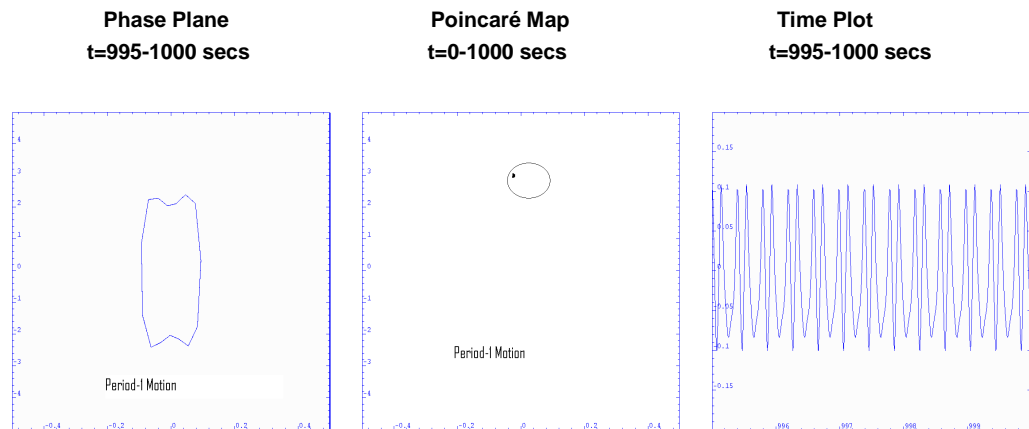


Figure 6- 11: Dynamical analysis of response to normalised excitation acceleration of models with the parametric force term in the horizontal direction

6.7 Numerical investigations in *Mathematica*TM code

In this section the numerical investigations of the systems dynamics has been carried out by employing the NDSolve integrator within *Mathematica*TM for the integration and prediction of the dynamics of the flexible rotor system for given initial conditions. The program code developed for the analysis of phase planes, Poincaré maps and time plots is presented in Appendix C2. The method used in the code is the Runge-Kutta method. All the plots in Figures 6-12 to 6-16 show stable periodic motions. The phase planes indicate periodic orbits in which the solutions start at the centre and moves outward in an elliptical motion. Corresponding Poincaré maps are plotted from the transient times as they converge to a period one motion and to darker areas in the middle. From these results there are no clear indications of chaos in the flexible rotor system.

More detailed analysis of Figure 6-3 are extended to phase planes, Poincaré maps and time plots at discrete normalised excitation acceleration points using the *Mathematica*TM program code and the results are presented in Figure 6-17. The program code is used for the prediction of chaos for the models by using the numerical data from table 6-1. Employing the NDSolve integrator within *Mathematica*TM in analysing the bifurcation plots in Figure 6-3 at normalised excitation accelerations of 618, 505, and 460 for $3m_u$, $4m_u$ and $5m_u$ respectively, the phase plane plots show overlaid, complicated and repeated orbit cross-overs. Their corresponding Poincaré maps show irregular shapes and are

indicative of chaotic motion. The time plots are non-periodic, the oscillations do not repeat and all the results mirror those in Figures 6-7(d) and 6-8 (c) and 6-9 (b) respectively.

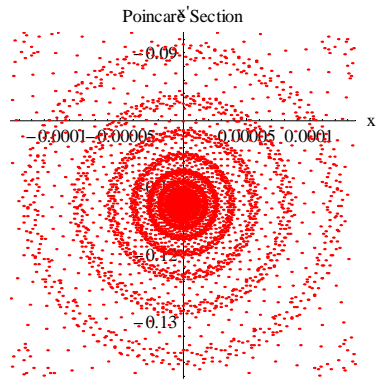
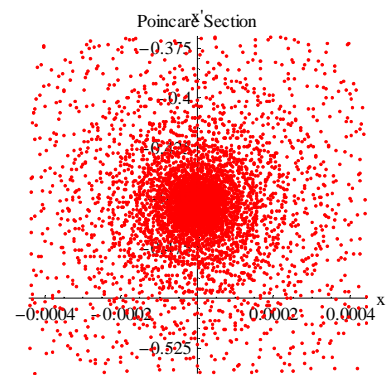
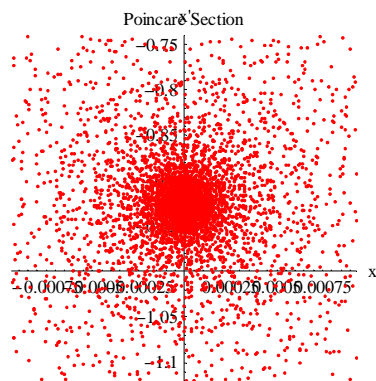
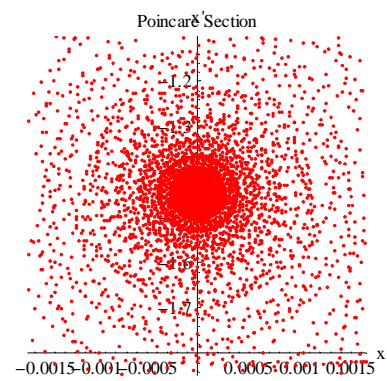
(a) m_u (b) $3m_u$ (c) $4m_u$ (d) $5m_u$

Figure 6- 12: Poincaré maps for the Models from solutions obtained from bespoke integration code in *Mathematica*TM.

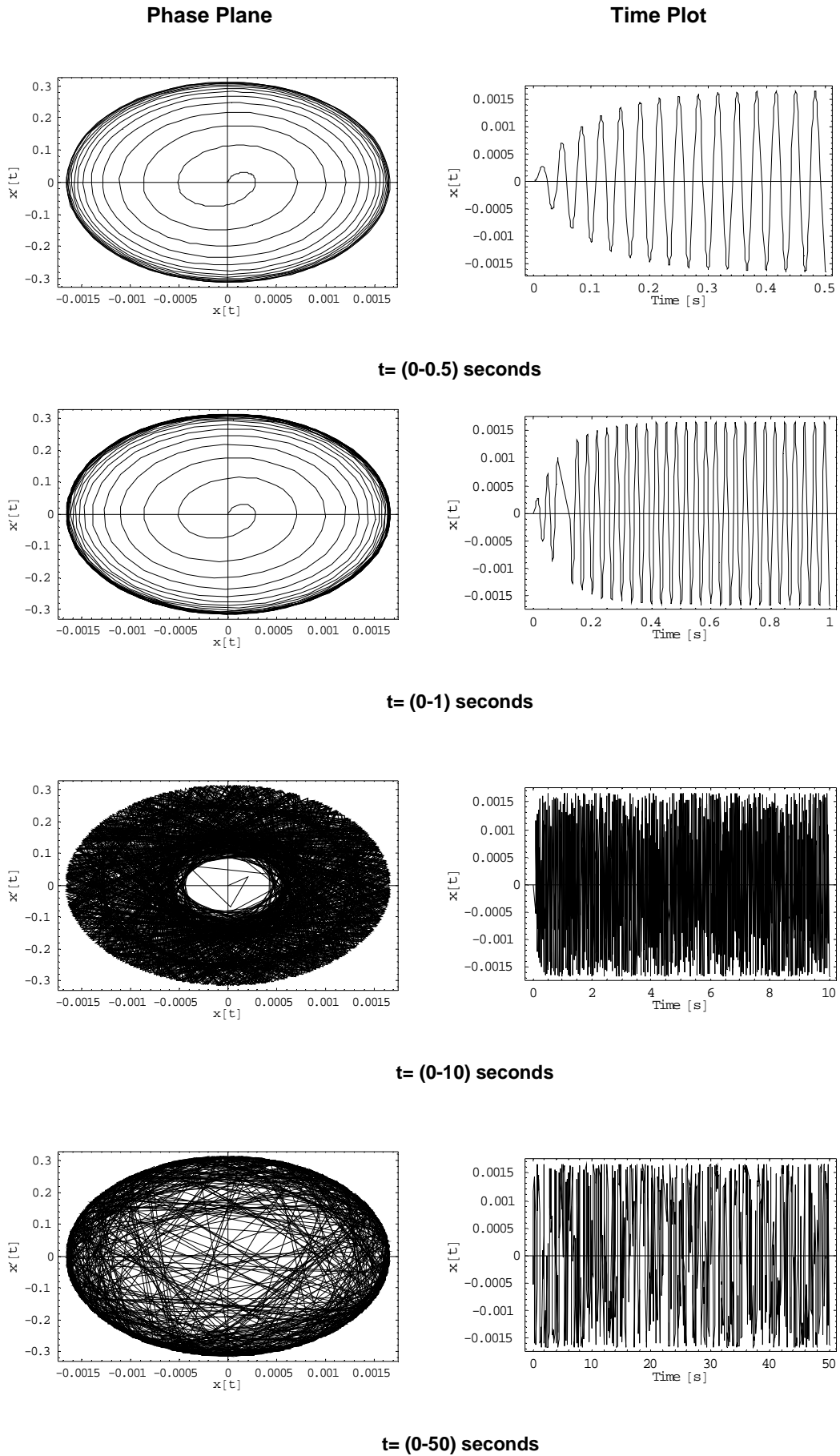


Figure 6- 13: Phase planes and Time plots for m_u from solutions obtained from bespoke integration code in *Mathematica*TM.

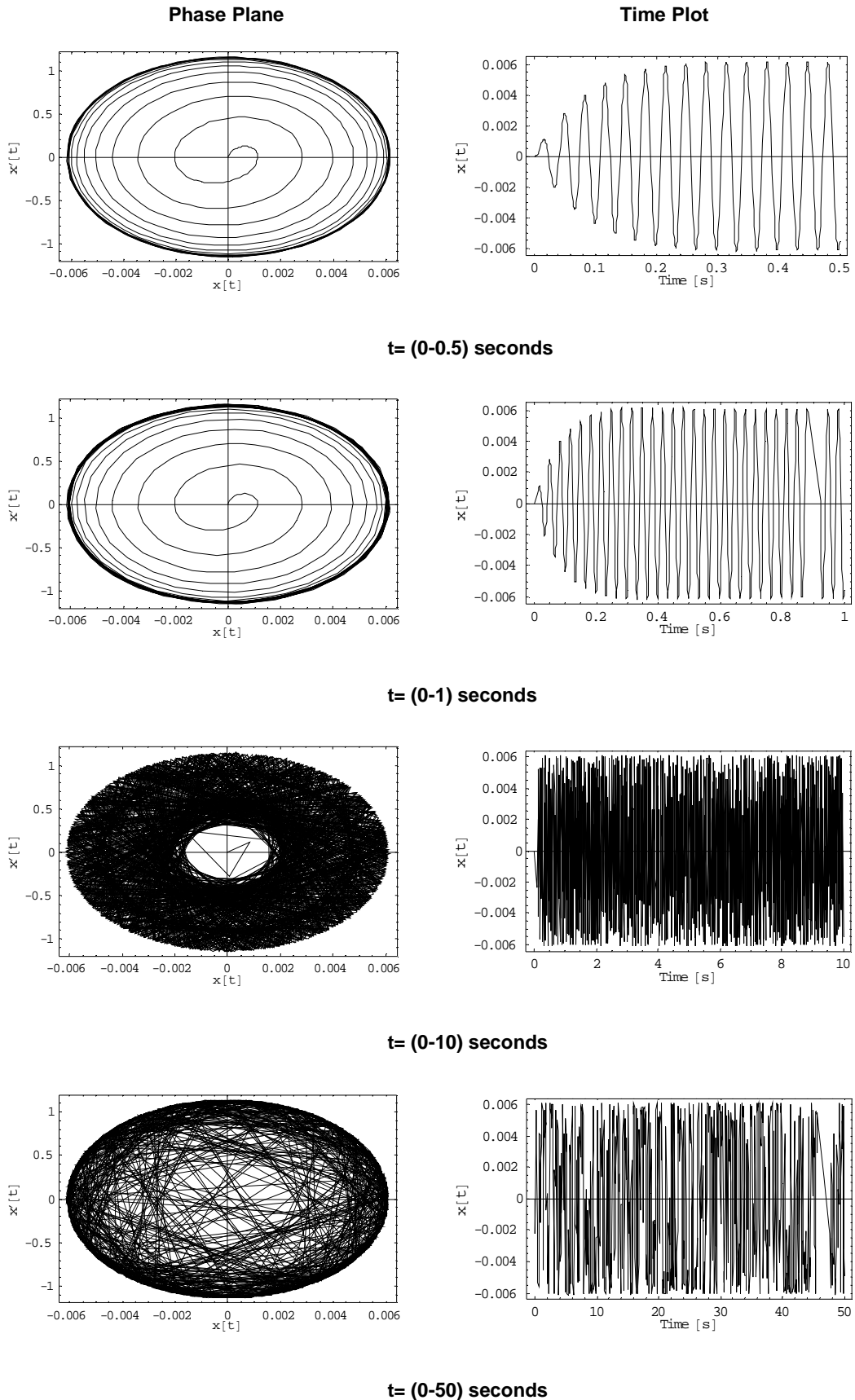


Figure 6- 14: Phase planes and Time plots for $3m_u$ from solutions obtained from bespoke integration code in *Mathematica*TM.

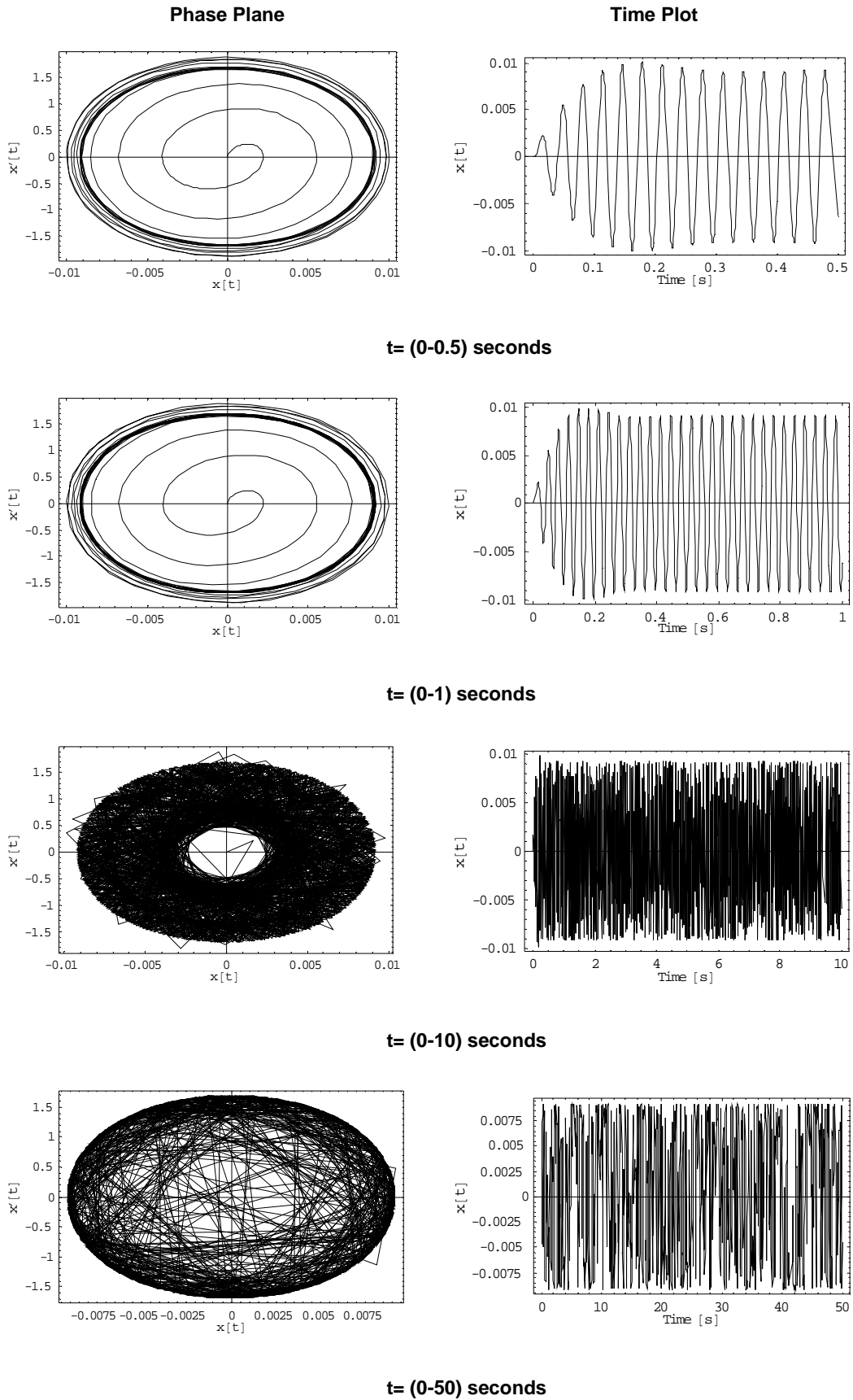


Figure 6- 15: Phase planes and Time plots for $4m_u$ from solutions obtained from bespoke integration code in *Mathematica*TM.

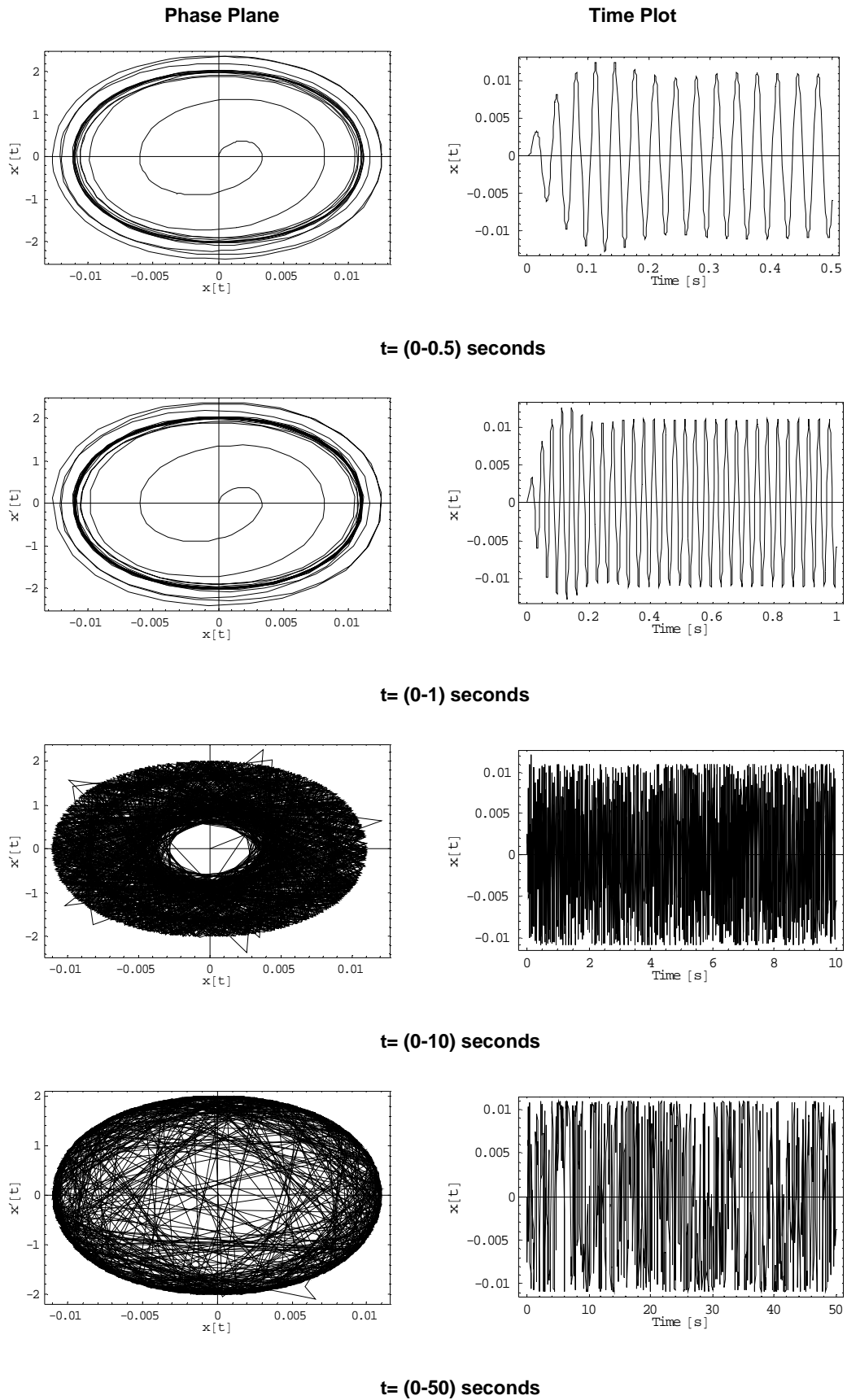
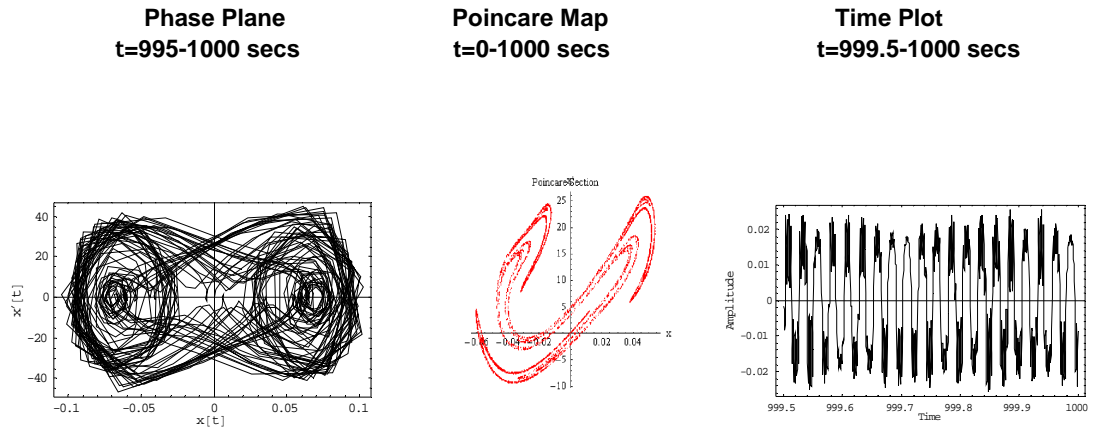
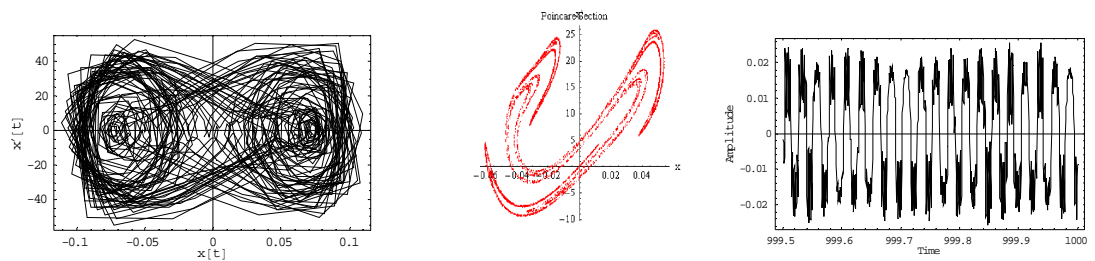


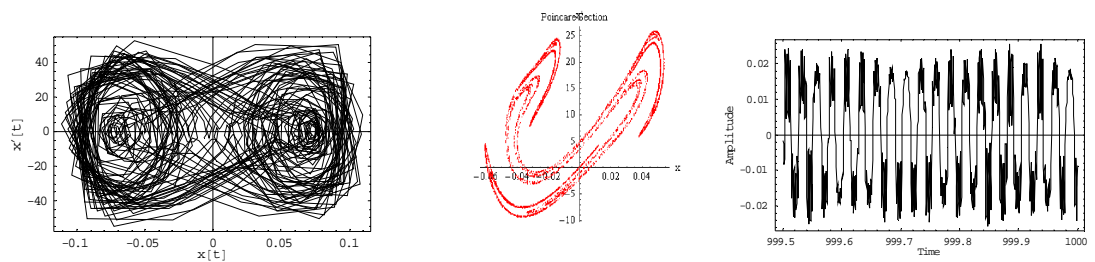
Figure 6- 16: Phase planes and Time plots for $5m_u$ from solutions obtained from bespoke integration code in *Mathematica*TM.



(a) At normalised excitation acceleration of 618 for $3m_u$.



(b) At normalised excitation acceleration of 505 for $4m_u$.



(c) At normalised excitation acceleration of 460 for $5m_u$.

Figure 6- 17: Dynamical analysis of response to normalised excitation acceleration at the various discrete points from solutions obtained from integration code in *Mathematica*TM

CHAPTER 7

EXPERIMENTAL INVESTIGATIONS

7.1 Controlling Flexible Rotor Vibration by means of an Antagonistic SMA/Composite Smart Bearing.

7.1.1 Introduction

The main themes of the research discussed in this chapter are the analysis and the testing of systems of integrated structural components and active actuators. In particular, systems are investigated comprising strategically designed and applied SMA and piezoelectric elements, i.e. SMA strips within glass/epoxy composites and piezoelectric stack actuators. Extensive recent research by Žak *et.al.*, (2003) and Inman *et.al.*, 2006 on the application of shape memory alloy (SMA) elements integrated within glass epoxy composite plates and shells has led to the design of a novel smart bearing based on the principle of antagonistic action. In a previous work by Žak *et.al.*, (2003), a sleeve ring composite host housing designed showed that a single SMA/composite active bearing could be very effective at both altering the natural frequency of the fundamental whirl mode as well as modifying the modal amplitude. The drawback of the single ended SMA/composite active bearing design is the disparity in the time constant between the relatively fast heating phase and the much slower cooling phase which is entirely reliant on externally supplied forced air cooling. This is principally because SMA can do no work when it is relaxing to its low temperature state, and so this was a significant limitation for the work as reported in the work of Žak *et.al.*, (2003). This has led to the antagonistic design in this thesis, in which each half of the new bearing has its separate heating as well as its own independent forced-air cooling system. The antagonistic design results in virtually equalising the time constants and giving faster responding push-pull loads on the centrally located bearing. This has the consequent knock-on effect of making the system generally more conducive to the control of resonant vibration.

It can often be useful to modify the frequencies of a rotor-shaft system. The main motivation in such cases is to avoid critical speeds whilst running up and running down rotors. The technique to be developed here is to use SMA/composite technology within bearing housings in rotating machinery in order to achieve optimal run-up and run-down of the rotor so that the effects of all significant resonances are modified. There are a number of ways in which variable pedestal properties may be devised to control the vibration levels and rotor stresses in a rotating machine. One option is to vary pedestal and/or bearing properties in such a way as to minimise the time a rotor spends at, or near, a critical speed. During operation, vibration levels may be substantially reduced by appropriate changes to support stiffness, causing changes to critical speeds.

The solution proposed here is to use the SMA effect to control the stiffness of a rotor bearing housing and hence manipulate the frequencies of the rotor system. The work proposed is an outgrowth of the previous work of Žak *et.al.*, (2003) and Segalman *et. al.*, (1993) to use an SMA composite to actively change the stiffness of the rotor system. This concept, attempted numerically in Segalman *et.al*, (1993) with basic models, is to avoid critical speeds during run up and was addressed by Žak *et.al.*, (2003) with improved modelling and experimental implementation. Žak *et. al.*, (2003), showed that for a laboratory rotor system supported on two bearings, one of which is an active component comprising a cylindrical sleeve with specially configured and integrated SMA strips, the critical speeds can be usefully shifted about their nominal values. The work shows how such an active bearing installation can be designed and discusses the many trade-offs required to optimise the performance in a useful way. It is shown that the principal trade-offs relate to stress in the composite host, the physical size and shape of this component, the quantity and distribution of SMA, and the local operating dynamics. The basic SMA effect is up to an 8% change in strain as the material's temperature is changed from the low temperature martensitic state to the high temperature austenitic state (Funakubo,1987). Usually, the SMA's temperature can be controlled either by direct or resistive heating. Here use is made of resistive heating by passing a controlled current of up to 35 A (at 12 V DC) through the SMA strips bonded to the bearing housing.

In the previous work of Žak *et. al.*, (2003) a simple flexible rotor system has been investigated. Different types of boundary conditions for the rotor have been examined theoretically: simply supported at both ends, one end simply supported, one end clamped, and then finally clamped at both ends. The dynamic behaviour of the rotor in terms of its modes of natural vibration, resonant frequencies and forced vibration amplitudes due to imbalance, have all been studied. The study showed conclusively that the dynamic response of a flexible rotor system could be substantially changed by adjusting the conditions at the shaft's boundary. With any rotor system operating above its first critical speed there are a number of issues to be addressed, the first, and perhaps most important, is the vibration level at the operating speed. The second issue to consider is the peak amplitude occurring during transient operation, such as run-up or run-down. A significant contribution to alleviating problems can be gained by varying the pedestal stiffness by the use of Shape Memory Alloys. A third area in which SMA technology can play an important role is in equalising the vertical and horizontal stiffness terms of a bearing support. This is particularly relevant in machines where gyroscopic terms are important, and this implies, almost invariably, high speed, overhung rotors.

7.1.2 Overview of the Experimental Rig

The rotor is supported by a heavy frame in order to be sure that all the vibrations, that are present and are to be detected by other devices, are due to the rotor itself and not to support structure effects. The mechanical core of the rig is an unbalanced rotor such that a force at the excitation frequency is generated during rotation. The rotor is supported by a frame as shown in Figure 7-3. The rotor-shaft is fixed on the left hand side by a normal ball bearing, whilst on the opposite side there is a special bearing comprising a composite tube fitted with axially equal-spaced SMA strips (Figure 7-2(a)). The shaft is located within a small ball bearing whose outer race is very tight press-fit into the composite tube. The electric motor (Figure 7-2(b)) is directly located within the lower part of the rig framework, and without the use of a special vibration damper to absorb vibration. The motion is transferred from the bottom of the rig to the top by a pulley-belt system (Figure 7-2 (c)) with a transmission ratio of one, so that shaft spin speed is equal to the electric motor speed. For monitoring the vibration produced, a laser vibrometer is used in connection with

a spectrum analyser. The SMA strip temperature is constantly kept under observation by means of thermocouples attached to the outer surface of the SMA strips. Thermocouples are used to detect the temperature of the strips and the room temperature. High current low voltage ohmic heating is used for SMA transformation, and the current levels are set by means of a series rheostat. High flow rate fans (Figure 7-2 (d)) are employed for the cooling of the SMAs. A special heater box designed such that switching on the heaters on one side of the antagonistic SMA/composite bearing automatically switches on the cooling fan on the other side and vice versa, is used to control the switching on and off of the heaters and the cooling fans.

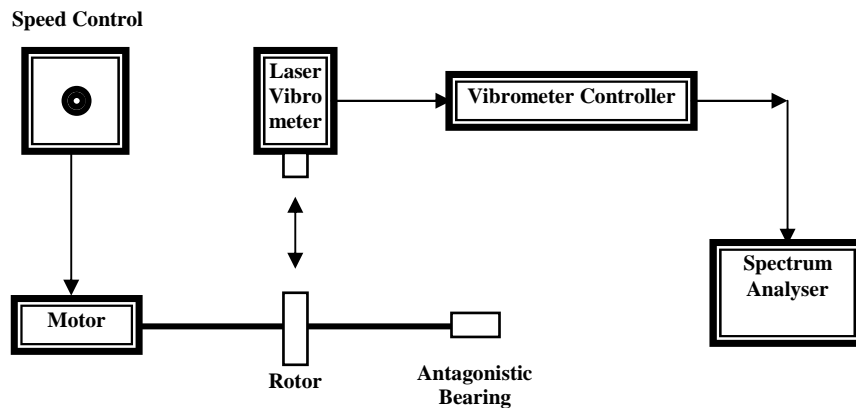
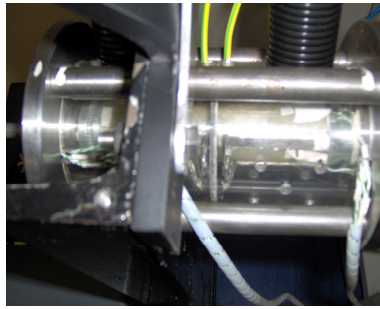


Figure 7- 1: SMA Experimental set-up for response measurements



(a) Antagonistic Bearing



(b) Electric Motor



(c) Pulley-belt system



(e) Cooling Fans

Figure 7- 2: Schematic view of Instruments used for the Antagonistic SMA/Composite Smart Bearing experiment

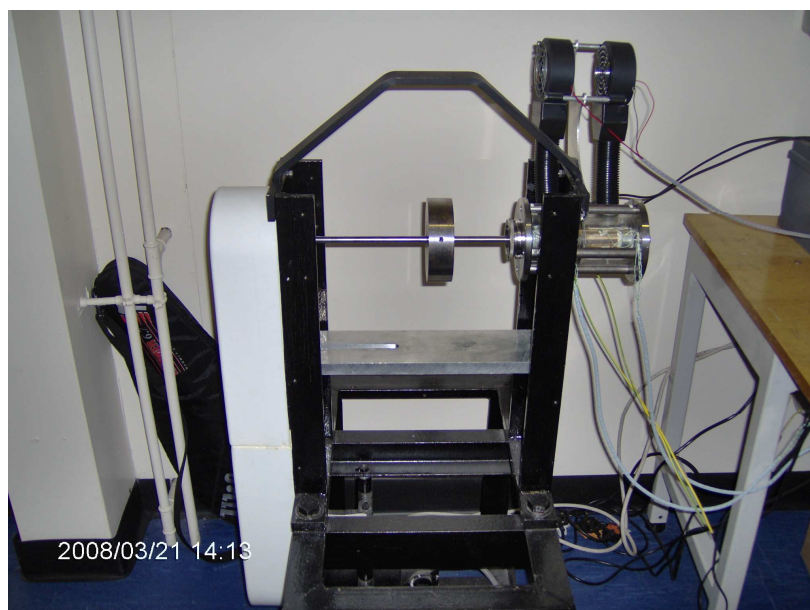


Figure 7- 3: The Antagonistic SMA/Composite Smart Bearing Test Rig

7.1.3 Active Bearing Concept

The basic concept proposed here is the use of integrated SMA/composites in the form of a cylindrical bearing housing, whose lateral stiffness properties could be actively controlled by means of SMA activation. This follows directly from the concept reported in Žak *et.al.*, (2003). However, one of the difficulties in using SMA as an actuator in a mechanical system is that SMA can do no work when it relaxes to its low temperature state. This was a limitation of the results given in Žak *et.al.*, (2003) that is rectified here by employing a new design using an antagonistic pair of SMA composite bearing housings. This new system has improved bandwidth and provides more control over the dynamics of the rotor system. A schematic of the antagonistic bearing system is given in Figure 7-4 where each end is actually fixed to ground. In this system a ball bearing is fitted halfway down a glass epoxy composite tube, entering through one end of the tube. The tube is divided into two regions, one on each side of the centrally located bearing. SMA strips are bonded in two independent sets of four, each set running axially along half the length of the tube and separated by 90 ° around the tube. The four strips in each set are electrically connected in series. This provides a convenient and fast way of heating each set of SMA strips through the martensite-to-austenite transformation temperature, and provides a significant axial contraction load on the tube in either direction indicated in Figure 7-4. The SMA can only perform work when heated and it would normally cool at the natural rate of convection with the surrounding medium (air in this case). Thus the relaxing rate of the SMA is not very controllable. To overcome this, two changes have been made. The first is to form the push-pull arrangement of Figure 7-4, which is termed *antagonistic* in this work. By alternating the current between the SMA strips between the left and the right sides of the bearing, the SMA actuation can perform work in both directions as illustrated by the arrows. So, as the SMA on the right relaxes, the SMA on the left is activated, giving both greater control authority and improved bandwidth of operation for the active bearing system. The second change in the design that was implemented in Žak *et. al.*, (2003) is to introduce active cooling of the SMA strips. The relaxation time of each strip is controlled by the convective heat transfer coefficient, following Newton's law of cooling. This coefficient ranges over several orders of

magnitude depending on the nature of the surroundings. In particular, the coefficient increases by an order of magnitude from still air to moving air. For example, for an SMA wire of 0.8mm, the heating time is about 50ms while the cooling time to 100% relaxation is about 1s under still air (Hunter *et.al.*, 1991). However, studies carried out by Shahin *et.al.*, (1994) showed that the time constant of relaxation improves up to four times if subjected to forced convection. Hence, an active cooling system was also added to the antagonistic active bearing system to achieve shorter relaxation times in the passive SMA.

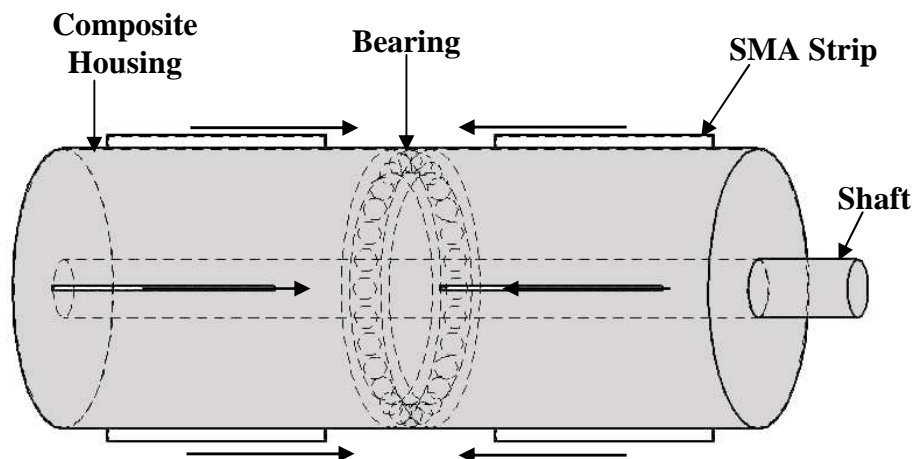


Figure 7- 4: Schematic of the antagonistic SMA/Composite bearing housing.

7.1.4 Active Bearing Experiment

The rotor-bearing system is set to the required excitation and the SMA elements are activated by passing a controlled current of up to 35A through them. The flexible rotor is stiffened by heating the outer SMA elements to about 120°C and then returned to the original state, just as quickly, by switching on the inner elements instead and simultaneously air cooling the outer elements to room temperature. The switch-over is performed again by switching off the inner elements, air-cooling them, and switching on the outer elements. The vibration response of the rotor-bearing system is then measured by means of a Polytech Laser Vibrometer allowing the response to be identified and monitored. A multi-channel data acquisition analyser is then used to analyse the responses. A series of timed tests is performed to assess the performance and average readings of

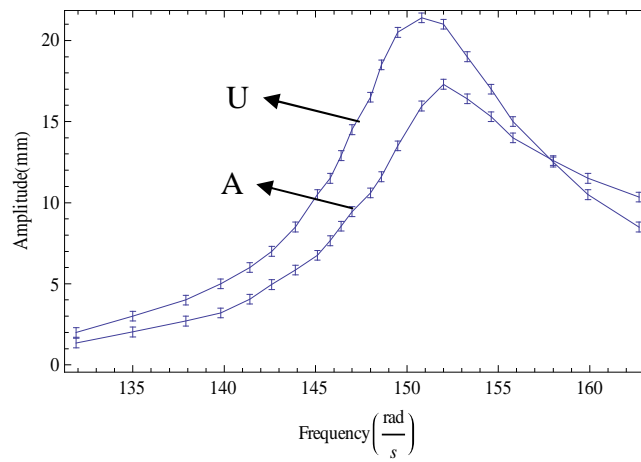
the amplitude values of the rotor system are taken. Sweep tests around the excitation frequency are performed, first without activating the SMA elements and then with the SMA elements activated.

7.1.5 Experimental Results

The results presented here are related to two states of the SMA strips. In the first state (not activated) it has been assumed that all the SMA strips are not activated, so no material properties are changed. In the second state (activated), however, when all the SMA strips on any one side are activated at the same time certain changes in the mechanical properties of the SMA material take place, namely Young's modulus (see table 7-1). No recovery stresses or recovery strains generated during the activation of the SMA strips are considered here. Such an activation scenario corresponds to the Active Property Tuning (APT) method (i.e. where only changes in the material properties of the SMA components are utilised (Rogers *et.al.*,1989)). In this thesis the dynamic responses of the rotor system are presented in terms of changes in amplitudes of forced vibration. The frequency sweep responses with their corresponding amplitudes of vibration for the antagonistic case are presented in Figures 7-5 and 7-6. As can be clearly seen from the results presented in Figures 7-5 and 7-6 the antagonistic configuration of the SMA strips is a fundamental factor in maximising the dynamic performance. The dynamic performance is defined here in terms of changes in the resonant frequencies of the rotor and in terms of the amplitudes of the disk vibration due to the activation of the SMA strips. The experimental results for the forward-whirl amplitude in the flexible rotor have demonstrated that the stiffness can be influenced by the SMA. The measured responses of the rotor system from repeated tests are shown in Figures 7-5 and 7-6. Resonant frequency shifts and amplitude reductions are observed when both the right hand and left hand sides of the SMA strips of the antagonistic bearing are activated. In the case of the unactivated SMA, an excitation frequency of the disk of 24 Hz is obtained, while the excitation frequency shifts to 24.2 Hz when the SMA is activated. It is thus shown that the first resonant frequency of the rotor is shifted by approximately 8% when the SMA strips are activated. At the same time the activation of the SMA strips reduces the amplitudes of the disk vibration by 19.4%.

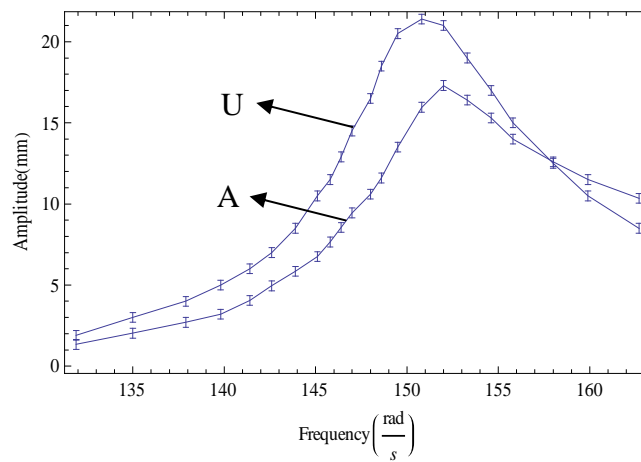
Property	Value	Property	Value
Martensite finish temperature M_F	20.7°C	Young's Modulus E_M	33.1 GPa
Martensite start temperature M_S	26.8°C	Young's Modulus E_A	69.6 GPa
Austenite start temperature A_S	37.2°C	Coefficient of thermal expansion α_M	$6.6 \times 10^{-6} / ^\circ C$
Austenite finish temperature A_F	47.0°C	Coefficient of thermal expansion α_A	$1.1 \times 10^{-5} / ^\circ C$
Stress influence coefficient C_M	10.6 MPa / °C	Critical Stress σ_S	80.0 MPa
Stress influence coefficient C_A	9.7 MPa / °C	Critical Stress σ_F	155 MPa
Maximum residual strain ϵ_L	0.058		

Table 7- 1: Material properties of a typical SMA material (Ni-Ti alloy), (<http://www.sma-inc.com>).



U- SMA unactivated, A- SMA activated

Figure 7- 5: The amplitudes of disc vibration versus excitation frequency for the right hand side of the Antagonistic Bearing.



U- SMA unactivated, A- SMA activated

Figure 7- 6: The amplitudes of disc vibration versus excitation frequency for the left hand side of the Antagonistic Bearing.

7.2 Controlling Flexible Rotor Vibration by means of a Piezoelectric Stack Exciter.

7.2.1 Introduction

Unbalance forces are the main source of vibration in rotating machines, but perfect balance is almost impossible to achieve. Moreover the distribution of unbalance can change in time because of wear or depositions all machines are subjected to. Reduction of rotor vibration is very important for safe and efficient functioning of all rotating machines. This section proposes an active vibration control scheme for controlling transverse vibration of a rotor shaft due to mass unbalance and presents an experimental study. The use of piezoelectric actuators in active vibration control has been considered in the past by Palazzolo *et.al.*, (1993) and Barret *et.al.*, (1993). Yabuno *et.al.*,(2001) used a piezoelectric actuator to stabilize the parametric resonance induced in a cantilever beam and to control bifurcation resulting in the shift of the bifurcation set and the expansion of the stable region. Carmignani *et.al.*,(2001) developed an adaptive hydrodynamic bearing made up of a mobile housing mounted on piezoelectric actuators. In their work they showed that imposing a harmonic displacement on the mobile bearing, in two orthogonal directions, a rotating force, and a correcting moment can be produced on the shaft of a rotor system to reduce the bending caused by the unbalance. Das *et.al.*,(2007) proposed an active vibration control scheme for controlling transverse vibration of a rotor shaft due to unbalance. These authors worked on the vibration control of rotors due to unbalance by placing electromagnetic exciters, at convenient locations on the span of the rotor away from the bearings. They showed that, locations distant from discs are in general convenient for exciters as they do not interfering in any way with the rotor operation. The technique looks good economically, as no change in the choice or design of the existing bearing or support system of the shaft is needed. Similar electromagnetic exciters were conceptualised by Janik *et.al.*, (1998) and were used to excite a rotor-shaft system for extracting the modal information by Janik *et.al.*, (2000) and Irretier *et.al.*, (2002).

There are many natural phenomena in which excited parametric and self-excited vibrations interact with one another. Examples are flow-induced vibrations and

vibrations in forced rotor systems. The responses of nonlinear excited systems to parametric excitations have been investigated by many researchers. Several authors, including Skalak and Yarymovych (1960), Struble, (1963), Dugundji *et. al.*,(1970), Chester (1975) and Cartmell (1990) have studied the effects of combined parametric and forced vibrations in dynamic systems. Frolov, (1967) examined a mechanical system excited simultaneously by parametric and periodic forced excitations. Frolov, (1967) showed that the resonant amplitude can be reduced by random variation of the system parameters. Kotera *et. al.*,(1985) studied a beam subjected to a periodic axial force and simultaneously to a flow-induced vibration. Mustafa and Ertas,(1995) theoretically and experimentally examined the effect of a pendulum (attached to the tip of a parametrically excited cantilever beam) whose natural frequency is tuned to be commensurable with a frequency of the beam in order to generate autoparametric resonance. For chosen external and internal resonance combinations, where the excitation frequency is twice the natural frequency of the first beam mode, and the linearised pendulum frequency is one-half that of the first beam mode, the results showed that, in some parametric excitation frequency ranges, the pendulum acts as a vibration-absorbing device in the same manner as the pendulum attached to the main system under external excitation. Nguyen and Ginsberg (2001), studied vibration control of a simple pendulum using parametric excitation. They showed that with judicious selection of the parametric excitation, a parametric frequency that is very high relative to the highest contemplated excitation frequency can substantially reduce the forced vibration response at any lower excitation frequency. The above ideas have led to the design of the piezoelectric exciter and the deliberate introduction of parametric excitations into a flexible rotor-bearing system axially to moderate the response of the pre-existing mass-unbalance vibration inherent to the rotor. The idea here is to use a piezoelectric stack actuator to put axial excitations into the shaft to investigate the interactions between forced vibrations, which emanate from rotor unbalance, and parametric excitation which results from the periodic stiffness variation caused by a periodic axial excitations from the actuator. No attempt of vibration control of rotor systems by the use of an axially placed piezoelectric exciter has, however been reported to the author's knowledge. Using the stability theory discussed in the previous chapters, a practically implementable strategy is proposed in which the inherent and

predominant instabilities in the flexible rotor-bearing system are manipulated in such a way that their effects on the overall performance of the rotor system can be effectively controlled. In justifying this work, a programme of experimental research has been carried out and the results show reductions in the resonant amplitudes for forward whirl in the flexible rotor-bearing system.

7.2.2 Instrumentation

A commercial rotor-kit (Bently Nevada rotor kit RK4) and a piezoelectric exciter specifically developed during this research are used for this experiment. The rotor kit provided a rotor supported by bearings, an electrical drive to run the rotor with a separate control box from which the desired rotational speed is selected. The torque is transmitted from the electrical motor to the rotor by means of a solid coupling. Provided are displacement transducers to measure the movements of the rotor, and a rigid V-shaped base, to which any components could be easily attached. The rotor kit is equipped with the piezoelectric exciter designed for active vibration control. The critical parts of the exciter unit are, a piezoelectric actuator supported by a helical compression spring, all placed inside a linear sliding bearing, and an aluminium casing. The piezoelectric actuator is driven by a function generator through a piezoelectric actuator amplifier. To avoid direct contact between the shaft and piezoexciter, and to allow free rotation and movement of the shaft end, a small self-aligned bearing is fixed in between the shaft and the piezoexciter. The vibration response of the rotor is then measured by means of a Polytec Laser Vibrometer allowing the displacement responses to be identified and monitored by a multi-channel data acquisition analyser. Figures 7-7 and 7-8 show the experimental configuration for activating the flexible rotor system. The leading principle here is to control, axially, the vibrations of the rotor, supported on conventional bearings, by using the piezoelectric actuator.

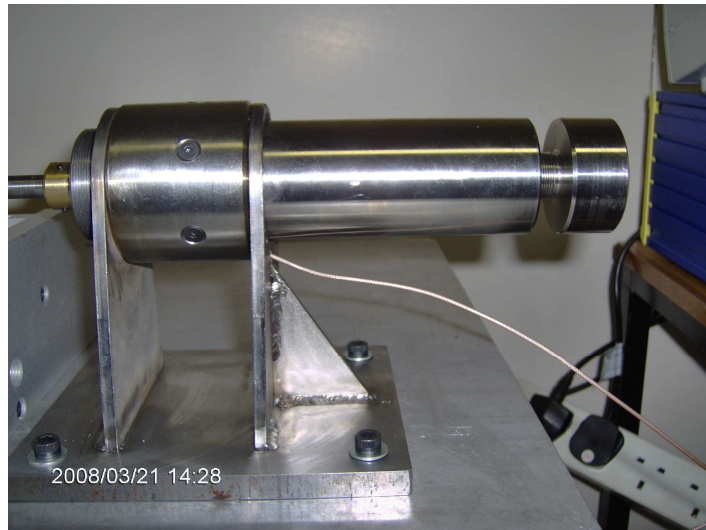


Figure 7- 7 : Close-up of the Piezoelectric Exciter

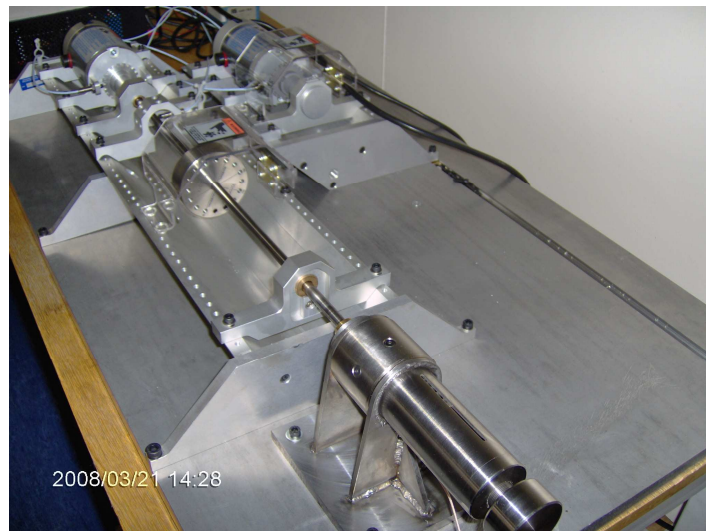


Figure 7- 8: Assembly of the Piezoexciter Test Rig

7.2.3 Design and Selection of Piezoexciter Component

To select a suitable piezoelectric actuator there is the need to determine the likely force levels needed to excite the rotor parametrically, and suitable exciters which can provide this, at appropriate levels of displacement. As the rotor whirls there will be millimetre level axial contraction of the shaft leaving a gap which will have to be taken up in one way or another. Use was made of the mathematical model including the axial excitation force term developed in Chapter 3 to find the parametric excitation force that is actually needed for the

rig, in order to get parametric resonances and the displacement due to the axial contraction of the shaft. The NDSolve integrator within *Mathematica*TM code was employed to solve the set of differential equations. All other parameters were completely fixed and the parametric excitation force value was varied until a parametric plot was obtained and the value at which the response is predicted was taken as a threshold value for the parametric excitation force. The reader is referred to Appendix D.1 for the obtained parametric plot. The actuator only displaces by micrometres so there will be a potential gap between the actuator and the shaft-end when the rotor is whirling. The actuator will therefore have to follow the end of the shaft as it contracts, but because the other end of the actuator has to react against something, a spring is needed to provide sufficient reaction, and to take up the space left as the shaft contracts. Figure 7-9(a) shows the system when the rotor is either stationary or spinning without whirl. The design work shown in Figure 7-9 was initiated by the supervisor of this research, with the candidate completing it and then doing the numerical calculations. The shaft-end is fully to the right because the shaft has not contracted due to whirl. Therefore the spring is fully compressed and exerting its maximum force onto the shaft-end (through the actuator which is merely a solid object transmitting that force from one side to the other (right to left)). The maximum force available is given in equation (7.2-1),

$$F_{S_{\max}} = k_s \delta_2 \quad (7.2-1)$$

where $F_{S_{\max}}$ is the maximum spring force, k_s is the spring constant, and δ_2 is the maximum spring compression.

Figure 7-9(b) shows the shaft-end having displaced to the left as a consequence of whirl. The spring has extended to fill the gap, Δ , and the remaining spring compression is δ_1 . This is a pre-compression and is set up via equation (7.2-2) such that it satisfies the need for the minimum spring force ($F_{S_{\min}}$) offered by the spring to equal at least the maximum force which the actuator is capable of ($F_{act(\max)}$), meaning

$$F_{S \min} = F_{act(\max)} = k_S \delta_1 \quad (7.2- 2)$$

where δ_1 is the ‘preload’ pre-compression.

As the minimum spring force available must be enough to resist the maximum force generated by the actuator, the actuator then can transmit its force to the shaft-end, even when the shaft-end has travelled by its maximum contraction to the left. The free length of the spring is shown in Figure 7-9(c) it can easily be seen that the relationship between the pre-compression δ_1 , the maximum compression δ_2 and the maximum shaft-end displacement, Δ , is given by equation (7.2-3)

$$\delta_1 = \delta_2 - \Delta \quad (7.2- 3)$$

This means that the maximum spring force can be written as in equation (7.2-4). The reader is referred to Appendix D.2 for the calculated data.

$$F_{S \max} = k_S (\delta_1 + \Delta) \quad (7.2- 4)$$

A spring was chosen based on the maximum required spring force and hence the spring stiffness was obtained.

7.2.4 Test Setup

The objective of this work has been the design and construction of a test rig to verify the feasibility of active control of vibration in rotor dynamics using a piezoelectric actuator. In particular the possibility of reducing the amplitude of vibrations of a flexible dynamically unbalanced rotor within acceptable levels is investigated. This is carried out by designing a piezoexciter excited by a high frequency drive. The active piezoexciter comprises a sliding bearing which houses the piezoelectric stack actuator which is serially attached to a compression spring. Since the actuator operates only in expansion, with small displacement, the reaction spring is set up against it.

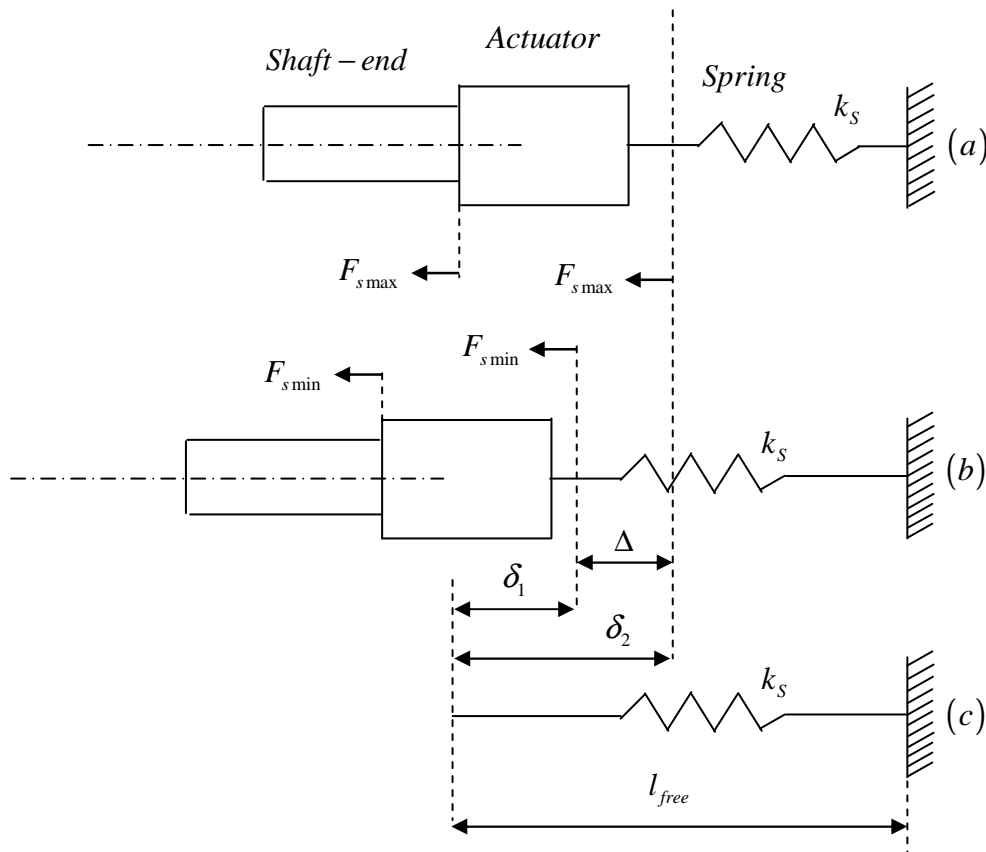


Figure 7- 9: (a) Shaft-end assembly when rotor is not whirling, (b) Shaft-end assembly when rotor is whirling at maximum amplitude and (c) Free length of spring.

The spring is adjusted to the required length by the spring compressor and voltage is applied through a piezoelectric voltage amplifier to the actuator which in turn develops the parametric excitation at a frequency of twice the first whirl frequency of the rotor system. The exciter is driven by a function generator through a high voltage amplifier. Activating the piezoelectric actuator at twice the excitation frequency of the rotor system generates the parametric excitation force to be introduced to the shaft, axially. The vibration response of the rotor-bearing system is then measured by means of the laser vibrometer. A multi-channel data acquisition analyser is then used to analyse the response.

The compression spring of the exciter unit is compressed to the required length and the rotor-bearing system is set to its first whirl resonance frequency. The piezoelectric actuator is then activated, first at a frequency twice the first whirl frequency of the rotor system. It is again activated at a frequency less than twice the first whirl resonance frequency. A series of timed tests are performed and average readings of the amplitude values of the rotor system are taken.

Sweep tests around the first whirl frequency are then performed, first without activating the piezoexciter, and then with the exciter activated at the parametric excitation frequency, and at a frequency less than the parametric excitation frequency.

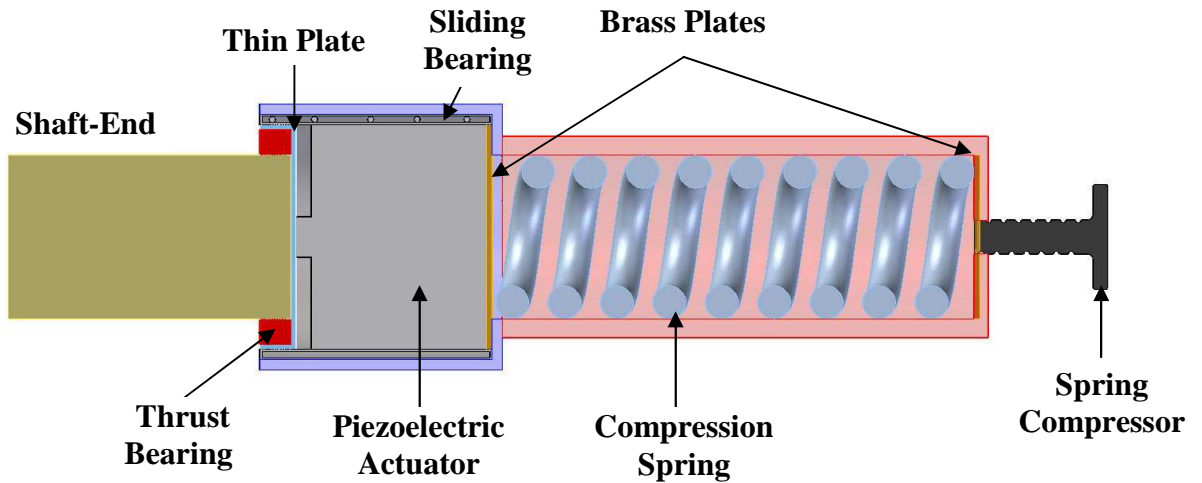


Figure 7- 10: Schematic of the piezoelectric exciter.

7.2.5 Experimental Results

In order to investigate the performance of the test rig three different loading conditions for the piezoexciter components have been considered. The influence of the activation of the piezoexciter for the cases when the spring is compressed to the lengths of 20.2 mm, 25.2 mm and greater than 25.2mm were all systematically examined. In the first case, the spring is compressed to a length of 20.2mm, giving the maximum and minimum spring forces as 426.8N and 426.4N respectively, with the minimum spring force acting as a ‘preload’ to the actuator. When the Piezoexciter is not activated, i.e. when no parametric excitation is applied to the shaft, and varying the shaft speed from 91.7 rad/s to 437.3 rad/s, Figure 7-11(a) shows a peak amplitude value of 17.6 mm at the resonance frequency of $\Omega_1 = 248.8$ rad/s or of 39.6 Hz. In Figure 7-11(b), activating the piezoexciter at a parametric frequency of $\Omega_2 = 497.6$ rad/s, or 79.2 Hz, i.e. at $\Omega_2 = 2\Omega_1$, the amplitude of disk vibration reduces by 8.6% to

16mm. However, in Figure 7-11(c) activating the piezoexciter at an arbitrarily chosen parametric frequency of 450 rad/s i.e. at $\Omega_2 < 2\Omega_1$ increases the amplitude of the disk vibration by 10.4% to 19.3mm.

In the second case, the spring is compressed to a length of 25.2mm, giving the maximum and minimum spring forces as 532.5N and 532N respectively, Figure 7-12(a) shows the peak amplitude of the disk vibration to be 15mm at the resonance frequency of $\Omega_1 = 248.8$ rad/s, or 39.6 Hz. Activating the piezoexciter at the parametric frequency of $\Omega_2 = 497.6$ rad/s, or 79.2 Hz, i.e. at $\Omega_2 = 2\Omega_1$, Figure 7-12(b) shows that the amplitude of disk vibration reduces by 13% to 13mm, which is a 4.4% increase in comparison with the previous case. Also activating the piezoexciter at an arbitrarily chosen parametric frequency of 450 rad/s, i.e. at $\Omega_2 < 2\Omega_1$, Figure 7-12(c) shows an increase in the amplitude of the disk by 10% to 16.5mm.

In the third case when spring is compressed at lengths greater than 25.2 mm, activating the piezoexciter showed no visible changes in the amplitudes of vibrations.

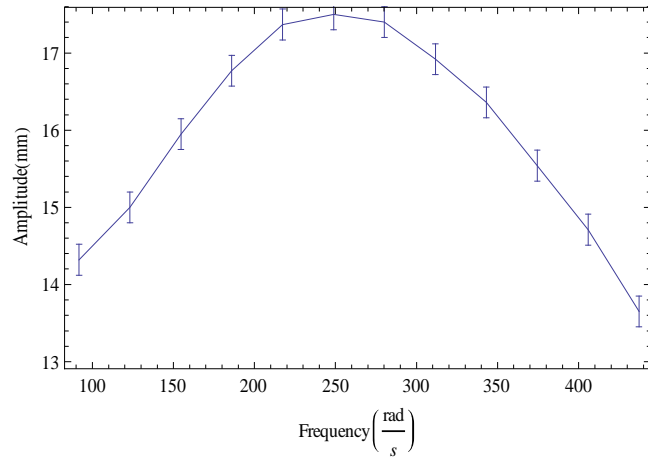
The experimental investigations show the same trend as explained in earlier chapters that the introduction of axial parametric excitation to a flexible rotor, which is also susceptible to mass unbalance, influences the amplitude of vibration of the disk. The greatest dynamic performance is obtained for the case when the spring is compressed to a length of 25.2mm, and on activating the piezoexciter, there was seen to be a reduction of 13% in the amplitude value at principal parametric resonance. On the other hand, an increase in amplitude value was observed when the exciter was activated at a parametric excitation frequency of less than twice the first whirl resonance frequency of the shaft. However, at a spring compression of 20.2mm, on activating the exciter, there was a reduction of 8.6% in amplitude at a parametric resonance of twice the resonance frequency of the shaft. Also, a higher increase in amplitude was observed when the exciter was activated at a parametric frequency less than twice the first whirl resonance frequency of the shaft at the spring length of 20.2mm. Making the compression length more than 25.2mm had no visible effect on the amplitude of vibration.

7.2.6 Piezoelectric Exciter Applications

It is desirable at this point to highlight the applications of this project. Although it is not common to find rotating machines equipped with exciters, there are a few special commercially available products such as the active magnetic bearing spindle, (Lee, *et.al.*, 1992). The authors used the active magnetic bearing (AMB), a special form of electromagnetic actuator, as an excitation device for imposing forces to the rotating shaft of a tool dynamometer. (Lee, *et.al.*, 1992) showed that vibrations of the rotating shaft can be drastically reduced by the electromagnetic exciter making the rotor operate right at the critical speed. This work discusses the benefits that can be derived by introducing exciters in rotating machinery. Although some investigations have been carried out with the possibility of introduction of exciters in machines either to control the machine vibration or to identify its system parameters by some authors like Lee, *et.al.*,(1992), it is likely that doubts would be raised about its practicality, particularly the cost of installation of such exciters in an existing machine. There is always a trade-off problem between the cost and benefits. However, if the benefits earned at the expense of installation of new exciters in a machine may even out the cost, such exciters will be considered as an important element of the machine.

The piezoelectric exciter can be used in tackling real vibrational issues encountered by manufacturers in the design of new rotating machines amongst which hydraulic turbines and generators feature very importantly. In almost all production of electricity the rotating machines serve as an important part of the energy transformation system. In hydropower units, a hydraulic turbine connected to a generator converts the potential energy stored in the water reservoir into electrical energy in the generator. An essential part of this energy conversion is the rotating system of which the turbine and generator are part. During the last century the machines for electricity production have been developed from a few mega Watts per unit up to several hundreds mega Watts per unit. Hydroelectric power generation supplies about 20 percent of the world's electricity and is the most important renewable energy converting industry. The installed capacity of hydroelectric power generation in 2000 was, according to the International Hydropower Association (2000) approximately 700GW with a production of 2600TWh/year. The technically feasible potential of

hydropower is 14000TWh/year. Most of the feasible potential is in developing countries in Africa, Asia and South America (Karlsson (2008). Ability to meet voltage control, energy storage and high efficiency are valuable characteristics of hydroelectric power generation. The development and increase of size of the hydropower machines have also brought a need for new techniques. The most important developments are the increased efficiency, i.e. speed and performance, of the turbines and generators. However, increasing the efficiency of the rotating machines may result in excessive vibration which could end up damaging the machines. The vibrations can thus be reduced by making the rotors stiffer and this can be achieved through active control which presents the opportunity to artificially increase the stiffness and damping properties of the rotor (Inman D.J., 2001). One possibility of incorporating the necessary stiffness and damping properties into the machines could be through the use of the piezoelectric exciter.



(a) Piezoexciter Unactivated

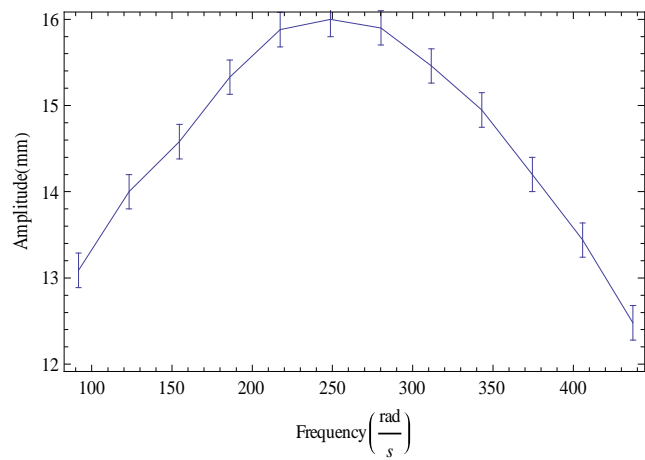
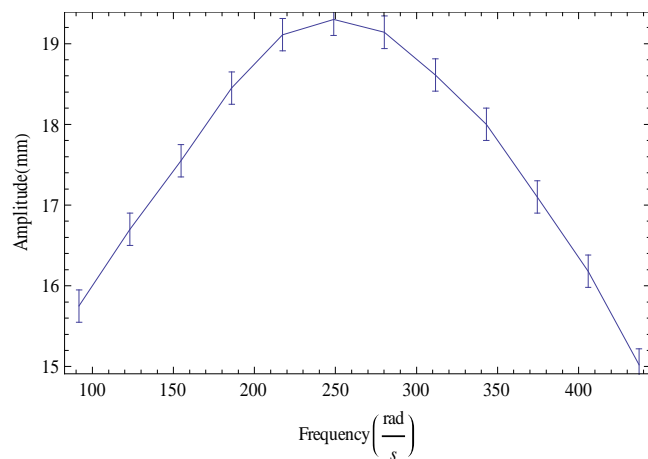
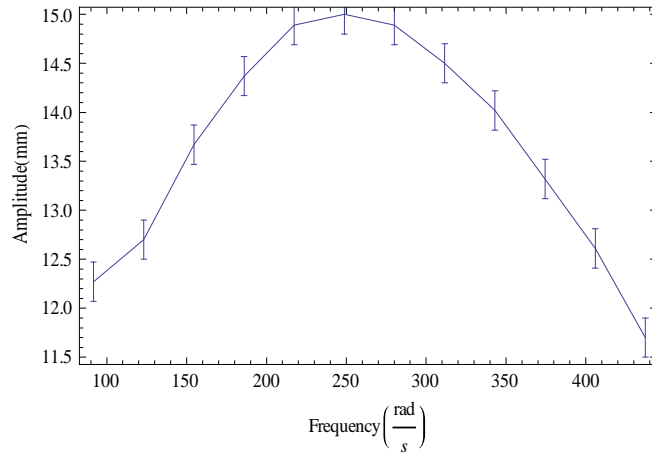
(b) Piezoexciter activated at $\Omega_2 = 2\Omega_1$ (c) Piezoexciter activated at $\Omega_2 < 2\Omega_1$

Figure 7- 11: The amplitudes of disc vibration versus frequency with a spring compression length of 20.2mm.



(a) Piezoexciter Unactivated

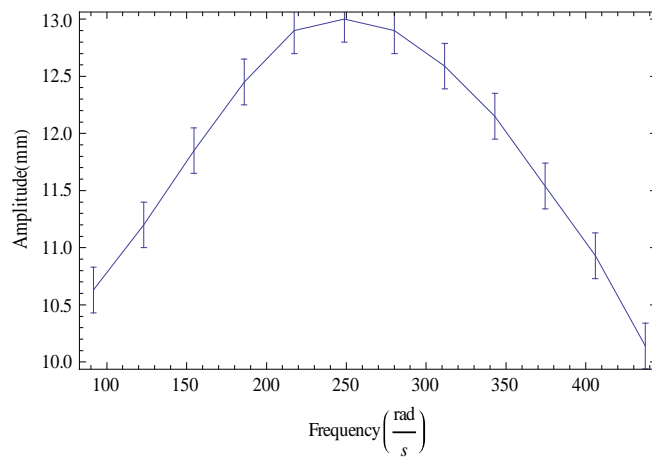
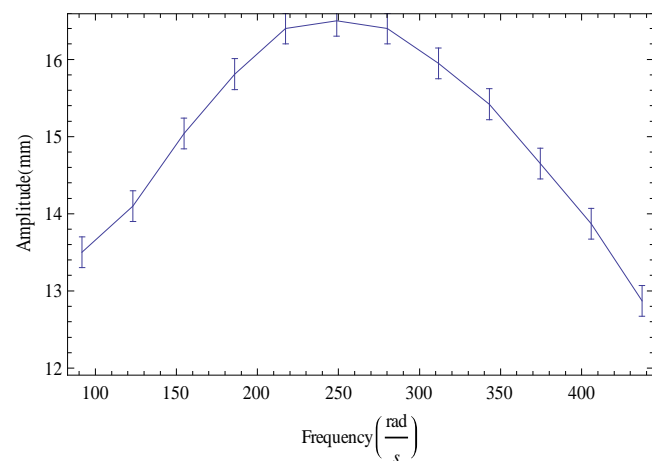
(b) Piezoexciter activated at $\Omega_2 = 2\Omega_1$ (c) Piezoexciter activated at $\Omega_2 < 2\Omega_1$

Figure 7- 12: The amplitudes of disc vibration versus frequency with a spring compression length of 25.2mm.

CHAPTER 8

DISCUSSIONS OF RESULTS

8.1 Introduction

The theoretical and experimental analyses for the flexible rotor system have been presented in Chapters 3 to 7. The derivation of the mathematical models for the rotor system was discussed in Chapter 3. The analytical and numerical techniques, including the method of multiple scales and direct numerical integration by the use of *Mathematica*TM, for the prediction of the response of the presented models as shown in Figures 3-1 to 3-5 were presented in Chapter 4. Chapter 5 presents a steady-state stability analysis of the rotor system via the Routh-Hurwitz stability criterion using the nonautonomous equations obtained from the multiple scales analysis in Chapter 4. A numerical study into the system's dynamics was extended in Chapter 6, where a study of the bifurcations and stability of the solutions via phase planes, Poincaré maps, time plots, bifurcation diagrams and the Lyapunov exponent were summarised. Chapter 7 summarised the novel methods of an antagonistic SMA/Composite bearing and a piezoelectric exciter for the control and reduction of vibration amplitudes in the flexible rotor system. The purpose of this chapter is to examine and extend the discussions where appropriate, the results from Chapters 3 to 7, allowing conclusions to be derived from the respective results.

8.2 Analytical Results

Mathematical models for the rotor system are proposed for vibration analysis and control. In the following are summarised points from the studies:

- Initially, the particular structure under investigation was a Jeffcott like flexible rotor system for which the systems kinematics are presented. The system equations were derived by first constructing the kinetic and strain energies of the rotor elements, followed by the formation of the virtual

work of external forces, including, bearing and axial forces. Rayleigh-Ritz method and Lagrange's equations were then applied to the obtained expressions resulting in coupled differential equations.

- The axial force terms included in the equations of motion provide a means for axially directed harmonic force to be introduced into the system, noting that this is not a follower force and that it maintains the line of the undisturbed equilibrium axis.

The analytical developments involved using the methods of multiple scales and direct numerical integration. In the following are summarised points which emerge from these studies:

The results from the method of multiple scales in Figures 4-1 to 4-4 showed good conclusive results for the cases of not including parametric force terms but increasing the mass unbalance and the damping coefficient, and including parametric force terms. The effect of increasing the mass unbalance of the rotor system does indeed have a global effect on the nonlinear response of the overall system. The response amplitudes increase as the mass unbalance increases.

Increasing the damping coefficient results in decreases in the amplitudes, but the decreases are very small and do not cause the elimination of the jump phenomena.

Including parametric force terms in the equations tend to reduce the peak whirl amplitudes of the whirling motion by approximately 23% and eliminate the jump in the rotating speed.

Numerically integrating the governing equations of motion (3.2-85) and (3.2-86) within *Mathematica*TM has produced results that corroborate those of the method of multiple scales. There is evidence of consistent phenomenon whereby both the responses in the first mode for q_1 and q_2 show a characteristic hardening effect and a jump phenomena, and reduction in the peak amplitudes when parametric excitation terms are introduced into the system.

The numerical integration results give the response for the first mode only whereas the method of multiple scales generates results related to the chosen resonance condition and around the region of perfect external tuning, by means of the detuning parameter, $\varepsilon\bar{\sigma}$ (equation 4.2-41).

8.3 Stability Analysis Results

In performing the stability analysis, the governing differential equations were solved analytically using the method of multiple scales and the ensuing nonautonomous slow-time modulation equations were used to construct a stability matrix and the stability of the system was then analysed using the Routh-Hurwitz stability criterion. The results show that there are values of mass unbalance for which the system can be stable or unstable.

Figures 5-1 and 5-2 and Table 5-1 give a summary of the stability of the steady-state solutions as the mass unbalance is varied. The results show that at mass unbalances of $m_u = 0.004kg$ the system's motion is stable and increasing the mass unbalances to $3m_u$, $4m_u$ and $5m_u$ the motion becomes unstable. Also, further increase of the mass unbalance values to $6m_u$ and $7m_u$ makes the motion stable again.

From Figures 5-1 and 5-2, at mass unbalance values between zero and 0.006kg, the system shows stable motions. At mass unbalance values from 0.006 to 0.022kg, the system is unstable and at mass unbalances greater than 0.022kg the system's motion again becomes stable.

The above results emphasize the intuitive expectation that mass unbalance affects the rotor system's stability under certain conditions.

8.4 Numerical Results

The subsequent numerical analyses were undertaken by generating problem-specific code within the public-domain software *Dynamics 2*.

Figure 6-2 gives plot of nondimensionalised bifurcatory behaviour of amplitude response as a function of the excitation frequency Ω . For the first response mode, it can be deduced that increase in the mass unbalance causes increase in the amplitude of vibration and shifts the amplitude peak more to the right mirroring the effects noticeable in the results of the multiple scales.

The calculated Lyapunov exponent supports the notion that nonlinearities can generate undesirable responses like chaos, but only in cases of very a high excitation level. However, no route to chaos is indicated in the plots of Figure 6-2.

Figure 6-3 shows the bifurcatory behaviour of the amplitude response in the x-direction as a function of nondimensionalised excitation acceleration, accompanied by its respective Lyapunov exponent. For the linear response from chapters 4 to 7, ($m_u = 0.004kg$), a periodic response for a wide range of excitation values is achieved. As the mass unbalance is increased, evidence of chaos surfaces.

The results in Figures 6-3(b), 6-3(c) and 6-3(d) show period doubling bifurcations as mass unbalance increases. In addition, a jump up to the zero level in the Lyapunov exponent plots occur, and indicates that the system has moved to higher period multiples.

Figure 6-4 shows the bifurcatory behaviour of the amplitude response in the x-direction as a function of normalised excitation acceleration accompanied by its respective Lyapunov exponent for the case of the introduced parametric excitation term. The results show stable periodic motions, indicating that all the period doubling and unstable motions observed in Figure 6-3 have become stable motions with the introduction of the parametric excitation term at the principal parametric resonance.

At discrete nondimensionalised excitation acceleration points of the bifurcations in Figures 6-3 and 6-4, phase planes, Poincaré maps and time plots are given in Figures 6-5 to 6-11. The following are general observations of the flexible rotor system as the mass unbalance is increased from m_u to $5m_u$:

- The periodic orbits in the phase planes move away from each other as the effect of the predominant systems nonlinearity is increased by manipulation of the mass unbalance, thus by the excitation acceleration. And therefore, the phenomena behind this behaviour, as shown on the phase planes, could represent a bifurcation to chaos.
- Complicated phase plots are obtained for higher values of mass unbalance, indicating likely chaotic motions as the system effectively becomes more nonlinear.
- In Figures 6-7(d), 6-8(c) and 6-9(b) strange attractors are obtained for the Poincaré maps for higher values of mass unbalance, again indicating likely chaotic motions.
- With the introduction of parametric excitation terms, the phase planes, Poincaré maps and time plots at the discrete nondimensionalised excitation acceleration points display periodic motions indicating stability or stable motions.

Figures 6-12 to 6-17 show the nonlinear dynamic system analyses by the use of specialised code written in *Mathematica*TM as the mass unbalance increases from m_u to $5m_u$:

- For all the discrete mass unbalance values, the motion is stable and periodic in the flexible rotor system.
- The Poincaré map converges to darker areas towards a point indicating a period one motion.
- Using the NDSolve integrator within *Mathematica*TM in analysing the bifurcation plots in Figure 6-3 at nondimensionalised excitation accelerations of 618, 505 and 460 for mass unbalance values of $3m_u$, $4m_u$ and $5m_u$ respectively, (i.e. for higher values of mass unbalance) complicated phase plots are obtained, and strange attractors are also obtained for the Poincaré maps (Figure 6-17), all indicating likely chaotic motions.

8.5 Experimental Results

The following results were obtained from two experimental programmes carried out on different flexible rotor systems. Vibrations in industrial rotating machines, can, for certain rotational speed, be so violent that they can cause significant damage, and the following are the resultant effects of introducing excitations axially into the shaft of such rotating machines using two types of smart material technologies, namely Shape Memory Alloys and Piezoactuators, in the forms of antagonistic SMA/Composite active bearing and Piezoelectric exciters respectively.

- The antagonistic SMA effect was successfully applied to control stiffness of a rotor bearing housing, and to manipulate the natural frequencies of the rotor system. The experimental results for the forward-whirl amplitude in the rotor system have demonstrated that the stiffness can be usefully affected by the SMA, with around a 19.4% reduction in the critical whirl amplitude.
- The piezoelectric exciter was successfully used to introduce parametric excitations into a second rotor system. The combined effects due to the existing forced vibration due to mass unbalance and also an additional parametric excitation in principal parametric resonance provided by the piezoexciter resulted in a more linear response than that provided by the rotor system alone. This has led to the moderation of the responses of the pre-existing mass unbalance vibration inherent to the rotor, with an approximately 13% reduction in the critical whirl amplitude.

8.6 Conclusions

The first three methods of investigating and identifying the response behaviour of rotor systems have all shown similar trends with regards to the effects of increasing the mass unbalance and introducing parametric force terms. Numerical studies have also indicated that chaos is evident as the system becomes more nonlinear due to the increase in mass unbalance and that with the introduction of parametric excitation terms the system's motion becomes

periodic. Prototypical experimental results from tests on rotor systems conclude that the novel antagonistic bearing and piezoelectric exciter concepts could be successfully applied to industrial applications, particularly installations where axial loading on the rotor shaft is also an inherent part of the control actuation.

CHAPTER 9

CONCLUSIONS AND RECOMMENDATIONS FOR FURTHER WORK

9.1 Summary

The research described in this thesis has been concerned with the issue of dynamic response modifications within flexible rotor systems by the use of Smart Materials in the form of shape memory alloys and piezoelectric actuators. The techniques that have been developed are based on the exploitation of the mitigating effects of a SMA/composite antagonistic bearing and piezoelectric exciters on the over all system response. It has been shown theoretically that certain nonlinear effects can be advantageously neutralised with the novel methodologies of introducing axial forces parametrically and through an active bearing component. It has been demonstrated in two different experiments, using different flexible rotor systems that the stiffness of the shaft can be usefully influenced by SMA and piezoelectric actuators. For a laboratory rotor system supported on two bearings, one of which was a two sided active component comprising a composite tube with specially configured and integrated SMA strips termed “antagonistic” in this work, the critical speed was usefully shifted about its normal value and the whirling amplitude reduced drastically. The antagonistic SMA effect was successfully applied to control the stiffness of a rotor bearing housing, and hence to manipulate the natural frequency of the rotor system. It has also been demonstrated that fitting a piezoexciter for axial excitation of the rotor, has greatly influenced the overall nonlinear response of the rotor system. There are some limited references to such systems in the literature but there have not been many reported phenomena relating to the design and application of bespoke antagonistic SMA/composite active bearings and axial piezoelectric exciter for the control of vibration in flexible rotors.

In order to gain an understanding of the behaviour of the flexible rotor system subjected to excitations due to rotating mass unbalance, it was decided firstly to develop an analytical model of which axial forces could be introduced into the system through an axial force term, and the equations were derived in the form of the well known Duffing equation. This can be used to determine the critical whirling amplitude in the rotor system with and without the introduction of the axial forces. These equations were solved analytically, to second order approximation, and the nonlinear vibration solutions were investigated when it was subjected to transverse vibration, using the method of multiple scales, and they were also numerically integrated by the use of NDSolve within *Mathematica*TM. Interesting nonlinear and interactive behaviour was observed for the primary resonance condition, $\frac{\Omega}{\omega} = 1 + \varepsilon\bar{\sigma}$, and for the parametric resonance condition, $\frac{\Omega_2}{\omega} = 2 + \varepsilon\bar{\sigma}$ when parametric excitations were deliberately introduced into the rotor system, where, Ω is the primary resonance frequency, Ω_2 is the parametric excitation frequency and $\varepsilon\bar{\sigma}$ is the internal detuning parameter. In this research it has been shown conclusively by using a second order multiple scales approximation that the nonlinear characteristics of the steady-state responses to the nonautonomous modulation equations can be manipulated by altering the mass unbalance and also by the introduction of a parametric force term. In particular it was shown that the effect of increasing the mass unbalance increases the amplitude of vibration. Further more, it was found that increasing the damping coefficient gives a very small decrease in the whirl amplitude of vibration. In addition to this, including a parametric force term results in the decrease in the amplitudes of vibration, effectively linearising the sub-system response amplitudes (Figure 4-4), notwithstanding the fact that such numerical relationships are necessarily system-data specific.

Stability of steady-state solutions analysis was performed for the rotor system. Nonautonomous equations taken from the multiple scales analysis were used for the analysis. Characteristics equation formed from the determinant of the equations was analysed using Routh-Hurwitz criterion for stability analysis. From the analysis a variety of stability information was extracted. Stability table and plots were obtained for various mass unbalance values and it was observed that

for certain increased values of mass unbalance the system becomes unstable and as it increases further the system becomes stable.

The effects were corroborated numerically and a further study of the bifurcations and stability of the solutions via phase planes, Poincaré maps, time plots, bifurcation diagrams and Lyapunov exponents showed that additional, and highly complex, dynamics could be observed, particularly in more strongly excited systems. A range of numerical results were obtained for both the second order analytical approximation and numerical integrations for the model of a rotor system in the physical co-ordinate space, and these underpinned the general finding that response amplitude characteristics could be effectively linearised and controlled for different combinations of data. This suggests that the useful mitigating effect might also be realisable in the more complex rotor system and so parallel programmes of experimental tests were carried out.

The response characteristics of physical industrial applications were thus determined. A rotor system is considered a vibrating system in the classical sense, and its excitations can be due to rotating mass unbalance. A resonance condition exists when the frequency of excitation due to the mass unbalance coincides with the natural frequency, which tends to increase the amplitude of vibration of the system. To find a practical design solution to the effects of nonlinear responses, it was first necessary to change the frequencies of the shaft rotor system, to avoid critical speeds whilst running up and running down rotors, and to control the vibration levels or rotor stresses in a rotating machine. The effect of this response of building one of two bearings of the rotor system into an active SMA/Composite antagonistic bearing and also deliberately introducing parametric resonance axially into the shaft of a second rotor system were also assessed. It was found that in the case of the antagonistic bearing, the fact that the bearing was fitted within the tube, half-way along, introduced the local dynamics of the tube into the dynamic end conditions of the rotor, and these dynamics were controlled by means of the embedded SMA strips. The SMA effect was thus applied to control the stiffness of the rotor bearing housing, and hence to manipulate the natural frequencies of the rotor system, and used to reduce the critical whirl amplitude. In the case of introducing parametric excitations into a flexible rotor system by means of a piezoexciter, it was found that the

responses of the pre-existed mass unbalance vibration got moderated and resulted in the reduction of the critical whirl amplitude when the exciter was excited parametrically at the principal parametric resonance.

This research provides some basic theory and understanding of how nonlinear and unstable rotor systems can be made more efficient and stable. The practical goal had been to try to control vibration, by reducing the whirl amplitude of the vibrating system. This was tackled by means of using (a) integrated SMA/composites in the form of a cylindrical antagonistic bearing housing component, whose radial and stiffness properties could be actively controlled by means of SMA actuation, and together with an additional axial force component as a result of SMA action on the rotor, (b) piezoelectric exciter fitted to the shaft of the rotor for parametric axial excitation of the rotor whose effects may be used to moderate the responses of the pre-existing mass unbalance vibration inherent to the rotor.

Engineers and scientists are encouraged to use these new approaches with prior understanding of the behaviour of rotating machines under the influence of mass unbalance. By obtaining a good basic understanding of each individual component, an ideal and robust overall linear and stable system can ultimately be configured and hence more reliable and efficient industrial systems can be designed.

9.2 Recommendations for Further Work

It would be good to develop a binary control strategy for the antagonistic active bearing and to check the performance for the flexible rotor at the first critical and possibly higher whirl speeds.

Then to investigate how such binary control can be integrated within a model-based controller (noting that the two-state behaviour is a fundamental feature of SMAs) so that the versatility of control is maximised both at critical speeds and above. This will require a minimised time constant for the antagonistic active bearing, which will, in turn, need maximised heating and cooling rates. This could introduce problems of thermal fatigue in the composite and

particularly in the epoxy adhesive used to secure the SMA strips, and these will have to be investigated.

The experimental test rig could be modified to an overhung configuration, in which gyroscopic forces will be highly significant, and then to see how backward travelling whirl can be mitigated at the first, and possibly higher, critical speeds, with attendant implications for the reduction of cyclic stress effects.

The experimental test rig for the piezoexciter case could also be modified and parametric excitations introduced axially at both ends of the shaft into the system to examine the combination effects on the system.

REFERENCES

Abduljabbar Z., ELMadany M.M., and AlAbdulwahab A.A., (1996), *Computers and Structures*, **58(3)**, pp.499-511, Active Vibration Control of a Flexible Rotor.

Active Materials Laboratory, MIT, USA. <http://aml.seas.ucla.edu>

AdaptaMat, Finland (MSM actuators).

Adiletta G., Guido A., and Rossi R. C., (1996), *Nonlinear Dynamics*, **10**, pp. 251-269, Chaotic motions of a rigid rotor in short journal bearings.

Adiletta G., Guido A., and Rossi R. C., (1997a), *Nonlinear Dynamics*, **14**, pp. 57-87, Nonlinear dynamics of a rigid unbalanced rotor in short bearings, Part I: Theoretical analysis.

Adiletta G., Guido A., and Rossi R. C., (1997b), *Nonlinear Dynamics*, **14**, pp. 157-189, Nonlinear dynamics of a rigid unbalanced rotor in short bearings, Part II: Experimental analysis.

Adiletta G., Guido A.R., and Rossi C., (1996), *Nonlinear Dynamics*, **11**, pp.251-269, Non-periodic motions of a Jeffcott rotor with non-linear elastic restoring forces.

Al-Bender F., Symens W., Swevers J., and Van Brussel H., (2004), *International Journal of Non-linear Mechanics*, **39**, pp. 1721-1735, Theoretical analysis of the dynamic behaviour of hysteresis elements in mechanical systems.

Allaire P.E., Humphris R.R., and Kelm R.D., (1986), *Rotordynamic instability problems in high-performance turbomachinery*, NASA CP-2443, pp. 419-430, Dynamics of a flexible rotor in magnetic bearings.

- Amabili M., and Paidoussis M., (2003), *Applied Mechanics Reviews*, **56**, pp. 349-381, Review of studies on geometrically nonlinear vibrations and dynamics of circular cylindrical shells and panels, with and without fluid-structure.
- Amer Y. A., and Banomy H.S., (2007), *Communications in Nonlinear Science and Numerical Simulation*, Vibration reduction in a 2DOF twin tail system to parametric excitations.
- An-Chen L., Yuan K., and Shin-Li L., (1993), *Int.J.Mech.Sci.* **35(6)**, pp. 479-490, Steady- state analysis of a rotor mounted on nonlinear bearings by the transfer matrix method.
- Anderson T.J., Nayfeh A.N., and Balachandran B., (1996a), *Nonlinear Dynamics*, **11**, pp.17-36, Coupling between high-frequency modes and a low-frequency mode: Theory and experiment.
- Anderson T.J., Nayfeh A.N., and Balachandran B., (1996b), *Journal of vibration and Acoustics*, **118**, pp. 21-27, Experimental verification of the importance of the nonlinear curvature in the response of a cantilever beam.
- Andronov A. A., and Pontryagin L., (1937), *Doklad Academia Nauk. SSSR.* **14**, pp.247-251(1937), Systems grossiers.
- Andronov A. A., Vitt E.A., and Khaiken, S. E., (1966), *Theory of oscillators*, (trans. F. Immirzi), Pergamon Press: Oxford.
- Arnold V. I., (1977), *Functional Anal. Appl.*, **11**, pp.85-92, Loss of stability of self-oscillations close to resonance and universal deformations of equivalent vector fields.
- Arnold V. I., (1983), *Springer-Verlag: New York*, Geometrical methods in the theory of ordinary differential equations.
- Asfar K.R., (1992), *International Journal of Nonlinear Mechanics*, **27(6)**, pp.947-954, Effect of non-linearities in elastometric materials dampers on torsional vibrational control.

-
- Asfar K. R., and Masoud K. K., (1994), *International Journal of Nonlinear Mechanics*, **29**, pp.421-428, Damping of parametrically excited single-degree-of-freedom systems.
- Atluri S., (1973), *Journal of Applied Mechanics*, **40**, pp. 121-126, Nonlinear vibrations of a hinged beam including nonlinear inertia effects.
- Azeez M. A. F., and Vakakis A. F., (1999), *International Journal of Non-linear Mechanics*, **34**, pp. 415-435, Numerical and experimental analysis of a continuously overhung rotor undergoing vibro-impacts.
- Aziz A., and Na T. Y., (1984). *Perturbation methods in heat transfer*, Hemisphere Publication Corporation, New York.
- Bailey T. and Hubbard J. E., (1985), *Journal of Guidance, Control, and Dynamics*, **8(5)**, pp. 605-611, Distributed piezoelectric-polymer active vibration control of a cantilever beam.
- Balckwood G. H., and Ealey M. A., (1993), *Material properties, Smart Materials and Structures*, **2(2)**, pp. 124-133, Electrostrictive behaviour in lead magnesium Niobate (PMN) actuators.
- Barret T. S., Palazzolo A.B., Kascak A. F., (1993), *Trans.ASME , J. Eng. Gas Turbine Power* **117** pp.176-187, Active vibration control of rotating machinery using piezoelectric actuators incorporating flexible casing effects.
- Barsoum R.G.S., (1997), *Smart Materials and Structures*, **6**, pp. 117-122, Active materials and adaptive structures.
- Baz A. and Poh S., (1988), *Journal of Sound and Vibration*, **126(2)**, pp. 327-343, Performance of an active control system with piezoelectric actuators.
- Baz A. and Poh S., (1990), *Journal of Sound and Vibration*, **139(2)**, pp. 133-149, Experimental implementation of the modified independent modal space control method.

-
- Baz A., and Ro L., (1994), *Composites Engineering*, **4(6)**, pp. 567- 576, Optimal vibration control of Nitinol-reinforced composites.
- Baz A., Ro J., and Gilheany J., (1995), *Journal of Sound and Vibration*, **185(1)**, pp. 171-185, Control of the natural frequencies of Nitinol-reinforced composite beams.
- Bender C. M., and Orszag S. A., (1978), *Advanced mathematical methods for scientists and engineers*, McGraw-Hill, New York.
- Bert C. W., (1982), *Journal of materials and science letters*, **1**, pp. 247-248, Simple method to determine nonlinear compressive and tensile stress-strain curves using sandwich beam.
- Bhattacharyya K., and Dutt J.K., (1997), *ASME Journal of Vibration and Acoustic*, **119**, pp. 539-544, Unbalance Response and Stability Analysis of Horizontal Rotor Systems Mounted on Nonlinear Rolling Element Bearings with Viscoelastic Supports.
- Bideaux J.-E., Bernet N., Sarwa C., Manson J.-A.E., and Gotthardt R., (1995), *Journal de Physique 1V, Coll.8*, **5**, pp. 1177-1182, Vibration frequency control of a polymer beam using embedded shape-memory-alloy fibres.
- Birkhoff G. D., (1927), *American mathematical society: Providence, RI*, Dynamical Systems.
- Bolotin V. V., (1964), *The dynamic stability of Elastic systems*, Holden-day, San Francisco, California.
- Brown R. D., Addison P. and Chan A. H. C., (1994), *Nonlinear Dynamics*, **5**, pp. 421-432, Chaos in the unbalance response of journal bearings.
- Buehler W.J., and Wiley C.R., (1965), *Nickel-based Alloys, US Patent 3*, pp.174, 851.

- Carlson J. D., and Spronston J.L., (2000), *Actuator2000. 7th International Conference on New Actuators and Drive Systems, Messe Bremen GMBH* pp. 126-130, Bremen, Controllable fluids in 2000- Status of ER and MR fluid technology. In: Borgamnn, H. (ed.).
- Carlson J. D., Catanzarite D.N. and St. Clair K. A., (1995), *Proceedings of 5th International Conference on ER Fluids, MR suspensions and Associated Technology, World Scientific*, pp.1-9, Sheffield, Commercial magneto-rheological fluid devices. In: Bullough, W. (ed.).
- Carmignani C., Forte P., and Rustighi E., (2001), *ASME Design Engineering Technical Conference and Computers and Information in Engineering Conference, Pittsburgh, September 9-12, 2001*, Active control of rotor vibrations by means of piezoelectric actuators.
- Cartmell M.P., (1984), *Combination Instabilities and Non-Linear Vibratory Interactions in Beam Systems*, Ph.D. Thesis, University of Edinburgh.
- Cartmell M.P., (1990), *Introduction to linear, parametric and nonlinear vibrations, Chapman and Hall*, London.
- Cartmell M.P., Ziegler S.W., Khanin R., and Forehand D.I.M., (2003), *Transactions of the American Society of Engineers Applied Mechanics Reviews*, **56(5)**, pp.455-492, Multiple Scales Analyses of the Dynamics of Weakly Nonlinear Mechanical Systems.
- Caughey T. K., and Vijayaraghavan A., (1970), *International Journal of Non-linear Mechanics*, **5**, pp. 533-555, Free and forced oscillations of a dynamic system with linear hysteric damping .
- Chang C.O., and Cheng J.W., (1993), *Journal of Sound and Vibrations*, **160(3)**, pp.433-454, Nonlinear dynamics and stability of a rotating shaft-disk system.
- Chang-Jian, Cai-Wan and Chen Chao-Kuang, (2007), *Chaos, Solutions and Fractals*, **34**, pp. 1160-1179, Bifurcation and chaos analysis of a flexible rotor supported by turbulent long journal bearings.

- Chen C.-L., Yau H.-T., (1998), *Nonlinear Dynamics*, **16**, pp.71-90, Chaos in the Imbalance Response of a Flexible Rotor Supported by Oil Film Bearings with Non-Linear Suspension.
- Chen L., and Hansen C. H., (2003), *Proceedings of the 42nd IEEE Conference on Decision and Control*, Hawaii USA, Nonlinear control of a parametrically excited system subjected to actuator saturation.
- Chenm J.H., and Lee A.C., (1997), *ASME Journal of vibration and Acoustics*, **119**, pp. 60-69, Identification of Linearised dynamic characteristics of rolling element bearings.
- Cheung L. Y., Dunn R.W., Daniels A. R. and Berry T., (1994), *Control '94. IEEE*. pp. 1157-1163, Active vibration control of rotor systems.
- Chester W., (1975), *Journal of Inst. Math. Applications*, **15**, pp. 289-306, The forced oscillations of a simple pendulum.
- Childs D., (1992), *Turbomachinery rotordynamics*. New York: Wiley and Sons.
- Childs D.W., (1982), *Journal of Engineering for Power*, **104**, pp. 533 - 541, Fractional- frequency rotor motion due to non-symmetric clearance effects.
- Chin W., Ott E., Nusse H.E., and Grebogi C., (1994), *Physical Review*, **E50(6)**, pp. 4427-4444, Grazing bifurcations in impact oscillations.
- Chivens D.R., (1973), *The Natural Frequencies and Critical Speeds of a Rotating Flexible Shaft-Disk System*. Ph.D. Thesis, Arizona State University, Tempe, Arizona.
- Choi S. K., and Libchaber A., (1994), *Journal of Applied Mechanics*, **61**, pp.131-137, Mode-locking and chaos in a Jeffcott rotor with bearing clearances.
- Choi S.-B., and Cheong C.-C., (1996), *Journal of Guidance, Control, and Dynamics*, **19(5)**, pp. 1178-1180, Vibration control of a flexible beam using shape memory alloy actuators.

-
- Chopra I., (2002), *American Institute of Aeronautics and Astronautics, Inc., (AIAA) Journal*, **40(11)**, pp. 2145-2187, Review of state of art of smart structure and integrated systems.
- Chow P.L., and Maestrello L., (2001), *International Journal of Nonlinear Mechanics*, **36**, pp.709-718, Vibrational control of a non-linear elastic panel.
- Choy F. K., Padovan J. and Li W. H.,(1987), *Mechanical systems and signal processing*, **2**, pp.133-133, Rub in high performance turbomachinery, modelling, solution methodology and signature analysis.
- Chu F. and Zhang Z., (1997), *International Journal of engineering science*, **35**,pp. 963-973, Periodic, Quasiperiodic and chaotic vibrations of a rub-impact rotor system supported on oil film bearings.
- Clark H. M., and Wayman C.M., (1970), *Phase transformation, American Society for Metals, eds., Chapman& Hall Ltd., London*, pp.59-114, Surface relief effects in solid states phase transformation.
- Cole J. D., (1968), *Perturbation methods in applied mathematics*, Blaisdell, Waltham, Mass.
- Cole J.D., and Kevorkian J., (1963), *Proceedings of International Symposium on Nonlinear Differential Equations and Nonlinear Mechanics*, pp. 113-120, Uniformly valid asymptotic approximations for certain non-linear differential equations.
- Crawley E. F., and de Luis J., (1987), *AIAA Journal*, **25(10)**, pp. 1373-1385, Use of piezoelectric actuators as elements of intelligent structures.
- Crespo Da Silva M. R. M. and Hodges D. H., (1986a), *I: Formulation, Vertica*, **10**, pp.151-169, Nonlinear flexure and torsion of rotating beams, with helicopter rotor blades.

-
- Crespo Da Silva, M. R. M. and Hodges D. H., (1986b), II: *Response and stability results, Vertica*, **10**, pp.171-186, Nonlinear flexure and torsion of rotating beams, with helicopter rotor blades.
- Cunningham R.E.,(1978), *ASME J. Mech. Des.* **100**,pp.563-573,Steady-state unbalance response of a three-disk flexible rotor on flexible, damped supports.
- Das A.S., Nighil M.C., Dutt J.K., and Irretier H., (2007), *Journal of Mechanism and Machine Theory*, Vibration control and stability analysis of rotor-shaft system with electromagnetic exciters.
- De Santiago O., and San Andrés L., (2003), , *ASME Paper GT 2003-38585, ASME Turbo-Expo 2003 Conference*, Atlanta, GA., Field Methods for Identification of bearing support parameters, Part II-Identification from rotordynamic response due to Imbalances .
- Den Hartog J .P., (1956), *Mechanical Vibrations*, *Dover, New York*.
- Der Hagopian J., Gaudiller L., Alauze C., and Voinis P.,(1999), *Proceedings of Eurodynamics'99*, Ulm, Germany, pp. 37-43, Synchronous control of large shafts lines by active balancing.
- DesRoches R.,(2002), *Application of Shape Memory Alloys in Seismic Rehabilitation of Bridges*, Technical Report NCHRP-IDEA project 65.
- Dimarogonas A.D., (1983), *Analytical Methods in Rotor Dynamics*, Applied Science Publishers, London and New York.
- Dimarogonas A.D., (1990), *Journal of Sound and Vibration*, **140(2)**, pp.181-189, The origins of Vibration Theory.
- Dimarogonas A.D., (1992), *Springer-Keynote Paper Session*, A Brief History of Rotor Dynamics.

- Dimitriadis E. K., Fuller C. R. and Rogers C. A., (1991), *Journal of Vibration and Acoustics*, **113**, pp. 100-107, Piezoelectric actuators for distributed vibration excitation of thin plates.
- Ditcher A.K. and Webber J.P.H., (1982), *Aeronautical Quarterly*. **33**, pp.1-24, Non-linear stress-strain effects in the flexural wrinkling of carbon fibre honey-comb sandwich beams.
- Dowell E. H., Traybar J., and Hodges D.H., (1977), *Journal of sound and vibration*, **50**, pp.533-544, An experimental-theoretical correlation study of non-linear bending and torsion deformations of a cantilever beam.
- Duchemin M., Berlioz A., and Ferraris G., (2006), *Transactions of the ASME*, **128**, pp. 576-585, Dynamic behaviour and stability of a rotor under base excitation.
- Dugundji J., and Chhatpar C.K., (1970), *Rev. Sci. Tech., Ser. Mech. Appl.*, **15(4)**, pp. 741-763, Dynamic stability of a pendulum under parametric excitation.
- Edwards S., Lees A. W. and Friswell M. I., (1999), *Journal of Sound and Vibration*, **225**, pp. 767 - 778, The influence of torsion on rotor/stator contact in rotating machinery.
- Ehmann C., Alizadeh A., and Nordmann R., (Feb. 2003), Schwingungsdämpfung aktiv gelagerter rotoren mit robuster Regelung, in Schwingungen in rotierenden Maschinen, Darmstadt
- Ehrich F. F., (1993), Handbook of rotordynamics. New York: McGraw Hill.
- Ehrich F.F., (1988), *Journal of Vibration, Acoustics, Stress and Reliability in Design*, **110**, pp. 9-16, High order subharmonic response of high speed rotors in bearing clearance.
- Ehrich, E. F., (1991), *Journal of vibration and Acoustics*, **113**, pp. 50-57, Some observations of chaotic vibration phenomena in high-speed rotordynamics.

- El-Bassiouny A. F., and Abdelhafez H.M.,(2001), *Mathematics and Computers in Simulation*, **57**, pp. 61-80, Prediction of bifurcations for external and parametric excited one-degree-of-freedom system with quadratic ,cubic and quartic non-linearities.
- El-Bassiouny, A. F., (2005), *Mechanics Research Communications*, **32**, pp. 337-350, Principal parametric resonances of nonlinear mechanical system with two-frequency and self-excitations.
- El-Marhomy A., (1994), *Journal of International Mathematics and Composite Science*, **7(1)**, pp.73-84, On the translational whirling motion of rotor-bearing systems.
- El-Marhomy A., (1998), *ASME Journal of Modelling, Measurement and Control*, **66(2)**, pp. 7-18, On dynamic response of disk-shaft-bearing system.
- El-Marhomy A., and Abdel-Sattar N.E., (2004), *Applied Energy*, **77**, pp. 287-308, Stability Analysis of Rotor-Bearing Systems Via Routh-Hurwitz Criterion.
- Fansen J. L. and Chen J.C., (1986), *Proceedings of NASA/DOD Control-Structures Interaction Conference, NASA CP 2447*, Part II, Structural control by the use of piezoelectric active members.
- Feigenbaum M. J., (1978), *Journal of Stats. Phys.*, **19**, pp. 25-52, Quantitative universality for a class of nonlinear transformation.
- Feigenbaum M. J., (1983), *Physica.*, **7D**, pp. 16-39, Universal behaviour in nonlinear Systems.
- Foepl A., (1895),*Der Civilingenieur*, **6**, pp.333-342, Das Problem der Delaval'schen Turbinenvelle.
- Frieman E.A., (1963), *Journal of Mathematical Physics*, **4**, pp.410-418, On a new method in the theory of irreversible processes.
- Friswell M. I., (2001), *Journal of Sound and Vibration*, **245(5)**, pp.960 - 967, Damping ratio and natural frequency bifurcations in rotating systems.

-
- Fritz R.J., (1970a), *ASME Journal of Basic Engineering*, pp.923-929, The effects of an annular fluid on the vibrations of a long rotor, part 1-theory.
- Fritz R.J., (1970b), *ASME Journal of Basic Engineering*, pp.930-937, The effects of an annular fluid on the vibrations of a long rotor, part 2-test.
- Frolov K.V.,(1967), *Proceedings of the 4th Conference on Nonlinear Oscillations*, pp. 327-336, Parametric and autoparametric oscillations of some nonlinear mechanical systems.
- Fukuchi N. and Okahata G., (2005), *Thin- Walled Structures*, **43**, pp. 225-236, Non-oscillatory behaviour and dynamic stability of a thin shell subjected to follower forces with small disturbances.
- Funakubo H., (1987), *Shape Memory Alloys*, Gordon Breach Science Publications, NY.
- Ganesan R., (1996), *Mechanical Machine Theory*,**31**, pp.781 - 798, Dynamic response and stability of a rotor-support system with non-symmetric bearing clearance.
- Genta G., (1999), *Vibration of structures and machines*, 3rd Ed. Springer, New York.
- Giglio M., Musazzi S., and Perini U., (1982), *Phys.Rev.Lett*, **47**, pp.245-248, Transition to chaotic behaviour via a reproducible sequence of period-doubling bifurcations.
- Goldman P. and Muszynska A., (1995), *Chaos, Solutions and Fractal*, **5**, pp. 1579-1601, Rotor-to-Stator, rub-related, thermal/mechanical effects in rotating machinery.
- Goldman P., and Muszynska A., (1994a), *ASME, Journal of Vibration and Acoustics*, **116(4)**, pp. 541-547, Dynamic effects in mechanical structures with gap and impacting: order and chaos.

- Goldman P., and Muszynska A., (1994b), *ASME, J Eng Gas Turbines Power*, **116(3)**, pp. 692-701, Chaotic behaviour of rotor-stator systems with rubs.
- Goldman P., and Muszynska A., (1995), *Chaos, Solitons and Fractals*, **5(9)**, pp.1683-1704, Chaotic responses of unbalanced rotor/bearing/ stator systems with looseness or rubs.
- Gonsalves D. H., Neilson R. D., and Barr A. D. S., (1995), *Nonlinear Dynamics*, **7**, pp. 451-470, A study of response of a discontinuously nonlinear rotor system.
- Grebogi C., Ott E., and Yorke J. A., (1982), *Phys. Rev. Lett.*, **48**, pp. 1507-1510, Chaotic attractors in crisis.
- Grebogi C., Ott E., and Yorke J. A., (1983a), *Phys. Rev. Lett.*, **50**, pp. 935-938, Fractal basin boundaries, long lived chaotic transients, and unstable-unstable pair bifurcation,.
- Grebogi C., Ott E., and Yorke J. A., (1983b), *Physica.*, **7D**, pp.181-200, Crisis, sudden changes in chaotic attractors, and transient chaos.
- Green R., (1948), *Journal of Applied Mechanics*, **15**, pp.369-376, Gyroscopic effects of the critical speeds of flexible rotors.
- Groll G. and Ewins D.J., (2001), *Journal of Sound and Vibration*, **241**; 233-233, The harmonic balance method with arc-length continuation in rotor/stator contact problems.
- Gustavsson R., (2005), Modelling and Analysis of Hydropower Generator Rotors, Licentiate Thesis, Luleå University of Technology.
- Hamdan M. N., Al-Qaisia A. A., and Al-Bedoor B.O., (2001), *International Journal of Mechanical Sciences*, **43**, pp. 1521-1542, Comparison of analytical techniques for nonlinear vibrations of a parametrically excited cantilever.
- Haxton, R. S., and Barr, A. D. S., (1972), *Journal of Engineering Industry*, **94**, pp. 119-125, The autoparametric vibration absorber..

-
- He Yong-Yong, Oi Satoko, Chu Fu-Lei, Li Han-Xiong, (2007), *Smart Materials and Structures*, **16**, pp.114-121, Vibration control of a rotor-bearing system using shape memory alloy: I. theory.
- Hietanen S., (2000-2002), *VTT Industrial Systems Espoo*, Finland.
- Hinch E. J., (1991), *Perturbation methods*, Cambridge University Press, New York.
- Hodges D.H. and Dowell E. H., (1974), *NASA Technical Note D-7818*, Nonlinear equations of motion for the elastic bending and torsion of twisted nonuniform rotor blades.
- Hodgson D.E., and Brown J.W.,(2000), *Using Nitinol Alloys*, Report of Shape Memory Applications Inc.
- Holmes A. G., Ettles C. M., and Mayes L. W., (1978), *International Journal for Numerical methods in Engineering*, **12**, pp. 695-702, Aperiodic behaviour of a rigid shaft in short journal bearings.
- Holmes P.J., (1977), *Appl. Math. Mod.*, **1**, pp. 362-366, Strange phenomena in dynamical systems and their physical implications.
- Holmes P.J., (1979), *Phil.Trans.R.Soc.Lond*, A; **292**, pp. 419-448, A nonlinear oscillator with a strange attractor.
- Holt C., and San Andrés L., (2001), *Turbomachinery laboratory, Texas A&M University*, MATHCAD Code for Identification of bearing support coefficients in flexible rotor-bearing systems.
- Horst H.G., and Wolfel H.P., (2004), *J. Int. Mat. Systems and Structures*, **15**, pp. 721-728, Active vibration control of a high speed rotor using PZT patches on shaft surface.
- Houlston P.R., (2007), *Active Vibration Control of Rotating Machines*, Ph.D. Thesis, University of Nottingham.

- Huang T.C., (1961), *Journal of Applied Mechanics*, 28, pp.579-584, The effect of rotatory inertia and of shear deformation on the frequency and normal mode equations of uniform beams with simple end conditions.
- Hunter I.W., Lafontaine S., Hollerbach J.M., and Hunter P.J., (1991), *In the Proceedings of the 1991 IEEE International Conference on MEMS*, pp.166-170, Fast Reversible NiTi Fibres for use in Microrobotics.
- Ikegami R., Wilson D.G., Anderson J.R., and Julien G.J.,(1990), *Journal of Intell. Mater. Syst. and Struct.*, 1, pp. 189-206, Active vibration control using Nitinol and Piezoelectric ceramics.
- Inman D.J., (2001), *Philosophical Transactions of the Royal Society of London Series A-Mathematical Physical and Engineering Sciences*, 359(1778), pp.205-219, Active Modal Control for Smart Structures.
- Inman D.J., Cartmell M.P., Lees A.W., Leize Th., and Atepor L., (2006), *Applied Mechanics and Materials*,5-6, pp.29-36, Proposals for Controlling Flexible Rotor Vibrations by means of an Antagonistic SMA/Composite Smart Bearing.
- Inoue K. and Hikiyara T., (1998), *T.IEE Japan D118* (11), pp. 1266-1271, Bifurcation phenomena of hunting in revolution speed of a rotor system with elastic shaft caused by whirling motion.
- Inoue K. and Ushio T., (2000), *International Journal of Bifurcation and Chaos*, 9, pp.1675-1684, Bifurcation and Hunting phenomena of rotating speed in a flexible rotor system caused by whirling motion.
- Inoue T., Ishida Y., and Isogai S., (2001), *Electromagnetics Symposium Proceedings*, Japan, 13, pp.131-136, Vibration Control of Rotor Systems using Electro-magnetic Mass Damper. Expansion to a Nonlinear System.
- International hydropower Association, International Commission on Large Dams, Implementing Agreement on hydropower and Canadian hydropower Association, (2000), *Hydropower and World's Energy Future; The role of*

hydropower in bringing clean, renewable, energy to the world. Downloaded from <http://www.ieahydro.org/Bur-Recl-web/Hydrofut.pdf> .

Ioannou P. A. and Sun J., (1996), *Robust adaptive control*. Prentice-hall, Inc. USA. 825 p. ISBN 0-13-439100-4.

Irretier H., and Lindemann S., (2002), *Proceedings of the 6th International Conference on Rotor Dynamics, Sydney, Australia*, pp.388-395, Improvement of damping parameters of flexible rotors by experimental modal analysis and modal updating.

Ishida Y., (1994), *JSME International Journal C37 (2)*, pp. 237-245, Nonlinear vibrations and chaos in rotordynamics.

Ishida Y., and Inoue T., (2007), *Journal of vibration and Control*, **13(8)**, pp. 1127-1143, Vibration suppression of nonlinear rotor systems using a dynamic damper.

Ishida Y., Ikeda T., and Yamamoto T., (1990), *ASME Journal of vibration and Acoustics*, **112**, pp. 288-297, Nonlinear forced oscillations caused by quartic nonlinearity in a rotating shaft system.

Ishida Y., Nagasaki I., Inoue T., and Seongwoo L., (1996), *Nonlinear Dynamics* **11(2)**, pp. 107-120, Forced oscillations of a vertical continuous rotor with geometrical nonlinearity.

Ishii Hiroaki, Fujisaka H., and Inoue M., (1986), *Phys. Lett.*, **116A**, pp. 257-263, Breakdown of chaos symmetry and intermittency in the double-well potential system.

Ishimatsu T., Shimomachi T. and Taguchi N., (1991), *International Conference on Industrial Electronics, Control and Instrumentation IEEE*. Pp 437- 441, Active vibration control of flexible rotor using electromagnetic damper.

-
- Iwata Y., and Nonami N., (1983), *Trans. Japan. Soc.Mech.Eng. (JSME) C49* pp.897-903,Vibration control of rotating shaft with Self-optimizing support system.
- Janik T.K., and Irretier H., (1998), *Proceedings of the IFTOMM Conference on Rotordynamics, Darmstadt*, pp. 695-708, New excitation and response measurement techniques for modal testing of flexible rotors.
- Janik T.K., and Irretier H., (2000), *International Journal of Rotating Machinery*,**6(1)**,pp.11-18, Experimental modal analysis-a tool for unbalance identification of rotating machines.
- Jeffcott H. H., (1919), *Philosophical magazine*, **37**, pp.304-315, The lateral vibration of loaded shafts in the neighbourhood of the whirling speed, The effect of want of balance.
- Ji Z., and Zu J.W., (1998), *Journal of Sound and Vibration*, **218(2)**, pp.293-305, Method of Multiple Scales for Vibration Analysis of Rotor-Shaft Systems With Non-Linear Bearing Pedestal Model.
- Ju D.-Y., and Shimamoto, (1999), *Journal of Intelligent Material Systems and Structures*, **10**, pp. 514-520, Damping property of epoxy matrix composite beams with embedded shape memory fibres.
- Karlsson M., (2008), *Modelling and Analysis of Multiphysical Interactions in Hydropower Rotor Systems*, Doctoral Thesis, Luleå University of Technology.
- Karpenko E. V., Wiercigroch M., and Cartmell M. P., (2002), *Chaos, Solitons and Fractals*, **13**, pp.1231-1242, Regular and chaotic dynamics of a discontinuously nonlinear rotor system.
- Keith F. J., and Allaire P., (1990), *Tribology transactions*, **33**, Digital control of magnetic bearings supporting a multimass flexible rotor.
- Kevorkian J., and Cole J.D., (1981), *Springer-Verlag*, **34**, Perturbation Methods in Applied Mathematics,

-
- Kim J. L., and Noah S. T., (1990), *Nonlinear Dynamics*, 1 , pp. 221-241, Bifurcation analysis for a modified Jeffcott rotor with bearing clearances.
- Kisk R.G., and Gunter E.J., (1964), *Journal Eng. for Industry* pp. 682-693, Transient Response of Rotor-Bearing Systems.
- Kunitoh T., Yabuno H., and Aoshima N., (2004), *The 30th Annual Conference of the IEEE Industrial Electronics Society*, November 2-6, Busan, Korea, Design of a Nonlinear Oscillator Using a Nonlinear Feedback.
- Lahmar M., Haddad A., and Nicolas D., (2000), *Eur J Mech A- Solids*, 19, pp. 151-177, An optimized short bearing theory for nonlinear dynamic analysis of turbulent journal bearings.
- Lalanne M., and Ferraris G., (1990), *Rotordynamics Prediction in Engineering*, John Wiley, Chichester.
- Lau S.L., Cheung Y.K., and Wu S.Y., (1982), *Journal of Applied Mechanics-Transactions of the American Society of Mechanical Engineers*, 49(4), pp. 849-853, A variable parameter incrementation method for dynamic instability of linear and nonlinear elastic system.
- Lawen J. L. and Flowers G. T., (1996), *EUROMECH-2nd European Nonlinear Oscillation Conference, Prague*, pp. 249-252, Influence of bearing housing dynamics on the response characteristics of a flexible rotor system with an auxillary clearance bearing .
- Lee A., Kang Y., and Liu S., (1993), *Int. J. Mech. Sci.*, 35(6), pp. 479-490, Steady-state analysis of a rotor mounted on nonlinear bearings by the transfer matrix method.
- Lee C. W., and Kim J. S., (1992), *ASME Journal of Dynamic Systems, Measurement, and Control*, 114, pp. 244-252, Modal testing and suboptimal vibration control of flexible rotor bearing system by using a magnetic bearing.

-
- Lee C. L., and Lee C. T., (1997), *Journal of sound and vibration*, **202(2)**, pp. 284-287, A higher order method of multiple scales.
- Lee C.-W.,(1993), *Vibration Analysis of Rotors*, Kluwer Academic Publishing, Dordrecht, The Netherlands.
- Lee S.U., Leontopoulos C. and Besant C., (1999), *Proceedings of the International Modal Analysis Conferences*, **2**, pp. 1692 - 1698, Backward whirl investigations in isotropic and anisotropic systems with gyroscopic effects.
- Lee W.K., and Park H.D., (1999), *International Journal of Non-Linear Mechanics*,**34**, pp.749-757, Second-order approximation for chaotic responses of a harmonically excited spring-pendulum system.
- Lewis D. W., Moore J.W., Bradley P.L., and Allaire P.G., (1982), *NASA CP-2250*, pp. 434-436, Vibration limiting of rotors by feedback control, Rotordynamic instability problems in high-performance turbomachinery.
- Liang C., and Rogers C.A., (1993), *Journal of Vibration and Acoustics*, **115**, pp.129-136, Design of Shape Memory Alloy Springs With Applications in Vibration Control.
- Libchaber A., Laroche C., and Fauve S., (1982), *Phys.Rev.Lett*, **43**, pp. L211-L216, Period doubling cascade in mercury: a quantitative measurement.
- Lichtenberg A. J., and Lieberman M. A., (1982), *Regular and stochastic motion*, Springer-Verlag: New York, Heidelberg, and Berlin.
- Liebowitz H., (1983), *NASA-CR-174495*, Vibration response of geometrically nonlinear elastic beams to pulse and impact loading.
- Lim F.C.N., (2003), *A Preliminary Investigation into the Effects of Nonlinear Response Modification within Coupled Oscillators*, Ph.D. Thesis, University of Glasgow.

-
- Lin C. C., and Segel L. A., (1988), *Society for Industrial and Applied Mathematics, Philadelphia*, Mathematics applied to deterministic problems in the natural sciences.
- Linsay P., (1982), *Phys.Rev.Lett*, **47**, pp.1349-1352, Period doubling and chaotic behaviour in a driven anharmonic oscillator.
- Lorenz E. N., (1964), *Tellous*, **16**, pp.1-11, The problem of deducing the comate from the governing equations.
- Lorenz, E. N., ,(1963), *J. Atmos. Sci.*, **20**, pp.130-141, Deterministic nonperiodic flow.
- Lyapunov A. M., (1949), *Probleme General de la stabilitee duMouvement (Annals of mathematical studies, 17) Princeton University Press: Princeton, NJ.*
- Malatkar p., (2003), *Nonlinear Vibrations of Cantilever Beams and Plates*, Ph.D. Thesis, Virginia Polytechnic Institute and State University.
- Marke K., Lahtinen R., and Koskinen J., (2002), *VTT Reseach Programme, VTT Symposium 225*, Smart Materials and Structures.
- Meirovitch L., (1970), *Methods of Analytical Dynamics*, McGraw-Hill Book Company, New York.
- Meirovitch L., (1990), *Dynamics and Control of Structures*, John Wiley, New York.
- Mitropolsky Y.A., (1967), *International Journal of Non-linear mechanics*, **2**, pp. 69-96, Averaging method in nonlinear Mechanics.
- Mockensturm E. M., Perkins N. C., and Galip Ulsoy A., (1996), *Journal of Vibration and Acoustics*, **118**, pp. 346-351, Stability and limit cycles of parametrically excited, axially moving strings.
- Moon F. C., (1987), *Chaotic Vibrations- An Introduction for Applied Scientists and Engineers*, Wiley, New York.

- Moore J.W., Lewis D. W., and Heinzman J., (1980), *Rotordynamic instability problems in high-performance turbomachinery*, NASA CP-2133, pp. 467-476, Flexibility of active feedback control of Rotordynamic instability.
- Moyer Jr. and Thomas E., (1984), *Computers and structures* ,**19**, pp. 339-344, Energy conservation in the transient response of nonlinear beam vibration problems subjected to pulse loading -A numerical approach.
- Murdock J.A.,(1999),*Perturbations: Theory and Methods*. SIAM: Philadelphia.
- Mustafa G., and Ertas A., (1994), *Journal of Sound and Vibration* , **182(3)**, pp. 393-413, Dynamics and bifurcations of a coupled column-pendulum oscillator.
- Muszynska A., (1996), *Journal of sound and vibration*, **192(1)**, pp.207 - 222, Forward and backward precession of a vertical anisotropically supported rotor.
- Muszynska A., and Goldman P., (1995), *Chaos, Solutions and Fractal*,**5**, pp.1983 - 1704 Chaotic responses of unbalanced rotor/bearing/stator systems with looseness or rubs.
- Nagata K., and Takeda S., (1987), *Journal of Sound and Vibration*.**113**, pp.307-315, Active control method for passing through critical speeds of rotating shafts by changing stiffness of the supports.
- Nagaya K., Takeda S., Tsukui Y., and Knmaido Y., (1987), *Journal of Sound and Vibration*, **113(2)**, pp.307-315,Active control method for passing through critical speeds of rotating shafts by changing stiffness of the supports with use of Memory metals.
- Nayfeh A .H., (1973), *Perturbation Methods*, Wiley-Interscience, New-York.
- Nayfeh A. H., and Mook D. T., (1979), *Nonlinear Oscillations*, Wiley, New York.
- Nayfeh A.H., (1965a), *Journal of Mathematical Physics*, **44**, pp.368-374, A perturbation method for treating nonlinear oscillation problems.

-
- Nayfeh A.H., (1965b), *Physics of Fluids*, **8**, pp.1896-1898, Nonlinear oscillations in a hot electron plasma.
- Nayfeh A.H., (1968), *IEEE Trans. Circuit Theory*, **15(3)**, pp. 192-200, Forced oscillations of the Van der Pol oscillator with delayed amplitude limiting.
- Nayfeh A.H., (1981), *Introduction to Perturbation Techniques*. John Wiley, New York.
- Nayfeh A.H., (1985), *Tropical course on Nonlinear Dynamics, Societa Italiana di Fisica, Santa Margherita di Pula, Sardinia*. Perturbation methods in nonlinear dynamics.
- Nayfeh A. H., and Mook D. T., (1995), *Nonlinear Oscillations*, Wiley, New York.
- Nayfeh, A. H., and Pai P. F., (2004), *Linear and Nonlinear Structural Mechanics*, Wiley-Interscience, New York.
- Neilson R. D., and Barr A. D. S., (1988), *Proc. Inst. Mech. Eng Part C*, **202(5)**, pp. 369-376, Dynamics of a rigid rotor mounted discontinuously nonlinear elastic supports.
- Nelson H.D., (1980), *ASME Journal of Mechanical Design*, **102**, pp.793-803, A finite rotating shaft element using Timoshenko beam theory.
- Nelson H.D., and McVaugh J.M., (1976), *ASME Journal of Engineering for Industry*, **98**, pp. 593-600, The dynamics of rotor-bearing systems using finite elements .
- Nguyen P.H., and Ginsberg J.H., (2001), *Journal of Vibration and Acoustics*, **123**, pp.359-364, Vibration control using parametric excitation.
- Nikolajsen J.L., Holmes R., and Gondholekar V., (1979), *Proc. Inst. Mech. Engrs (London)*, **193**, pp. 331-336 , Investigation of an electromagnetic damper for vibration control of a transmission shaft.

-
- Nonami K., and Flexming D.P., (1985), *Int. Conf. on Rotordynamics, Tokyo*, pp.429-436, Quasi-model vibration control by means of active control bearings.
- Nonami K., Kawamata S., and Hotote M., (1986), *Trans. JSME* **54**, pp. 1073-1078, Active vibration control of flexible rotor supported by active control bearings, part 2.
- Nusse H.E., and York J.A., (1994), *Dynamics: Numerical Explorations*, Springer-Verlag: New York.
- Nusse H.E., and York J.A., (1998), *Dynamics: Numerical Explorations* (2nd Edition). Springer-Verlag: New York.
- Nusse H.E., Ott E., and York J.A., (1994), *Physical Review*, **E49 (2)**, pp. 1073-1076, Border-collision bifurcations: An explanation for observed bifurcation phenomena.
- Nusse H.E., Ott E., and York J.A., (1995), *Physical Review Letters*, **75 (13)**, pp. 2482-2485, Saddle-node bifurcations on fractal basin boundaries.
- Otsuka K. and Ren X., (1999), *Intermetallics*, **7**, pp.511- 528, Recent developments in the research of shape memory alloys.
- Ott E., Grebogi C., and Yorke J.K., (1990), *Physical Review Letters*, **64(11)**, 1196-1199. Controlling Chaos.
- Pai P. F. and Nayfeh A.H., (1990a), *Nonlinear Dynamics*, **1**, pp.477-502, Three-dimensional nonlinear vibrations of composite beams. I: equations of motion.
- Pai P. F. and Nayfeh A.H., (1990b), *International Journal of Non-linear Mechanics*, **25**, pp.455-474, Nonlinear non-polar oscillation of a cantilever beam under lateral base excitations.
- Pakdemirli M., (2003), *Journal of sound and vibration***262**, pp. 989-998, Comparison of higher order versions of the method of multiple scales for an odd non-linearity problem.

-
- Palazzolo A. B., Kascak A. F., Montague G.T., and Kiraly L.J., (1989), *Trans. ASME*, **111**, pp.298-305, Piezoelectric pusher for active vibration control of rotating machinery.
- Palazzolo A. B., Lin R.R., Alexander R.M., Kascak A.F., and Montague, J., (1989), *Journal of Vibration , Acoustics, Stress, and Reliability in Design*, **111**, pp. 298-305, Piezoelectric pushers for active vibration control of rotating machinery.
- Palazzolo A.B., Jogannathan S., Kascak A. F., Montague G.T., and Kiraly L.J., (1993), *Journal of vibration and Acoustics*, **115**, pp. 111-119, Hybrid active vibration control of rotor bearing systems using piezoelectric actuators.
- Papirno R., (1982), *ASTM Journal of testing and evaluation*, **10**, pp.263-268, Goodness-of-fit of the Ramberg-Osgood analytic stress-strain curve to tensile test data.
- Perkins J., Shape memory effects in Alloys, *Plenum Press*, (1975).
- Pierre C., and Dowell E. H.,(1985), *Journal of Applied Mechanics-Transactions of the American Society of Mechanical Engineers*, **52(3)**, pp. 693-697, A study of dynamic instability of plates by an extended incremental harmonic balance method .
- Poincaré H. Les Methods Nouvelle de la Mécanique Céleste, I, II, III, Gauthier-Villars, paris : pp. 1893-1899.English translation edited by Goroff D., (American Institute of Physics, NY).
- Poisson D.,(1829), *Mem. de l' Academie des Sciences*, **8** , Me'moire sur l'equilibre et le mouvement des corps élastiques.
- Polk S.R., .(1974), *M.S.E Engineering Report, Arizona State University, Tempe, AZ*, Finite element formulation and solution of flexible rotor-rigid disc systems for natural frequencies and critical whirl speeds.

-
- Prohl M.A., (1945), *ASME Journal of Applied Mechanics*, **67**, A-142, A general Method for Calculating Critical speeds of Flexible Rotors.
- Queini S. S., and Nayfeh A. H., (1999), *Journal of sound and Vibration*, **224**, pp. 33-47, Single-mode control of a cantilever beam under principal parametric excitation.
- Rahman Z., and Burton T. D., (1989), *Journal of sound and vibration*, **133(3)**, pp. 369-379, On higher order methods of multiple scales in non-linear oscillations-periodic steady state response.
- Rankine W.J.M.,(1869), *Engineer (London)*,27,pp.249, On the Centrifugal Force of Rotating Shaft.
- Rao J.S.,(1991), *Rotor Dynamics*, 2nd Edition, John Wiley, New York.
- Ray J.D., and Bert C.W., (1969), *Journal of Engineering for Industry*, **91**, pp. 997-1004, Nonlinear vibrations of a beam with pinned ends.
- Rhee S.W.,(1992), *Robust Control of Smart Materials*, Ph.D. Thesis, University of Missouri, USA.
- Richards C. M., and Singh R., (2001), *Journal of sound and Vibration*, **247**, pp, 907-834, Characterization of rubber isolator nonlinearities in the context of single-and multi-degree-of -freedom experimental systems.
- Ritz W., (1909), *Crelle's Journal*,**85**.
- Rogers C.A, Fuller C.R., and Liang C., (1989), *Journal of sound and Vibration*, **136(1)**, pp. 164-170, Active control of sound radiation from panels using embedded shape memory alloy fibres.
- Rogers C.A, Liang C., and Jia J., (1991), *Computers and Structures*, **38(5/6)**, pp. 569-580, Structural modification of simply-supported laminated plates using embedded shape memory alloy fibres.

-
- Rogers C.A., (1988), *Proceedings of the American Society for Composites 3rd Technical Conference on Composite Materials, Seattle* ,Novel design concepts utilizing shape memory alloy reinforced composites.
- Rosen A. and Friedmann P., (1979), *Journal of Applied Mechanics*, **46**, pp. 161-168, The nonlinear behaviour of elastic slender straight beams undergoing small strains and moderate rotations.
- Ruelle D., and Takens F., (1971), *Commun. Math. Phys.*, **20**, pp.167-192, On the nature of turbulence.
- Ruhl R.L., and Booker J.F., (1972), *ASME Journal of Engineering for Industry*, **68**, pp.128-132, A finite element model for distributed parameter turbo rotor systems.
- San Andrés L., (2003), *TRC-B&C-2-03, Research progress report to the Turbomachinery research consortium, Texas A&M university* ,A method for Identification of force coefficients in flexible rotor-bearing systems.
- Sandri G., (1965), *In Nonlinear Partial Differential Equations: A Symposium on Methods of Solutions (Edited by Ames W.F.)*, Academic: New York, pp. 259-277. Uniformization of asymptotic expansions.
- Sandri G., (1965), *Nuovo Cimento*, B36,pp. 67-93, A new method of expansion in mathematical physics.
- Santos I.F., (1993), *Proceedings of the IUTAM Symposium on Active Control of Vibration*, Bath, UK, pp. 79-87, Design and evaluation of two types of active tilting-pad bearings.
- Sathyamoorthy M., (1982a), *Shock and Vibration Digest*, **14**, pp.19-35, Nonlinear analysis of beams. Part I: A survey of recent advances.
- Sathyamoorthy M., (1982b), *Shock and Vibration Digest*, **14**, pp.7-18, Nonlinear analysis of beams. Part II: Finite element methods.

-
- Sathyamoorthy M., (1997), *Nonlinear analysis of structures*. CRC Press, New York.
- Schultze J. F., Hemez F. M., Doebling S. W., and Sohn H., (2001), *Shock and Vibration*, **8**, pp.325-337, Application of non-linear system model updating using feature extraction and parameter effect analysis.
- Schweitzer G., Lange R., (1976), *ImechE Conference on Vibrations in Rotating Machinery*, Cambridge, Paper no. C239/76, Characteristics of a magnetic rotor bearing for active vibration control.
- Segalman D.J., Parker G.G., and Inman D.J., (1993), *ASME Journal of Intelligent Structures, Materials and Vibration*, **58**, pp.1-5, Vibration suppression by modulation of elastic modulus using shape memory alloy.
- Sethna P.R.,(1965), *Journal of Applied Mechanics*, **32**, pp. 576-582, Vibration of dynamical systems with quadratic nonlinearities.
- Shabaneh N. and Zu J. W., (2003), *Transactions of the ASME*, **125**, pp. 290-298, Nonlinear dynamic analysis of a rotor shaft system with viscoelastically supported bearings.
- Shahin A.R., Meckl P.H., Jones J.D., and Thrasher M.A., (1994), *Journal of Intelligent Materials, Systems, and Structures*, **5**, pp. 95-104, Enhance Cooling of Shape Memory Alloy Wires using Semiconductor 'Heat Pump' Modules.
- Shahin A.R., Meckl P.H., and Jones J.D., (1997), *Journal of Intelligent Materials, Systems, and Structures.*, **8**, pp. 51-70, Model of SMA tendons for active control of structures.
- Shakeri C., Noori M.N. and Hou Z., *Smart materials and structures*.
<http://me.wpi.edu/~cirrus/Publications/SmartMaterials/SmartMaterialsExtension.htm>

-
- Shaw R., (1981), *Z. Naturf.*, **36a**, pp. 80-112, Strange attractors, chaotic behaviour, and information flow.
- Shaw S. W., (1988), *Journal of sound and vibration and Acoustics*, **124**, pp.329-343, Chaotic dynamics of a slender beam rotating about its longitudinal axis.
- Sherif A. H., and Abu Omar T. M., (2004), *Tribology International*, **37**, pp., 235-244, Mechanism of energy dissipation in mechanical system with dry friction.
- Simões R.C., Steffen Jr V., Der Hagoplan J., and Mahfoud J., (2007), *Journal of Vibration and Control*, **13(1)**, pp.45-64 Modal active vibration control of a rotor using piezoelectric stack actuators.
- Simoyi R.H., Wolf A., and Swinney H. L., (1982), *Physical Review Letters* **49**, pp.245-248, One-dimensional dynamics in a multicomponent chemical reaction.
- Sims N.D., Stanway R. and Johnson A.R., (1999), *The shock and Vibration Digest*, **31(3)**, pp.195-203, Vibration control using smart fluids: a state of the art review.
- Singer J., Wang Y. Z., and Bau Haim H., (1991), *Physical Review Letters*, **66(9)**, pp. 1123-1125, Controlling a chaotic system.
- Singh R., Davies P., and Bajaj A. K., (2003), *Nonlinear Dynamics*, **34**, pp. 319-346, Identification of nonlinear and viscoelastic properties of flexible polyurethane foam.
- Skalak R., and Yarymovych M.I., (1960), *Journal of Applied Mechanics*, **27**, pp.159-164, Subharmonic oscillations of pendulum.
- Solamone D. J., (1980), *Journal of Engineering for power* **102**, PP.749-755, Synchronous unbalance response of an overhung rotor with disk screw.
- Stanway R., and Burrows C.R., (1981), *ASME Journal of Dynamical Systems, Measurement and control* **103**, pp. 383-388, Active vibration control of flexible rotor on flexible-mounted journal bearings.

-
- Steinkopff T and Wolff A., (2000), *Functional Materials, EUROMAT, Wiley, Germany, 13*, pp.381-390, (Siemens AG), Modelling of piezoelectric actuators.
- Stodola A.,(1918), , *Gesante Tubinenwes,15*, PP.269-275, Neve Kristische Drehzahlen als folye der kreisel wirkuag der laufrader.
- Strogatz S. H., (1994), *Nonlinear dynamics and chaos, with applications to physics, biology, chemistry, and engineering*, Addison-Wesley publishing company, Reading, UK.
- Struble R.A., (1963), *ASME Journal of Applied Mechanics, 30*, pp. 301-303, On the subharmonic oscillations of a pendulum.
- Sturrock P.A., (1957), *Proc, Roy, Soc. London, A242*, pp.277-299, Nonlinear effects in electron plasmas.
- Sturrock P.A., (1963), *Stanford University Microwave laboratory Rept., No.1004*. Nonlinear theory of electromagnetic waves in plasmas.
- Subbiah R., and Rieger N., (1988), *ASME Journal of Vibration, Acoustics, Stress and Reliability in Design*, vol. 110, On the transient analysis of rotor bearing systems.
- Sun J.C., Wang X.G. and Xi F.J., (2000), *International Conferences on Control Application, IEEE*, pp.953-958, Sliding mode active vibration control of circular saws.
- Sun L., and Krodkiewski J.M., (1998), *Journal of Sound and Vibration, 213*, pp. 1-14, Self-tuning adaptive control of forced vibration in rotor systems using an active journal bearing.
- Sun L., Krodkiewski J.M. and Cen Y., (1998), *Journal of sound and vibration, 213 (1)*, pp. 1- 14, Self-turning adaptive control of forced vibration in rotor systems using an active journal bearing.

-
- Tammi K., (2003), VTT *Publications* **498**, Active vibration control of rotor in desk top test environment.
- Testa J., Perez J ., and Jeffries C., (1982),), *Physical Review Letters*, ,**48**, pp.714-717, Evidence of universal chaotic behaviour of a driven nonlinear oscillator.
- Thomson W. T., (1993), Theory of Vibration with Applications, *Nelson Thornes ltd.* U.K.
- Timoshenko S.P., and Goodier J.N., (1970), Theory of Elasticity, McGraw-Hill, New York.
- Timoshenko, S.P., (1921), *Philosophical Magazine and Journal of Science*, **41**, pp.744-747, On the correction for shear of the differential equation for transverse vibrations of prismatic bars.
- Timoshenko, S.P., (1922), *Philosophical Magazine and Journal of Science*, **43**, pp.125-131, On the transverse vibrations of bars of uniform cross-section.
- Timoshenko, S.P., (1983), History of Strength of Materials, Dover, New York.
- Timoshenko, S.P., and Young, D.H., (1968), Elements of Strength of Materials, Litton Educational Publishing, New York.
- Tomlinson G. R., and Hibbert J.H., (1979), *Journal of Sound and vibration*, **64**, pp., 233-242, Identification of the dynamic characteristics of a structure with Coulomb friction.
- Tondl A., (1965), Some problems of rotor dynamics, Publishing House, Czechoslovak Academy of Science, Prague.
- Uchino K., (1986), *Ceramic Bulletin*, **65**, pp. 647-652, Electrostrictive actuators.
- Ueda, Y., (1979), *Journal of Statistics and Physics*, **20**, pp.181-196, Randomly transitional phenomena in the system governed by Duffing's equation.

-
- Ueda, Y., (1991), *Journal of Chaos, Solutions and Fractals*, **1(3)**, pp. 199-231, Survey of regular and chaotic phenomena in forced Duffing Oscillator.
- Ueda, Y., (2001), *The road to chaos-II*, Aerial Press, Inc. Santa Cruz. USA.
- Ueda, Y.,(1958), *International Journal of Nonlinear Mechanics*,**20**, pp. 481-491,Random phenomena resulting from nonlinearity in the system described by Duffing's equation.
- Van de Vorst E.L.B., (1996), *Long Term Dynamics and Stabilization of Nonlinear Mechanical Systems*, Ph.D. Thesis, Eindhoven University of Technology.
- Van de Vorst E.L.B., Fey R.H.B., De Kraker A., and Van Campen D.H., (1994),*In Proceedings of the WAM of the ASME, Symposium on Nonlinear and Stochastic Dynamics, New York, USA, 192*, pp.107-114.
- Van de Vrande B.L., (2001), *Nonlinear Dynamics of Elementary Rotor Systems with Compliant Plain Journal Bearings*. Ph.D. Thesis, Eindhoven University of technology.
- Van der Pol, B., (1972 *Philosophical Magazine and Journal of Science*,**7(3)**, pp.65-80, Forced oscillations in a circuit with nonlinear resistance (reception with reactive triode).
- Van Dyke, M., (1964), *Perturbation methods in fluid mechanics*, Academic Press, New York.
- Vance J M., (1988), *Rotordynamics of turbomachinery. John Wiley & Sons, Inc. New York .*
- Vassilopoulos L., and Ghosh P.K., (1983), *VIII Congress, Pan-American Institute of naval engineering, Washington, DC*, Simplified techniques for studying nonlinear shaft vibration problems.
- Viderman Z., and Porat I., (1987), *ASME journal of dynamics systems, measurement and control*, vol. 109, An optimal control method for passage of a flexible rotor through resonances.

-
- Wang J., and Meng G., (2002), *Sixth International Conferences on Rotor Dynamics*, **2**, pp .615-620, Instability of a cantilever rotor supported on MR fluid damper and sliding bearing.
- White S.W., Kim S. K., Bajaj A. K., Davies P., Showers D. K., and Liedtke P. E., (2000), *Nonlinear Dynamics*,**22**,pp. 281-313, Experimental techniques and identification of nonlinear and viscoelastic properties of flexible polyurethane foam.
- Wickert J. A., (1992), *International Journal of Non-Linear Mechanics*, **27**, pp. 503-517, Nonlinear vibration of a travelling tensioned beam.
- Woafu P., Fotsin H.B., and Chedjou J.C., (1998), *Physica script* **57**, pp. 195-200, Dynamics of two nonlinearly coupled oscillators.
- Wolf A., Swift J. B., Swinney H. L., and Vastano J. A., (1985), *Physica*, **16D**, pp. 285-317, Determining Lyapunov exponents from a time series.
- Wolfram S., (1996), *The Mathematica Book*, 3rd Edition, Wolfram Media and Cambridge University Press.
- Wong S.B.,(1988),The Identification of Non-Linear Stabilisation Parameter on a Simple parametric oscillator, BSc. Thesis, University of Aberdeen, UK.
- Yabuno H., (1997), *Nonlinear Dynamics*, **12**, pp. 263-274, Bifurcation control of parametrically excited Duffing system by a combined linear plus-nonlinear feedback control.
- Yabuno H., Saigusa S., and Aoshima N., (2001), *Nonlinear Dynamics*, **26**, pp. 143-161, Stabilization of the parametric resonance of a cantilever beam by bifurcation control with a piezoelectric actuator.
- Yalcintas M. and Dai H., (1999), *Smart Materials and Structures*, **8**, pp.560-573, Magnetorheological and electrorheological materials in adaptive structures and their performance comparison.

-
- Yamamoto T., and Ishida Y., (2001), *Linear and Nonlinear Rotordynamics*, Wiley, NY.
- Yamamoto T., Ishida I., and Kawasumi J., (1975), *Bulletin of the JSME* **18(123)**, pp.965-975, Oscillations of a rotating shaft with symmetrical nonlinear spring Characteristics.
- Yamamoto T., Ishida Y., Ikeda T., and Yamada M., (1981), *Bulletin of the JSME*, **24**, pp.192, Subharmonic and summed-and- differential harmonic oscillations of an unsymmetrical rotor.
- Yamamoto T., Yasuada K., and Nagasaka I., (1976), *Bulletin of the JSME*, **19(138)**, pp.1442-1447, Ultra-Subharmonic oscillations in a nonlinear vibratory system (1976).
- Yan X., Nie J., Sun C., (2000), *Journal of Aerospace Power*, **15**, pp.63-66, Intelligent support system for passing through critical speed of high-speed rotor by changing stiffness.
- Yang T., and Chaung W.C., (2000), *ASME paper 2000 GT-400*, Identification of bearing coefficients of flexible rotor- bearing systems.
- Yao G.Z., Qiu Y., Meng G., and Fang T., (1999), *Journal of Sound and Vibration*, **219**, pp. 175-188, Vibration control of a rotor system by disk type electrorheological damper.
- Yeh J.Y., Chen L. W., and Wang C. C., (2004), *Composite Structures*, **64(1)**, pp. 47-54, Dynamic instability of a sandwich beam with a constraining layer and electrorheological fluid core.
- Yeh Z., and Shih Y., (2005), *Composite Structures*, **40(15)**, pp.1333-1359, Dynamic characteristics and dynamic instability of Magnetorheological material-based adaptive beams.

- Yi K. A., Veillette R. J., (2005), *IEEE Transactions on Control Systems Technology*, **13**, pp. 517-526, A charge Controller for linear operation of a Piezoelectric stack actuator.
- Young L. S., (1984), *Physica*, **124A**, pp. 639-646, Dimension entropy, and Lyapunov exponents in differentiable dynamical systems.
- Žak A.J., Cartmell M.P., and Ostachowicz W.M., (2003), Dynamics and control of a rotor using an Integrated SMA/Composite active bearing actuator, Glasgow University.
- Zhao C., (2001), *Advanced materials and processes*, Shape memory stainless steels.
- Zheng T., and Hasebe N., (2000), *Journal of Applied Mechanics*, **67**, pp. 485-495, Nonlinear dynamic behaviours of a complex rotor-bearing system.
- Zorzi E.S., and Nelson H.D., (1977), *ASME Journal of Engineering for Power*, **99**, pp.71-76, Finite element simulation of Rotor-bearing systems with internal damping.

Note: Total number of references in this dissertation is 328.

PUBLICATIONS

Inman D.J., Cartmell M.P., Lees A.W., Leize Th., and **Atepor L.**, “Proposals for Controlling Flexible Rotor Vibrations by means of an Antagonistic SMA/Composite Smart Bearing”, *Applied Mechanics and Materials Vols.5-6 (2006)*, pp.29-36.

Cartmell M.P., Inman D.J., Lees A.W., Ganilova O.A., and **Atepor L.**, “Smart Material Applications to Structural Dynamics and Rotating Machines”, *Proceedings of the Euromech 498 Colloquium on the Nonlinear Dynamics of Composite and Smart Structures*, pp. 19-28, 21-24 May 2008, Kazimierz Dolny, Poland.

CONTENTS OF APPENDICES

APPENDIX A	A-2
A.1 Smart Material Force using Lagrange's Equation.....	A-2
A.2 Mathematica Validation of Equations (3.2-75) and (3.2-76)	A-8
A.3 Linear Viscous Damping Factor.....	A-9
A.4 Damping Coefficient Estimation.....	A-11
A.5 Experimental Determination of the Value b for the Nonlinear Cubic Stiffness Term.....	A-12
APPENDIX B	B-1
B.1 Simultaneous Solution of Amplitudes p, q, r, s - without Parametric Force Term.....	B-1
B.2 Simultaneous Solution of Amplitudes p, q, r, s - with Parametric Force Term.....	B-2
B.3 Coefficients of the Characteristic Equation	B-4
APPENDIX C	C-1
C.1 Screen Dump of the Code for the Analysis of the Coupled Differential Equations	C-1
C.2 Specialized Code written in <i>Mathematica</i> TM	C-2
C.3 Dynamics 2 Commands	C-4
APPENDIX D	D-1
D.1 Parametric Plots	D-1
D.2 Calculation of Maximum Spring Force.....	D-1

APPENDIX A

A.1 Smart Material Force using Lagrange's Equation.

A disk of mass m is attached to the middle of a shaft of length $2l$, which is subjected to an initial tensile force denoted by the symbol F_v with the mass displaced a distance q from its equilibrium position as indicated in Figure A.1-1. The q is a theoretical generalised coordinate in the YZ plane on the system. In practice the lateral displacement of the shaft is given by two orthogonal coordinates q_1 and q_2 , and this is due to the combined effect of the whirl dynamics of the shaft (driven by the two generalised forces $Q_1(t)$ and $Q_2(t)$ which in turn are based on the physically defined unbalanced mass in the disk, which is parameterised by the eccentricity quantity d), and the axial load due to the active bearing.

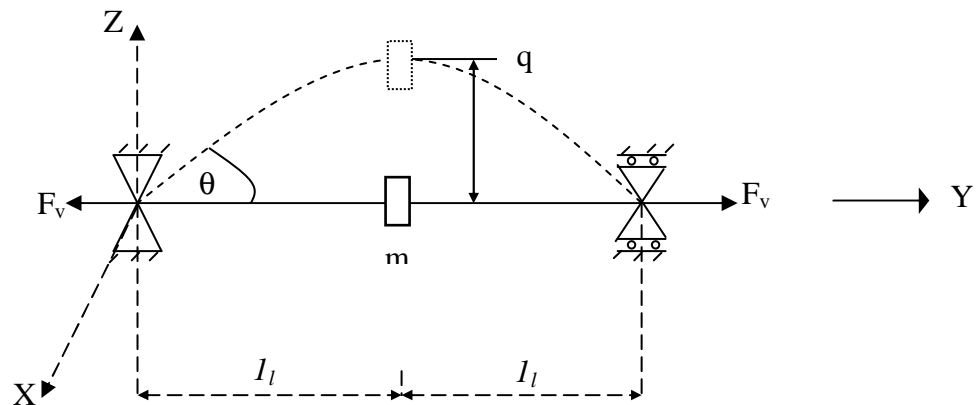


Figure A.1- 1: Model of the rotor

Applying Lagrange's equation of the form

$$\frac{d}{dt} \left(\frac{\partial T}{\partial \dot{q}_i} \right) - \frac{\partial T}{\partial q_i} + \frac{\partial U}{\partial q_i} = Q_i(t) \quad (\text{A.1- 1})$$

where, T is the total kinetic energy of the system; U is the potential or strain energy.

Applying Lalanne and Ferraris methods in Rotor dynamics Prediction in Engineering, kinetic energy can be written as;

$$T = \frac{1}{2}m(\dot{q}_1^2 + \dot{q}_2^2) + \Omega^2 \left(\frac{1}{2}I_{dy} + \rho IL \right) - \Omega a_2 \dot{q}_1 \sin(1.325q_2) \quad (\text{A.1- 2})$$

where, m is the mass; q_1, q_2 are the vertical and horizontal displacements respectively; Ω is the angular velocity.

Applying Lagrange's equation (A.1-1) to the kinetic energy expression (A.1-2) we have

$$\frac{d}{dt} \left(\frac{\partial T}{\partial \dot{q}_1} \right) - \frac{\partial T}{\partial q_1} = m\ddot{q}_1 - \Omega a_5 \dot{q}_2 \cos(1.325q_2) \quad (\text{A.1- 3})$$

$$\frac{d}{dt} \left(\frac{\partial T}{\partial \dot{q}_2} \right) - \frac{\partial T}{\partial q_2} = m\ddot{q}_2 + \Omega a_5 \dot{q}_1 \cos(1.325q_2) \quad (\text{A.1- 4})$$

The strain energy

$$U = U_1 + U_2 \quad (\text{A.1- 5})$$

where, U_1 is the strain energy in terms of lateral elasticity; U_2 is the strain energy in terms of elasticity in the axial direction.

Using Timoshenko's expression due to beam extension/compression

$$U_1 = \frac{F_v}{2} \int_0^l \left[\left(\frac{\partial z}{\partial y} \right)^2 + \left(\frac{\partial x}{\partial y} \right)^2 \right] dy \quad (\text{A.1- 6})$$

where, F_v is the axial force; z and x can be related to q_1 and q_2 by a Galerkin representation, which separates the independent variables "y" and "t", on the basis that $q_1 = q_1(t)$ and $q_2 = q_2(t)$.

$$\text{Thus,} \quad z = W(y)q_1(t) \quad (\text{A.1- 7})$$

$$x = W(y)q_2(t) \quad (\text{A.1- 8})$$

where, $W(y)$ is a deflection shape function. The q_1 and q_2 notations are functions of time t whereas $W(y)$ is a function of y . The deflection shape, $W(y)$

as given by Timoshenko in the treatment of the theory of beams having a fixed end and freely supported at the other (approximation)

$$W(y) = \frac{Py}{12EI} \left(\frac{3l^2}{4} - y^2 \right) \quad (\text{A.1- 9})$$

where, P is the applied load, E is the Young's Modulus of the material, I is the area moment of Inertia, l is the length of the beam, y is the distance of the applied load from the fixed end. Proceeding to normalise the deflection shape and applying $W(y)=1$ at $y = \frac{l}{2}$ leads to

$$\frac{pl^3}{48EI} = 1 \quad (\text{A.1- 10})$$

hence

$$W(y)_{norm} = \frac{3y}{l} - \frac{4y^3}{l^3} \quad (\text{A.1- 11})$$

$$W'(y) = \frac{3}{l} - \frac{12y^2}{l^3} \quad (\text{A.1- 12})$$

Substituting equations (A.1-7) and (A.1-8) into (A.1-6) we have

$$U_1 = \frac{F_v}{2} (q_1^2 + q_2^2) \int_0^l [W'(y)]^2 dy \quad (\text{A.1- 13})$$

Substituting (A.1-12) into (A.1-13) and proceeding to integrate with respect to y and finally on evaluating within the limits of the integral, we get,

$$U_1 = \frac{F_v}{2} \left(\frac{14}{l} \right) (q_1^2 + q_2^2) \quad (\text{A.1- 14})$$

Let

$$H = \frac{14F_v}{l} \quad (\text{A.1- 15})$$

Therefore,

$$U_1 = \frac{H}{2} (q_1^2 + q_2^2) \quad (\text{A.1- 16})$$

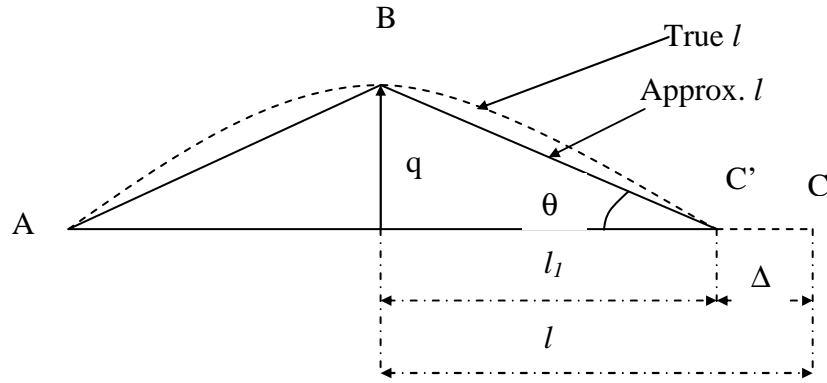


Figure A.1- 2: Schematic of the shafts movements.

Inspection of the geometry in Figure A.1-2, assuming C is free to move (implying A is also free) then when shaft deflects through q point C moves to C' . So, axial displacement required at C (CC') is $CC' = \Delta$ (Similarly at A).

Denoting horizontal length OC as $OC' = l_1$, the potential energy of the system can be written as

$$U_2 = \frac{1}{2}k\Delta^2 = \frac{1}{2}k(l-l_1)^2 \quad (\text{A.1- 17})$$

Also from Figure A.1-2,

$$l_1 = \left(l_{approx}^2 - q^2\right)^{\frac{1}{2}} \quad (\text{A.1- 18})$$

Therefore

$$\Delta = l - \left(l_{approx}^2 - q^2\right)^{\frac{1}{2}} \approx l - \left(l^2 - q^2\right)^{\frac{1}{2}} \quad (\text{A.1- 19})$$

where, $l_{approx} \approx l$

Simplifying (A.1-19) using binomial expansion of the form

$$(a+b)^n = a^n + na^{n-1}b + \frac{n(n-1)}{2!}a^{n-2}b^2 \dots \quad (\text{A.1- 20})$$

and letting $a = l^2$, $b = -q^2$ and $n = \frac{1}{2}$, we have

$$(l^2 - q^2)^{\frac{1}{2}} = (l^2)^{\frac{1}{2}} + \frac{1}{2}(l^2)^{-\frac{1}{2}}(-q^2) + \frac{\left(\frac{1}{2}\right)\left(-\frac{1}{2}\right)}{2*1}(l^2)^{-\frac{3}{2}}(-q^2)^2 + \dots \quad (\text{A.1- 21})$$

$$\approx l - \frac{q^2}{2l}$$

Therefore

$$l - (l^2 - q^2)^{\frac{1}{2}} \approx l - l + \frac{q^2}{2l} \approx \frac{q^2}{2l} \quad (\text{A.1- 22})$$

Thus from equation (A.1-22) equation (A.1-19) may be replaced with a simpler (but less accurate) equation by using the approximate relationship

$$\Delta \approx \frac{q^2}{2l} \quad (\text{A.1- 23})$$

Substituting equation(A.1-23) back into equation(A.1-17) we have,

$$U_2 = \frac{1}{2}k\left(\frac{q^2}{2l}\right)^2 \quad (\text{A.1- 24})$$

For a shaft of length l , axial force F_v produces an extension Δ . Force acts over cross-sectional area A , producing normal stress

$$\sigma = \frac{F_v}{A} \quad (\text{A.1- 25})$$

The compression produces normal strain

$$\varepsilon = \frac{\Delta}{l} \quad (\text{A.1- 26})$$

Combining equations (A.1-25) and (A.1-26) yields relationship between force and extension:

$$F_v = \frac{EA}{l}\Delta = k\Delta \quad (\text{A.1- 27})$$

where k is the shaft stiffness and $k = \frac{EA}{l}$. Substituting for k and considering vertical and horizontal displacements (A.1-24) becomes

$$U_2 = \frac{AE}{8l^3} (q_1^4 + q_2^4) \quad (\text{A.1- 28})$$

Substituting equations (A.1-16) and (A.1-28) into equation (A.1-5) we get

$$U = \frac{H}{2} (q_1^2 + q_2^2) + \frac{AE}{8l^3} (q_1^4 + q_2^4) \quad (\text{A.1- 29})$$

Therefore,

$$\frac{\partial U}{\partial q_1} = Hq_1 + \frac{AE}{2l^3} q_1^3 \quad (\text{A.1- 30})$$

And

$$\frac{\partial U}{\partial q_2} = Hq_2 + \frac{AE}{2l^3} q_2^3 \quad (\text{A.1- 31})$$

Substituting equations (A.1-30), (A.1-31), (A.1-3) and (A.1-4) into equation (A.1-1) we have

$$m\ddot{q}_1 - \Omega a_5 \dot{q}_2 \text{Cos}(1.325q_2) + Hq_1 + \frac{AE}{2l^3} q_1^3 = Q_1(t) \quad (\text{A.1- 32})$$

$$m\ddot{q}_2 + \Omega a_5 \dot{q}_1 \text{Cos}(1.325q_2) + Hq_2 + \frac{AE}{2l^3} q_2^3 = Q_2(t) \quad (\text{A.1- 33})$$

Substituting equation (A.1-15) into equations (A.1-32) and (A.1-33) gives

$$m\ddot{q}_1 - \Omega a_5 \dot{q}_2 \text{Cos}(1.325q_2) + \frac{14F_v}{l} q_1 + \frac{AE}{2l^3} q_1^3 = Q_1(t) \quad (\text{A.1- 34})$$

$$m\ddot{q}_2 + \Omega a_5 \dot{q}_1 \text{Cos}(1.325q_2) + \frac{14F_v}{l} q_2 + \frac{AE}{2l^3} q_2^3 = Q_2(t) \quad (\text{A.1- 35})$$

A.2 Mathematica Validation of Equations (3.2-75) and (3.2-76)

$$T = 1/2 * m * ((D[q1[t], t])^2 + (D[q2[t], t])^2) + (\Omega^2 * (l_{dy}/2 + \rho * l * L)) - (\Omega^2 * a^2 * (D[q1[t], t]) * \sin[\gamma * q2[t]])$$

$$U = 1/2 * k * ((q1[t])^2 + (q2[t])^2)$$

$$\text{FullSimplify}[\text{Expand}[\partial_t (\partial_{q1} T) - \partial_{q1} T + \partial_{q1} U]] = 0$$

$$\text{FullSimplify}[\text{Expand}[\partial_t (\partial_{q2} T) - \partial_{q2} T + \partial_{q2} U]] = 0$$

$$\Omega^2 * (l_{dy}/2 + \rho * l * L) - a^2 * \Omega^2 * \sin[\gamma * q2[t]] * q1^{[t]+1/2 * m} (q1^{[t]2} + q2^{[t]2})$$

$$1/2 * k * (q1[t]^2 + q2[t]^2)$$

$$k * q1[t] - a^2 * \gamma * \Omega^2 * \cos[\gamma * q2[t]] * q2^{[t]+m} q1^{[t]} = 0$$

$$k * q2[t] + a^2 * \gamma * \Omega^2 * \cos[\gamma * q2[t]] * q1^{[t]+m} q2^{[t]} = 0$$

$$T = 1/2 * m * ((D[q1[t], t])^2 + (D[q2[t], t])^2) + (\Omega^2 * (l_{dy}/2 + \rho * l * L)) - (\Omega^2 * a^2 * (D[q1[t], t]) * (\gamma * q2[t]))$$

$$U = 1/2 * k * ((q1[t])^2 + (q2[t])^2)$$

$$\text{FullSimplify}[\text{Expand}[\partial_t (\partial_{q1} T) - \partial_{q1} T + \partial_{q1} U]] = 0$$

$$\text{FullSimplify}[\text{Expand}[\partial_t (\partial_{q2} T) - \partial_{q2} T + \partial_{q2} U]] = 0$$

$$\Omega^2 * (l_{dy}/2 + \rho * l * L) - a^2 * \gamma * \Omega^2 * q2[t] * q1^{[t]+1/2 * m} (q1^{[t]2} + q2^{[t]2})$$

$$1/2 * k * (q1[t]^2 + q2[t]^2)$$

$$k * q1[t] - a^2 * \gamma * \Omega^2 * q2^{[t]+m} q1^{[t]} = 0$$

$$k * q2[t] + a^2 * \gamma * \Omega^2 * q1^{[t]+m} q2^{[t]} = 0$$

A.3 Linear Viscous Damping Factor.

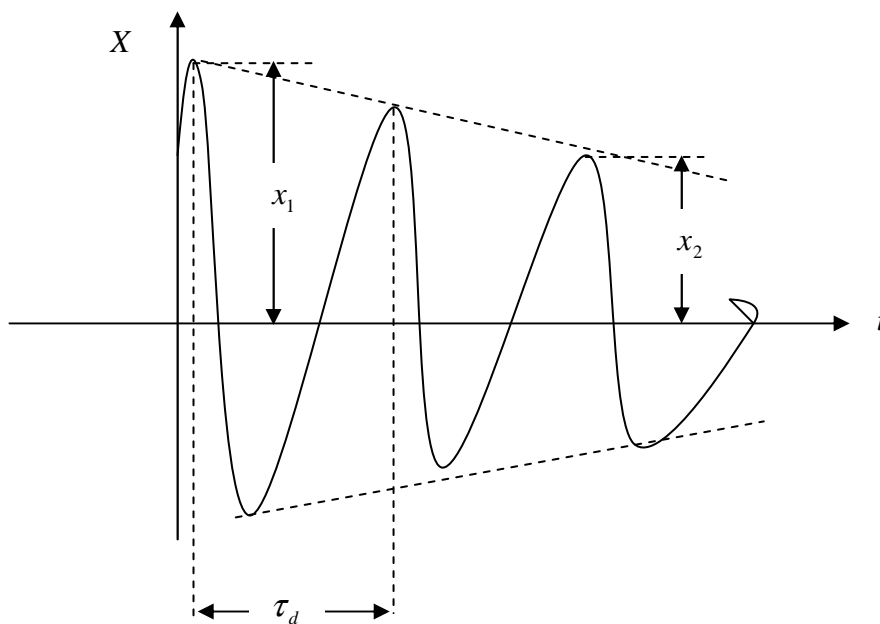
A measurement of the rate of decay of free oscillations will be a convenient way to determine the amount of damping present in the system. If the damping is larger, the rate of decay will be greater.

A damping vibration expression can be given by the general equation,

$$x = X e^{-\xi \omega t} \sin(\sqrt{1 - \xi^2} \omega t + \phi) \quad (\text{A.3-1})$$

Where, ϕ is the phase angle.

This is illustrated as in Figure A3-1



A.3- 1: Graphical Representation of Decay

A term called logarithmic decrement is introduced which is defined as the natural logarithm of the ratio of any two successive amplitudes. The expressions for the logarithmic decrement then becomes

$$\delta = \ln\left(\frac{X_1}{X_2}\right) = \ln\frac{e^{-\xi\omega t} \text{Sin}\left(\sqrt{1-\xi^2}\omega t + \phi\right)}{e^{-\xi\omega(t+\tau_d)} \text{Sin}\left(\sqrt{1-\xi^2}\omega(t+\tau_d) + \phi\right)} \quad (\text{A.3- 2})$$

And since the values of the sines are equal when the time is increased by the damping period, τ_d , the above relation reduces to

$$\delta = \ln\frac{e^{-\xi\omega t}}{e^{-\xi\omega(t+\tau_d)}} = \ln e^{\xi\omega\tau_d} = \xi\omega\tau_d \quad (\text{A.3- 3})$$

Substituting for the damped period, $\tau_d = \frac{2\pi}{\omega\sqrt{1-\xi^2}}$, the expression for the logarithmic decrement becomes

$$\delta = \frac{2\pi}{\sqrt{1-\xi^2}} \quad (\text{A.3- 4})$$

This is an exact equation.

For a small damping ratio $x_1 \approx x_2$, and $\delta \ll 1$, so that

$$\xi \cong \frac{\delta}{2\pi} \quad (\text{A.3- 5})$$

If x_1 and x_2 are so close in value that experimental distinction between them is impractical, the above analysis may be modified by using two observed amplitudes which are n cycles apart. The damping factor for the rig is found experimentally in the following section.

A.4 Damping Coefficient Estimation

The damping coefficient is determined experimentally, and the objective is to determine the linear damping factor ξ for the rig, and then estimate the damping coefficient c . The electric motor is switched off and the flexible rotor system is excited by striking the disk with a tapping hammer. The amplitudes X_1 and X_2 for two consecutive displacements which are measured at three cycles apart for the decaying oscillations are read off from the oscilloscope. This procedure is repeated several times and the average of the peak to peak values are taken. The peak to peak values of X_1 and X_2 are 0.46 volts and 0.2 volts respectively. The calculation of the damping factor utilizes the derivation of logarithmic decrement equation (A.3-2), and upon substitution of values for X_1 and X_2 gives

$$\delta = \frac{1}{n} \ln \left(\frac{X_1}{X_2} \right) = \frac{1}{3} \left(\frac{0.46}{0.2} \right) = 0.276 \quad (\text{A.3- 6})$$

where, n is the number of cycles elapsed.

To find the damping factor the logarithmic decrement value $\delta = 0.276$ is back substituted into equation (A.3-5) giving

$$\xi = \frac{\delta}{2\pi} = 0.044 \quad (\text{A.3- 7})$$

The damping coefficient is then calculated as

$$c = 2m\xi\omega = 13.6 \text{ Ns} / \text{m} \quad (\text{A.3- 8})$$

A.5 Experimental Determination of the Value b for the Nonlinear Cubic Stiffness Term.

The objective of this experiment is to determine the value of b for the cubic stiffness term. This experimentally based method of identifying cubic nonlinearities for nonlinear systems was first used by Wong in 1988. In the usual manner of carrying out the experiment, the rig was excited at its experimental nonlinear frequency of 39.6 Hz and with the aid of the spectrum analyser the amplitude in volts was obtained and recorded as A_1 with $\omega_{nl(1)}$ as its resonance frequency. The next step forward was to shift the frequency of excitation slightly and new amplitude of vibration A_2 with its corresponding frequency $\omega_{nl(2)}$ was recorded. This is repeated for several times and amplitudes of 0.12 volts and 0.119 volts were obtained for A_1 and A_2 respectively. The voltages are then converted into metres and the values of $\omega_{nl(1)}$, $\omega_{nl(2)}$, A_1 and A_2 are substituted into equation (3.2-93) to get

$$b = \frac{4(\omega_{nl(1)}^2 - \omega_{nl(2)}^2)}{3(A_1^2 - A_2^2)} - \frac{4F}{3A_1A_2(A_1 + A_2)} = 5.05 \times 10^9 \frac{\text{rad}^2}{\text{s}^2\text{m}^2} \quad (\text{A.4- 1})$$

APPENDIX B

B.1 Simultaneous Solution of Amplitudes p, q, r, s- without Parametric Force Term

$$\{\Gamma, \omega, \hat{a}_5, \Omega, \hat{c}, \hat{b}\} = \{0.69, 1, 0.001, 248.8, 21.9, 8.15 \cdot 10^9\}$$

$$\text{Solve}\left[\left\{\left(-\frac{\hat{c} \cdot p}{2 \cdot \omega} + \frac{\Omega \cdot \hat{a}_5 \cdot r}{2 \cdot \omega} + \frac{\hat{c}^2 \cdot q}{8 \cdot \omega^2} - \frac{\Omega \cdot \hat{c} \cdot \hat{a}_5 \cdot s}{4 \cdot \omega^2} - \frac{3 \cdot \Omega^2 \cdot \hat{a}_5^2 \cdot q}{8 \cdot \omega^2} - \frac{3 \cdot \hat{b} \cdot p^2 \cdot q}{2 \cdot \omega^2} - \frac{3 \cdot \hat{b} \cdot q^3}{2 \cdot \omega^2}\right) + 0.164 = 0,\right.\right.$$

$$\left.\left(-\frac{\hat{c} \cdot q}{2 \cdot \omega} + \frac{\Omega \cdot \hat{a}_5 \cdot s}{2 \cdot \omega} + \frac{\hat{c}^2 \cdot p}{8 \cdot \omega^2} - \frac{\Omega \cdot \hat{c} \cdot \hat{a}_5 \cdot r}{4 \cdot \omega^2} - \frac{3 \cdot \Omega^2 \cdot \hat{a}_5^2 \cdot p}{8 \cdot \omega^2} - \frac{3 \cdot \hat{b} \cdot q^2 \cdot p}{2 \cdot \omega^2} - \frac{3 \cdot \hat{b} \cdot p^3}{2 \cdot \omega^2}\right) + 0.94 = 0,\right.$$

$$\left.\left(-\frac{\hat{c} \cdot r}{2 \cdot \omega} - \frac{\Omega \cdot \hat{a}_5 \cdot p}{2 \cdot \omega} + \frac{\hat{c}^2 \cdot s}{8 \cdot \omega^2} + \frac{\Omega \cdot \hat{c} \cdot \hat{a}_5 \cdot q}{4 \cdot \omega^2} - \frac{\Omega^2 \cdot \hat{a}_5^2 \cdot s}{8 \cdot \omega^2} - \frac{3 \cdot \hat{b} \cdot r^2 \cdot s}{2 \cdot \omega^2} - \frac{3 \cdot \hat{b} \cdot s^3}{2 \cdot \omega^2}\right) + 0.94 = 0,\right.$$

$$\left.\left(-\frac{\hat{c} \cdot s}{2 \cdot \omega} - \frac{\Omega \cdot \hat{a}_5 \cdot q}{2 \cdot \omega} + \frac{\hat{c}^2 \cdot r}{8 \cdot \omega^2} + \frac{\Omega \cdot \hat{c} \cdot \hat{a}_5 \cdot p}{4 \cdot \omega^2} - \frac{\Omega^2 \cdot \hat{a}_5^2 \cdot r}{8 \cdot \omega^2} - \frac{3 \cdot \hat{b} \cdot s^2 \cdot r}{2 \cdot \omega^2} - \frac{3 \cdot \hat{b} \cdot r^3}{2 \cdot \omega^2}\right) + 0.164 = 0\right\},$$

$$\{p, q, r, s\}$$

$$\{0.69, 1, 0.001, 248.8, 21.9, 8.15 \cdot 10^9\}$$

$$\left\{\left\{p \rightarrow -0.00211902258821777, q \rightarrow 0.00041952572031022116\right\}, \left\{p \rightarrow 0.0010603879792571763 - 0.0016899612702690975 i, q \rightarrow -0.00020473606482728724 + 0.000254657775694461 i\right\}, \left\{p \rightarrow 0.0010603879792571763 + 0.0016899612702690975 i, q \rightarrow -0.00020473606482728724 - 0.000254657775694461 i\right\}, \left\{p \rightarrow 0.0075527239412491445 - 0.04329451602546732 i, q \rightarrow -0.04330005477589113 - 0.007550667319177746 i\right\}, \left\{p \rightarrow 0.0075527239412491445 + 0.04329451602546732 i, q \rightarrow -0.04330005477589113 + 0.007550667319177746 i\right\}, \left\{r \rightarrow -0.00016644670174246828 - 0.00033437589022070584 i, s \rightarrow -0.0010630247650816708 - 0.0016830682814302487 i\right\}, \left\{r \rightarrow -0.00016644670174246828 + 0.00033437589022070584 i, s \rightarrow -0.0010630247650816708 + 0.0016830682814302487 i\right\}, \left\{r \rightarrow 0.00031931322453801616, s \rightarrow 0.0021284184422404335\right\}, \left\{r \rightarrow 0.04256287130820719 - 0.007423398857843448 i, s \rightarrow 0.007423493543825637 + 0.04255585754269378 i\right\}, \left\{r \rightarrow 0.04256287130820719 + 0.007423398857843448 i, s \rightarrow 0.007423493543825637 - 0.04255585754269378 i\right\}\right\}$$

B.2 Simultaneous Solution of Amplitudes p, q, r, s- with Parametric Force Term

$$\{\Gamma, \omega, \hat{a}_5, \Omega, \Omega_2, \hat{c}, \hat{b}, F, \phi\} = \{0.69, 1, 0.001, 248.8, 497.6, 21.9, 8.15 \times 10^9, 19873.3, 0\}$$

Solve[

$$\left\{ \begin{aligned} & \left(-\frac{\hat{c} * p}{2 * \omega} + \frac{\Omega * \hat{a}_5 * r}{2 * \omega} + \frac{\hat{c}^2 * q}{8 * \omega^2} - \frac{\Omega * \hat{c} * \hat{a}_5 * s}{4 * \omega^2} - \frac{\Omega^2 * \hat{a}_5^2 * q}{8 * \omega^2} - \frac{3 * \hat{b} * p^2 * q}{2 * \omega^2} - \frac{3 * \hat{b} * q^3}{2 * \omega^2} + \left(\frac{F^2}{(8 * \Omega_2^2 * \omega^2) + (16 * \Omega_2 * \omega^3)} q \right) \right. \\ & \left. \left(\frac{\Gamma}{4} * \left(1 - \frac{\Omega * \hat{a}_5}{2 * \omega} \right) * \text{Cos}[\phi] \right) - \left(\frac{\hat{c} * \Gamma}{16 * \omega} * \text{Sin}[\phi] \right) + \left(\left(\frac{F}{4 * \omega^2} * p - \frac{\hat{c} * F}{16 * \omega^3} * q + \frac{\Omega * \hat{a}_5 * F * s}{16 * \omega^3} \right) * \text{Sin}[\phi] \right) - \right. \\ & \left. \left(\left(\frac{F}{4 * \omega^2} * q - \frac{\hat{c} * F}{16 * \omega^3} * p + \frac{\Omega * \hat{a}_5 * F * r}{16 * \omega^3} \right) * \text{Cos}[\phi] \right) \right) = 0, \\ & \left(-\frac{\hat{c} * q}{2 * \omega} + \frac{\Omega * \hat{a}_5 * q}{2 * \omega} + \frac{\hat{c}^2 * p}{8 * \omega^2} - \frac{\Omega * \hat{c} * \hat{a}_5 * p}{4 * \omega^2} - \frac{\Omega^2 * \hat{a}_5^2 * p}{8 * \omega^2} - \frac{3 * \hat{b} * q^2 * p}{2 * \omega^2} - \frac{3 * \hat{b} * p^3}{2 * \omega^2} + \left(\frac{F^2}{(8 * \Omega_2^2 * \omega^2) + (16 * \Omega_2 * \omega^3)} p \right) \right. \\ & \left. \left(\frac{\Gamma}{4} * \left(1 - \frac{\Omega * \hat{a}_5}{2 * \omega} \right) * \text{Sin}[\phi] \right) - \left(\frac{\hat{c} * \Gamma}{16 * \omega} * \text{Cos}[\phi] \right) - \left(\left(\frac{F}{4 * \omega^2} * p - \frac{\hat{c} * F}{16 * \omega^3} * q + \frac{\Omega * \hat{a}_5 * F * s}{16 * \omega^3} \right) * \text{Sin}[\phi] \right) + \right. \\ & \left. \left(\left(\frac{F}{4 * \omega^2} * q - \frac{\hat{c} * F}{16 * \omega^3} * p + \frac{\Omega * \hat{a}_5 * F * r}{16 * \omega^3} \right) * \text{Cos}[\phi] \right) \right) = 0, \\ & \left(-\frac{\hat{c} * r}{2 * \omega} - \frac{\Omega * \hat{a}_5 * r}{2 * \omega} + \frac{\hat{c}^2 * s}{8 * \omega^2} + \frac{\Omega * \hat{c} * \hat{a}_5 * s}{4 * \omega^2} - \frac{\Omega^2 * \hat{a}_5^2 * s}{8 * \omega^2} - \frac{3 * \hat{b} * r^2 * s}{2 * \omega^2} - \frac{3 * \hat{b} * s^3}{2 * \omega^2} + \left(\frac{F^2}{(8 * \Omega_2^2 * \omega^2) + (16 * \Omega_2 * \omega^3)} r \right) \right. \\ & \left. \left(\frac{\Gamma}{4} * \left(1 - \frac{\Omega * \hat{a}_5}{2 * \omega} \right) * \text{Sin}[\phi] \right) + \left(\frac{\hat{c} * \Gamma}{16 * \omega} * \text{Cos}[\phi] \right) + \left(\left(\frac{F}{4 * \omega^2} * p - \frac{\hat{c} * F}{16 * \omega^3} * q + \frac{\Omega * \hat{a}_5 * F * s}{16 * \omega^3} \right) * \text{Sin}[\phi] \right) - \right. \\ & \left. \left(\left(\frac{F}{4 * \omega^2} * q - \frac{\hat{c} * F}{16 * \omega^3} * p + \frac{\Omega * \hat{a}_5 * F * r}{16 * \omega^3} \right) * \text{Cos}[\phi] \right) \right) = 0, \\ & \left(-\frac{\hat{c} * s}{2 * \omega} - \frac{\Omega * \hat{a}_5 * s}{2 * \omega} + \frac{\hat{c}^2 * r}{8 * \omega^2} + \frac{\Omega * \hat{c} * \hat{a}_5 * r}{4 * \omega^2} - \frac{\Omega^2 * \hat{a}_5^2 * r}{8 * \omega^2} - \frac{3 * \hat{b} * s^2 * r}{2 * \omega^2} - \frac{3 * \hat{b} * r^3}{2 * \omega^2} + \left(\frac{F^2}{(8 * \Omega_2^2 * \omega^2) + (16 * \Omega_2 * \omega^3)} s \right) \right. \\ & \left. \left(\frac{\Gamma}{4} * \left(1 - \frac{\Omega * \hat{a}_5}{2 * \omega} \right) * \text{Cos}[\phi] \right) + \left(\frac{\hat{c} * \Gamma}{16 * \omega} * \text{Sin}[\phi] \right) - \left(\left(\frac{F}{4 * \omega^2} * p - \frac{\hat{c} * F}{16 * \omega^3} * q + \frac{\Omega * \hat{a}_5 * F * s}{16 * \omega^3} \right) * \text{Sin}[\phi] \right) + \right. \\ & \left. \left(\left(\frac{F}{4 * \omega^2} * q - \frac{\hat{c} * F}{16 * \omega^3} * p + \frac{\Omega * \hat{a}_5 * F * r}{16 * \omega^3} \right) * \text{Cos}[\phi] \right) \right) = 0, \end{aligned} \right.$$

{p, q, r, s}

$$\{0.69, 1, 0.001, 248.8, 497.6, 21.9, 8.15 * 10^9, 19873.3, 0\}$$

$$\begin{aligned} & \{p \rightarrow -894.7379882695416 - 0.9729102385553624 i, \\ & q \rightarrow -0.9779853527565429 + 895.1785380877246 i\}, \\ & \{p \rightarrow -894.7379882695416 + 0.9729102385553624 i, \\ & q \rightarrow -0.9779853527565429 - 895.1785380877246 i\}, \\ & \{p \rightarrow -0.0032642071606207228 - 0.03256906353255708 i, \\ & q \rightarrow -0.032617320406510907 - 0.0027971079970158974 i\}, \\ & \{p \rightarrow -0.0032642071606207228 + 0.03256906353255708 i, \\ & q \rightarrow -0.032617320406510907 + 0.0027971079970158974 i\}, \\ & \{p \rightarrow -0.000012132187738244567, q \rightarrow -0.00003742338553602895\}, \\ & \{p \rightarrow 0.0033653530222304304 - 0.03262057366766362 i, \\ & q \rightarrow 0.032651548148452246 - 0.0026947631597000793 i\}, \\ & \{p \rightarrow 0.0033653530222304304 + 0.03262057366766362 i, \\ & q \rightarrow 0.032651548148452246 + 0.0026947631597000793 i\}, \\ & \{p \rightarrow 895.1553564118768 - 0.982031010887873 i, \\ & q \rightarrow 0.9779698367073695 + 895.178443007957 i\}, \\ & \{p \rightarrow 895.1553564118768 + 0.982031010887873 i, \\ & q \rightarrow 0.9779698367073695 - 895.178443007957 i\}, \end{aligned}$$

$$r \rightarrow -0.0019614024487508972, s \rightarrow -0.019791428012050954,$$

$$\{r \rightarrow -1.1174595304377865 * 10^{-6}, s \rightarrow -0.00003513406798268923\},$$

$$\{r \rightarrow 3.1667071803621055 * 10^{-7} - 0.019786282522361136 i, s \rightarrow -0.00001753142221042751 - 0.001714560160168787 i\}, \{r \rightarrow 3.1667071803621055 * 10^{-7} + 0.019786282522361136 i, s \rightarrow -$$

```
0.00001753142221042751`+0.001714560160168787`  
i},{r→0.001967245099456199`,s→0.01982653707275483`},{r→88038.13746949122`  
-107213.08058734308`i,s→4145.347064433491`+4197.079934276428`  
i},{r→88038.13746949122` +107213.08058734308` i,s→4145.347064433491` -  
4197.079934276428`i},{r→105938.7465238797` +0.` i,s→-4145.347046889566`-  
4197.079931597161` i},{r→105938.7465238797`+0.` ,s→-  
4145.347046889566`+4197.079931597161`i}}
```

B.3 Coefficients of the Characteristic Equation

$$k_1 = a_0 b_0$$

$$k_2 = \frac{a_0 b_0 \bar{c}}{\omega} + \frac{b_0 \Gamma \text{Cos} \gamma_{10}}{2} - \frac{a_0 \Gamma \text{Sin} \gamma_{20}}{2} + \frac{a_0^2 \Omega \bar{a}_5 \text{Cos} \psi_{10}}{2\omega} + \frac{b_0^2 \Omega \bar{a}_5 \text{Cos} \psi_{10}}{2\omega}$$

$$k_3 = \frac{a_0 b_0 \bar{c}^2}{4\omega^2} + \frac{b_0 \bar{c} \Gamma \text{Cos} \gamma_{10}}{2\omega} + \frac{a_0 \Gamma \alpha'_{20} \text{Cos} \gamma_{20}}{2} - \frac{b_0 \Gamma \alpha'_{10} \text{Sin} \gamma_{10}}{2} - \frac{a_0 \bar{c} \Gamma \text{Sin} \gamma_{20}}{2\omega}$$

$$- \frac{\Gamma^2 \text{Cos} \gamma_{10} \text{Sin} \gamma_{20}}{4} + \frac{a_0^2 \bar{c} \Omega \bar{a}_5 \text{Cos} \psi_{10}}{2\omega^2} + \frac{b_0^2 \bar{c} \Omega \bar{a}_5 \text{Cos} \psi_{10}}{2\omega^2} + \frac{a_0 \Gamma \Omega \bar{a}_5 \text{Cos} \gamma_{10} \text{Cos} \psi_{10}}{4\omega}$$

$$- \frac{b_0 \Gamma \Omega \bar{a}_5 \text{Cos} \psi_{10} \text{Sin} \gamma_{20}}{4\omega} - \frac{b_0^2 \alpha'_{10} \Omega \bar{a}_5 \text{Sin} \psi_{10}}{2\omega} + \frac{a_0^2 \alpha'_{20} \Omega \bar{a}_5 \text{Sin} \psi_{10}}{2\omega} + \frac{a_0 b_0 \Omega^2 \bar{a}_5^2 \text{Cos}^2 \psi_{10}}{4\omega^2}$$

$$k_4 = \frac{b_0 \bar{c}^2 \Gamma \text{Cos} \gamma_{10}}{8\omega^2} - \frac{a_0 \bar{c} \Gamma \alpha'_{20} \text{Cos} \gamma_{20}}{4\omega} - \frac{\Gamma^2 \alpha'_{20} \text{Cos} \gamma_{10} \text{Cos} \gamma_{20}}{4} - \frac{b_0 \bar{c} \Gamma \alpha'_{10} \text{Sin} \gamma_{10}}{4\omega}$$

$$- \frac{a_0 \bar{c}^2 \Gamma \text{Sin} \gamma_{20}}{8\omega^2} - \frac{\bar{c} \Gamma^2 \text{Cos} \gamma_{10} \text{Sin} \gamma_{20}}{4\omega} + \frac{\Gamma^2 \alpha'_{10} \text{Sin} \gamma_{10} \text{Sin} \gamma_{20}}{4} + \frac{a_0^2 \bar{c}^2 \Omega \bar{a}_5 \text{Cos} \psi_{10}}{8\omega^3}$$

$$+ \frac{b_0^2 \bar{c}^2 \Omega \bar{a}_5 \text{Cos} \psi_{10}}{8\omega^3} + \frac{a_0 \bar{c} \Gamma \Omega \bar{a}_5 \text{Cos} \psi_{10} \text{Cos} \gamma_{10}}{4\omega^2} - \frac{b_0 \Gamma \alpha'_{20} \Omega \bar{a}_5 \text{Cos} \gamma_{20} \text{Cos} \psi_{10}}{4\omega}$$

$$- \frac{a_0 \Gamma \alpha'_{10} \Omega \bar{a}_5 \text{Cos} \psi_{10} \text{Sin} \gamma_{10}}{4\omega} - \frac{b_0 \bar{c} \Gamma \Omega \bar{a}_5 \text{Cos} \psi_{10} \text{Sin} \gamma_{20}}{4\omega^2} - \frac{b_0^2 \bar{c} \alpha'_{10} \Omega \bar{a}_5 \text{Sin} \psi_{10}}{4\omega^2}$$

$$+ \frac{a_0^2 \bar{c} \alpha'_{20} \Omega \bar{a}_5 \text{Sin} \psi_{10}}{4\omega^2} + \frac{a_0 \Gamma \alpha'_{20} \Omega \bar{a}_5 \text{Cos} \gamma_{10} \text{Sin} \psi_{10}}{4\omega} + \frac{b_0 \Gamma \alpha'_{10} \Omega \bar{a}_5 \text{Sin} \gamma_{20} \text{Sin} \psi_{10}}{4\omega}$$

$$+ \frac{b_0 \Gamma \Omega^2 \bar{a}_5^2 \text{Cos} \gamma_{10} \text{Cos}^2 \psi_{10}}{8\omega^2} - \frac{a_0 \Gamma \Omega^2 \bar{a}_5^2 \text{Cos}^2 \psi_{10} \text{Sin} \gamma_{20}}{8\omega^2}$$

$$+ \frac{a_0 b_0 \alpha'_{10} \Omega^2 \bar{a}_5^2 \text{Cos} \psi_{10} \text{Sin} \psi_{10}}{4\omega^2} + \frac{a_0 b_0 \alpha'_{20} \Omega^2 \bar{a}_5^2 \text{Cos} \psi_{10} \text{Sin} \psi_{10}}{4\omega^2}$$

$$+ \frac{b_0 \Gamma \Omega^2 \bar{a}_5^2 \text{Cos} \psi_{10} \text{Sin} \gamma_{10} \text{Sin} \psi_{10}}{4\omega^2} - \frac{b_0 \Gamma \Omega^2 \bar{a}_5^2 \text{Cos} \gamma_{10} \text{Sin}^2 \psi_{10}}{8\omega^2}$$

$$- \frac{a_0 \Gamma \Omega^2 \bar{a}_5^2 \text{Sin} \gamma_{20} \text{Sin}^2 \psi_{10}}{8\omega^2} + \frac{a_0^2 \Omega^3 \bar{a}_5^3 \text{Cos}^3 \psi_{10}}{8\omega^3} + \frac{b_0^2 \Omega^3 \bar{a}_5^3 \text{Cos}^3 \psi_{10}}{8\omega^3}$$

$$+ \frac{a_0^2 \Omega^3 \bar{a}_5^3 \text{Cos} \psi_{10} \text{Sin}^2 \psi_{10}}{8\omega^3} + \frac{b_0^2 \Omega^3 \bar{a}_5^3 \text{Cos} \psi_{10} \text{Sin}^2 \psi_{10}}{8\omega^3}$$

$$\begin{aligned}
k_5 = & -\frac{\bar{c}\Gamma^2\text{Cos}\gamma_{10}\text{Cos}\gamma_{20}}{8\omega} + \frac{\Gamma^2\alpha'_{10}\alpha'_{20}\text{Cos}\gamma_{20}\text{Sin}\gamma_{10}}{4} - \frac{\bar{c}^2\Gamma^2\text{Cos}\gamma_{10}\text{Sin}\gamma_{20}}{16\omega^2} \\
& + \frac{\bar{c}\Gamma^2\alpha'_{10}\text{Sin}\gamma_{10}\text{Sin}\gamma_{20}}{8\omega} + \frac{a_0\bar{c}^2\Gamma\Omega\bar{a}_5\text{Cos}\gamma_{10}\text{Cos}\psi_{10}}{16\omega^3} \\
& - \frac{b_0\bar{c}\Gamma\alpha'_{20}\Omega\bar{a}_5\text{Cos}\gamma_{20}\text{Cos}\psi_{10}}{8\omega^2} - \frac{a_0\bar{c}\Gamma\alpha'_{10}\Omega\bar{a}_5\text{Cos}\psi_{10}\text{Sin}\gamma_{10}}{8\omega^2} \\
& - \frac{b_0\bar{c}^2\Gamma\Omega\bar{a}_5\text{Cos}\psi_{10}\text{Sin}\gamma_{20}}{16\omega^3} + \frac{a_0\bar{c}\Gamma\alpha'_{20}\Omega\bar{a}_5\text{Cos}\gamma_{10}\text{Sin}\psi_{10}}{8\omega^2} \\
& + \frac{b_0\Gamma\alpha'_{10}\alpha'_{20}\Omega\bar{a}_5\text{Cos}\gamma_{20}\text{Sin}\psi_{10}}{4\omega} - \frac{a_0\Gamma\alpha'_{10}\alpha'_{20}\Omega\bar{a}_5\text{Sin}\gamma_{10}\text{Sin}\psi_{10}}{4\omega} \\
& + \frac{b_0\bar{c}\Gamma\alpha'_{10}\Omega\bar{a}_5\text{Sin}\gamma_{20}\text{Sin}\psi_{10}}{8\omega^2} + \frac{a_0\Gamma\alpha'_{10}\Omega^2\bar{a}_5^2\text{Cos}\gamma_{20}\text{Cos}^2\psi_{10}}{8\omega^2} \\
& - \frac{b_0\Gamma\alpha'_{20}\Omega^2\bar{a}_5^2\text{Cos}^2\psi_{10}\text{Sin}\gamma_{10}}{8\omega^2} - \frac{\Gamma^2\Omega^2\bar{a}_5^2\text{Cos}\gamma_{10}\text{Cos}^2\psi_{10}\text{Sin}\gamma_{20}}{16\omega^2} \\
& + \frac{b_0\Gamma\alpha'_{20}\Omega^2\bar{a}_5^2\text{Cos}\gamma_{10}\text{Cos}\psi_{10}\text{Sin}\psi_{10}}{8\omega^2} + \frac{a_0\bar{c}\Gamma\Omega^2\bar{a}_5^2\text{Cos}\gamma_{20}\text{Cos}\psi_{10}\text{Sin}\psi_{10}}{16\omega^3} \\
& - \frac{\Gamma^2\Omega^2\bar{a}_5^2\text{Cos}\gamma_{10}\text{Cos}\gamma_{20}\text{Cos}\psi_{10}\text{Sin}\psi_{10}}{16\omega^2} + \frac{b_0\bar{c}\Gamma\Omega^2\bar{a}_5^2\text{Cos}\psi_{10}\text{Sin}\gamma_{10}\text{Sin}\psi_{10}}{16\omega^3} \\
& - \frac{a_0\Gamma\alpha'_{10}\Omega^2\bar{a}_5^2\text{Cos}\psi_{10}\text{Sin}\gamma_{20}\text{Sin}\psi_{10}}{8\omega^2} - \frac{\Gamma^2\Omega^2\bar{a}_5^2\text{Cos}\psi_{10}\text{Sin}\gamma_{10}\text{Sin}\gamma_{20}\text{Sin}\psi_{10}}{16\omega^2} \\
& - \frac{b_0\bar{c}\Gamma\Omega^2\bar{a}_5^2\text{Cos}\gamma_{10}\text{Sin}^2\psi_{10}}{16\omega^3} - \frac{\Gamma^2\Omega^2\bar{a}_5^2\text{Cos}\psi_{10}\text{Sin}\gamma_{10}\text{Sin}^2\psi_{10}}{16\omega^2} \\
& - \frac{a_0\bar{c}\Gamma\Omega^2\bar{a}_5^2\text{Sin}\gamma_{20}\text{Sin}^2\psi_{10}}{16\omega^3} + \frac{a_0\Gamma\Omega^3\bar{a}_5^3\text{Cos}\gamma_{10}\text{Cos}^3\psi_{10}}{16\omega^3} \\
& - \frac{b_0\Gamma\Omega^3\bar{a}_5^3\text{Cos}^3\psi_{10}\text{Sin}\gamma_{20}}{16\omega^3} - \frac{b_0\Gamma\Omega^3\bar{a}_5^3\text{Cos}\gamma_{20}\text{Cos}^2\psi_{10}\text{Sin}\psi_{10}}{16\omega^3} \\
& + \frac{a_0\Gamma\Omega^3\bar{a}_5^3\text{Cos}^2\psi_{10}\text{Sin}\gamma_{10}\text{Sin}\psi_{10}}{16\omega^3} + \frac{a_0\Gamma\Omega^3\bar{a}_5^3\text{Cos}\gamma_{10}\text{Cos}\psi_{10}\text{Sin}^2\psi_{10}}{16\omega^3} \\
& - \frac{b_0\Gamma\Omega^3\bar{a}_5^3\text{Cos}\psi_{10}\text{Sin}\gamma_{20}\text{Sin}^2\psi_{10}}{16\omega^3} - \frac{b_0\Gamma\Omega^3\bar{a}_5^3\text{Cos}\gamma_{20}\text{Sin}^3\psi_{10}}{16\omega^3} \\
& + \frac{a_0\Gamma\Omega^3\bar{a}_5^3\text{Sin}\gamma_{10}\text{Sin}^3\psi_{10}}{16\omega^3}
\end{aligned}$$

APPENDIX C

C.1 Screen Dump of the Code for the Analysis of the Coupled Differential Equations

```

Dynamics for Windows
Enter vector field:
-Documentation: (allowed process parameters: c1,...,c9,phi,rho,sigma,beta)
X'+C1*X'-C2*Y'*cos(1.325*Y)+C3*X+C4*X^3=rho*sin(phi*t)
Y'+C1*Y'+C2*X'*cos(1.325*Y)+C3*Y+C4*Y^3=rho*cos(phi*t)
y[0]=s;y[1]=t;y[2]=X';y[3]=Y';y[4]=X;y[5]=Y;

-Vector field: can use p,q,...,x,y,z; phase space: u,v,...,z only; set t':=1
s' := 1 ! this is time
t' := 1 ! this is time mod 2* pi/ phi (see window below)
x' := u
y' := v
u' := rho*sin(phi*t)-C1*u+C2*v*cos(1.325*y)-C3*x-C4*x^3 ! EOM1
v' := rho*cos(phi*t)-C1*v-C2*u*cos(1.325*y)-C3*y-C4*y^3 ! EOM2

-Initialize variables & parameters; use only u,v,...,z for phase space
t:=0;x:= 0 y:= 0 u:=0 v:=0 ! Set initial conditions
XCO :=4 YCO :=2 ! Plot X(x-axis) vs X'(y-axis)
x_upper :=0.05 x_lower :=-0.05 y_upper := 4 y_lower := -2
C1 :=1.4 C2 :=0.025 C3 :=248.8 C4:=32800000 rho:=0.048
phi :=248.8
spc := 30 ipp := 30 ! Take 30 steps per 2pi/phi and plot once in 30 steps.
! If you have an autonomous system, include a line like step := .01
-Modulo function: (Optional; this is evaluated once per time step)
t := mod(t,0,2*pi/phi

Esc=Cancel Tab=Next F3=Map F1=Compile

```

Figure C- 1: Dynamics 2 Program Code for coupled Duffing equations

C.2 Specialized Code written in *Mathematica*TM

C.2.1 Numerical Integration

$$\begin{aligned} eqns = & q_1''[t] + \hat{c} * q_1'[t] - \Omega * \hat{a}_5 * q_2'[t] * \cos[\gamma * q_2[t]] + \omega^2 * q_1[t] + \hat{b} * (q_1[t])^3 \\ & - \mu * d * \Omega^2 * \sin[\Omega * t] \end{aligned}$$

$$\begin{aligned} eqnt = & q_2''[t] + \hat{c} * q_2'[t] - \Omega * \hat{a}_5 * q_1'[t] * \cos[\gamma * q_2[t]] + \omega^2 * q_2[t] + \hat{b} * (q_2[t])^3 \\ & - \mu * d * \Omega^2 * \cos[\Omega * t] \end{aligned}$$

system= NDSolve[{eqns==0,eqnt==0, q₁[0]==0, q₂[0]==0, q'₁[0]==0,

q'₂[0]==0},{q₁,q₂},{t,0,50},MaxSteps→Infinity,AccuracyGoal→Automatic,
PrecisionGoal→Automatic,WorkingPrecision→20]

Plot[Evaluate[q₁[t]/.system],{t,0,50},Frame→True,FrameTicks→Automatic,
GridLines→Automatic,FrameLabel→{Time,q₁[t]}

Plot[Evaluate[q'₁[t]/.system],{t,0,50},Frame→True,FrameTicks→Automatic,
GridLines→Automatic,FrameLabel→{Time,q'₁[t]}

C.2.2 Plotting of Poincaré Map

system=NDSolve[{eqns==0,eqnt==0,x[0]==0,u[0]==0,v[0]==0,{x},{t,0,T},
Method→Runge-Kutta,

MaxSteps→Infinity,AccuracyGoal→Automatic,PrecisionGoal→Automatic,
WorkingPrecision→20]

ParametricPlot[Evaluate[{x[t],u[t]}/.system],{t,0,T},PlotRange→All,
Frame→True,FrameLabel→{x[t],u[t]}Textual=2*π/ω

ParametricPlot[Evaluate[{x[t],v[t]}/.system],{t,0,T},PlotRange→All,
Frame→True,FrameLabel→{x[t],v[t]}Textual=2*π/ω

```
tstart=10* Texternal  numperiods=20
```

```
Poincarepts=Flatten [Table [Evaluate [{x[timeperiod [i]], u[timeperiod [i]]}
/.system],{i,0,numperiods}],1]ListPlot[Poincarepts,AspectRatio→1,
ImageSize →{300,300},PlotRange →{{-π,π},{-2,2}},
```

```
PlotLabel →StyleForm[“PoincaréSection”], AxesOrigin → {-π,0}, Axeslabel →{x,
u}, PlotStyle →{PointSize [0.015],RGBColour[1,0,0]}
```

C.2.3 Plotting of Time plots and Phase planes

```
Solution[tmax]= NDSolve[{eqns==0, eqnt==0, x[0]==0, u[0]==0, v[0]==0},
{x, u},{t,999.5,1000},Method →Runge-Kutta,
MaxSteps →Infinity,AccuracyGoal →Automatic,PrecisionGoal →Automatic,
WorkingPrecision →20]; sol1=solution[1000];
```

```
{x, v},{t,999.5,1000},Method →Runge-Kutta,
MaxSteps →Infinity,AccuracyGoal →Automatic,PrecisionGoal →Automatic,
WorkingPrecision →20]; sol1=solution[1000];
```

For time plots

```
graph1[tmin_,tmax_]:=Plot[Evaluate x[t] /.sol1},{t,tmin,tmax},Frame →True];
graph[999.5,1000];
```

For phase planes

```
graph[tmin_,tmax_]:=ParametricPlot[Evaluate x[t], u[t] /.sol1},{t,tmin,tmax},
AxesStyle →{AbsoluteThickness[1]},Frame →True]; graph[995,1000];
```

```
graph[tmin_,tmax_]:=ParametricPlot[Evaluate x[t], v[t] /.sol1},{t,tmin,tmax},
AxesStyle →{AbsoluteThickness[1]},Frame →True]; graph[995,1000];
```

C.3 Dynamics 2 Commands

C.3.1 General

* : to get help with commands (e.g. *MM-help with menu)

. : pause the program after plotting one dot.

<space bar> returns the program to normal

& : Cycle through the most important menus

<Enter> : Fetch previous menu

<Esc> : current routine terminates or fetches parent menu of current
menu

<space bar> : removes menu and continues plotting

<Tab> : prints the speed (in dots per second) and a selection of parameter
values.

Dynamics : Starts the program

MM : Main menu

C : clear screen & core memory

R : refresh screen

C.3.2 Colour

<F7> : decrease colour number by 1

<F8> : increase

<F9> : choose colour number

CT : displays colour table

C.3.3 Change Parameters:

PM : Parameter Menu

<+> : increase PRM (e.g.RHO) by the amount PS (i.e. Parameter Step)

<-> : decrease PRM by the amount PS

<Home> or <Shift 3> : halve PS

<PgUp> or <Shift 4> : double PS

C.3.4 Plotting

I : initialize y using y1

II : initialize and iterate

CON : connects conservative dots

PT : toggle 'Plot Time' to have time on the horizontal axis

T : plots the trajectory

C.3.5 Storing Data

DD : Dump Data to disk

FD : retrieve picture from disk

AFD : add from disk-adds the old picture onto the screen

TD : save picture to disk

C.3.6 Lyapunov Plotting Commands

- L : sets number of Lyapunov exponents ($0 \leq L \leq 2$) to be computed.
- LL : prints the current values of the Lyapunov exponents, numbers and dimension on the screen.

C.3.7 Bifurcation Plotting Commands

- BIFM : Bifurcation Diagram Menu
- BIFD : sets the number of dots to be plotted (per horizontal line).
- BIFPI : sets the number of pre-iterates.
- BIFR : specifying range of the bifurcation parameter (e.g.RHO).
- BIFS : plots bifurcation diagram on screen.
- BIFV : for higher quality picture
- PRM : parameter to be varied

APPENDIX D

D.1 Parametric Plots

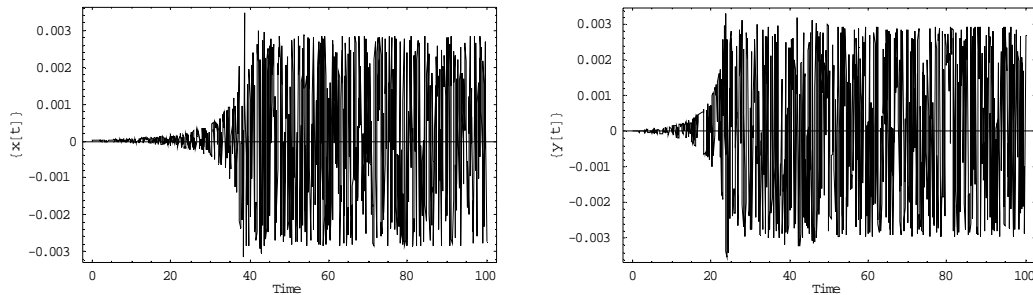


Figure D- 1: Parametric Plots

D.2 Calculation of Maximum Spring Force

The axial loading relationship $P = \frac{AE}{l} \Delta$ is used in finding the maximum displacement Δ , where the parameters for the calculation of spring are as follows: P is the actuator force of 532N, $A = \pi r^2$ where r is the radius of the shaft, E is the modulus of elasticity of steel and l is the shaft length of 0.56m.

Therefore

$$\Delta = \frac{Pl}{AE} = 0.018 \quad (\text{D- 1})$$

Now

$$\delta_2 = L_0 - L_n = 25.2mm \quad (\text{D- 2})$$

Giving

$$\delta_1 = \delta_2 - \Delta = 25.182mm \quad (\text{D- 3})$$

Spring constant is

$$k_s = \frac{F_{S\min}}{\delta_1} = 21131Nm^{-1} \quad (\text{D- 4})$$

Therefore

$$F_{S\max} = k_s \delta_2 = 532.5N \quad (\text{D- 5})$$